

LONDON  
SCHOOL of  
HYGIENE  
& TROPICAL  
MEDICINE



**BUG-BEATS : UNDERSTANDING WINGBEAT  
FREQUENCIES FOR AUTOMATED DETECTION OF  
MOSQUITOES**

**FREDERICK ARVIND SARATHCHANDRA**

Thesis submitted in accordance with the requirements for the degree  
of  
Doctor of Philosophy  
of the

University of London

**December 2024**

Department of Disease Control

Faculty of Infectious and Tropical Diseases

**LONDON SCHOOL OF HYGIENE & TROPICAL MEDICINE**

Funded by the Biotechnology and Biological Research Council  
(BBSRC)

and

Rentokil-Initial Plc

I, Frederick A Sarathchandra, confirm that the work presented in this thesis is my own. Where information has been derived from other sources, I confirm that this has been indicated in the thesis.

Signed: F. Sarathchandra

Date: December 2024

# ABSTRACT

Deepening our understanding of the mosquito wingbeat is essential for the development of future acoustic mosquito surveillance approaches. Here, a series of measurement arenas together with acoustic methods, were developed and evaluated to explore novel approaches of capturing and describing the wingbeat. The range of measurement arenas designed provided semi-anechoic and reverberant conditions which facilitated the generation of acoustic datasets for free-flight and tethered mosquitoes

The semi-anechoic arena created, facilitated investigations into the acoustic effects of post-emergence age and bloodmeals, which were performed on *Aedes aegypti*, *Anopheles gambiae* and *Culex quinquefasciatus*. The arena developed could produce descriptions of the mosquito wingbeat with exceptional clarity, for tethered or free flight mosquitoes. This facilitated a further investigation using *Ae. aegypti* to describe the effects of tethering on the mosquito wingbeat.

The devices developed also enabled investigation into the acoustic effects of position on a measured wingbeat. A remotely operated positioning tool was designed, to alter the angle and distance of a tethered mosquito relative to the measurement microphone, whilst in the sealed semi-anechoic arena.

Using the tightly controlled acoustic conditions of the arenas generated low noise data that permitted exploration of new acoustic processing approaches. These led to the development of novel metrics to explore mosquito acoustics beyond the wingbeat frequency. The utility of these novel metrics was evaluated alongside the wingbeat frequency for the investigations undertaken in this project.

Through this project, a high-quality dataset has been compiled of mosquito wingbeats, which furthered understanding of how to sample, process and interpret them, which may facilitate development of future tools for mosquito surveillance

# Acknowledgements

“it takes a village to raise a child”

I will be forever grateful for the multiple villages, literal and metaphorical, that have raised the child that is not only me, but also this PhD! My parents, sister, and wider family across the world (especially in Sri Lanka & South Africa) have been instrumental in their support and this project would not have been completed without you all. This particularly includes my parents' garage, which rapidly became my prototyping and acoustic entomology HQ during all the COVID lockdowns.

I must acknowledge the generous support offered by my “academic villages”, with a special thank you to Dr Alicia Showering for your unwavering guidance, support & inspiration from day 1. The team at the LSHTM malaria centre are all rock-stars to me, and I will forever be grateful for you adopting a rogue engineer into your spectacular group of malaria scientists. I'd also especially like to thank Cheryl, Shahida and Pat for kindly explaining all things entomology to me, and for providing me with the mosquito eggs / larvae / adults throughout the project after I crashed yet another colony! I'd also like to acknowledge the patience and kind guidance of Ruby Chan of the RVC for your numerous sessions with me to guide me through all things statistics.

A special mention is also needed for the most amazing team at UCL with the LIDo DTP and the tireless efforts of Nadine who make the PhD experience second to none.

None of this project would have happened without the generous support of the industrial partner Rentokil, and I must say an enormous thank you to the staff there who kindly accommodated me throughout, especially during COVID. Matt, Greg and Fabio, you have all been incredible! Without you, there would be no mosquitoes or test lab! But more importantly, the whimsical and tangential chats in the office have been ridiculous but amazing!

To my friends in the four corners of the world, new and old, I think I owe you all apologies! I've been so pre-occupied by this project and oftentimes trapped you in my latest rant about either a literal fire, or philosophical one. Thank you so much for putting up with me, and always encouraging me to keep going. Especially Tom, Rahul<sup>2</sup>, Nick, Vasko, James R, Roz, Claire & Seb, I'll do my best to make up for all your (probably) days of lost time!

Finally, to my supervisory team, Mary, Matt, Richard thank you for your efforts and extreme patience with me throughout this project, especially with getting this thesis over line! It's been a pleasure to learn from you all, and I'm especially grateful for your time and expertise you kindly shared with me.

I hope you, the reader, may take something of interest from this thesis and I am grateful for you taking the time to find it. It has been a privilege to be given the chance of understanding the concept of mosquito control, through my strange mixed lenses of entomology, engineering, product design and of course acoustics, and I hope there may be some thought-provoking ideas for you here as a result!

# TABLE OF CONTENTS

<b>Abstract</b>	<b>iii</b>
<b>Acknowledgements</b>	<b>iv</b>
<b>Table of Contents</b>	<b>v</b>
<b>List of Figures</b>	<b>x</b>
<b>List of Tables</b>	<b>xvi</b>
<b>1. Connecting acoustics, mosquito surveillance and vector control</b>	<b>1</b>
1.1. Introduction	1
1.1.1. Overview	1
1.1.2. Mosquito borne disease	2
1.1.3. Overview of vector surveillance	5
1.1.4. Simplifying the identification process through new approaches	10
1.1.5. Metrics used in vector control epidemiological models	12
1.2. Mosquito acoustics	14
1.2.1. Why develop our understanding of mosquito acoustics	14
1.2.2. Factors affecting the wingbeat frequency	19
1.2.3. Overview of acoustic sampling and processing techniques	24
1.2.4. Connecting acoustic measures to vector control	29
1.3. Project aims and objectives	32
1.3.1. Project scope	32
1.3.2. Aims and objectives	33

<b>2. Describing mosquito free flight acoustics with simple arenas</b>	<b>36</b>
2.1. COVID impact statement	36
2.2. Introduction	38
2.2.1. The application of mosquito acoustics for surveillance	38
2.2.2. Aims and objectives	39
2.3. Materials and methods 1 – acoustic measurement using acrylic tunnels	41
2.3.1. Overview	41
2.3.2. Mosquito rearing and handling	41
2.3.3. Measurement arenas and sampling equipment development	41
2.3.4. Introduction to acoustic analysis of mosquitoes using MKII hardware and PAK 5.8	52
2.3.5. Measurement setup	53
2.3.6. Analysis setup	53
2.3.7. Experimental design: Free flight measurements in four acrylic flight tunnels	56
2.4. Results and discussion 1 - acoustic measurement using acrylic tunnels	57
2.4.1. Results	57
2.4.2. Discussion of the Ø40, Ø76, Ø120 & Ø230 tunnel performance	60
2.4.3. Conclusions of the Ø40, Ø76, Ø120 & Ø230 tunnel assessment	62
2.5. Materials and methods 2 – assessment of <i>Aedes aegypti</i> , <i>Anopheles gambiae</i> & <i>Culex quinquefasciatus</i>	64
2.5.1. Overview	64
2.5.2. Measurement arena optimisation	64
2.5.3. Experimental design	65
2.6. Results and discussion 2 – Assessment of <i>Aedes aegypti</i> , <i>Anopheles gambiae</i> & <i>Culex quinquefasciatus</i>	66
2.6.1. Results	66
2.6.2. Discussion of the Ø80 tunnel measurements	68
2.7. Chapter summary	70
2.7.1. Conclusions and next steps	70

<b>3. Developing controlled measurement approaches</b>	<b>72</b>
3.1. COVID impact statement	72
3.2. The need for a controlled measurement space	73
3.2.1. The compromise of design simplicity, precision and accuracy	73
3.2.2. Acoustic control	74
3.2.3. Environmental control	75
3.2.4. Position control	76
3.2.5. Aims and objectives	76
3.3. Developing the novel tools	77
3.3.1. Semi-anechoic measurement chamber – free flight	77
3.3.2. Semi-anechoic measurement chamber – tethered flight	83
3.3.3. Variable aspirator	86
3.3.4. Equipment summary	88
3.4. Developing a tethered flight method	89
3.4.1. Airflow based tethering	92
3.4.2. Preliminary evaluation of distance on measured mosquito acoustics	92
3.4.3. Preliminary evaluation of angle on measured mosquito acoustics	97
3.4.4. Discussion of the tethered distance and angle evaluations	100
3.5. The repeatability of tethered flight	104
3.5.1. The acoustic profile	104
3.5.2. Why should flight effort be quantified during a long time period measurement?	105
3.5.3. Development of an analysis approach to describe the variation fundamental flight tones	107
3.5.4. Development of a vibration based mosquito tether metric	112
3.6. Developing a semi-anechoic free flight method	124
3.6.1. Assessment of the free flight tunnel	124
3.6.2. Results of semi-anechoic free-flight tunnel comparison measurements	125
3.6.3. Discussion of semi-anechoic free flight tunnel measurements	127
3.7. Chapter summary	128
3.7.1. Controlling mosquito acoustics	128

<b>4. Flight type and species comparisons</b>	<b>130</b>
4.1. Introduction	130
4.1.1. Understanding free flight and tethered acoustics	130
4.1.2. Mosquito species	132
4.1.3. Aims and objectives	132
4.2. Materials and methods	133
4.2.1. Experimental design: free flight vs tethered flight	133
4.2.2. Experimental design: free flight species comparison	135
4.2.3. Mosquito rearing and handling	135
4.2.4. Acoustic setup	136
4.2.5. Analysis workflow	137
4.3. Results	139
4.3.1. Tethered vs free flight	139
4.3.2. Free flight species comparison	143
4.4. Harmonic convergence – an example	145
4.4.1. Harmonic convergence of flight tones	145
4.4.2. Results	146
4.5. Discussion	151
4.5.1. Tethered vs free flight	151
4.5.2. Free flight species comparison	153
4.5.3. Harmonic convergence	156
4.6. Chapter summary	157
<b>5. Physiological effects on mosquito acoustics</b>	<b>159</b>
5.1. Introduction	159
5.1.1. Exploring physiology with the tethered approach	159
5.1.2. Selection of physiology to investigate	160
5.1.3. Aims and objectives	162
5.2. Materials and methods	163
5.2.1. Mosquito rearing and handling	163
5.2.2. Acoustic setup	165
5.2.3. Analysis workflow	166
5.2.4. Statistical analyses & data visualisation	166

5.3. Results	168
5.3.1. Effect of age	168
5.3.2. Effect of bloodmeals	171
5.3.3. Accelerometer vs microphone metrics	174
5.4. Discussion	175
5.4.1. Effect of age	175
5.4.2. Effect of bloodmeals	177
5.4.3. Comparison of microphone and accelerometer metrics	178
5.5. Chapter summary	179
<b>6. General discussion</b>	<b>181</b>
6.1. Summary	181
6.1.1. Methods, devices, acoustic recordings & frequency analysis	181
6.2. Measurement approaches	183
6.2.1. Design trade-offs during development of measurement spaces	183
6.2.2. Longer time-period measurements	186
6.2.3. Considerations of tether and free flight approaches	187
6.2.4. Further development of accelerometer-based measurements	189
6.3. Application to vector control	191
6.3.1. Integrating the acoustic descriptions into vector surveillance	191
6.3.2. Flight patterns and surveillance tool design	193
6.3.3. Acoustic physiological state identification and vector surveillance	198
6.4. Conclusions	201

## **Abstract**

- A1. Latin square design for free flight – tether investigation (4.3.1)
- A2. Example Spectrogram Tethered Flight
- A3. Example Frequency Descriptions Tethered Flight (PAK 5.8 Output)
- A4. Engineering development drawings for acrylic tunnels (Ø40, Ø76, Ø120)

## LIST OF FIGURES

<b>1. Connecting acoustics, mosquito surveillance and vector control</b>	<b>1</b>
1.1. Vector-borne disease transmission ecological system	4
1.2. WHO Global response framework	6
1.3. Generalised process of mosquito identification	6
1.4. CDC Light trap function description	7
1.5. a) Unsorted catch from a CDC light trap, b) Catch sorted manually on petri dish to identify morphological features on mosquitoes	8
1.6. Example sorting of wet catch (sandflies) from a CDC light trap	9
1.7. Mosquito identification approaches following sampling	10
1.8. Generalised process of novel acoustic mosquito identification	14
1.9. Einige Beispiele für die Höhe der Stimmen und Töne der Insecten – An example of the pitches of insect voices and tones” - mosquito and insect wingbeat classification using sheet music notation by Landois Herman	15
<b>2. Flight type and species comparisons</b>	<b>36</b>
2.1. Ø230 x 1000 flight tunnel, suspended on vibration isolation springs	42
2.2. Ø40 x 1000 flight tunnel	43
2.3. Ø76 x 1000 flight tunnel	44
2.4. Ø120 x 1000 flight tunnel	45
2.5. End capsule assembly drawing	46
2.6. Ø40 tunnel visualisation	47
2.7. Ø76 tunnel visualisation	48
2.8. Ø120 tunnel visualisation	49
2.9. Ø230 tunnel visualisation	50
2.10. Engineering drawing of the specimen cartridge assembly	51

2.11. Field aspirator, specimen cartridge and suction tube assembly	51
2.12. Frequency analysis template visualises measured flight bursts within the tunnel, from the LHS and RHS microphones. Average FFT content during flight bursts and no flight zones (top), spectrograms (bottom left & right) and bandpass magnitude plot between 500 & 550 Hz	53
2.13. Frequency analysis summary report. Frequency content for the four measurement arenas, with sum level information is summarised for specimen S85 <i>Aedes aegypti</i>	55
2.14. Background noise compensated frequency analysis summary. Example frequency content for the four measurement arenas, along with frequency information is summarised for single <i>Ae. aegypti</i> specimen	57
2.15. Summarised background noise compensated mean fundamental frequencies for the four measurement tunnels	58
2.16. Summarised background noise compensated mean fundamental frequencies amplitudes for the four measurement tunnels	58
2.17. Summarised background noise compensated average fundamental & harmonic frequency amplitude ratios for the four measurement tunnels	59
2.18. Ø80 x 500mm tunnel [PU-13h] visualisation	65
2.19. Ø80 measured frequency content for <i>Cx. quinquefasciatus</i> , <i>An. gambiae</i> & <i>Ae. aegypti</i> . Letters above the boxplots indicate which groups differ significantly from one another	67
2.20. Ø80 measured frequency amplitudes for <i>Cx. quinquefasciatus</i> , <i>An. gambiae</i> & <i>Ae. aegypti</i>	67
<b>3. Developing controlled measurement approaches</b>	<b>72</b>
3.1. Semi-anechoic measurement chamber (shown with Ø100 tunnel installed inside)	78
3.2. Ø76 acoustically transparent flight tunnel, with shakers	79
3.3. a) Specimen cartridge magnetically secures to chamber, with card barrier keeping mosquito out of chamber, b) card removed, allowing entry to “air lock”, c) outer “air lock” gate open, permitting entry of mosquito into “airlock”, d) outer “airlock” closed, securing mosquito between outer & inner	

“airlock) Ø3.4 (left), b (right) –. a) Specimen is inside airlock with both gates closed, b) inner airlock opened, permitting mosquito to enter chamber	80
3.4. a) Specimen is inside airlock with both gates closed, b) inner airlock opened, permitting mosquito to enter chamber	80
3.5. Control Centre allows monitoring of the chamber environmental sensors and displays status of chamber controls	81
3.6. Control Centre switchgear	82
3.7. Interior view showing mosquito entry to flight tunnel, following opening of interior “airlock” (Ø40 tunnel shown installed)	82
3.8. Exterior view showing acoustic plug in place, secured before opening interior airlock gate	83
3.9. a) Linear actuator with rotary platform to allow 150 mm linear positioning of tethered mosquito combined with 360° rotation. b) Rotary cage with tethered mosquito	83
3.10. Mosquito positioning tool installed in the chamber	84
3.11. a) overview of the Position Controller, b) detail view of the PU13g-890 user interface for programming the distance and angle	85
3.12. 5-120 mm distances measured (30 mm, side view shown)	85
3.13. Angular reference frame used (30 mm, 0°, top view shown)	86
3.14. VN-11b Variable Aspirator	86
3.15. a) Detachable magnetic nozzle, b) nozzle removed with cartridge installed, c) VN-11b speed control dial and power button shown with screen to display fan power %	86
3.16. Performance curve for the VN-11b	87
3.17. Overall equipment setup, for both free-flight and tethered measurements	88
3.18. Mounting of a tethered mosquito	90
3.19. Detail view of tether position ( <i>Aedes aegypti</i> female shown)	90
3.20. Three stages to the airflow mosquito tethering method	91
3.21. Individual spectrograms for tethered <i>Ae. aegypti</i> at each measured distance. (5-120mm)	94

3.22. Example frequency spectra and amplitudes of tethered individual <i>Aedes aegypti</i> mosquito, with increasing microphone-mosquito distances. Automated peak finder script shows fundamental and harmonics and amplitudes identified	95
3.23. Summary of fundamental and harmonic amplitudes for tethered <i>Aedes aegypti</i> for 5-120 mm microphone-mosquito distances. <i>Top</i> (a) frequency amplitudes including spread, <i>bottom left</i> (b) means of frequency content, <i>bottom right</i> (c), summarised frequency content for all distances with mean amplitude line	96
3.24. Summary of fundamental frequency and harmonic amplitudes across all measured angles	98
3.25. Measured fundamental and harmonic directivity patterns for four female individuals	99
3.26. 800s measurement of tethered <i>Aedes aegypti</i> female	106
3.27. 10s frequency power spectra for <i>Aedes aegypti</i> female measurement (specimen represented in figure 3.35)	107
3.28. 500s spectrogram with tracked fundamental frequency and frequency amplitude profile for tethered <i>Ae. aegypti</i>	109
3.29. “Ramp” frequency and frequency amplitude profile	110
3.30. “Constant” frequency and frequency amplitude profile	110
3.31. “Flight manoeuvre” frequency and frequency amplitude profile	111
3.32. “Long constant flight” frequency and frequency amplitude profile	111
3.33. Tethered accelerometer mounting diagram	113
3.34. Tethered mosquito positioning relative to microphone mounting diagram	114
3.35. Example frequency data (1800s window) from accelerometer (left column) and microphone (right) for <i>Aedes aegypti</i>	115
3.36. Example frequency data (20s window) from accelerometer (left column) and microphone (right) for <i>Ae. aegypti</i>	116
3.37. [a-i] Example representations of tethered <i>Aedes aegypti</i> flight using sound pressure level (dB) and acceleration based approaches	118
3.38. [a,b] Example comparison of frequency and frequency amplitude by sound pressure level (dB) & acceleration (m/s <sup>2</sup> )	120

3.39. [a-f] Detailed time domain (linear) representation of tethered <i>Aedes aegypti</i> flight using sound pressure level and acceleration based approaches	123
3.40. Comparison of semi anechoic free flight, tethered flight, and reverberant free flight (Ø80) spectrograms	125
3.41. Frequency comparison for individual <i>Aedes aegypti</i> under tethered and free-flight (anechoic) conditions	126
3.42. Frequency amplitude comparison for individual <i>Aedes aegypti</i> under tethered and free-flight (anechoic) conditions	126
<b>4. Flight type and species comparison</b>	<b>130</b>
4.1. Fundamental frequencies by order for tethered and free flight measurements. Outliers represented by circle	140
4.2. Mean fundamental frequencies by order for the three flight type combinations	140
4.3. Fundamental frequency standard deviations by order for tethered and free flight measurements. Outliers represented by asterisks	141
4.4. Mean fundamental frequency standard deviations by order for the three flight type combinations	142
4.5. Mean free flight fundamental frequencies by species. Letters above the boxplots indicate which groups differ significantly from one another (One way ANOVA with Tukey post-hoc analyses $P < 0.05$ )	143
4.6. Mean free flight fundamental frequency standard deviation by species. Letters above the boxplots indicate which groups differ significantly from one another (One way ANOVA with Tukey post-hoc analyses $P < 0.05$ )	144
4.7. Labelled spectrograms and frequency spectra before, during and after copulation for <i>Culex quinquefasciatus</i>	147
4.8. Detailed 300s spectrogram before, during and after copulation for <i>Culex quinquefasciatus</i>	148
4.9. Detailed spectrogram during copulation for <i>Culex quinquefasciatus</i> (0.085s time resolution at 11.71 Hz frequency resolution)	149

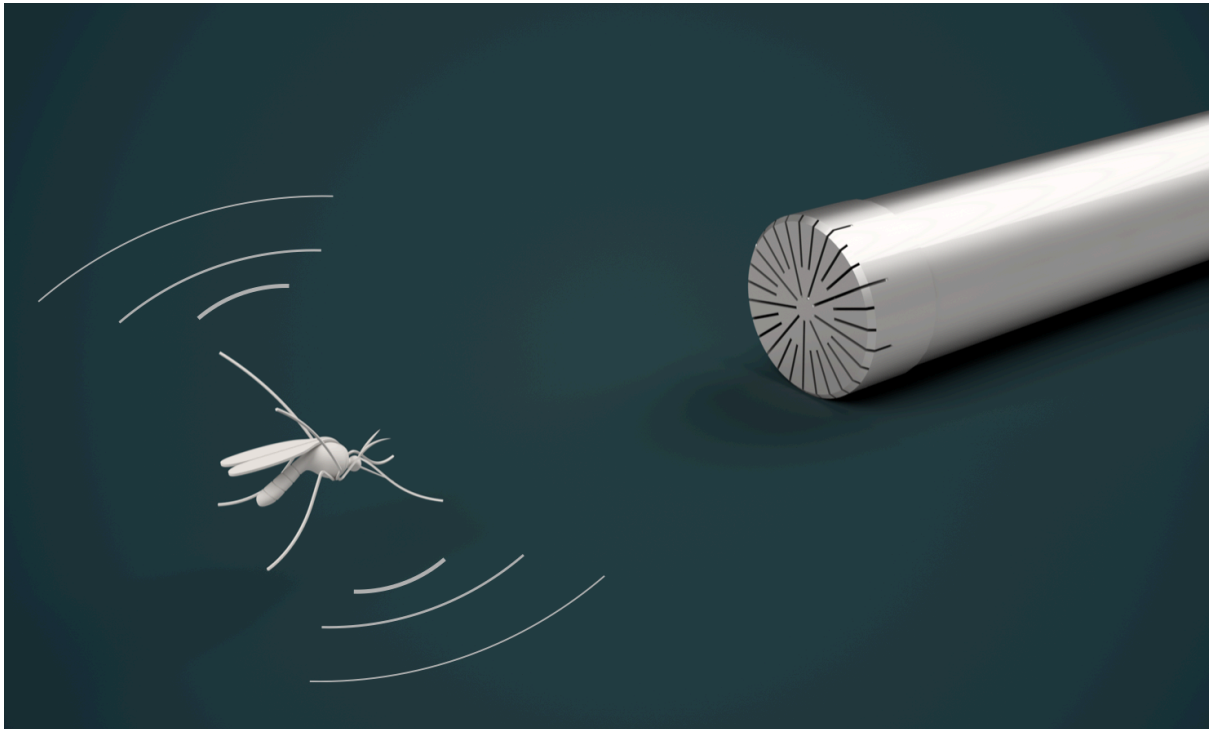
4.10. 0s - 900s spectrograms (labelled) before, during and after copulation for <i>Culex quinquefasciatus</i>	150
4.11. Spectrogram comparison of <i>Cx. quinquefasciatus</i> , <i>Ae aegypti</i> and <i>An gambiae</i>	155
<b>5. Physiological effects on mosquito acoustics</b>	<b>159</b>
5.1. Microphone wing-beat frequencies measured by age and species, box and whisker plots	168
5.2. Microphone wing-beat frequencies amplitudes measured by age and species, box and whisker plots. Letters above the boxplots indicate which groups differ significantly from one another (One way ANOVA with Tukey post-hoc analyses $P < 0.05$ ). Outliers represented by circles	170
5.3. Microphone wing-beat frequencies standard deviations, measured by age and species, box and whisker plots. Outliers represented by circles and asterisks	170
5.4. Microphone wing-beat frequencies measured by blood meals and species, box and whisker plots. Outliers represented by circles	172
5.5. Microphone wing-beat frequencies amplitudes measured by blood meals and species, box and whisker plots. Outliers represented by circles	172
5.6. <i>Cx. quinquefasciatus</i> (left) and <i>An. gambiae</i> (right) tethered	179
<b>6. General discussion</b>	<b>181</b>
6.1. Two <i>Cx. quinquefasciatus</i> tethered specimens featuring varying adhesive. sizes	190
6.2. From top to bottom, fundamental frequency spectrograms under semi- anechoic free flight for <i>Cx. quinquefasciatus</i> , <i>Ae. aegypti</i> and <i>An. gambiae</i>	194
6.3. From top to bottom, fundamental frequency amplitudes under semi- anechoic free flight for <i>Cx. quinquefasciatus</i> , <i>Ae. aegypti</i> and <i>An. gambiae</i>	195
6.4. Radar plot showing amplitude of fundamental and harmonics by angle relative to microphone from Chapter 3 (selected from figure 3.24)	197

## LIST OF TABLES

<b>1. Connecting acoustics, mosquito surveillance and vector control</b>	<b>1</b>
1.1. Examples of mosquito-borne diseases and estimates of local & global burdens	3
1.2. Reported wingbeat frequencies for a range of mosquitoes	18
1.3. Example applications of acoustic measurement and analysis	24
1.4. Frequency resolution and bin sizes at 44.1 kHz sampling rate	27
1.5. Frequency resolution and bin sizes at 16 kHz sampling rate	27
1.6. Frequency resolution and bin sizes at 8 kHz sampling rate	27
1.7. Frequency resolution and time resolution by bin size at 44.1 kHz sampling rate	28
1.8. Frequency resolution and time resolution by bin size at 16 kHz sampling rate	28
1.9. Frequency resolution and time resolution by bin size at 8 kHz sampling rate	28
<b>2. Flight type and species comparisons</b>	<b>36</b>
2.1. Averaged flight tone frequency data for <i>Aedes aegypti</i> with calculated ratios of measured harmonic frequencies relative to the observed fundamental	59
2.2. Averaged (LHS & RHS microphones) sum levels of ambient and flight tone throughput signal for <i>Aedes aegypti</i> in the four tunnels	59
2.3. Ø80 measured frequency & amplitude content for <i>Culex quinquefasciatus</i> , <i>Anopheles gambiae</i> & <i>Aedes aegypti</i>	66
2.4. Averaged (LHS & RHS microphones) sum levels of ambient and flight tone throughput signal for <i>Aedes aegypti</i> , <i>Anopheles gambiae</i> & <i>Culex quinquefasciatus</i> in the Ø80 tunnel	68

<b>3. Developing controlled measurement approaches</b>	<b>72</b>
3.1. Summary of frequency content across all distances measured	92
3.2. Summary of frequencies across all angles measured	97
3.3. Variation in described frequencies and frequency amplitudes by flight type	111
3.4. R <sup>2</sup> values for flight analysis lengths analysed using time-domain analysis (figure 3.35)	119
3.5. Mean fundamental frequency and amplitudes for tethered <i>Aedes aegypti</i> using accelerometer and microphone measurement data	120
3.6. Fundamental frequency content for anechoic free-flight and tethered flight for individual <i>Aedes aegypti</i>	126
<b>4. Frequency comparison for individual <i>Aedes aegypti</i> under tethered and free-flight (anechoic) conditions</b>	<b>130</b>
4.1. Acoustic metrics (and labels) used for analysis of tethered mosquito flight	137
<b>5. Physiological effects on mosquito acoustics</b>	<b>159</b>
5.1. Acoustic metrics (and labels) used for analysis of tethered mosquito flight	166
5.2. Overview of experiments and treatments investigating mosquito age and blood meal effects	166
5.3. Overview of microphone fundamental frequencies [M1] by age and species	169
5.4. Overview of microphone fundamental frequency amplitudes [M2] by age and species	169
5.5. Overview of microphone fundamental frequencies [M1] by blood meals	173
5.6. Overview of microphone fundamental frequencies [M1] by blood meals	173

# CHAPTER 1: CONNECTING ACOUSTICS, MOSQUITO SURVEILLANCE AND VECTOR CONTROL



Mosquito with a measurement microphone

## 1.1 Introduction

### 1.1.1 - OVERVIEW

The relationship between humans and mosquitoes is complex and has been the subject of study for many years. Belonging to the order Diptera, mosquitoes are found throughout the world with around 3600 species and 41 genera described (Rueda and Debboun, 2019). Within these, mosquitoes belonging to the genera of *Anopheles*, *Aedes* and *Culex*, act as vectors to humans and animals of many diseases (Dahmana and Mediannikov, 2020). Understanding their populations is

key to implementing effective control against them, however conventional entomological surveillance methods to do this are labour intensive and can be challenging to conduct. Vector borne diseases (VBDs) disproportionately affect communities residing in low and middle income countries from lower socioeconomic status, with the most affected regions covering countries within sub-Saharan Africa, South Asia, Central and South America (Golding et al., 2015; World Health Organization, 2020a). Climate change is also altering the habitats of mosquitoes, with vectors emerging in new areas, as well as those where they had previously been eradicated (Grobbelaar et al., 2016; World Health Organization, 2020a).

In the face of these challenges, enhanced surveillance methods that can simply provide large-scale datasets are needed (Franklinos et al., 2019). This project investigates the feasibility of using the acoustic wingbeat of mosquitoes for their identification, by exploring the underlying principles of how their sound profile during flight may be captured and analysed to perform classification.

### 1.1.2 - MOSQUITO BORNE DISEASE

Mosquitoes linked to disease transmission, pass on a variety of pathogens during their blood-feeding on humans. Most mosquitoes are anautogenous, requiring blood to produce their eggs (Harrison et al., 2021). This means that exclusively the female mosquitoes act as disease vectors. Diseases these pathogens cause include malaria, dengue, Zika, Chikungunya, lymphatic filariasis and West Nile fever (Dahmana and Mediannikov, 2020). Whilst there are differences between the specific transmission and development mechanisms within the pathogens that cause these diseases (Table 1.1), the common factor is that the mosquito acts as the vector during blood-feeding. Therefore, the concept of vector control, which controls the presence of mosquitoes is of high importance to effectively control the spread of these diseases.

Globally, an estimated 249 million cases of malaria occurred in 2022, which resulted with an estimated 608,000 deaths (World Health Organization, 2023). The number of deaths is stabilising over time, however there are new challenges facing the control of mosquitoes that must be addressed, such as insecticide resistance and changing mosquito habitats due to climate change (World Health Organization, 2023)

**Table 1.1** – Examples of mosquito-borne diseases and estimates of local & global burdens (World Health Organization, 2020b) . Data sources: a - (World Health Organization, 2023), b - (Kyu et al., 2018), c - (Roth et al., 2018), d - (Quan et al., 2020) , e-(PAHO, 2017), f-(ECDC, 2018), f-(Kimani et al., 2016), h. Institute of Health Metrics and Evaluation (IHME 2019a),

Disease	Reference	Year	Region	Disability adjusted life years (x1000) or cases	Deaths
malaria	a	2021	Global	-	608000
Dengue	b, c	2017	Global	2923	49779
Lymphatic filariasis	b, c	2017	Global	1364	NA
Japanese encephalitis	d	2015	Global	-	25125
Yellow fever	b, c	2017	Global	314	13761
Chikungunya	e	2017	Americas	61613 (suspected Nr cases)	101
West Nile fever	f	2018	Europe	2083 (reported autochthonous infections)	180
Zika virus disease	b, c	2017	Global	2.2	57

As shown by table 1.1, mosquito-borne diseases impose a significant health burden on a global scale, with the greatest burden being caused by malaria. As a result, significant efforts have been made to prevent and control the spread of these diseases, which can be grouped into the following categories of countermeasures (World Health Organization, 2020b):

- Vector control
- Personal protection
- Environmental and agricultural management
- Community education and mobilisation campaigns
- Mass drug or vaccine administration

These methods of controlling mosquitoes (the vector) are tailored to the specific disease, vector and community to reduce the spread of the disease by targeting different parts of the disease transmission chain.

To understand whether an intervention is effective, a system of surveillance is required. In simple terms, this is a process of understanding the current status of a disease in a population so that the risk of subsequent disease transmission can be assessed (Sivagnaname and Gunasekaran, 2012). The spread of VBDs can be described as a dynamic relationship between the vector, its pathogen, humans and the environment (World Health Organization, 2020a), which are in a continuous, dependant cycle (World Health Organization, 1975) as illustrated by figure 1.1. Therefore, to understand how a VBD could spread through a population, appropriate surveillance of the pathogen, vector and human host needs to be undertaken.

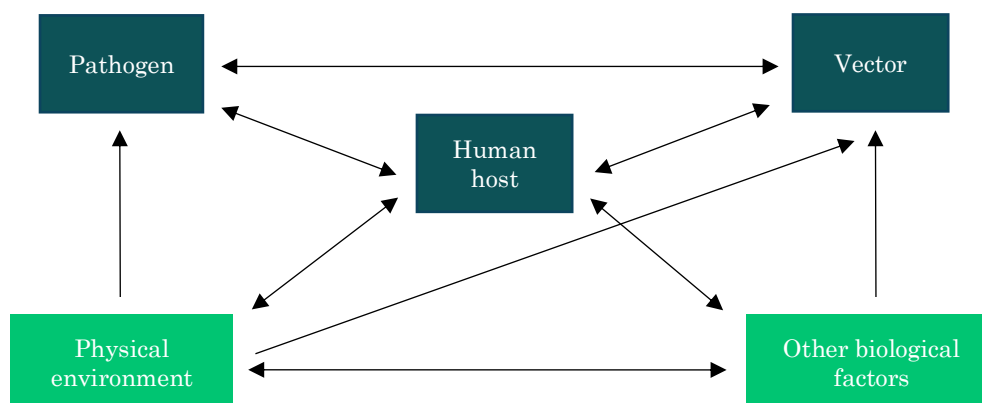


**Figure 1.1** – Vector-borne disease transmission ecological system (adapted from (World Health Organization, 1975b))

With the aim of reducing the impact of VBDs, either the pathogen, vector or human hosts must be monitored. In practice this is done with data collection, which fall into two categories: epidemiological and entomological data. Case data (epidemiological) uses confirmed cases of the VBD from health facilities, with methods such as microscopy, or rapid diagnostic tests used to confirm a case from a patient who presents with symptoms of the VBD. This method of data collection allows the human population and the pathogens in circulation to be understood and monitored.

Collection of entomological data can deepen understanding of transmission dynamics by describing the populations of vectors in an area under surveillance (Garjito et al., 2021). However, there are many different approaches to collecting entomological data, in terms of collection methods but also analysis approaches (Kouassi et al., 2023) and data outputs. By collecting entomological data, a detailed picture can be created to better describe the dynamics and potential for disease transmission. A greater understanding of the vector landscape in an area can allow for monitoring of insecticide resistance and pathogens (with further testing using xenomonitoring). However, depending on the methods used the work required and cost of acquiring this data can vary greatly.

### 1.1.3 - OVERVIEW OF VECTOR SURVEILLANCE

Vector surveillance is defined by the World Health Organization as “the collection of entomological data used to plan and assess anti-vector measures” (World Health Organization, 2020b) and it aims to understand vector populations in a way that supports strategic decision making (Kouassi et al., 2023). This activity could be undertaken in a number of different scenarios where vector control is required, such as for baseline vector population studies prior to the implementation of a control intervention, or for the ongoing monitoring of an interventions efficacy. Vector surveillance can also be used to track changes in mosquito populations following deployment of interventions, or for tracking changes in their efficacy due to increasing insecticide resistance.

Developing novel vector surveillance methods has also been described as an important point of action by the World Health Organization’s Global Vector Response 2017-2030 framework (figure 1.2), which highlights the need to “enhance vector surveillance and monitoring”.

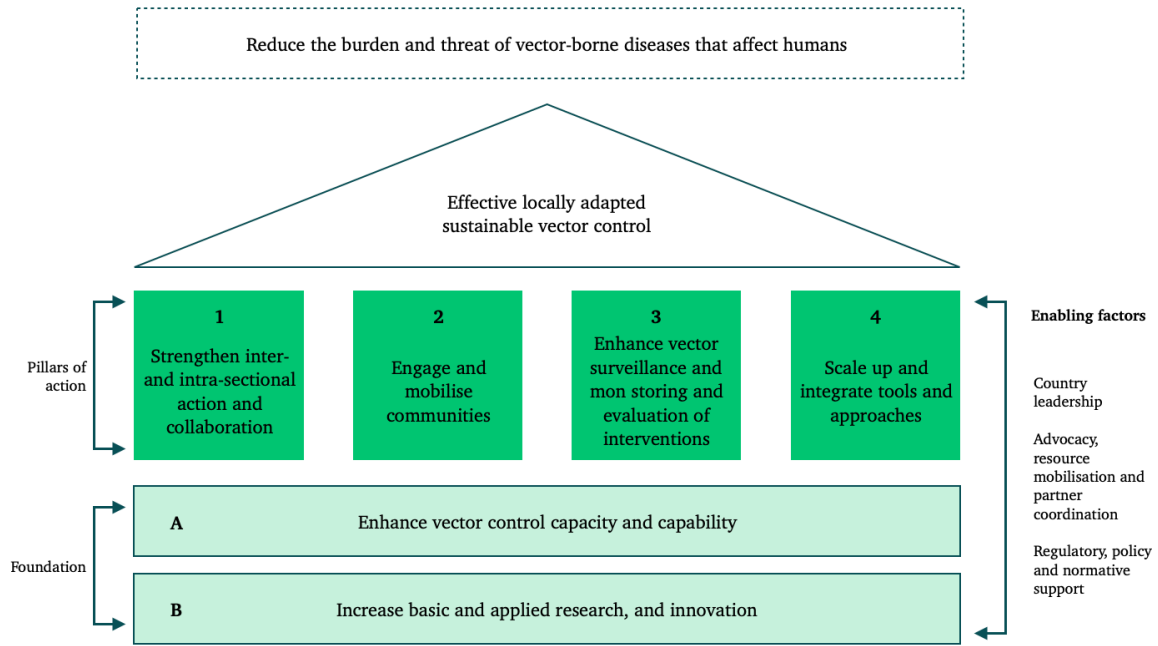


Figure 1.2 – WHO Global response framework (World Health Organization, 2017)

In general, different approaches to sampling mosquitoes are taken depending on their lifecycle stage and respective physiological state, but they follow the same general workflow as shown by figure 1.3. Mosquitoes have different lifecycle stages that they must progress through (eggs, larvae, pupae, adults) with certain stages preferred when conducting surveillance. Currently preferred methods for understanding the distribution of mosquito vectors include larval surveys, light traps and mechanical aspirators (Azil et al., 2011; Sikaala et al., 2013), which target the mosquitoes either when in water sources, or when as emerged adults.

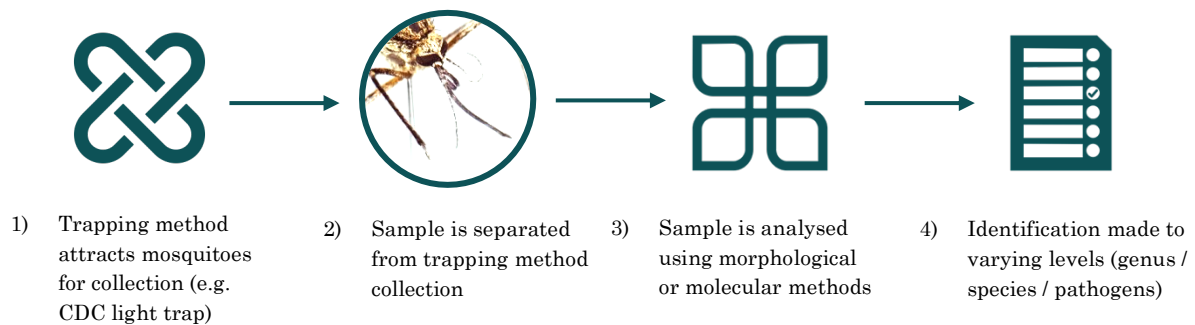


Figure 1.3 – Generalised process of mosquito identification

The data collected using these methods provides information about the vector and how they relate to its environment. However, the spread of methods used for vector

sampling can result with data of varying specificity and sensitivity (World Health Organization, 2009).

Sampling larvae in urban environments can be deemed as more practical than the sampling of adult mosquitoes (Li et al., 2014; World Health Organization, 2009), as the collection of specimens from artificial water sources in the urban environment can be simpler. Sampling and analysis of adults however can yield more information, especially should they have completed host-feeding and contain a blood meal. Analysis of the blood meal in the vector known as xenomonitoring (Cameron and Ramesh, 2021) can potentially reveal how pathogen loads are in circulation within a mosquito population in an area being studied.

Therefore, traps that target adult, female mosquitoes following blood-feeding would be the most suited for identifying potential pathogen loads. The responsiveness of mosquitoes to a trap is also highly dependant upon their behaviour and physiology, and a number of distinct trap designs have been developed to target these different stages and states (Tong Qiu et al., 2007). The most used of these traps, is the CDC light trap, which was developed by the US Center for Disease Control (figure 1.4).



**Figure 1.4** – CDC Light trap function description (Sarithchandra, 2015)

Here, the general principal of a light trap is illustrated. Mosquitoes respond to different stimuli depending on their physiological state, which can be split into the four categories of mechanical, thermal, chemical and visual stimuli (Gullan and Cranston, 2014). When conducting sampling of mosquitoes that are host seeking, a trap must replicate some or all the stimuli that are created by a host, from these four categories. The CDC light trap, with its simple design, is able to produce visual and odour stimuli, through its large black lid, and possibly odour lures (e.g. with the addition of CO<sub>2</sub> or artificial chemical blends). Once mosquitoes are near the area most attractive (where odour is released) a fan actively draws the mosquito into the trap where it is trapped in a collection cup.

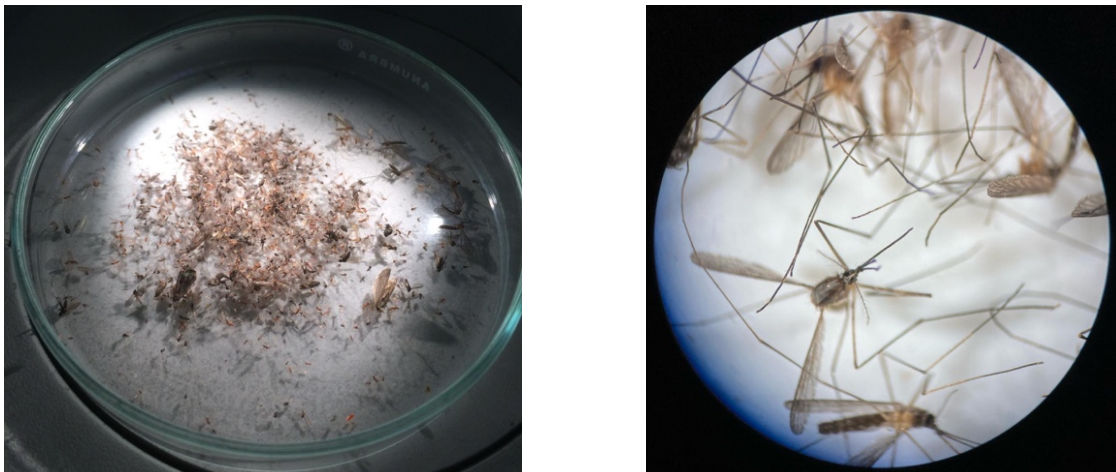


**Figure 1.5a** – *left* Unsorted catch from a CDC light trap , **1.5b** *right* Catch sorted manually on petri dish to identify morphological features on mosquitoes. Images courtesy of Dr J. Stokes

However, identifying what has been caught in the collection cup can be a slow, labour intensive and challenging process, that can also cause damage to the mosquitoes (Russell and Hunter, 2010). This collection cup can contain a mixture of other non-mosquito insects (figure 1.5a), which must first be separated out from the mosquitoes desired for identification (figure 1.5b). Depending upon the type of setup used, the collection cup stores the caught specimens either using an airflow (dry catch) or with a liquid (wet catch) (figure 1.6), which can further compound the difficulty of specimen sorting.

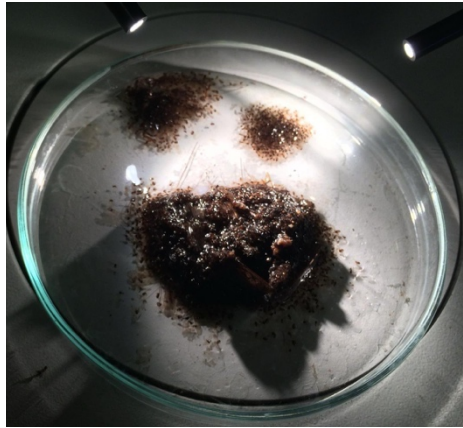


**Figure 1.6** –Example sorting of wet catch (sandflies) from a CDC light trap. Image courtesy of Dr J. Stokes

Once a trap catch has been successfully sorted, the mosquitoes must then be identified. There are two approaches to this, which are molecular and morphological (Walker, 2020). The wet catch approach is not well suited for morphological identification as this can damage identification features on the specimen. Expanded upon in in figure 1.7, molecular and microscopy methods are very different in their approaches, featuring different associated costs and feasibilities. Both methods allow for the identification of a mosquito specimen, but molecular methods, such as ELISA or qPCR can also be used to screen for pathogens. However, they both still require the initial sorting of the catch, which is labour intensive and requires high operator skill.

Molecular methods allow high throughput (Kothera et al., 2017), but this approach requires specialist operator training (Kittichai et al., 2023). Equipment required can also have high initial and running costs (e.g. PCR), and can require cold chain logistics for supplying buffers which is not always feasible in remote field environments.

Morphological methods of species identification on the other hand are well established and generally considered the gold standard incurring much lower material costs (Kittichai et al., 2023). However highly experienced and skilled personnel are needed for incriminating samples with high sensitivity using microscopy (Chan et al., 2014). Using this approach for high throughput can be challenging due to the expertise required to conduct morphological ID. It is also

worth noting, that if larval sampling is conducted with morphological identification, only the fourth instar can be feasibly identified using microscopy since identifying features are not fully developed in the earlier larval stages (Chan et al., 2014).

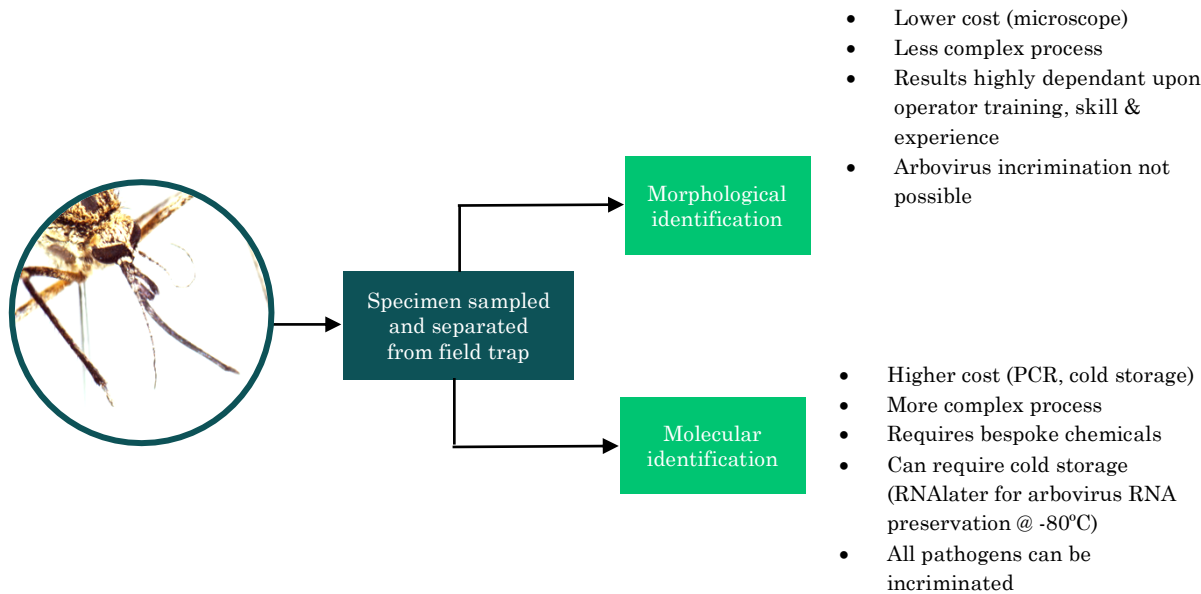


**Figure 1.7** – Mosquito identification approaches following sampling (Walker, 2020)

#### 1.1.4 - SIMPLIFYING THE IDENTIFICATION PROCESS THROUGH NEW APPROACHES

Innovative approaches are being explored to identify sampled mosquitoes, away from the traditional morphological and molecular methods. For example, a novel approach using light has been used to identify *Aedes aegypti*, *Culex quinquefasciatus* and *Anopheles gambiae* together with a machine learning using an approach known as Raman spectroscopy (Omucheni et al., 2023). This novel approach still required manual sampling and separation of mosquitoes, however the identification process presented is novel, and potentially well suited to a field application due to its comparably lower cost to a PCR approach. Automated vision approaches are also under development, with some able to distinguish unfed, blood fed, semi-gravid and gravid mosquitoes (Azam et al., 2023), or others focussing on gender identification (Kittichai et al., 2021). Wing morphology was also focussed on by Kittichai et al. (2023), whereby an image based machine learning workflow

was developed to process and identify mosquitoes from stereomicroscope and mobile phone sources.

Satellite imagery has also been evaluated in Nicaragua for dengue control, whereby these images were used to identify and monitor potential breeding sites, which were combined with epidemiological data (homes of identified dengue cases). This then allowed for identification of potential larval development sites to be targeted by control measures (Chang et al., 2009). More recently, instead of using satellite imagery, drones with deep learning image processing were evaluated for use in malaria control efforts in Côte d'Ivoire and Burkina Faso whereby vector breeding sites could be automatically identified (Trujillano et al., 2023) to implement targeted control.

The important role of entomological surveillance data in supporting control efforts has been demonstrated in the control efforts of numerous countries. For example, in Sri Lanka, this data formed part of epidemic forecasting and integrated vector management approaches for malaria control (Abeyasinghe et al., 2012; Beier et al., 2008). In the Americas, robust entomological surveillance has been demonstrated as a potential method to determine risks of West Nile virus (WNV) infections, with mosquito data being used to strongly predict variation in WNV cases (Kilpatrick and Pape, 2013). Being able to establish impending risk from entomological surveillance data, can also facilitate decisions of when to implement control measures (such as insecticide or larvicide deployment). Since these decisions may involve government officials, having data that can be readily understood by their electorate can greatly help achieve critical community support for implementing control measures proactively (Kilpatrick and Pape, 2013).

With the end aim of identifying mosquito populations in an area for vector control, the identification step is key to generating reliable data from sampled mosquitoes. It is how this step is performed, that determines the reliability of entomological data which is crucial for vector control planning and surveillance.

### 1.1.5 – METRICS USED IN VECTOR CONTROL EPIDEMIOLOGICAL MODELS

At this point, it is helpful to consider the way mosquitoes would become infected, and then infectious which is when they are most dangerous. As with many aspects of vector control, the complex cycle between pathogens, human hosts and the vectors (figure 1.1) is affected by a multitude of factors which is why effective vector control can be so challenging. From the perspective of an acoustic surveillance tool, it would therefore be helpful to consider what specific elements of mosquito physiology would be useful to describe, so they could be of value when exploring acoustic metrics for vector control activities.

Vectorial capacity is a mathematical approximation of the overall efficiency of vector-borne disease transmission. Also known as the ‘daily reproductive rate’, it describes the intensity of transmission by mosquitoes. This is the number of infectious bites that would eventually arise from all the mosquitoes that bite a human on a single day (Smith et al., 2014). It is affected by multiple elements of mosquito biology such as their survival, population densities, feeding preferences, as well as environmental conditions which affect these elements (Kramer and Ciota, 2015; Mitchell and Catteruccia, 2017).

Understanding vector competence through experiments is of great importance for supporting effective vector-borne disease outbreak responses, however undertaking the experiments is extremely complex and challenging (Wu et al., 2022). The classical model expressed by Equation 1 comes from the work of MacDonald and Garret-Jones, however some of the assumptions, whilst useful approximations, are inconsistent with the underlying mosquito biology (Novoseltsev et al., 2012; Smith and McKenzie, 2004). New challenges posed to the field of vector control, such as climate change induced dynamic temperature and rainfall patterns, have further necessitated efforts to re-examine the assumptions underpinning these classical models (Lambrechts et al., 2011; Novoseltsev et al., 2012; Paaijmans et al., 2010; Pascual et al., 2009).

$$C = \frac{ma^2p^nv}{-lnp} \quad (1.1)$$

Equation 1.1 shows how vectoral capacity is calculated (Garrett-Jones, 1964a; MacDonald, 1957; West et al., 2020).

### **Human biting rate – $ma$**

Representation of the incidence of biting-contact between mosquito and people in terms of bites per night. Indicates the average number of vector females liable to become infected per case per day (Garrett-Jones, 1964a)

### **Human biting habit – $a$**

Average number of humans bitten by one mosquito in one day (Garrett-Jones, 1964a; MacDonald, 1957).

### **Vector daily probability of survival – $p$**

Also denoted as daily survivorship, this represents the probability of vector survival through one day (Garrett-Jones, 1964b; West et al., 2020)

### **Vector competence – $v$**

Also described as vector efficiency (Hardy et al., 1983), this describes the ability of a mosquito to become infected following a pathogen uptake from an infected blood meal, and then successfully transmit the pathogen (Kramer and Ciota, 2015).

### **Extrinsic incubation period – $n$**

The time taken for completion of the extrinsic cycle of the pathogen (MacDonald, 1957; West et al., 2020).

For a mosquito to be able to transmit a pathogen, its extrinsic incubation period must be completed. Historically, this period was considered to be only affected by climatic conditions, but there is growing evidence to suggest it is also influenced by the vectors genetic diversity, diversity of the parasite and a range of abiotic and

biotic factors that affect the mosquito condition (Ohm et al., 2018). For malaria, dengue and Zika, this is typically between 9-14 days (Johnson et al., 2020a).

This background overview has been included to contextualise how entomological data is incorporated into vector control models used to predict epidemiological outcomes. The various factors used in their calculations require a deep understanding of the complex vector-host-pathogen interactions, of which some data is sourced from entomological measures.

From a surveillance perspective, it is here where the utility of acoustically derived measures will be explored, to assess how they could supplement existing methods for predicting epidemiological outcomes. Since this is the intended end application of acoustically derived measures, this perspective helps frame the project scope. The acoustics of mosquitoes will be explored to identify what metrics could be realistically extracted, that could have utility in supporting vector control.

## 1.2 Mosquito acoustics

### 1.2.1 - WHY DEVELOP OUR UNDERSTANDING OF MOSQUITO ACOUSTICS?

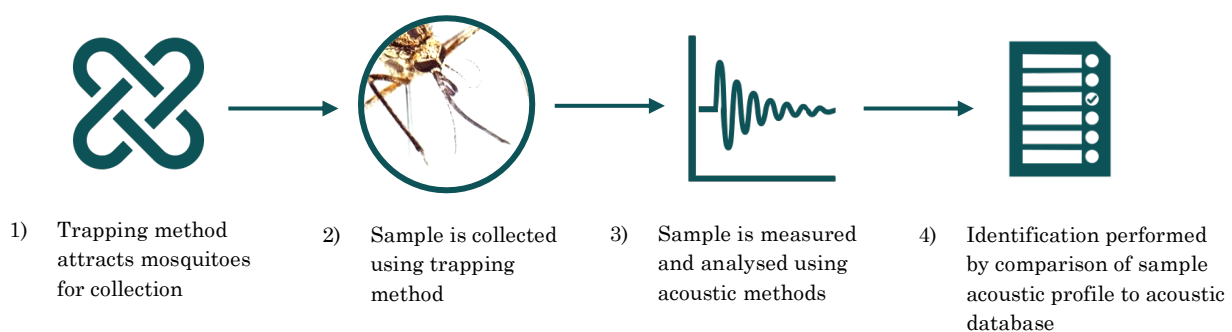


**Figure 1.8** – Generalised process of novel acoustic mosquito identification

Where the scope of this project lies, is with exploring the feasibility of performing the mosquito identification step using wingbeat acoustics of mosquitoes (figure 1.8). Unlike the aforementioned approaches, the mosquito will need to be alive,

such that it can still generate its signature wingbeat. This distinct sound created as mosquitoes flap their wings for flight, has been long studied and hypothesised as a viable method of identifying them. The earliest reported acoustic identification can be traced back to 1867 where Landois Hermann used his musically trained ear and a tuning fork to identify a variety of insect wingbeats, including *Culex pipiens* as a note d” (figure 1.9), which we would describe as 594 Hz today.

Einige Beispiele für die Höhe der Stimmen und Töne der Insecten.

The figure displays a musical score with two main parts: 'Stimme' (voice) and 'Flugton' (flight tone). Each part is represented by a treble clef staff with a key signature of one flat (Bb) and a 2/4 time signature. The 'Stimme' part shows various melodic lines for different insects, while the 'Flugton' part shows rhythmic patterns, some with notes and some with rests. The insects listed are: Musca vomitoria (Schmeissfliege.), Mesembrina meridiana, Musca domestica (Stubenfliege.), Syrphus ribesii, Eristalis tenax (Schlammfliege.), Haematopota pluvialis (Regenbreme.), Rhyngia rostrata, Culex annulatus ♀, Culex pipiens (Stechmücke.), and Apis mellifica (Honigbiene.).

**Figure 1.9** – “Einige Beispiele für die Höhe der Stimmen und Töne der Insecten – An example of the pitches of insect voices and tones” - mosquito and insect wingbeat classification using sheet music notation by Landois Hermann (Landois Hermann, 1867a)

Since the description of Hermann, a significant body of literature on mosquito acoustics has followed. The most used acoustic metric for flight remains the wingbeat frequency which is the fundamental frequency produced from flapping wings during their flight. However an implementation of acoustic metrics into a solution which reliably performs acoustic identification of mosquitoes, whilst remaining economically and culturally realistic is yet to receive widespread adoption.

Descriptions of mosquito acoustics have become more sophisticated since the 1867 acoustic assessments of Hermann. The range of modern methods to describe

mosquito flight is substantial (Spitzen and Takken, 2018), encompassing diverse approaches such as high-speed image tracking, tethered flight mills, and mobile phones to record mosquitoes flight acoustics (Li et al., 2017; Nayar, J.K.; Sauerman Jr., 1972; Vasconcelos et al., 2019). Their sound is generated from the regular, cyclical flapping of their wings which produces a sound that we perceive as a “tone” and the rate at which wings beat at, is known as the wingbeat frequency (Landois Hermann, 1867b; Sotavalta, 1952a, 1952b).

The literature is consistent on the expected differences between male and female mosquitoes within a species, with males demonstrating higher wingbeat frequencies than their respective females (Belton and Costello, 1979; Park et al., 2023; Pennetier et al., 2010a). The field of mosquito acoustics has been greatly expanded upon by studies exploring its role during mating, which have demonstrated its importance during this specific stage of the mosquito lifecycle (Lauren J Cator et al., 2009a; Pantoja-Sánchez et al., 2019a; Pennetier et al., 2010b).

It has also been hypothesised that the acoustic role in sexual selection has led to characteristic sound signatures that are unique to individual mosquito species (Mukundarajan et al., 2017a). Because of this, the concept of acoustic species identification has been explored with a variety of approaches. Mukundarajan et al (2017) used mobile-phone microphones to sample and process wingbeats for identification. Commercially available solutions are also being developed, with solutions for mosquito monitoring developed by Irideon S.L (Barcelona, ES) and Biogents AG (Regensburg, DE) (González-Pérez et al., 2024; Johnson et al., 2022). The Irideon S.L developed system demonstrated the ability to classify the *Aedes* and *Culex* genera with a 95.5% accuracy, whilst sex and genus classification was performed to an 88.8% accuracy (González-Pérez et al., 2024). This was achieved by combining a their unique device design with a machine learning method of automated classification.

The wingbeat frequency of mosquitoes has been sampled with a variety of different methods which do not exclusively use microphones as a sensor (Santos et al., 2019a). Acoustic methods employ microphones to record the flight tones of a mosquito by sampling sound pressure level or particle velocity. Particle velocity microphones measure the velocity and direction of particles in the direction of a sound wave (vector quantity), whilst pressure microphones measure changes in sound pressure at a fixed point (scalar quantity). Both approaches provide metrics to describe sound intensity, the power per unit area which when measured normal to the sound source, is the product of the sound waves pressure and particle velocity (Bennet-Clark, 1984; Brüel & Kjær, 1986). Optical methods use a light source and optical receiver to identify the wingbeat frequency by detecting interference patterns caused whilst the light beam is broken by flapping wings. This approach is used for both the Irideon and Biogents developed devices (González-Pérez et al., 2024; Johnson et al., 2022). Regardless of the sampling methods used, a subsequent data processing stage is carried out, using digital signal processing techniques. These convert the raw sampled throughput data signal, into a frequency spectrum. This is commonly conducted with a Fast Fourier Transform (FFT), however machine learning acoustic classification approaches have also been demonstrated to great effect (Batista et al., 2011a; Yin et al., 2023). Machine vision approaches have also been demonstrated using optically acquired data for other winged insect detection such as aphids Homoptera: Aphidae (Moore and Miller, 2002). A general drawback however with machine learning based approaches, is that they can require a substantial set of training data, which can be challenging to acquire.

As mentioned, notable acoustic-based studies include investigating how mobile devices can be used as acoustic sensors to conduct low-cost mosquito identification. The “HumBug” project has developed an impressive workflow to sample mosquitoes in the field using an audio capture app, which exploits machine learning to perform identification by processing on the mobile device (Kiskin et al., 2020; Mesaros et al., 2018). The preliminary success of this ongoing project serves as a good illustration of how acoustic vector identification could potentially

be realised with a citizen science approach. A separate group is also using mobile devices in a similar way, with promising results as well (Mukundarajan et al., 2017a). Beyond optical and acoustic sensors for sampling, there are further sensor methods which have been demonstrated, including the use of radar (Wang et al., 2017) or ultrasonics (Staunton et al., 2019a), which directed an ultrasonic transducer at mosquitoes in free-flight to capture wing-beat frequency through Doppler shift measurement of a reflected ultrasonic continuous wave signal.

**Table 1.2** – Reported wingbeat frequencies for a range of mosquitoes

Author	Temperature	Species	Sex	WBF
Landois, 1867	-	<i>Cx. pipiens</i>	?	594 Hz*
(Sotavalta, 1952b)	-	<i>Ae. aegypti</i>	F	480 Hz
(Moore et al., 1986)	22°C	<i>Ae. aegypti</i>	F	508 Hz
(Arthur et al., 2014)	23°C	<i>Ae. aegypti</i>	F	511 Hz
(Aldersley et al., 2014)	26 °C	<i>Ae. aegypti</i>	F	481 Hz
(Cator et al., 2011)	32.6°C	<i>Ae. aegypti</i>	F	664 Hz
(Batista et al., 2011b)	23°C	<i>Ae. aegypti</i>	F	645 Hz
(Batista et al., 2011b)	23°C	<i>Cx. quinquefasciatus</i>	F	528 Hz
(Staunton et al., 2019)	24°C	<i>Ae. aegypti</i>	F	515 Hz
(Staunton et al., 2019)	24°C	<i>Ae. aegypti</i>	M	740 Hz
(Staunton et al., 2019)	28°C	<i>Ae. aegypti</i>	F	562 Hz
(Staunton et al., 2019)	28°C	<i>Ae. aegypti</i>	M	786 Hz
(Staunton et al., 2019)	32°C	<i>Ae. aegypti</i>	F	580 Hz
(Staunton et al., 2019)	32°C	<i>Ae. aegypti</i>	M	878 Hz
(Bomphrey et al., 2017a)	26°C	<i>Cx. quinquefasciatus</i>	M	717 Hz
(Mujres et al., 2017)	28.5°C	<i>An. coluzii</i>	F	579 Hz
(Penetier et al., 2010b)	-	<i>An. gambiae s.s [M]</i>	M	704 Hz
(Penetier et al., 2010b)	-	<i>An. gambiae s.s [S]</i>	M	682 Hz
(Penetier et al., 2010b)	-	<i>An. gambiae s.s [M]</i>	F	467 Hz
(Penetier et al., 2010b)	-	<i>An. gambiae s.s [S]</i>	F	460 Hz
(Göpfert et al., 1999a)	22-23°C	<i>Ae. aegypti</i>	M	668 Hz
(Göpfert et al., 1999a)	22-23°C	<i>Ae. aegypti</i>	F	459 Hz
(Brogdon, 1994)	25°C	<i>Ae. aegypti</i>	M	715 Hz
(Brogdon, 1994)	25°C	<i>Ae. aegypti</i>	F	458 Hz
(Brogdon, 1994)	25°C	<i>An. albopictus</i>	M	724 Hz
(Brogdon, 1994)	25°C	<i>An. albopictus</i>	F	544 Hz
(Duhrkopf and Hartberg, 1992)	26°C	<i>Ae. aegypti</i>	F	350-550 Hz
(Villarreal et al., 2017a)	18-31°C	<i>Ae. aegypti</i>	F	300-600 Hz

Table 1.2 demonstrates the ranges of wingbeat frequencies that have been reported across mosquito genera. What is of interest, is that for the species that are measured across multiple independent studies (such as *Ae. aegypti*), there is a wide range in the wingbeat frequencies reported. This can be attributed to methodological and environmental differences between the approaches taken to

obtain these recordings, with temperature included as simple example. The physiology of the mosquito, its measurement method and subsequent acoustic analysis also did not follow one approach since it is not standardised, so understanding the impact of these differences for an application of acoustic mosquito detection is challenging.

### 1.2.2 - FACTORS AFFECTING THE WINGBEAT FREQUENCY

Throughout prior work, it has been hypothesised and demonstrated, that mosquito behaviour and wingbeat frequency are influenced by certain factors. Within a species these can be environmental or physiological such as ambient temperature, age or body size (Staunton et al., 2019a; Tripet et al., 2004). A summary of the main factors that have been demonstrated to impact wingbeat acoustics is included below.

#### *Species*

Understanding the acoustic differences between mosquito species which would be useful for identification would be extremely useful. This has therefore been the subject of numerous previous studies, with notable species comparisons being performed with mobile devices between 20 species including *Ae. aegypti*, *An. gambiae* and *Cx. quinquefasciatus* (Mukundarajan et al., 2017b). These three species are some of the most medically important mosquitoes, acting as the vectors for malaria, dengue and Zika, and West Nile Virus amongst others. In this study, it was observed that classification between species that exhibited overlapping wingbeat frequencies could be challenging, which has also been reported by other studies, such as the optical classification approach of T.-H. Ouyang et al. (2015).

### *Flight mode*

The wingbeat sound pressure level is highly directional, and from the flapping wing sound source, what is detected by a sensor (e.g. microphone) is a function of distance and angle (Arthur et al., 2014b; Seo et al., 2020). To ensure control and better repeatability between measurements, many studies opt to use a tethering approach to mosquito fixation. The mosquito is physically constrained using either a hair, entomological pin or wire, which is then glued to the mosquito scutellum (Attisano et al., 2015; Cator and Zanti, 2016; Vinauger and Riffell, 2023). This allows the mosquito to flap its wings, whilst being constrained such that it does not change its distance or angle relative to a measurement sensor. Whilst tethering allows for controlled measurements to take place, mosquitoes in the field are not physically constrained in this manner. So, from the perspective of understanding their flight tones for application into a surveillance device that would be field deployed, describing their acoustics whilst tethered may not be entirely representative without further investigation of the acoustic effect of tethering, compared to their more natural free flight.

There is not a clear consensus on the extent to which tethering affects the wingbeat frequency. Both increases and decreases in wingbeat frequency have been attributed to tethered mosquitoes when compared to those in free flight (Arthur et al., 2014c; Montoya et al., 2021; Staunton et al., 2019b). A comparison conducted by Villarreal (2017) found that whether or not a female was tethered had no significant effect on their flight tone, for *Ae. aegypti*. On the other hand, a novel wingbeat frequency characterisation method that used free flight was the chosen flight mode of Staunton (2019a). They stated tethering may cause lower wingbeat frequencies, and by excluding free flight, it may restrict detection of differences in frequencies between hovering or forward flight, and even increase the variance of wingbeat frequency distributions detected (Staunton et al., 2019a).

### *Size*

There are also conflicting accounts in the literature between the impact wing size has on wingbeat frequency. It was found that recordings taken with *Ae. aegypti* mosquitoes exhibiting wing lengths between 2.5-3.2 mm, demonstrated minor variation of female flight tones attributable to wing size in the study of Villarreal et al. (2017b). Conversely, Staunton et al. (2019b) concluded wingbeat frequency of differently sized females were significantly different when comparing wing lengths between 2.31-2.61 mm. Mosquito size descriptions are not only restricted to wing size however, with measured body mass also used as a metric when investigating the impact of environment during *Ae. aegypti* larval development (Walker et al., 2021). The effect of size on the wingbeat frequency of *An. gambiae* females was evaluated with those with larger wings (3.38 mm) exhibiting higher, (465.5 Hz) but not significantly different wingbeat frequencies than smaller (2.82 mm) mosquitoes (433.1 Hz).

### *Temperature*

It is well documented that temperature is a significant factor that can affect mosquito behaviour (Lahondère et al., 2023; Staunton et al., 2019a; Villarreal et al., 2017a). The effect of temperature on the wingbeat frequency has been described across numerous studies, starting with the work on dipterans (genus *Musca*) by Sotovalta (1952), through to more recent work on mosquitoes where the wingbeat frequency has been demonstrated to generally increase with rising ambient temperatures (Staunton et al., 2019a; Villarreal et al., 2017a), with increases in *Ae. aegypti* females reported between 6-13Hz / °C (Costello, 1974; Staunton et al., 2019b; Villarreal et al., 2017b). Accordingly, it is of importance to control this during wingbeat frequency investigations

## Age

The importance of understanding age from a vector control perspective has been introduced in section 1.1, and previous studies have explored how ageing of mosquitoes can impact their wingbeat frequency. However, the effect of age on mosquito acoustics is relatively understudied with few recent studies investigating this. Staunton et al. (2019b) reported increases in wingbeat frequency within female *Ae. aegypti* from their first week post emergence to third week (503 Hz to 531 Hz). In their study, three age categories post emergence were investigated (1 week, 2 weeks and 3 weeks post emergence).

A subsequent study of Park et al. (2023) aligned their age investigation of wingbeat frequency to these age categories, with a reported increase in wingbeat frequency between the youngest to oldest groups, although this was not found to be significant. However, a significant rise in wingbeat frequency was reported between their own age categories of freshly emerged (1-4 days post emergence) and non-blood fed (5-9 days post emergence) mosquitoes, which aligns with the description of Costello (1974), which reported an sharp increase in wingbeat frequency freshly post emergence. This effect, which was also observed in blowflies and cockroaches, was hypothesised to be due to an increase of cytochrome c titre in insect flight muscles (Farnworth, 1972; Levenbook and Williams, 1956; Park et al., 2023).

## Sex

There is broad consensus for most mosquito species of medical importance that males exhibit higher wingbeat frequencies than females (Clements, 1999; Warren et al., 2009a), with the substantial work around the acoustic patterns of mating behaviour, known as harmonic convergence (Lauren J. Cator et al., 2009) describing this difference between male and female wingbeat frequencies for *Ae. aegypti*, *Cx. quinquefasciatus* and *An. gambiae* (Cator et al., 2010; Lauren J. Cator et al., 2009; Warren et al., 2009a).

## *Pathogens*

Understanding whether a mosquito poses a danger by having a pathogen load, would be useful information to obtain acoustically however there are points to consider with this. One potential approach would be to explore whether pathogen loads cause a measurable change in the wingbeat frequency of a mosquito. There is already evidence that when a mosquito is infected with certain pathogens, it can experience altered flight behaviours. This has been quantitatively described by Somerville et al. (2019a), where it was shown that the flight distance, average flight speed, maximum flight speed and number of flight bursts were significantly affected (detrimentally) by a *Brugia malayi* infection in *Ae. aegypti*, which causes lymphatic filariasis (Somerville et al., 2019b). This study did not however assess impact on wingbeat frequency, but the effect of a *B. malayi* infection on the aforementioned flight characteristics warrants further exploration of this.

More recently a study into the impact of the filarial nematode *Dirofilaria immitis* (which causes canine heartworm disease) on *Ae. aegypti* wingbeat frequency has been undertaken (Park et al., 2020). This study used the same mobile-phone based acoustic setup as Mukundarajan et al. (2017b), and found that as L3 stage larvae increased within the mosquito, there was a significant reduction on wingbeat frequency. With the setup used, a significant difference between infected and non-infected mosquitoes could not be found however.

## 1.2.3 – OVERVIEW OF ACOUSTIC SAMPLING AND PROCESSING TECHNIQUES

**Table 1.3** – Example applications of acoustic measurement and analysis

Discipline	Domain	Example measurements	Measurement set-up	Analysis method	Quality assurance
Entomology	Academia	Mosquito wing-beat frequency characterisation	Bespoke prototype test chambers, wide variety of sensor types (sound pressure microphones, particle velocity microphones, mobile phones, optical sensors, ultrasonic sensors, laser vibrometers)	Custom scripts (e.g. MATLAB, Python), statistical analysis	Published peer-review
Marine biology	Academia	Interpretation of marine (e.g. whales, dolphins) acoustic communication	Industry-grade underwater measurement microphones	Custom scripts (MATLAB, Python), statistical analysis	Published peer-review
Food science	Academia / Industry	Objective quantification of subjective textures (e.g. biscuits)	Industry-grade microphones	Commercial analysis software	Subjective quality perception, Published peer review
Automotive engineering	Industry	Homologation acoustic pass-by noise tests, Noise Vibration & Harshness (NVH) development measurements	Anechoic chamber, field measurements, industry-grade measurement microphones, accelerometers & laser vibrometers	Commercial analysis software (e.g. PAK - Müller BBM, LMS – Siemens,)	ISO / EN / ASTM / DOT standards
Civil engineering, Architecture	Industry	Building acoustics	Room acoustics, industry-grade measurement microphones	Commercial analysis software	ISO / EN / ASTM standards
Creative arts	Industry	Musical instruments, film recording, vocals	Anechoic studio, studio-grade microphones	Creative analysis software (e.g. Logic Pro X, Audacity)	Subjective quality perception

Regardless of application, describing the acoustic profile of any sound source can be generalised into two stages: acquisition and processing. Techniques, equipment and methods for performing these two stages can be found across diverse applications. Examples include sound engineering in the music industry, end-of-line factory acoustic testing of machinery, automotive acoustic development and speech recognition in smart devices. The underlying fundamentals used across

these diverse applications are shared, but it is of interest to note differences between them to help identify elements that should be considered during the development of a method for describing mosquito acoustics (table 1.3).

### *Acquisition*

The first step is acquisition. Acquiring a sound source is commonly performed with sound pressure microphones, however newer sensor technologies such as pressure gradient microphones and particle velocity probes are used across applications. The exact mechanism these sensors work by, can vary. Several acoustic wingbeat frequency studies microphones follow the setup of Göpfert and Robert (2000), which used pressure gradient microphones, with a significant benefit being that they offer the ability to describe particle velocity with a relatively inexpensive sensor (Knowles NR-3158, NR-21358). Particle velocity can also be directly acquired with MEMS based probes, such as those offered by Microflow Technologies, which operate by acquiring particle velocity through measuring temperature differentials across heated platinum wire element (Microflow Technologies, 2024).

It is common practice in highly regulated industrial applications, to use calibrated condenser microphone sets for acquisition of sound sources, such as the GRAS 46AE (GRAS Sound & Vibration, 2024). These microphones are calibrated for frequency and amplitude response, and are specifically designed to deliver stable outputs across a range of temperatures and humidities. It is due to this traceable stability in acoustic performance they offer, that their use in legally binding acoustic measurements in different industries is permitted (e.g. automotive, aerospace).

Selecting a suitable sensor is a design decision that needs to consider the intended application. As this project is intended to capture and understand mosquito wingbeat acoustics, the accuracy and stability of the sensor is critical in ensuring that wingbeat acoustics are captured with accuracy and precision.

## *Processing*

Once a sensor is selected and exposed to the sound source, its output needs to be captured. For a conventional microphone, its analogue output needs to be sampled by an analogue to digital converter (ADC). ADCs available range widely in cost and functionality depending on their applications, with ultra small form factor units available for on-device processing such as the Texas Instruments ADS1013 es were tethered, with one spe(Texas Instruments, 2024), through to standalone calibrated data acquisition units for capturing sensors in industrial applications such as the Müller BBM MKII (Müller BBM VibroAkustik Systeme, 2024).

Once a signal is captured, its frequency content will need to be obtained which is undertaken by application of a Fast Fourier Transform (FFT). An important trade off occurs here, which affects the way that frequency descriptions are made, known as the Nyquist sampling theorem. This detail will directly affect the manner in which wingbeat frequencies can be described, and could also affect the approach taken to sample the wingbeat frequency.

The Nyquist Sampling Theorem depicts how the sensor signal (microphone) sampling rate and maximum frequency that can be represented are connected (Oshana, 2006) . It states that the sampling rate used must be at least twice the maximum frequency to be captured. In conventional acoustic applications, sampled audio must cover the human hearing range, so since the upper limit of human hearing is roughly 20 kHz, a sampling rate of at least 40 kHz must be used. This is why a standard CD is sampled at 44.1 kHz (Oshana, 2006).

In addition to ensuring an appropriate sampling rate, the frequency resolution required from the processed measurement must also be considered. The frequency resolution can be described as a “function of how many parts the maximum signal can be divided into” (National Instruments, 2019). When using an FFT, a parameter known as a bin / window / block size must be chosen. This value will divide the sampled signal into a number of equally spaced parts, or bins, and the

measurement signal amplitude will be calculated at each frequency bin. An example of this relationship is given below:

Sample rate: 44.1 kHz, Bin size: 32

$$\text{Frequency resolution} = \frac{\text{Sample rate}}{\text{Bin size}} = \frac{44100}{32} = 1378.1 \text{ Hz} \quad (1.2)$$

**Table 1.4** - Frequency resolution and bin sizes at 44.1 kHz sampling rate

Bin size	Frequency resolution (Hz)
8	5512.50
16	2756.25
32	1378.13
64	689.06
128	344.53
256	172.27
512	86.13
1024	43.07
2048	21.53
4096	10.77
8192	5.38
16384	2.69
32768	1.35

**Table 1.5** - Frequency resolution and bin sizes at 16 kHz sampling rate

Bin size	Frequency resolution (Hz)
8	2000.00
16	1000.00
32	500.00
64	250.00
128	125.00
256	62.50
512	31.25
1024	15.63
2048	7.81
4096	3.91
8192	1.95
16384	0.98
32768	0.49

**Table 1.6** - Frequency resolution and bin sizes at 8 kHz sampling rate

Bin size	Frequency resolution (Hz)
8	1000.00
16	500.00
32	250.00
64	125.00
128	62.50
256	31.25
512	15.63
1024	7.81
2048	3.91
4096	1.95
8192	0.98
16384	0.49
32768	0.24

Equation 1.2 shows the specific relationship between the bin size chosen and the resultant frequency resolution. This can be expanded to further available bin sizes, which must be powers of 2 to function. Tables 1.4, 1.5 and 1.6 expand this relationship for 44.1 kHz, 16 kHz and 8 kHz sampling rates.

Sample rate: 44.1 kHz, Bin size: 32

$$\text{Time resolution} = \frac{\text{Bin size}}{\text{Sampling rate}}$$

$$\frac{32}{44100} = 0.0007 \text{ secs} \quad (1.3)$$

**Table 1.7** - Frequency resolution and time resolution by bin size at 44.1 kHz sampling rate

Bin size	Frequency resolution (Hz)	Time resolution (s)
8	5512.50	0.0002
16	2756.25	0.0004
32	1378.13	0.0007
64	689.06	0.0015
128	344.53	0.0029
256	172.27	0.0058
512	86.13	0.0116
1024	43.07	0.0232
2048	21.53	0.0464
4096	10.77	0.0929
8192	5.38	0.1858
16384	2.69	0.3715
32768	1.35	0.7430

**Table 1.8** - Frequency resolution and time resolution by bin size at 16 kHz sampling rate

Bin size	Frequency resolution (Hz)	Time resolution (s)
8	1000.00	0.001
16	500.00	0.002
32	250.00	0.004
64	125.00	0.008
128	62.50	0.016
256	31.25	0.032
512	15.63	0.064
1024	7.81	0.128
2048	3.91	0.256
4096	1.95	0.512
8192	0.98	1.024
16384	0.49	2.048
32768	0.24	4.096

**Table 1.9** - Frequency resolution and time resolution by bin size at 8 kHz sampling rate

Bin size	Frequency resolution (Hz)	Time resolution (s)
8	2000.00	0.0005
16	1000.00	0.001
32	500.00	0.002
64	250.00	0.004
128	125.00	0.008
256	62.50	0.016
512	31.25	0.032
1024	15.63	0.064
2048	7.81	0.128
4096	3.91	0.256
8192	1.95	0.512
16384	0.98	1.024
32768	0.49	2.048

The bin size has a clear impact on the frequency resolution, however the sampling rate is also a significant factor that must be considered when sampling signals with the intention of conducting FFT analysis. Unfortunately, whilst it is tempting to conclude that a higher bin size allows for higher frequency resolution, the time resolution must now be considered (equation 1.3). Time resolution indicates how many samples are required to calculate half the sampling frequency of a signal, known as the Nyquist frequency. The number of samples taken per second is the sampling rate. The time resolution, is simply the number of samples required, divided by the sampling rate. This is the final relationship to describe, as the bin size is equal to the number of samples required (equation 1.3). Therefore, the above tables can be updated to reflect how the time resolution is affected by bin size and sampling rate.

What tables 1.7, 1.8 and 1.9 can show us is that increasing the frequency resolution comes at the expense of sampling time, whereby longer measurements are required to be able to obtain a finer frequency resolution.

This simple mathematical exercise also demonstrates that lower sampling rates allow the calculation of finer frequency resolutions at smaller bin sizes, although the time resolution remains comparable (e.g tables 1.8 and 1.9). What is important to consider, is that measurements that require longer time resolutions must use samples that are stable events. Therefore, appropriate selection of sampling rate and bin size must be done whilst considering the length of a wingbeat measurement and the nature of how stable it is, during the period to be analysed.

#### 1.2.4 - CONNECTING ACOUSTIC MEASURES TO VECTOR CONTROL

Being able to acquire vector data (e.g. species, age, sex) that is accurate whilst also operationally feasible (cheaper, low labour requirements) is crucial to improving understanding of disease transmission likelihood.

### *Flight acoustics acquisition*

The process of capturing mosquito acoustics in the literature varies as previously discussed, with a wide range of sensors, processing techniques and devices developed to capture the wingbeat frequency of mosquitoes. However, the setups created for laboratory studies are not necessarily translatable to a device ready for field operation. Compounded by the mixture of approaches taken in the literature that use both mosquitoes which are tethered or able to fly freely, it would be useful to explore a range of flight capture designs that use tethered and free flight to evaluate both approaches. This would allow a better understanding of an optimised design for capturing acoustics in a field setting, as well as a lab environment. Approaches should be considered that offer a good trade-off between imposed Nyquist sampling limitations (frequency and time resolution), physical geometries and mosquito flight behaviours.

### *Species*

The approach taken when implementing vector control measures is highly species specific, due to the different behaviours between mosquito species. The majority of malaria control is based on deployment of indoor residual spraying and insecticide treated bednets, which are effective against the primary malaria vectors *An. gambiae* and *An. funestus*. These mosquitoes bite primarily at night, and indoors (Sougoufara et al., 2014). On the other hand, the primary vector of Zika virus and dengue, *Ae. aegypti*, is diurnal, expressing biting behaviour in the early morning and afternoon (Rund et al., 2020). This means deploying bednets, which are effective against the night active malaria vectors, would be less effective against day biting *Ae. aegypti*. In areas that experience mixed populations of mosquitoes which can exhibit both biting behaviours, understanding the species composition of mosquitoes would be critical to implementing appropriate, targeted control.

## *Age*

The range of control interventions available is diverse (Johnson et al., 2020a). This includes the release of *Wolbachia* infected mosquitoes that block virus transmission or sterilise vectors (Hoffmann et al., 2014; Zheng et al., 2019), gene drives (Hammond et al., 2016), insecticide treated nets (Protopopoff et al., 2018), larviciding (Seixas et al., 2019), indoor residual spraying (Vazquez-Prokopec et al., 2017) and the mass deployment of lethal ovitraps (Johnson et al., 2017). What is common between these diverse control approaches, is that they all reduce mosquito survival, thus greatly impacting transmission potential as they reduce the possibility of extrinsic incubation period completion (Garrett-Jones, 1964a; Johnson et al., 2020a). Improving our understanding of mosquito population ages, would allow comparison against the expected extrinsic incubation period for their respective pathogens. This in turn could be used to determine whether mosquito ages measured (either before, after or during an intervention) would have reached an infectious stage to understand the risk of pathogen transmission. Therefore, it would be useful to explore the feasibility of describing mosquito age, through acoustic measurement.

## *Blood meals*

Ultimately, it is of importance to understand whether a mosquito carries a pathogen and has also completed its extrinsic incubation period, to quantify risk of onward transmission. Typically, this is performed with molecular analysis of their blood-meals (Reeves and Burkett-Cadena, 2023). Before investigating this pathogen load effect, the simpler influence of a blood meal on the wingbeat frequency would be extremely useful to understand, and more feasible to investigate.

## 1.3 Project aims and objectives

### 1.3.1 – PROJECT SCOPE

The essence of the work undertaken in this thesis, is to further our understanding of how mosquito acoustics could be used specifically to conduct vector surveillance. This understanding could then support the development of a future device that performs automated vector surveillance.

This project is approached from two perspectives. The first, is to explore how flight acoustics can be captured simply, in a way that is reflective of designs that would be realistically feasible to create in the field. The second, is to identify when under tightly controlled conditions, how mosquito acoustics could generate descriptions of use within the field of vector control. The second approach removes the design constraints imposed by a field application, and allows focus to shift to capturing with accuracy and precision the mosquito acoustics under a range of physiological conditions.

The project scope was also uniquely affected due to its timing, from Autumn 2019 – Spring 2024. The substantial disruption due to the COVID-19 pandemic resulted with the project scope being expanded such that in addition to the two distinct approaches mentioned, a third aspect of operational autonomy was developed. Development of a range of new supplementary devices and methods was incorporated into the project scope, which allowed the acoustic investigations to continue across multiple locations despite the period of uncertainty from the pandemic.

### 1.3.2 – AIMS AND OBJECTIVES

#### **Thesis Aims**

The aim of this project is to investigate mosquito wingbeat acoustics from the perspective of integration into a future vector surveillance application. This will quantitatively evaluate aspects that impact the acquisition, analysis and outcomes of mosquito acoustic descriptions across entomology, engineering, and signal processing.

#### **Thesis Objectives**

The objectives of this project are:

1. To design a simple free flight methodology to capture mosquito wingbeats.  
**(Chapter 2)**

A range of simple measurement arenas will be designed using basic geometries that would be realistically feasible to implement into a field device. A methodology to capture and process wingbeat acoustics of *Ae. aegypti* female mosquitoes whilst under free flight will be developed

2. To conduct an initial free flight comparison between *Ae. aegypti*, *Cx. quinquefasciatus* and *An. gambiae* using a simple measurement arena.  
**(Chapter 2)**

Using the most suitable methods and arenas of objective 1, an initial species comparison will be conducted to assess the suitability of the method for describing differences in measured wingbeat acoustics.

3. To design a semi-anechoic arena, for capturing wingbeat acoustics under tethered conditions. **(Chapter 3)**

Develop a semi-anechoic measurement arena that permits controlled, tethered measurements of mosquito wingbeat acoustics whilst adjusting mosquito distance and angle relative to measurement microphone. A preliminary assessment to describe the effect of distance and angle on measured wingbeat acoustics will be conducted.

4. To establish an acoustic processing workflow under semi-anechoic conditions to generate metrics of mosquito wingbeat acoustics. **(Chapter 3)**

Using the semi-anechoic setup developed in Chapter 3, a method of processing sampled mosquito wingbeats will be established using preliminary *Ae. aegypti* measurements, with the aim of sampling with repeatability.

5. To design bespoke methods of mosquito handling, to allow contact free mosquito handling in the lab **(Chapters 2, 3)**

A suite of devices will be developed to allow mosquitoes to be handled efficiently in the lab. Damage to mosquitoes is to be minimised through airflow design of handling equipment, and automated mosquito entry to measurement chambers is to be incorporated into arena design, to reduce exposure and influence of breath volatiles. Novel approaches to tethering that require no ice, gases or chemicals are to be established.

6. To evaluate a novel approach to capturing tethered mosquito wingbeats using vibration (**Chapter 3, 5**)

A preliminary comparison of microphone and accelerometer derived wingbeat patterns will be conducted for tethered *Ae. aegypti*. This will be expanded upon for *Ae. aegypti*, *An. gambiae* and *Cx. quinquefasciatus* in Chapter 5. The null hypothesis to be evaluated is that wingbeat frequency derived from an accelerometer and microphone are not different.

7. To compare wingbeat acoustics under free flight and tethered semi-anechoic conditions (**Chapter 4**)

A repeated measures comparison is to be undertaken, describing the effect of tethering and free flight capture approaches of wingbeat acoustics for *Ae. aegypti*, using the methods and devices developed in Chapter 3

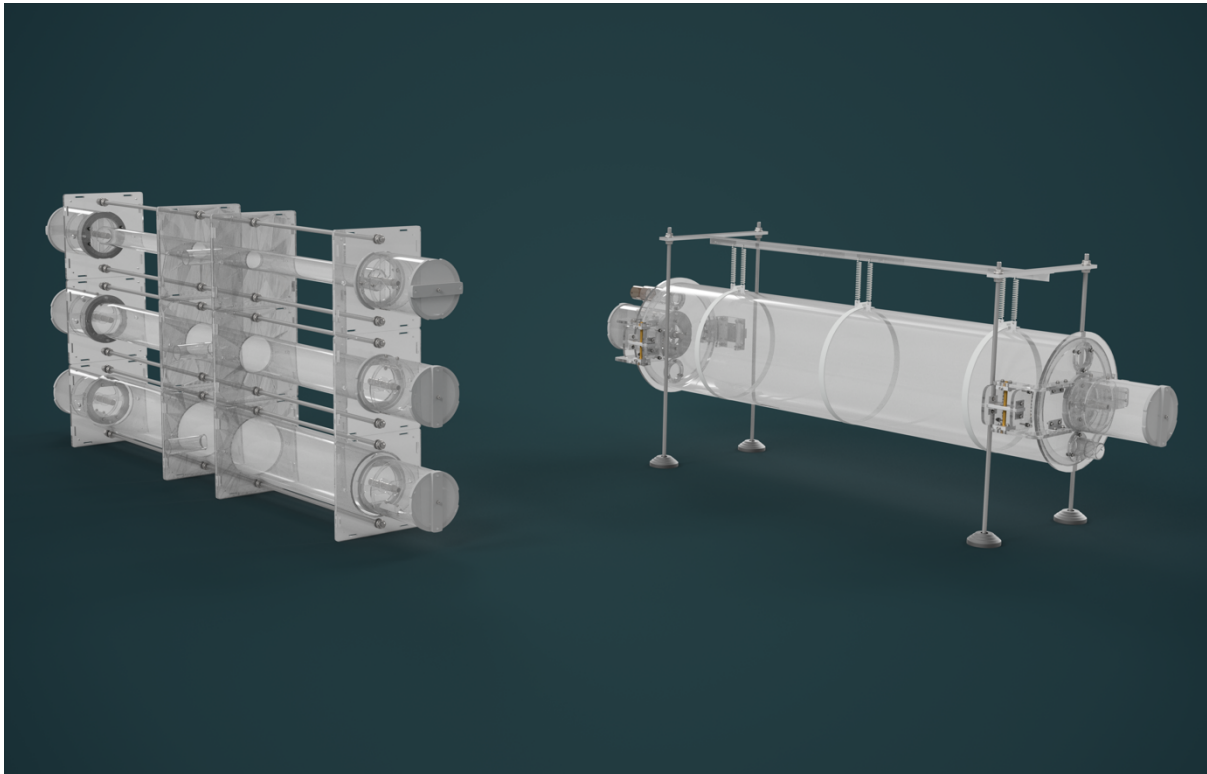
8. To compare the free flight wingbeat acoustics between *Ae. aegypti*, *Cx. quinquefasciatus* and *An. gambiae*. (**Chapter 4**)

Using the free flight method developed in Chapter 3, a comparison will be made between the acoustic profiles of the three species

9. To independently compare the effects of age and blood meals on the tethered acoustics of *Ae. aegypti*, *Cx. quinquefasciatus* and *An. gambiae* (**Chapter 5**)

Using the tethered method defined in Chapter 3, the effects on wingbeat acoustics of age, and blood meals will be compared for the three mosquito species. Comparison between species will be done exclusively in the free flight investigation of Chapter 4

# CHAPTER 2: DESCRIBING MOSQUITO FREE-FLIGHT ACOUSTICS WITH SIMPLE ARENAS



Measurement tunnels evaluated

## 2.1 COVID impact statement

The direction of this chapter was greatly affected by the COVID lockdowns between March 2020 to June 2021. Basic mosquito flight behaviour and their associated acoustics were to be described and understood, however the unpredictable lockdowns imposed in this period by the government of the United Kingdom, created a substantial challenge to preparing this investigation. Mosquito colonies to be used at the insectaries of LSHTM were lost, laboratory

access was unpredictable and critical materials including acrylic and microchips suffered acute shortages.

It was initially envisioned to prepare a bespoke acoustic insectary, which would combine the required temperature, light and humidity requirements needed for the mosquitoes of medical importance, with low background noise such that uninterrupted acoustic measurements could be performed. From March 2020, it became clear that the proposed acoustic rework of an insectary would not be feasible, as access to this space was highly unpredictable for the following years. As a result, a radical design change was taken to ensure that all measurement arenas to be used throughout this project were portable. This would allow for mosquito measurements to continue across multiple locations, should COVID lockdowns be imposed at short notice. The result was that between 2020-2023, data acquisition of mosquito acoustics could continue across three separate test labs.

Therefore, the measurement arenas and methodologies outlined in this chapter were not optimised for perfect acoustic conditions, however they illustrate the compromise that was made to start describing mosquito acoustics in environments whilst under severe resource restrictions.

## 2.2 Introduction

### 2.2.1 – THE APPLICATION OF MOSQUITO ACOUSTICS FOR SURVEILLANCE

As covered in Chapter 1, prior studies investigating mosquito acoustics can be distinguished by their applications and technological approaches (Santos et al., 2019b). Considerable focus has been paid to understanding the role of acoustics on the interactions between sexes, as well as their auditory perception mechanisms. Accordingly, these investigations required controlled spaces to take acoustic measurements of mosquitoes, known as flight arenas. A variety of spaces have been developed, using a wide range of sensors however there is no *standardised* acoustic flight arena, and as such most studies either use previously developed apparatus, or develop their own bespoke arenas to suit a specific focus of the investigation. A common design requirement when performing acoustic measurements, is that the effects of background noise need to be mitigated, to ensure recorded flight tones are as noise-free as possible. These spaces are either designed for free-flight or tethered measurements, and depending on the nature of the study either a single mosquito is recorded, or multiple mosquitoes can be recorded concurrently.

However, in the context of the current application, the primary focus was to assess the feasibility of using wingbeats as a method of identification in a *simple* device. A simple field device would need to be low-cost and robust but compromising the design by not using sound attenuation materials could result in the quality of any acoustic signal to be corrupted by background noise. Nevertheless, it would be of great utility to validate whether the wing-beat frequency of a mosquito in free flight could be captured within a compromised, simple measurement arena that could be feasibly deployed in a field setting.

A simple arena should feature a form and design that does not necessitate complex manufacturing processes, and its materials should be easy to obtain. Moreover, its

design simplicity would be improved by reduction of assembly complexity, so use of multiple materials or components should be minimised. This would greatly facilitate the translation of a design concept into a real device. Arenas developed for laboratory wingbeat characterisation in the literature have understandably not incorporated design *translatability* into their designs. This design constraint is only necessary should field surveillance be set as a desired outcome, which is not always the case. However, by the inclusion of this constraint into the design specification of the initial flight arenas, it would greatly simplify the next steps of arena translation into a field surveillance device.

When considering the basic form available for an arena, a tunnel would be one of the simplest forms to choose. Mosquito behavioural assays that examine flight behaviour or odour responses routinely use this form as a flight space, since tubes are simple to construct (Castillo et al., 2023) and readily available. However an understanding of the influence tube size has on mosquito flight and their acoustics has not been explicitly described. A solid acrylic tube would act as a reverberant sound field, which could make identifying the wingbeat challenging (Brüel & Kjær, 1984). Without sound attenuation measures, there would also be uncontrolled background noise. However, the simplicity of design would mean that translating such a design into a field device would be much more straightforward than implementing a design that required more extensive features to create an anechoic, or semi-anechoic arena.

### 2.2.2 – AIMS AND OBJECTIVES

Here, I focus on wing-beat characterisation using simple arenas. The devices and methods that have been developed used readily available materials and assessed the viability of describing mosquito acoustics with severely limited resources. This unique perspective could prove to be useful in guiding the development of a future, simple field surveillance device.

## Chapter Aim

This chapter aims to explore how acoustic measurements of freely flying mosquitoes can be achieved using simple measurement arenas that are constructed with methods, materials & analysis approaches realistically transferrable to the field. The effect of the arenas' geometry on the flight tones produced by a mosquito in free flight will be assessed.

## Chapter Objectives

1. Design, construct & evaluate multiple simple arenas for measuring mosquito flight acoustic recordings.
2. Develop a data acquisition and processing workflow to analyse mosquito flight recordings.
3. Develop a system of sampling and transporting mosquitoes for field and lab use during COVID restrictions
4. Conduct an initial comparison of the flight arenas using *Aedes aegypti* in free flight to assess the relative suitability of four tunnels.
5. Evaluate an optimised tunnel geometry with *Ae. aegypti*, *Anopheles gambiae* and *Culex quinquefasciatus*.

## **2.3 Materials and methods 1 – acoustic measurement using acrylic tunnels**

### 2.3.1 – OVERVIEW

A series of hardware builds were undertaken, to design and produce flight arenas based around a tunnel concept. An acoustic measurement and analysis methodology was then developed, which were evaluated with *Ae. aegypti* females.

### 2.3.2 – MOSQUITO REARING AND HANDLING

*Ae. aegypti* females were reared from eggs originating from the stock colonies maintained at the London School of Hygiene & Tropical Medicine. Eggs were floated in distilled water and fed on a fish flake diet (TetraMin fish-flakes, Tetra, VA, USA). Pupae were transferred to emergence cages (BugDorm), where each cage was labelled by the emergence date of the pupae. A 12:12 light/dark cycle was used and insectaries were maintained at 29°C, with a humidity of 60% at all times. Acoustic tests were conducted in the same insectary, under the same climatic conditions. Adults were not blood fed prior to testing and were provided with 10% sucrose solution ad libitum, which was delivered via a soaked cotton wool ball placed on top of the rearing cage.

### 2.3.3 – MEASUREMENT ARENAS AND SAMPLING EQUIPMENT DEVELOPMENT

Four arenas were constructed based on cylinders with diameters of 40, 76, 120 and 230 mm. The range of measurement arenas designed and constructed are listed, alongside support equipment that was developed to streamline mosquito handling in field and laboratory environments. Complete engineering drawings for flight arenas are included in the appendix.

1) Ø230 x 1000MM FLIGHT TUNNEL

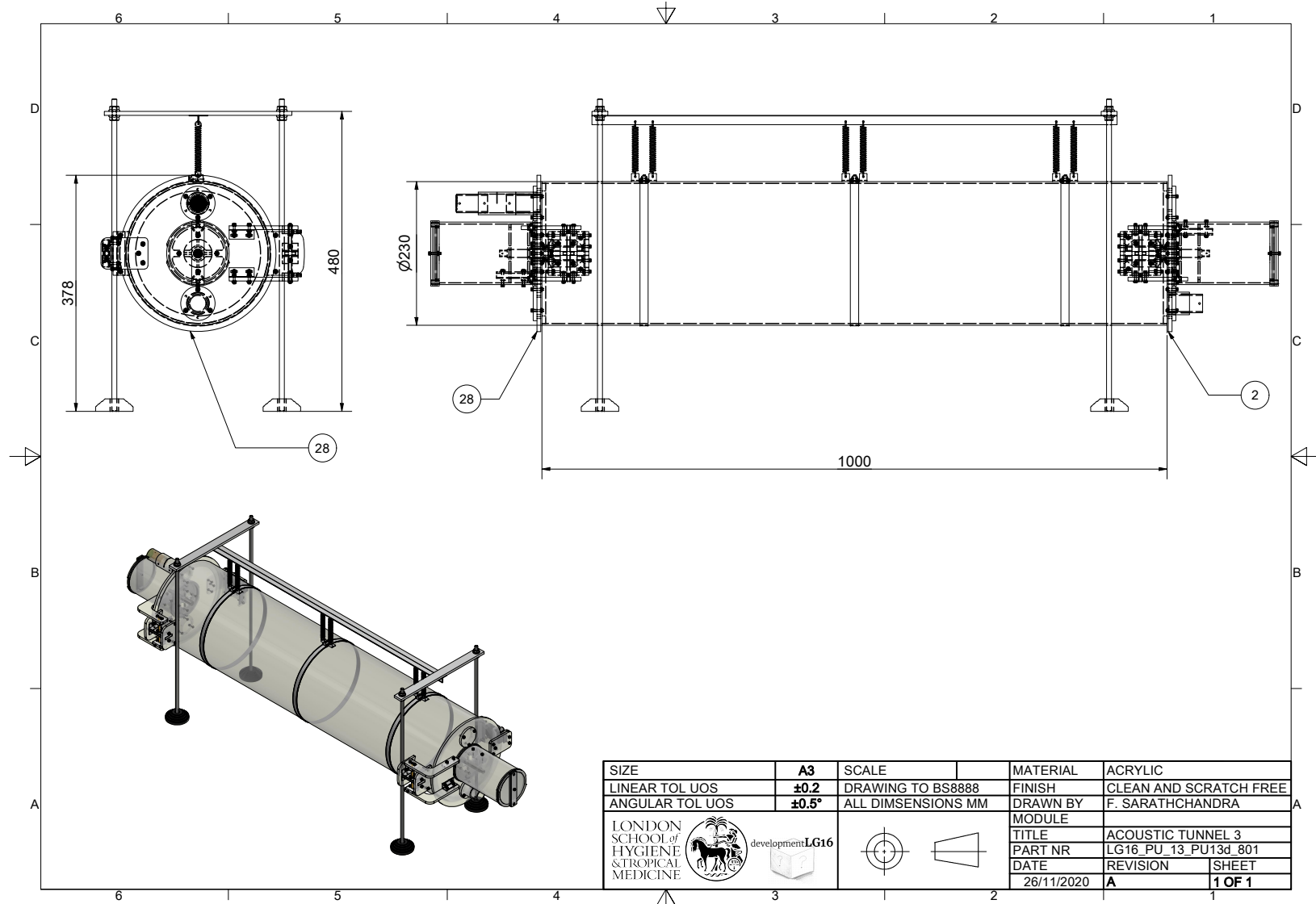


Figure 2.1 – Ø230 x 1000 flight tunnel, suspended on vibration isolation springs

### 2) Ø40 x 1000MM FLIGHT TUNNEL GENERAL ASSEMBLY DRAWING

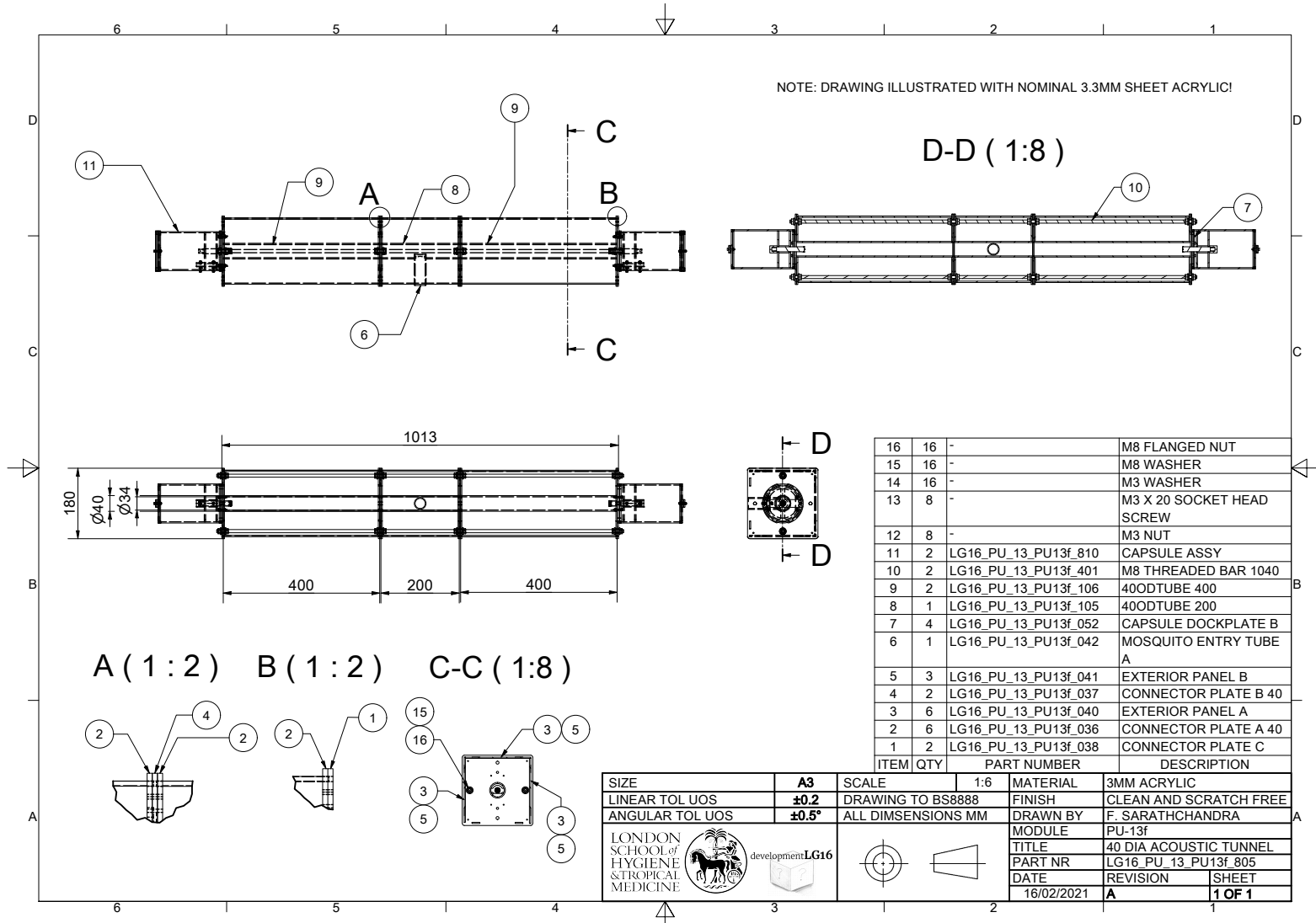


Figure 2.2– Ø40 x 1000 flight tunnel

### 3) Ø76 x 1000MM FLIGHT TUNNEL GENERAL ASSEMBLY DRAWING

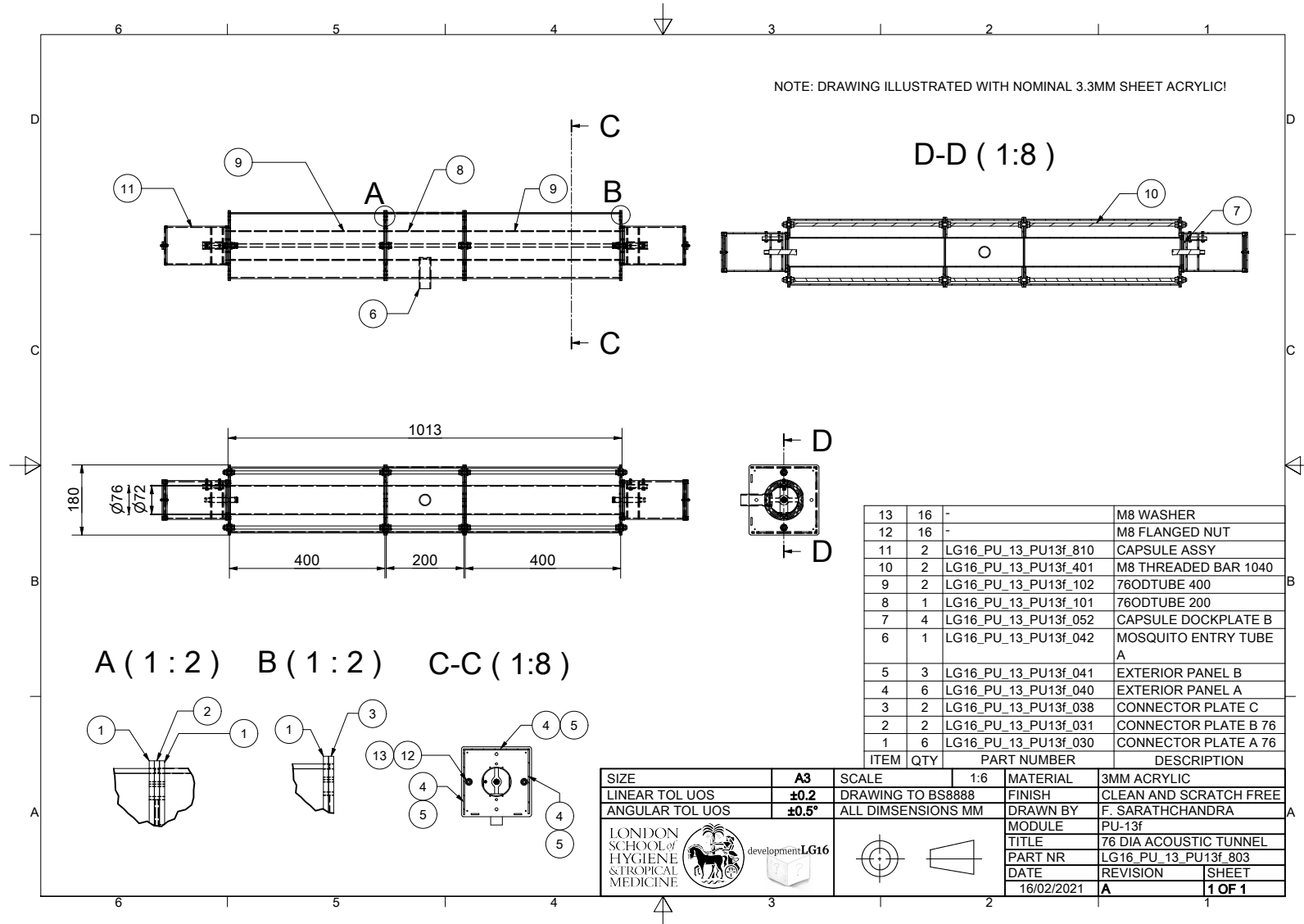


Figure 2.3– Ø76 x 1000 flight tunnel

### 4) Ø120 x 1000MM FLIGHT TUNNEL GENERAL ASSEMBLY DRAWING

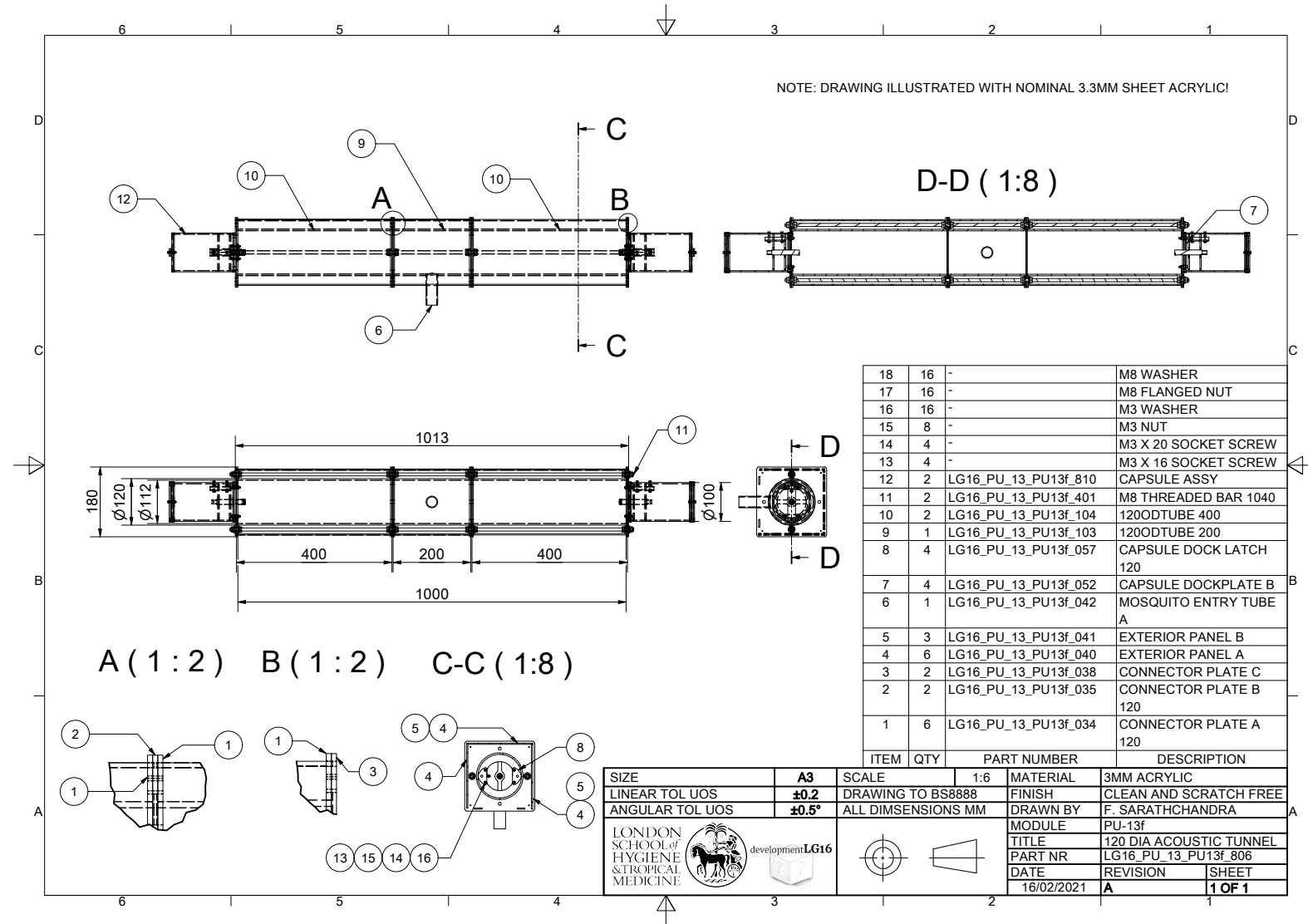


Figure 2.4 – Ø120 x 1000 flight tunnel

### 5) END CAPSULE ASSEMBLY DRAWING

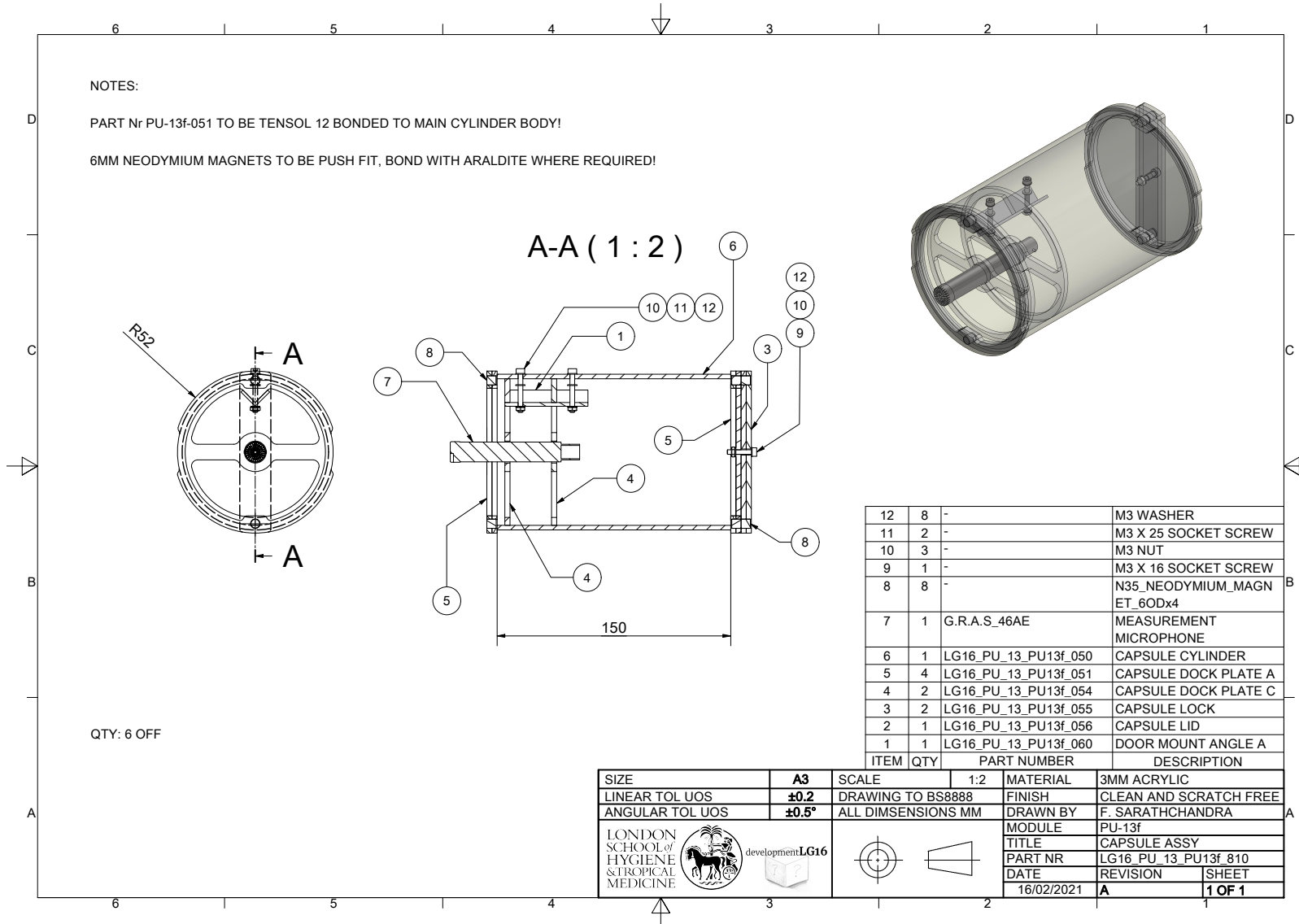
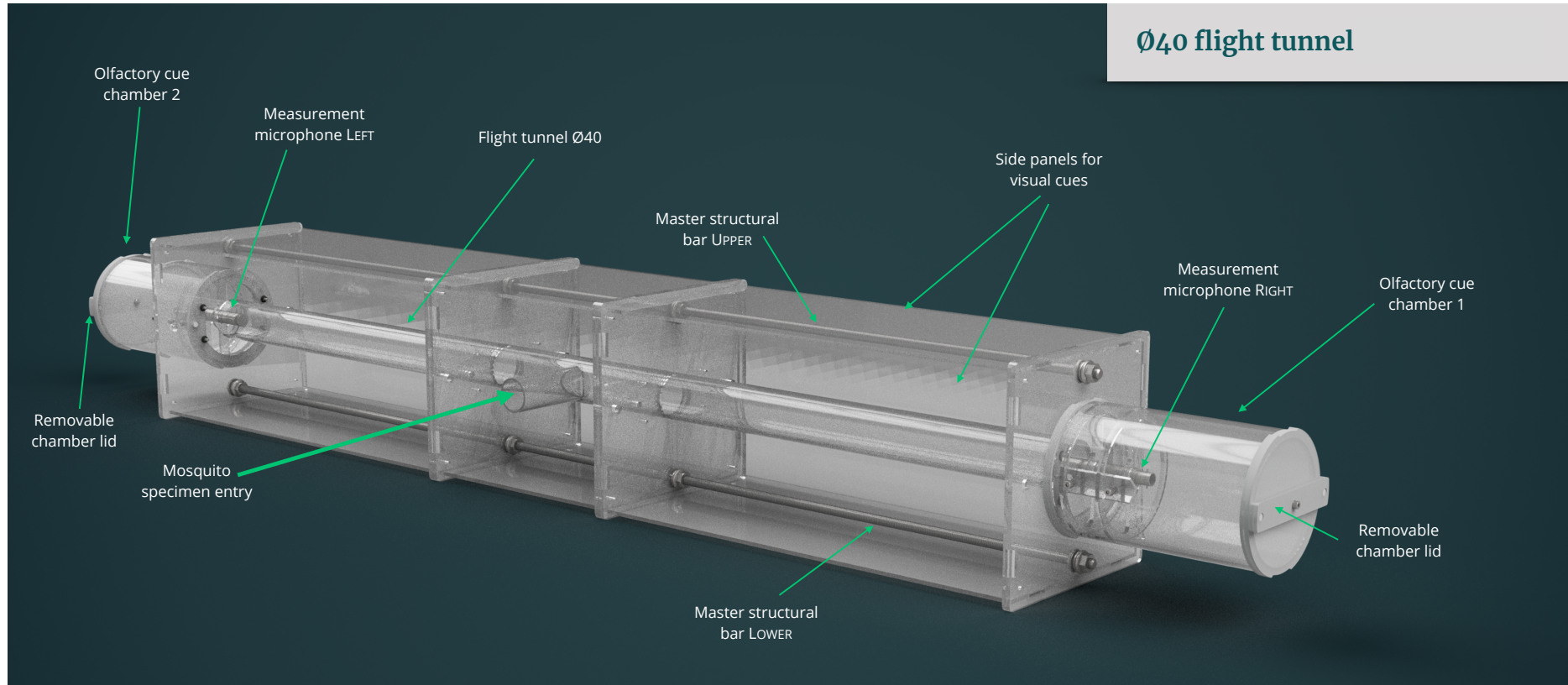


Figure 2.5 – End capsule assembly drawing

## 6) TUNNEL VISUALISATIONS



**Figure 2.6** – Ø40 tunnel visualisation

The Ø40, Ø76 and Ø120 tunnels were designed to be flatpack, for quick assembly & disassembly. All three tunnels have been designed modularly, and all follow parametric design principles. Mosquitoes are loaded centrally, where they can then fly along the length of the 1000 mm tunnel, with or without an odour cue. At each end of the tunnel are the magnetic measurement end capsules. The complete assembly is held together by the two master structural bar elements as illustrated on Figure 2.6

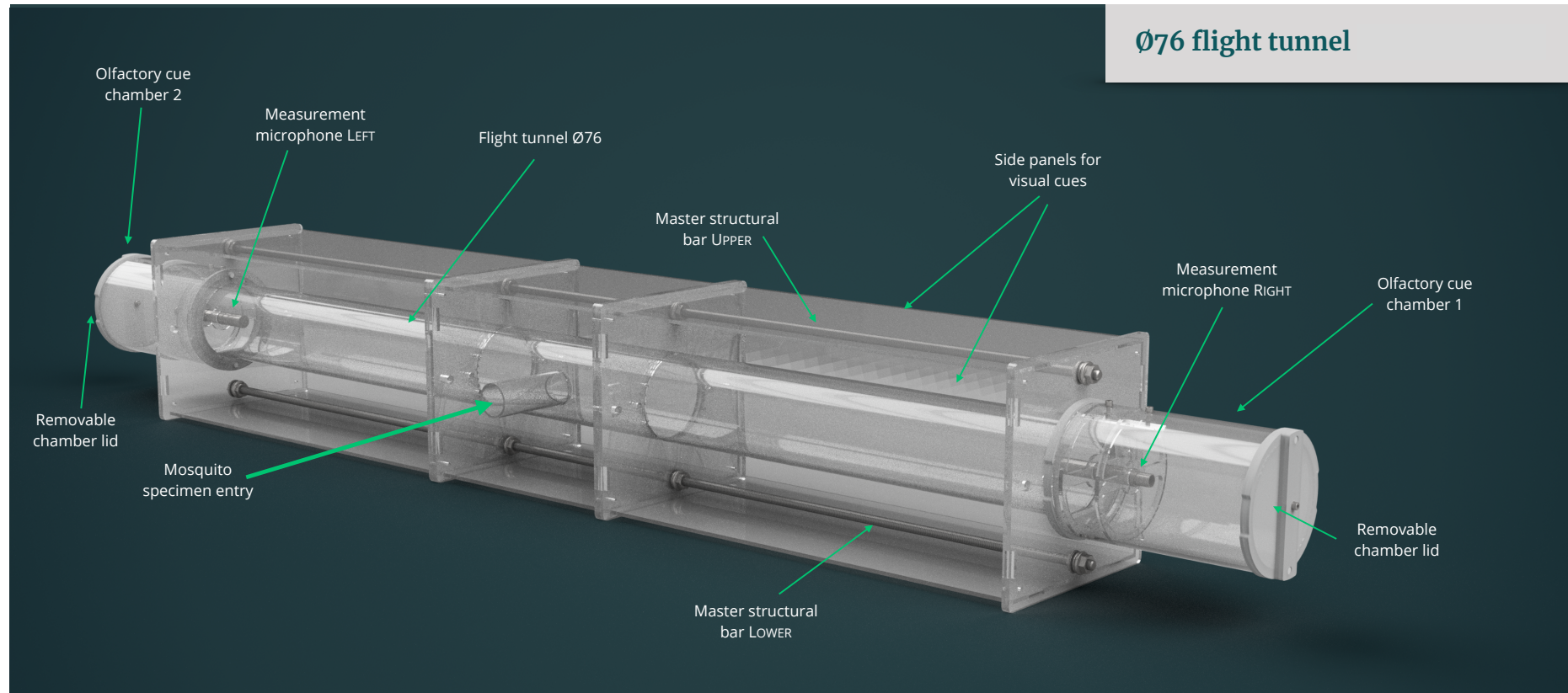


**Figure 2.7** – Ø76 tunnel visualisation

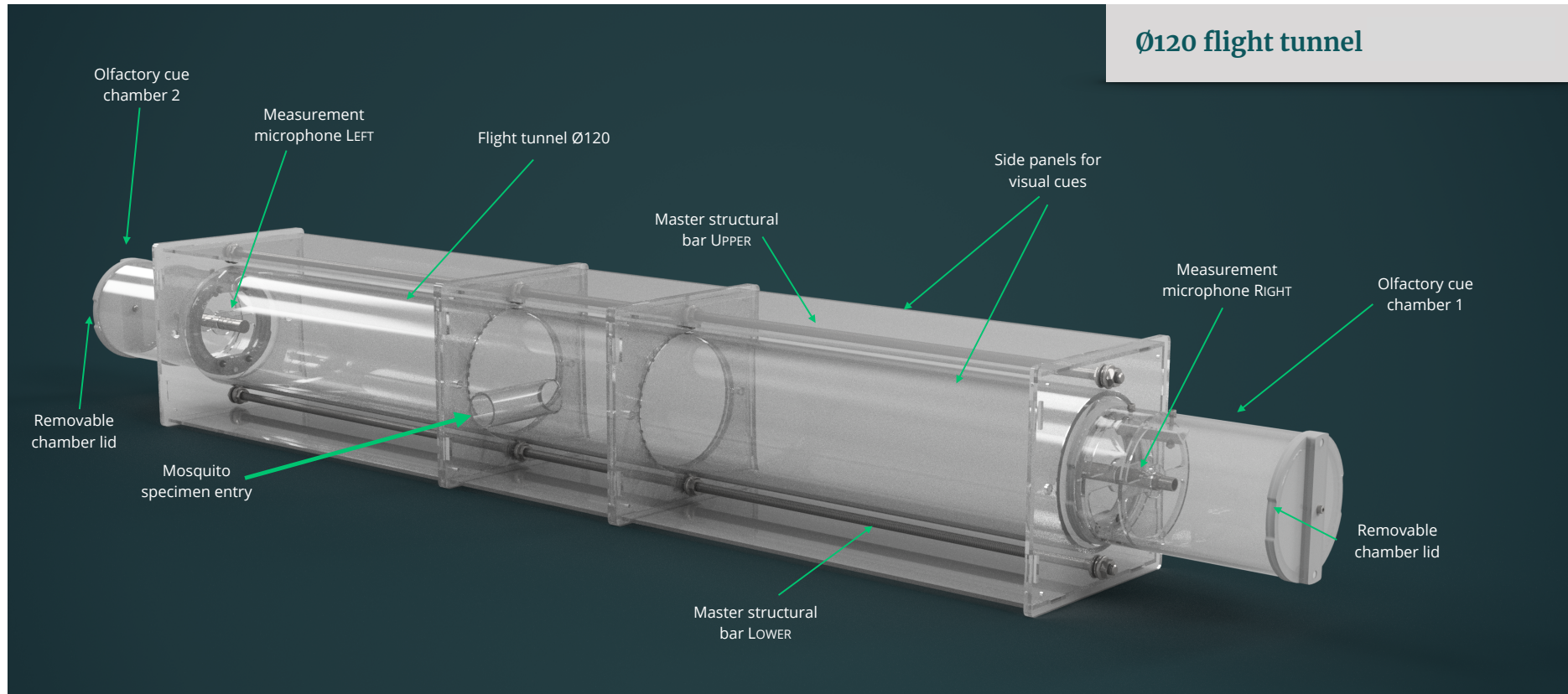


**Figure 2.8–** Ø120 tunnel visualisation

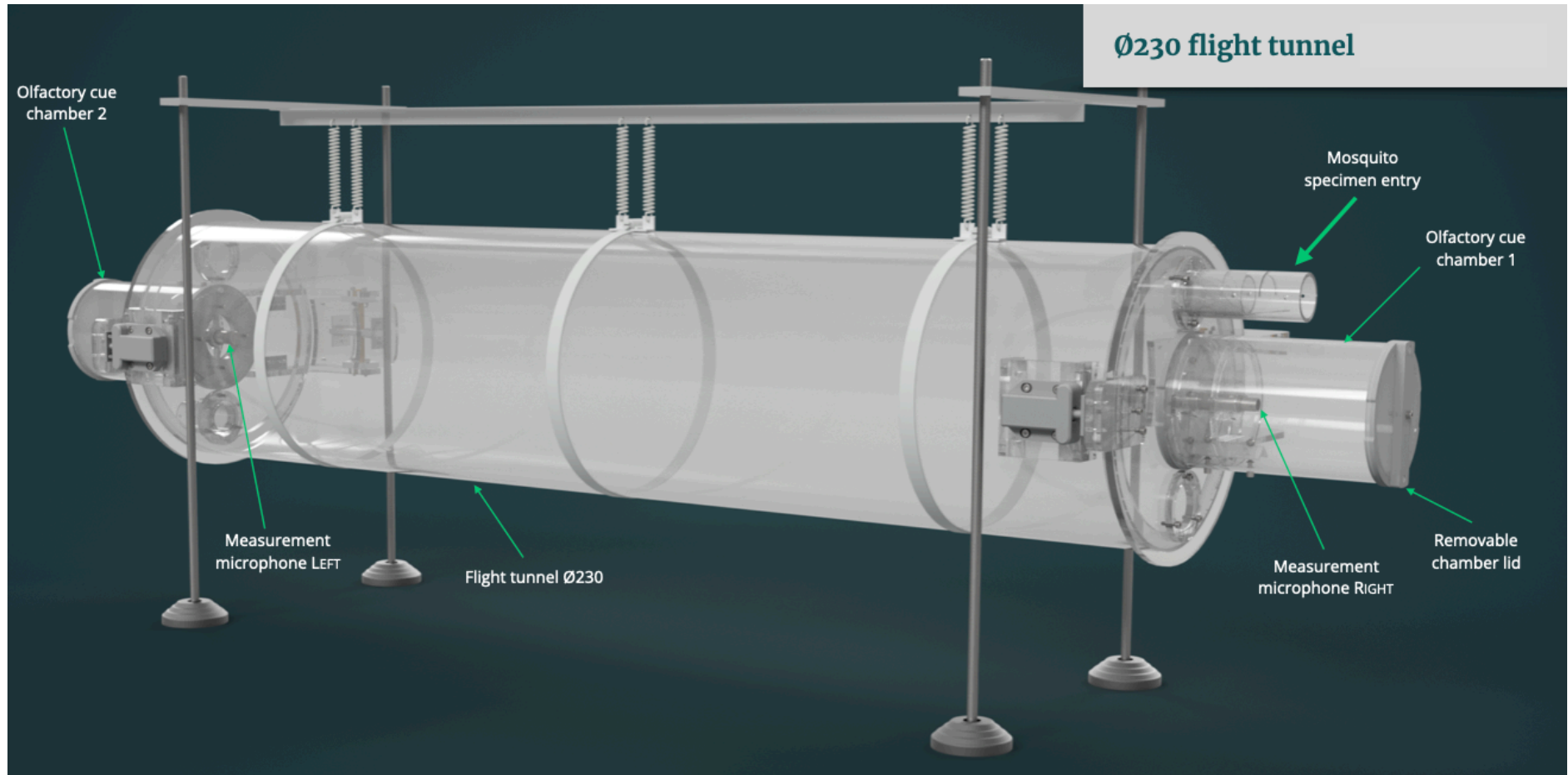


Figure 2.9 – Ø230 tunnel visualisation

### 7) MOSQUITO MAGNETIC SPECIMEN CARTRIDGE

The cartridge was designed to allow simple containment & transfer of live mosquitoes between capture / measurement devices. Magnetic latches allow the lid to remain secure, and also permit direct connections to measurement arenas.

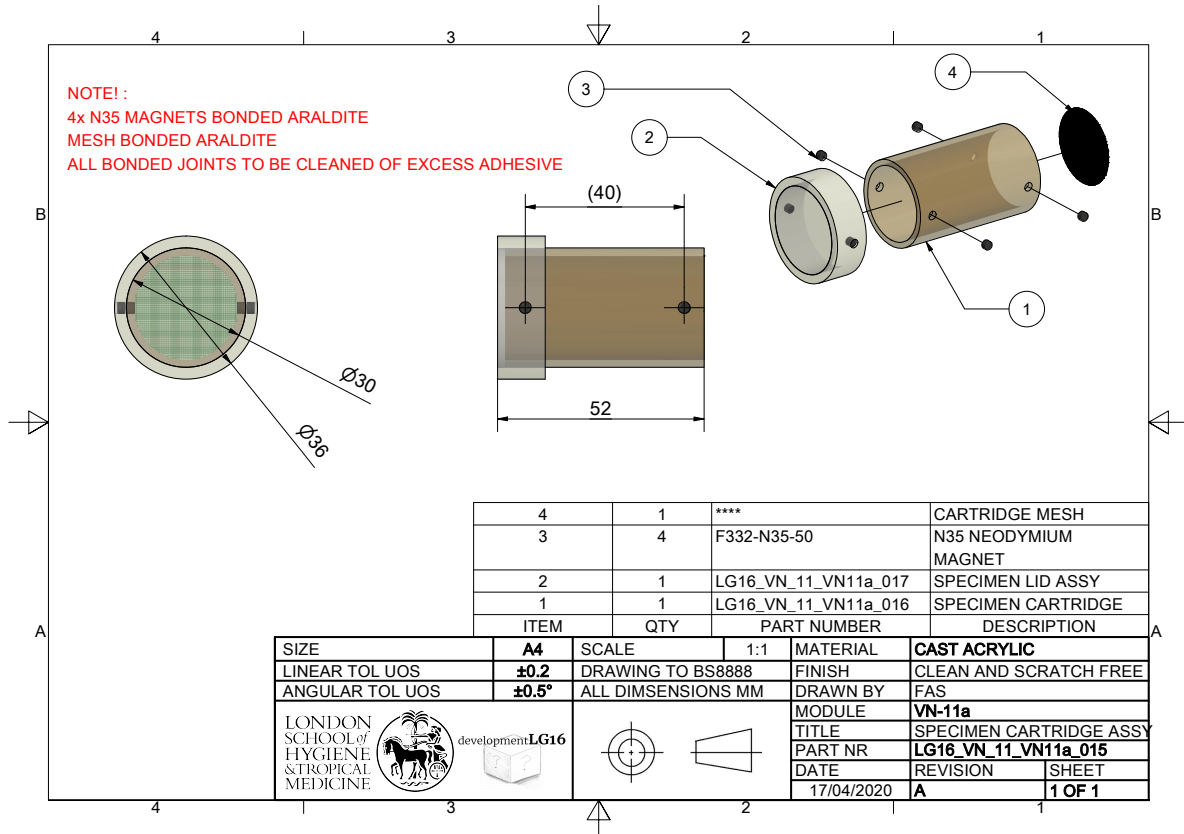


Figure 2.10 - Engineering drawing of the specimen cartridge assembly

### 8) FIELD ASPIRATOR COLLECTION SYSTEM

A USB powered aspirator was designed to allow wild samples to be collected into bespoke magnetic measurement cartridges that were used to introduce mosquitoes into the arenas.

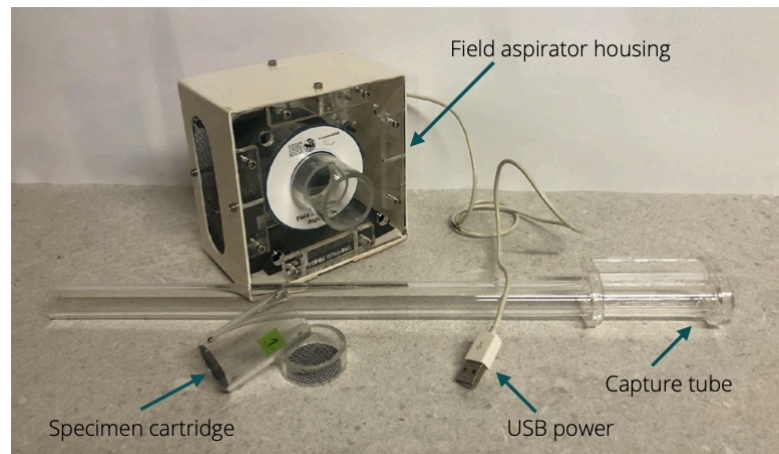


Figure 2.11 – Field aspirator, specimen cartridge and suction tube assembly

#### 2.3.4 - INTRODUCTION TO ACOUSTIC ANALYSIS OF MOSQUITOES USING MKII HARDWARE & PAK 5.8

A traceable measurement and analysis approach was used for mosquito acoustic measurements. A GRAS 46AE ½” free-field condenser-pressure microphone (GRAS Sound & Vibration, Holte, Denmark) was used, ensuring it remained calibrated in accordance to IEC 61094-6:2004 (traceable to the Danish National Metrology Institute / Danmarks Nationale Metrologiinstitut - DFM).

Microphones were connected to a PAK MKII measurement system (Müller-BBM VibroAkustik Systeme, Planegg, Germany), (MECALC, Centurion, South Africa) which allowed up to four analysis channels to be captured at up to 204 kHz. Acoustic data acquisition, pre-processing, post-processing and visualisation was performed with the PAK 5.8 software suite (Müller-BBM VibroAkustik Systeme, Planegg, Germany), with further post-processing using custom Python scripts and visualisations with the Plotly graphing library.

Prior to measurements, a daily calibration of the microphones was performed using a 42AG Multifunction Sound Calibrator, Class 1 (GRAS Sound & Vibration, Holte, Denmark). A calibration tone at 250 Hz and 94 dB was exposed to the test microphone, and the V/Pa response registered by the MKII measurement system was cross-checked against its calibrated response certificate. This process ensured that sound pressure levels registered during measurements remained accurate.

### 2.3.5 – MEASUREMENT SETUP

Pre-processing and sample rates can be defined in PAK 5.8. A sample rate of 12 kHz was used, with an FFT blocksize of 16384 to provide a 0.73 Hz frequency resolution for a 1.36s block duration. Measurements were manually started and stopped, once a period of mosquito flight had been observed that was uninterrupted by background noises.

### 2.3.6 – ANALYSIS SETUP

A custom report was generated in PAK 5.8 for each mosquito measured, to visualise the frequency content recorded in each of the four measurement arenas. This was achieved by first generating a spectrogram for the flight to identify captured flight bursts, with an example measurement shown by figure 2.12.

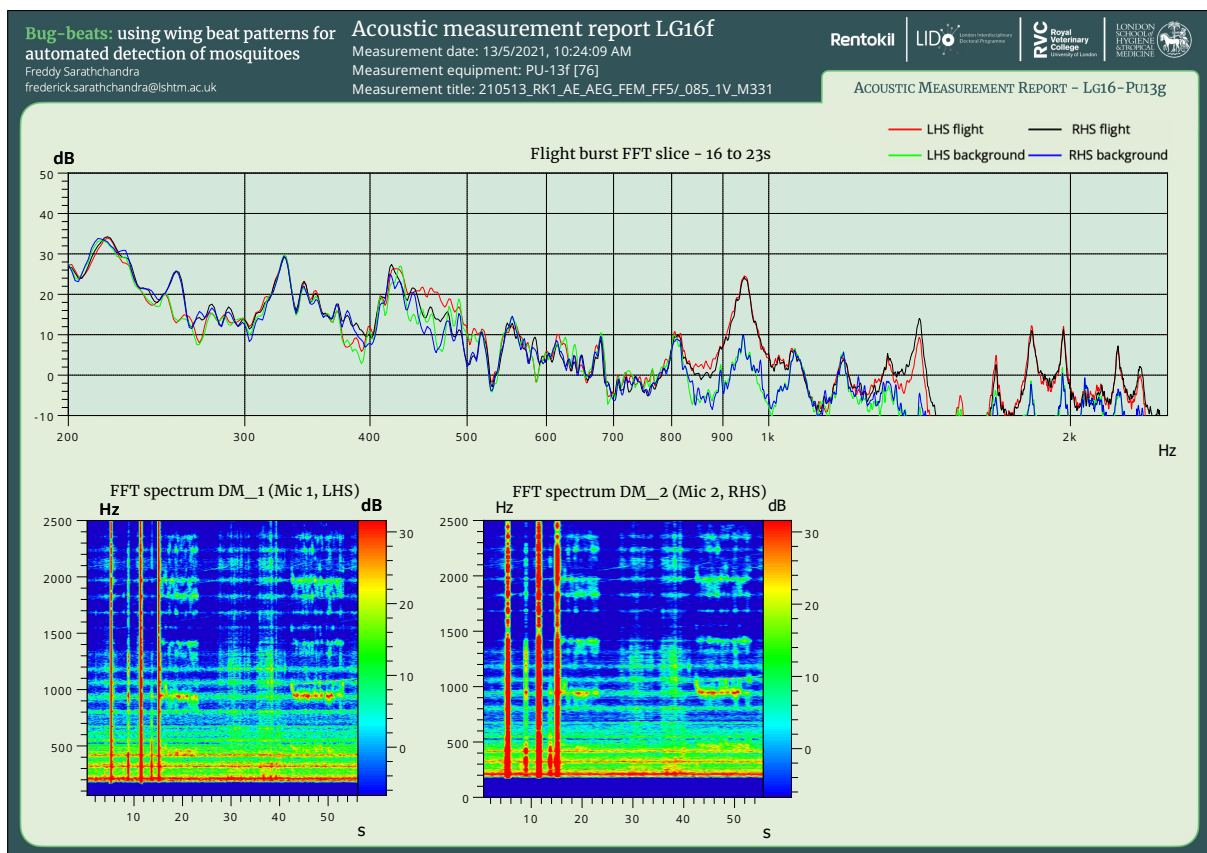


**Figure 2.12** – Frequency analysis template visualises measured flight bursts within the tunnel, from the LHS and RHS microphones. Average FFT content during flight bursts and no flight zones (top), spectrograms (bottom left & right) and bandpass magnitude plot between 500 & 550 Hz.

The two frequency spectrograms (bottom left / centre) shown in figure 2.12 show a typical soundscape captured in the measurement arena for the LHS and RHS microphones. Vertical lines are indicative of the broadband noise associated with flight initiation by the experimenter; tapping was the most effective method. Continuous horizontal lines are indicative of ambient background noise, which was mostly from HVAC system in the test lab.

Various external noise sources are clearly present, but two flight bursts in this example can be identified. Following manual identification, the flight bursts frequency spectra plot is generated, which shows the frequency content for the duration of the flight burst selected (16-23s). This is plotted for both the LHS and RHS microphones up to 2500 Hz. Background frequency content is also plotted using manually selected regions where the mosquito was not in flight. By repeating this workflow for all four measurement arenas, a summary report is generated for each specimen, as shown by figure 2.13. This report also shows the overall level (sum level) during a flight burst, and during a period of no flight.

From this report, further analysis was performed using a custom Python script to visualise the frequency content for each arena, with background noise compensation, as shown by figure 2.14. This makes comparison of the four arenas much simpler, as the different impacts of background noise between the arenas can be compensated for. This was achieved by averaging the LHS and RHS microphone frequency spectra and amplitudes for periods of flight and no flight, and subtracting their frequency amplitudes. A simple peak finder was incorporated into the script to identify the fundamental and first 3 harmonic frequencies and amplitudes, which was automatically visualised and exported to a .csv file for final comparison.

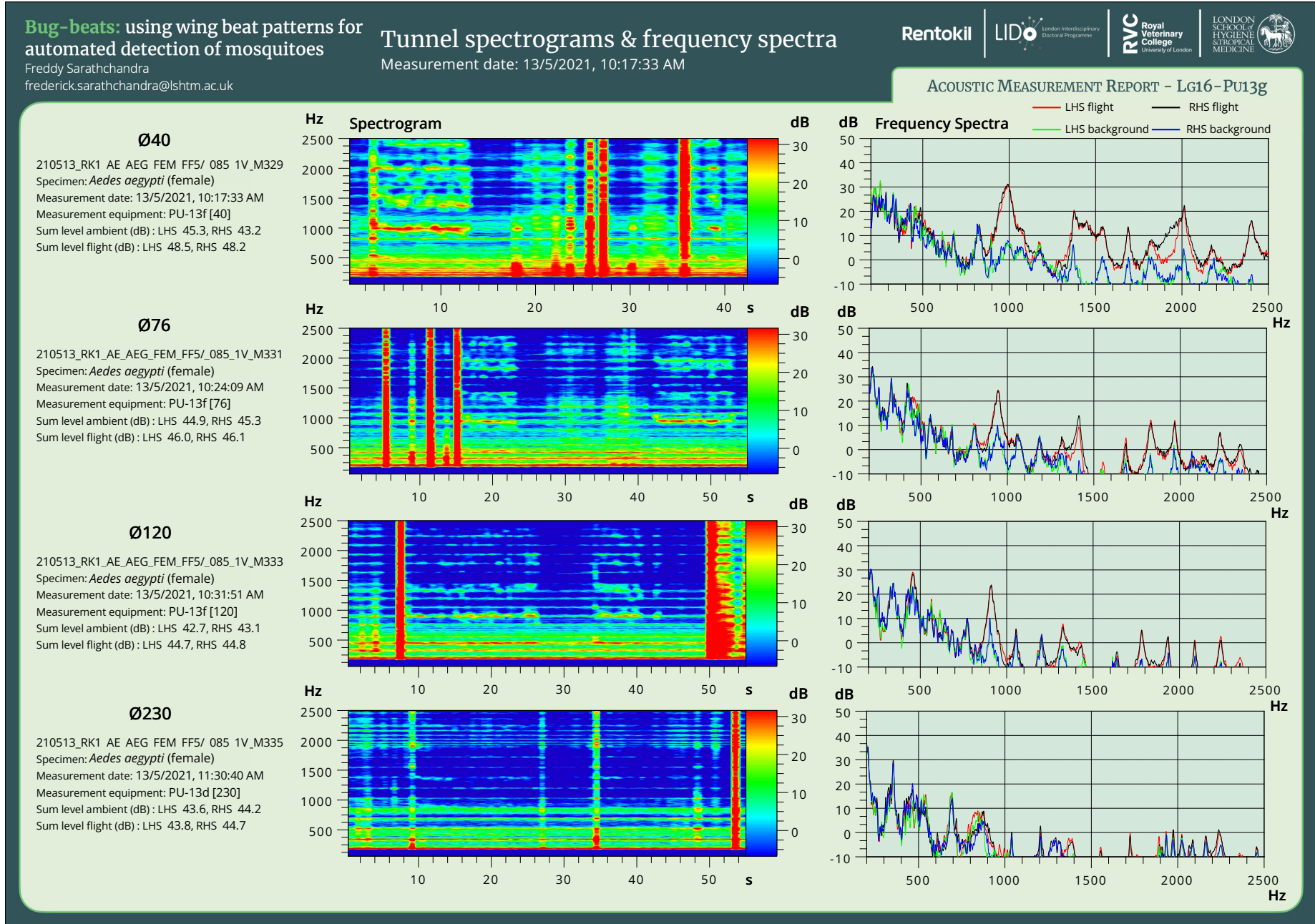


**Figure 2.13** – Frequency analysis summary report. Frequency content for the four measurement arenas, with sum level information is summarised for specimen S85 *Aedes aegypti*.

### 2.3.7 – EXPERIMENTAL DESIGN: FREE-FLIGHT MEASUREMENTS IN FOUR ACRYLIC FLIGHT TUNNELS

Mosquitoes were introduced individually into one of the four tunnels (Ø40, Ø 76, Ø 120, Ø 230) in a randomised order. It would then be permitted to fly, such that a flight time above 2 seconds was obtained. The mosquito would then be aspirated out from the tunnel, and introduced to a new tunnel, until measurements had been completed with the same specimen in all four tunnels. Initial assessment was performed with *Aedes aegypti* females, which were non-blood fed between the ages of 5-30 days post emergence.

Twelve individual recordings were analysed across the four acrylic flight tunnels, using *Ae. aegypti* females (n=4). All measurements took place in the same test lab, with ancillary HVAC equipment powered down, to minimise background noise. Temperature was maintained between 22-25°C with relative humidity between 40-60 %. Following post-processing with the Python script, comparisons were performed using the mean frequency and mean amplitude data for each tunnel diameter.

## 2.4 Results and discussion 1 – acoustic measurement using acrylic tunnels

### 2.4.1 – RESULTS

Frequency spectra for *Aedes aegypti* specimen S85 for Ø40, Ø76, Ø120 & Ø230 tunnels

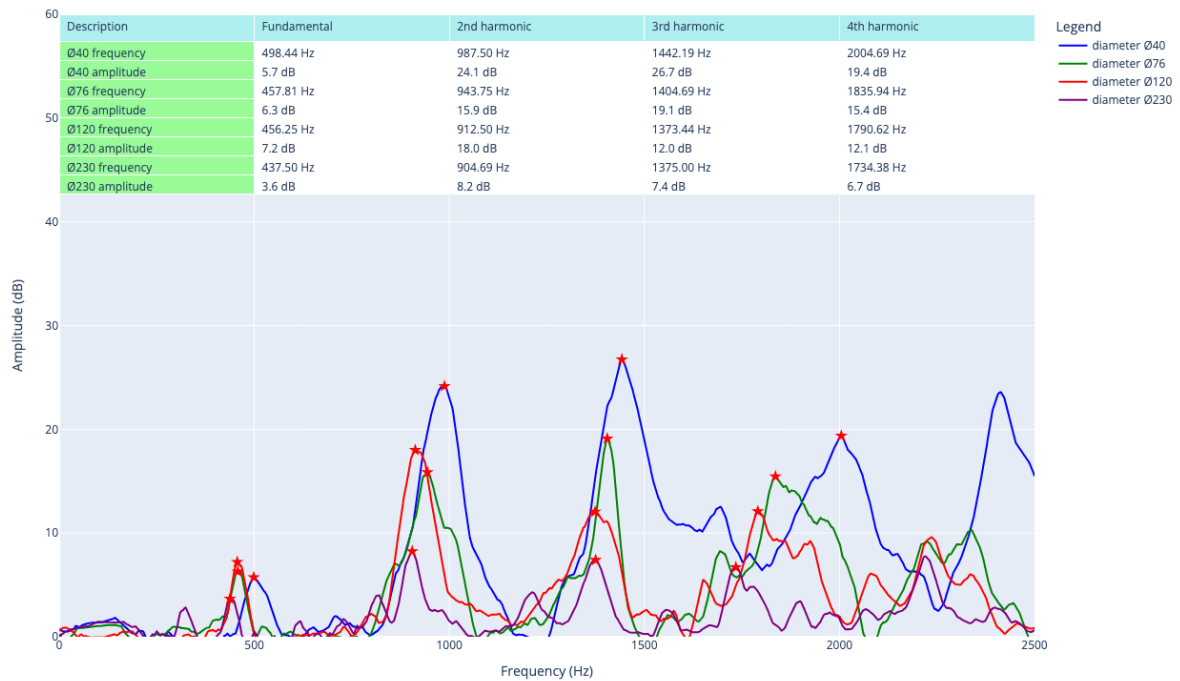


**Figure 2.14** – Background noise compensated frequency analysis summary. Example frequency content for the four measurement arenas, along with frequency information is summarised for single *Ae. aegypti* specimen

Following post-processing with the Python script (output on figure 2.14), comparisons were performed using the frequency and amplitude data for each tunnel diameter (figure 2.15). Mean fundamental frequency across the four tunnels was 498.4 Hz at an amplitude of 8.03 dB with an IQR of 22.3 Hz and 1.7 dB. The amplitude of the fundamental decreased as tunnel diameter increased (figure 2.16).

When considering the amplitude of the fundamental with harmonics, the fundamental frequency always featured the lowest amplitude across all four tunnels (figure 2.17). The third harmonic exhibited the highest amplitude for the

Ø40 & Ø230 tunnels and the second harmonic showed the highest amplitude for the Ø76 & Ø120 tunnels (figure 2.17)

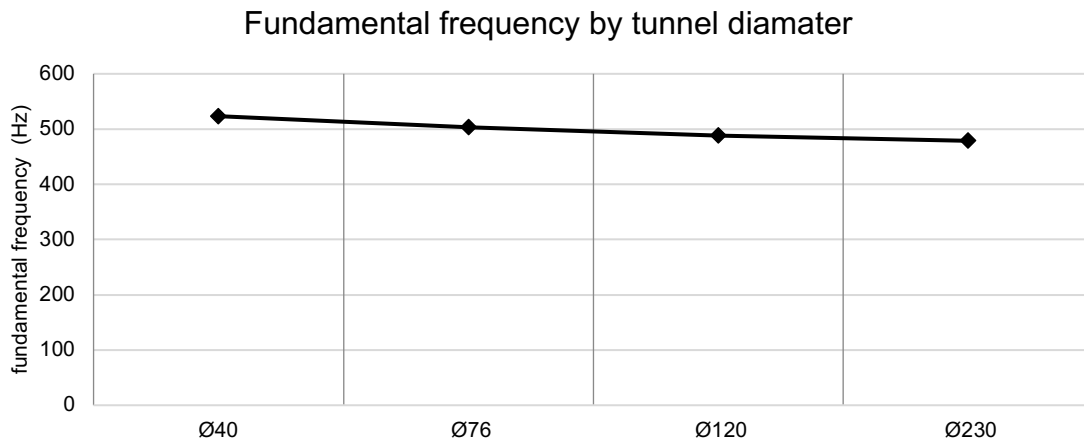


**Figure 2.15** – Summarised background noise compensated mean fundamental frequencies for the four measurement tunnels,

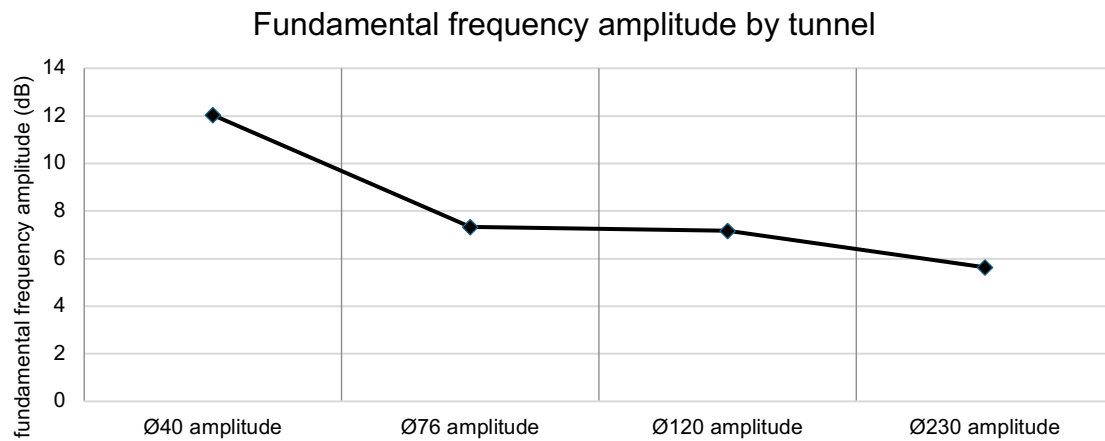


**Figure 2.16** – Summarised background noise compensated mean fundamental frequencies amplitudes for the four measurement tunnels,

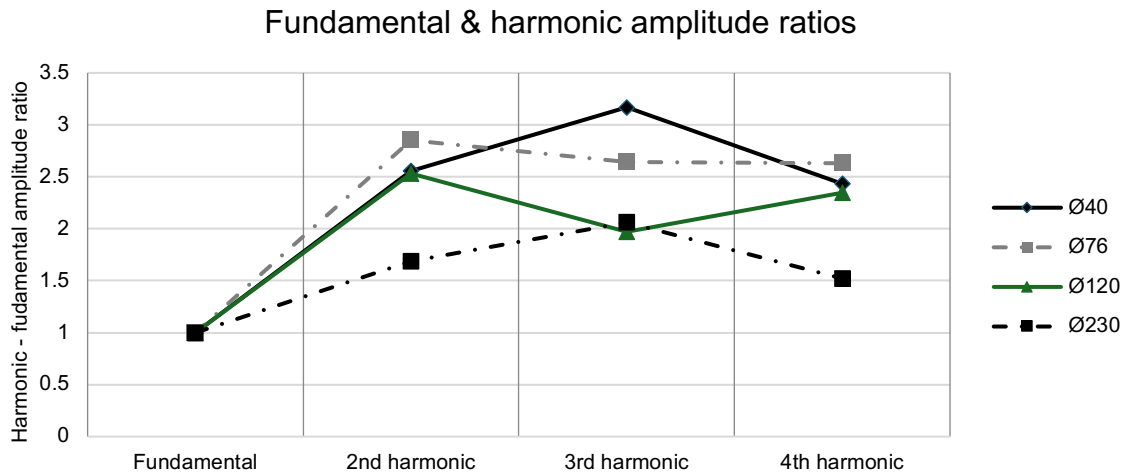


**Figure 2.17** – Summarised background noise compensated average fundamental & harmonic frequency amplitude ratios for the four measurement tunnels

**Table 2.1** – Averaged flight tone frequency data for *Aedes aegypti* with calculated ratios of measured harmonic frequencies relative to the observed fundamental

Flight tone	Ø40 frequency (Hz)	Ø76 frequency (Hz)	Ø120 frequency (Hz)	Ø230 frequency (Hz)	Ø40 fundamental - harmonic ratio	Ø76 fundamental - harmonic ratio	Ø120 fundamental - harmonic ratio	Ø230 fundamental - harmonic ratio
fundamental	523.3	503.1	488.3	478.7	1.00	1.00	1.00	1.00
2 <sup>nd</sup> harmonic	1025.7	1016.0	978.3	995.8	1.96	2.02	2.00	2.09
3 <sup>rd</sup> harmonic	1533.3	1522.5	1478.6	1489.2	2.93	3.03	3.03	3.12
4 <sup>th</sup> harmonic	2060.7	2000.8	1939.5	1957.0	3.94	3.98	3.97	4.09

**Table 2.2** – Averaged (LHS & RHS microphones) sum levels of ambient and flight tone throughput signal for *Aedes aegypti* in the four tunnels

Species & measurement type	Combined average (dB)	Delta (dB)
Ø40 ambient	44.5	9.1
Ø40 flight	53.6	
Ø76 ambient	45.6	1.0
Ø76 flight	46.6	
Ø120 ambient	43.9	1.7
Ø120 flight	45.6	
Ø230 ambient	42.6	1.5
Ø230 flight	44.1	

The harmonics measured deviated from their theoretically expected values (integer multiples of the fundamental) across all four tunnels, represented by the fundamental-harmonic ratios in table 2.1. Deviation from the expected harmonics was averaged for each tunnel, with harmonic deviations of 4% [Ø40], 2% [Ø76], 1% [Ø120] & 8% [Ø230].

The sum level data in table 2.2 demonstrates that periods of flight within the Ø40 tunnel flight exhibited the greatest difference (9.1 dB) in overall amplitude with comparison to ambient background noise levels, whilst the smallest difference was with the Ø76 tunnel (1.0 dB).

#### 2.4.2 – DISCUSSION OF THE Ø40, Ø76, Ø120 & Ø230 TUNNEL PERFORMANCE

The dataset evaluated here is relatively small, but sufficient to compare the four tunnels and their suitability for characterising mosquito flight tones. Using the background noise compensation approach, the fundamental frequency of *Ae. aegypti* was identified straightforwardly. However, as figure 2.17 shows, the described acoustic profiles and their specific harmonic content varied between the tunnels.

It was easier to identify flight bursts from the smaller tunnel diameters, than the larger tunnels, with the smaller tunnels exhibiting a higher signal to noise ratio than the larger tunnels. This is shown in figure 2.13, whereby the delta between background noise and flight tones (red / black) is much greater for the Ø40 tunnel than Ø230. Following background noise compensation, the effect is more clearly visualised, with the fundamental amplitude reducing with increasing tunnel diameters (Fig. 2.16).

As tunnel diameter increases, there would be higher dissipation of sound energy since the averaged distance from the sound source to the microphone would be lower (Brüel & Kjær, 1984), reducing the overall amplitude of the wingbeats

measured by the microphones at both ends of the tunnels. However, a constraint with the analysis approach taken, is that the distance of the mosquito from the measurement microphone was not measured and could not be controlled. The setup used the average of two measurement microphones positioned at both ends of the tunnel (both for frequency and amplitude), but this could not identify or compensate for scenarios where the mosquito may have exclusively flown at one region of the tunnel (e.g the LHS predominantly).

The fundamental amplitude with this dataset correlates with tunnel diameter, whereby it decreased with increasing tunnel diameter. What is less clear, is the connection between the sum level of all frequencies (table 2.2), during a flight burst and whilst under ambient noise. Except for the Ø40 tunnel, which demonstrated a 9 dB delta in the sum level measured under ambient and flight, the larger diameters did not show such a difference (between 1.0 -1.7 dB). From the perspective of the surveillance device, this would mean that monitoring changes in sum level to identify a flight burst, would only be feasible for the smallest diameter.

As stated in the introduction of this chapter, these tunnels are an engineering compromise, and they are intended to create distinct reverberant sound fields from their cylindrical and acrylic constructions at low cost. These are the sound fields that a simple field detection device could realistically be expected to feature.

Since the sum level is obtained from a raw microphone output, its use as a metric is a computationally attractive approach since it requires no post-acquisition processing unlike frequency calculations (FFT). However, further development to quantify expected sum levels with and without flight would be required to exploit this. This would be dependent upon the material properties of the tunnel (e.g. its acoustic absorption and reflectivity) but also the acoustic environment the tunnel is situated in. This relationship between the wingbeat and the measured level could be described through further experimental validation. The signal is also

confounded by the mosquito distance and orientation relative to the measurement microphones, which have been previously shown to change (Arthur et al., 2014b).

Figure 2.13 illustrates how the ambient noise frequency spectra varied for the four tunnels. Although they were designed with the same 1000 mm length, with a theoretical resonant frequency of 86 Hz (closed ended pipe assumption), the real frequency spectra show that all four tunnels exhibited very different acoustic behaviours. Despite the application of a 200 Hz high-pass filter, low frequency noise was present in all tunnels, and the signal-to-noise ratio of unprocessed signals (the sum level data) was not proportional to tunnel diameter as shown by table 2.2, which can be attributed to the complex manner in which the reverberant field interacted with the mosquito flight tone, ambient noise and resonant properties of the tunnels.

Measurement of amplitude will also require further investigation under more controlled acoustic conditions, as it is unclear from this dataset how the sum level amplitude and individual frequency amplitudes are affected by resonance, tunnel geometry and mosquito positioning. Whilst all four tunnels limited mosquitoes in flight to be always < 500mm from a microphone along the tunnel axis, as the diameter increased, this distance could potentially increase by movements away from the axis, towards the tunnel walls. As mosquito position was not tracked, the amplitudes of this dataset cannot be a position within the arena.

#### 2.4.3 – CONCLUSIONS OF THE Ø40, Ø76, Ø120 & Ø230 TUNNEL ASSESSMENT

From the perspective of identifying a mosquito within an enclosed space, all four tunnels produced signals that, when transformed into the frequency domain, allowed for identification and description of the mosquito flight tones in free flight. Using the sum level, a computationally simpler approach without frequency transforms, would require further understanding of the effects of distance and angle on the wingbeat of mosquitoes, in conjunction with a better understanding

of the acoustic properties of the tunnels. The tunnels, whilst reverberant, exhibited complex frequency spectra beyond the expected fundamentals and associated harmonics. However, the simple background noise compensation approach did permit the fundamental and their harmonics to be identified clearly.

As tunnel diameter increased, the amplitude of the frequencies identified decreased and, intriguingly, the fundamental was not the frequency with the highest amplitude in any tunnel. As the tunnel lengths were equal, this resonant frequency across the tunnels should also be comparable. The observed amplitude differences could instead be due to varying acoustic interference of the tunnels, from differing respective rates of absorption, reflection, or transmission. Accordingly, a more controlled flight space will be required to describe the true amplitudes of the wing-beat frequency spectra. Such a space would lack the design simplicity of the tunnels in this chapter that is necessary for use in the field, but would return an accurate description of the wingbeat acoustics, with reduced influence from tunnel geometries these arenas offer.

## 2.5 Materials and methods 2 - assessment of *Aedes aegypti*, *Anopheles gambiae* & *Culex quinquefasciatus*

### 2.5.1 – OVERVIEW

As the results of section 2.4 demonstrated, using acrylic tunnels to describe mosquito acoustics was shown to be feasible, however the mosquito distance from the microphone was difficult to control with the 1000 mm tunnels. Due to the reflective nature of the acrylic tunnels the exact manner in which mosquito position affects amplitude could not be quantified without further empirical validation. This could be through incorporation of a video tracking approach, which has been achieved in a number of approaches in previous flight behaviour studies (Jones et al., 2021; Muijres et al., 2023). This would be feasible but is outside the scope of this chapter, which focuses on the themes of simplicity and engineering compromise. The purpose of the compromise is to ensure methods and approaches developed can be efficiently transferred for field applications.

### 2.5.2 – MEASUREMENT ARENA OPTIMISATION

To therefore mitigate the uncontrolled variation of amplitude due to mosquito position, a simpler solution was developed which was to use a shorter tunnel length of 400 mm. This would reduce the possibility of multiple paths being taken from the source to reach the receiver.

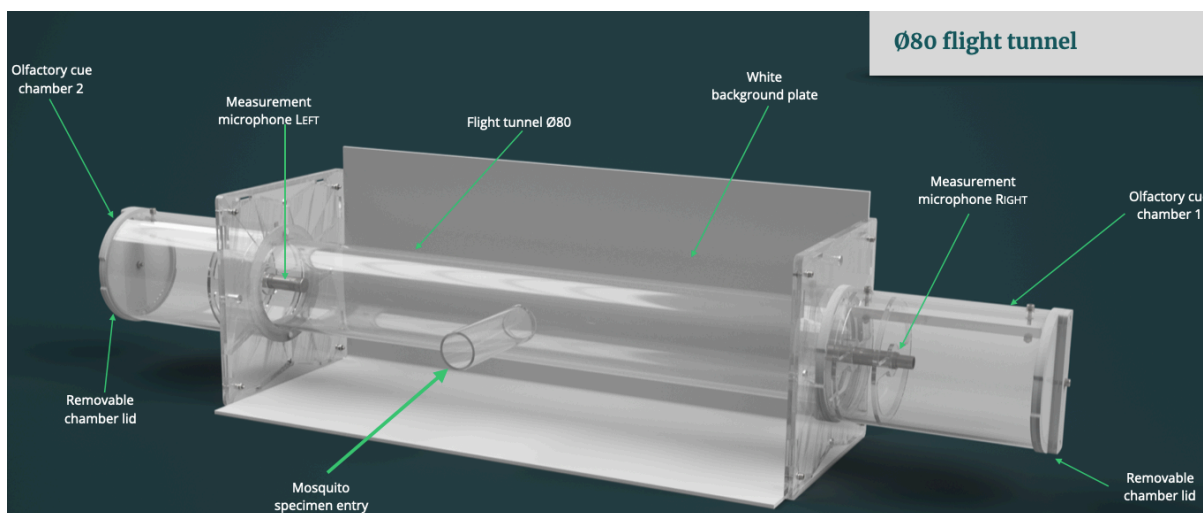


**Figure 2.18** – Ø80 x 400mm tunnel [PU-13h] visualisation

The Ø80 diameter was chosen as it offered a good compromise between material availability (Ø76 unavailable due to extremely restricted acrylic product availability during 2020-2022 due to its use in COVID related PPE), and a strong signal-noise ratio for mosquito flight bursts (based off the Ø76) and feasible flight.

### 2.5.3 – EXPERIMENTAL DESIGN

Building upon the findings from section 2.4, this optimised flight tunnel was used to explore its suitability at identifying the acoustic metrics produced by *Aedes aegypti*, *Anopheles gambiae* and *Culex quinquefasciatus*. The same measurement and analysis approach was taken as described in sections 2.3. Ten individuals of each species were used for these measurements: unfed females, 5-30 days post emergence. Rearing was conducted in the same manner as described in section 2.3.3. The three species were analysed against each other using a one-way ANOVA with Tukey HSD post hoc analyses ( $P < 0.05$ ). This was performed using the mean fundamental frequency of the LHS and RHS microphones for each measurement during identified flight bursts. Prior to the one-way ANOVA proceeding, a normality test of residuals based on the Shapiro-Wilkes test was performed to validate the normal distribution of the data to be analysed.

## 2.6 Results and discussion 2 - assessment of *Aedes aegypti*, *Anopheles gambiae* & *Culex quinquefasciatus*

### 2.6.1 – RESULTS

Ten flight bursts were analysed from each female *Aedes aegypti* (n=10), *Anopheles gambiae* (n=6), & *Culex quinquefasciatus* (n=10). Mean fundamental frequencies were 579.5 Hz (SD = 55.3 Hz) at 13.0 dB (SD = 3.5 dB), 600.6 Hz (SD = 39.4 Hz) at 10.2 dB (SD = 4.7 dB) and 463.8 Hz (SD = 25.7 Hz) at 16.46 dB (SD = 3.9 dB). As seen previously, across all three species the measured fundamental frequency means exhibited the lowest amplitude and the 3<sup>rd</sup> harmonic means exhibited the highest amplitude. Differences detected between fundamental frequencies of *Ae. aegypti* or *An. gambiae* vs *Cx. quinquefasciatus* were statistically significant (SE = 18.7 Hz, p < 0.001) but no significant difference was detected between *An. gambiae* and *Ae. aegypti* (SE = 18.7 Hz, p = 0.507).

**Table 2.3** – Ø80 measured frequency & amplitude content for *Culex quinquefasciatus*, *Anopheles gambiae* & *Aedes aegypti*

		<i>Aedes aegypti</i>			<i>Anopheles gambiae</i>			<i>Culex quinquefasciatus</i>		
		Mean	Fundamental-harmonic ratio	SD	Mean	Fundamental-harmonic ratio	SD	Mean	Fundamental-harmonic ratio	SD
Frequency (Hz)	Fundamental	<b>579.5</b>	1.00	55.3	<b>600.6</b>	1.00	39.4	<b>463.8</b>	1.00	25.7
	2nd harmonic	1153.7	1.99	100.9	1189.7	1.98	75.5	927.2	2.00	54.6
	3rd harmonic	1727.6	2.98	150.1	1781.5	2.97	102.0	1371.1	2.96	77.4
	4th harmonic	2312.4	3.99	199.4	2363.4	3.94	180.5	1848.0	3.98	95.6
Amplitude (dB)	Fundamental	<b>13.0</b>	1.00	3.5	<b>10.2</b>	1.00	4.7	<b>16.5</b>	1.00	3.9
	2nd harmonic	17.4	1.34	4.9	18.8	1.85	2.9	18.0	1.09	18.0
	3rd harmonic	23.6	1.82	5.7	24.4	2.40	2.0	20.4	1.24	20.4
	4th harmonic	13.3	1.02	3.4	10.8	1.07	4.0	18.0	1.09	18.0

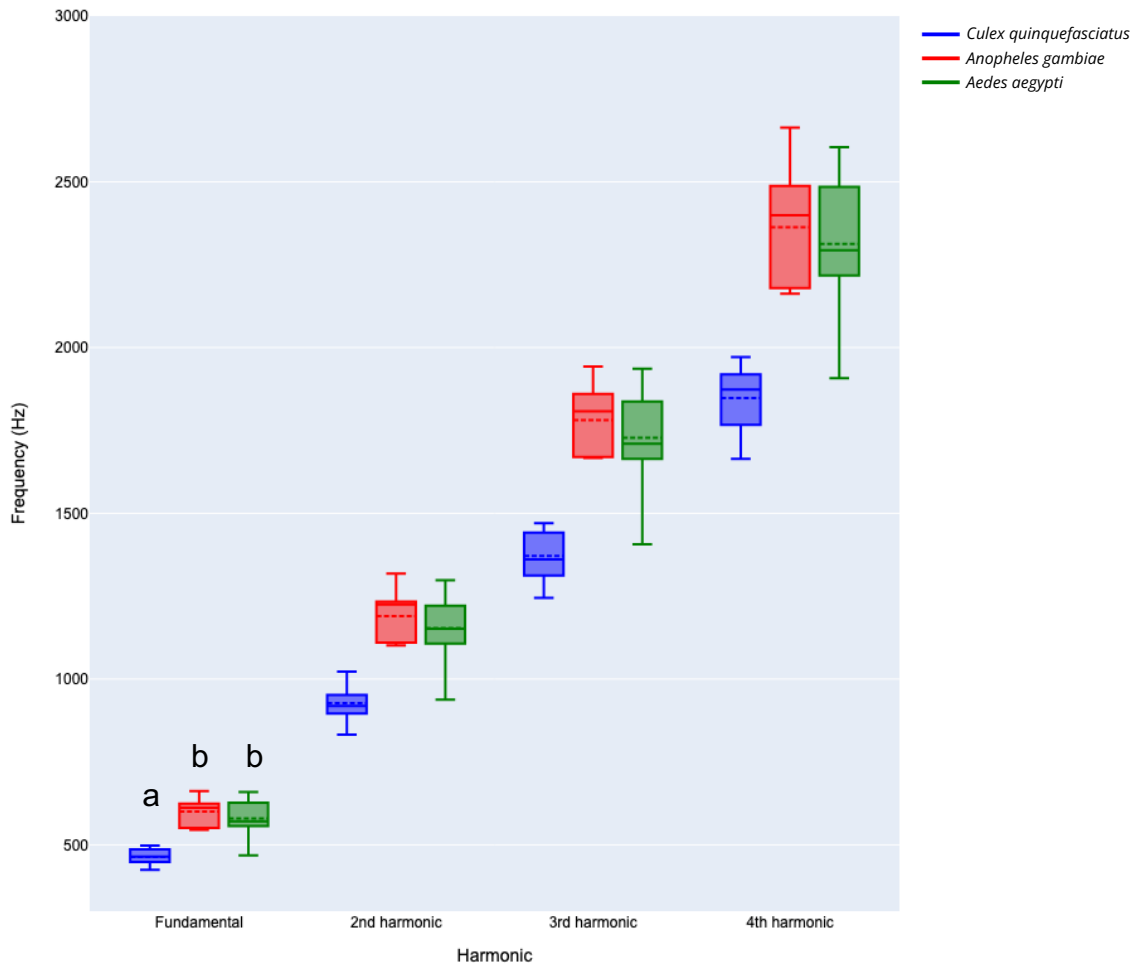


**Figure 2.19** – Ø80 measured frequency content for *Cx. quinquefasciatus*, *An. gambiae* & *Ae. aegypti*. Letters above the boxplots indicate which groups differ significantly from one another

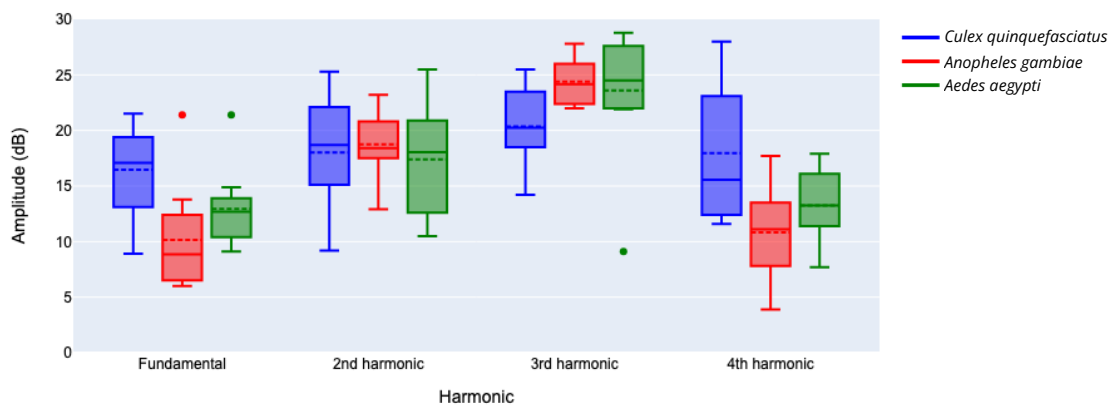


**Figure 2.20** – Ø80 measured frequency amplitudes for *Cx. quinquefasciatus*, *An. gambiae* & *Ae. aegypti*

Linear regressions were applied to the mean fundamental and harmonic frequencies measured, with  $R^2$  values of 0.9998 for *Cx. quinquefasciatus*, and 1.000 for *Ae. aegypti* and *An. gambiae*.

**Table 2.4** – Averaged (LHS & RHS microphones) sum levels of ambient and flight tone throughput signal for *Aedes aegypti*, *Anopheles gambiae* & *Culex quinquefasciatus* in the Ø80 tunnel

Species & measurement type	Combined average (dB)	Delta (dB)
<i>Aedes aegypti</i> ambient	32.0	6.0
<i>Aedes aegypti</i> flight	38.0	
<i>Anopheles gambiae</i> ambient	31.8	6.1
<i>Anopheles gambiae</i> flight	37.9	
<i>Culex quinquefasciatus</i> ambient	31.5	11.5
<i>Culex quinquefasciatus</i> flight	42.9	

LHS and RHS microphone averaged sum level data represented in table 2.4 shows a consistent ambient background noise level around 32 dB across all species measured. Measurements during all flights featured higher sum levels than their ambient references, with 6 dB increases measured for *Ae. aegypti* and *An. gambiae*, whilst *Cx. quinquefasciatus* measured a 11.5 dB sum level increase.

### 2.6.2 – DISCUSSION OF THE Ø80 TUNNEL MEASUREMENTS

The Ø80 tunnel allowed flight activity across all three species to be successfully measured, with fundamental and harmonic frequencies and amplitudes captured (figures 2.19, 2.20). Due to the higher sample sizes used for each species than in section 2.5, the spread for frequency and amplitude metrics has been summarised (table 2.3). Fundamental and harmonic frequencies, were strongly correlated for all three species, confirming that the harmonic components during their flight could be identified when using a reverberant sound-field tunnel environment.

What is most encouraging from this dataset, is that the amplitude of the harmonics exceeded that of the fundamental. This would suggest that obtaining higher signal to noise ratio with low-cost microphones would be feasible, since the

wingbeat could potentially be identified in a the higher frequencies where there is less background noise (figure 2.20).

It is also notable that all three species followed the same amplitude trend (figure 2.20), as first illustrated by the preliminary dataset of section 2.5 (figure 2.17). The fundamental, when measured in the Ø80 tunnel environment, always featured the lowest amplitude. The 2<sup>nd</sup> harmonic would feature a higher amplitude than the fundamental and the 3<sup>rd</sup> harmonic featured the highest amplitude. As the theoretical resonant frequency of the Ø80 tunnel is different from those tested in section 2.5 due to the different tunnel length, the effect of resonance of the tunnel on the recorded signal will be different. Without further acoustic testing of the tunnel (such as modal analysis to measure the exact tunnel harmonic and fundamental frequencies), the influence of resonance cannot be explicitly excluded as influencing this amplitude trend. Such investigations would confirm whether this amplitude trend represents the *true* mosquito wing-beat, or represents version of it *altered* by the acoustic properties of the tunnel. This difference is critical to understand, as it would define the accuracy and precision of a mosquito dataset captured within reverberant sound fields.

The initial comparison of wingbeat frequency demonstrated that the acoustic profiles captured for *Cx. quinquefasciatus* were significantly lower than *Ae. aegypti* and *An. gambiae*. However the overlapping wingbeats, which here were between *Ae. aegypti* and *An. gambiae*, were not significantly different. This would suggest that in this arena, with this analysis approach, it would not be possible to identify between these two species, using exclusively the wingbeat frequency.

Featuring the standard deviation has provided useful insight into potentially novel metrics for describing mosquito acoustics. The aim of all metrics in this application, is to find measurable acoustic traits that illustrate ways to differentiate species. Table 2.3 illustrates the SD for the fundamental frequencies to vary between 25.7 Hz (*Cx. quinquefasciatus*), 55.5 Hz (*Ae. aegypti*) and 39.4 Hz (*An. gambiae*). This representation of the spread in the mean fundamental

frequencies could potentially be used as a metric, should multiple measurement be made.

The shorter 400 mm tunnel length improved the signal to noise ratio over the 1000 mm counterparts, by forcing flight activity to be nearer the measurement microphones and therefore measuring higher amplitude. Whilst mosquito position within the tunnel was not tracked (as discussed previously), the sum level delta between ambient levels and flight bursts (table 2.4) illustrated the impact on signal to noise ratio. Using sum level amplitude as the metric, this greater delta is a vast improvement over the delta measured (with the limited dataset) with the 10000 mm Ø76 tunnel for *Ae. aegypti* (1.0 dB, table 2.2).

It is of interest to note that both *Ae. aegypti* and *An. gambiae* featured comparable sum level amplitudes, whilst *Cx. quinquefasciatus* exhibited a 5.5 dB higher sum level. However when this sum level is decomposed into the energies of each frequency (table 2.6.2.1, figure 2.6.2.2) the higher amplitude of *Cx. quinquefasciatus* is represented clearly only by the fundamental, with harmonic amplitudes varying in rankings relative to the other species measured.

## 2.7 Chapter summary

### 2.7.1 – CONCLUSIONS AND NEXT STEPS

This chapter has illustrated how five bespoke acrylic flight arenas, in addition to support equipment, were designed, constructed and tested, then used to measure the flight tones of *Ae. aegypti*, *An. gambiae* and *Cx. quinquefasciatus* female mosquitoes. A simple, yet accurate measurement methodology was developed to allow calibrated acoustic measurements to be taken of mosquitoes in free flight within the tunnels. A post-processing workflow compensated for background noise, revealing the frequency content of mosquitoes in flight.

Larger tunnel diameters had lower signal-noise ratios than their smaller diameter counterparts, but tunnel length was also influential. Reducing both the diameter and length led to improved signal-noise ratios when using overall sum-level, and the three species could be described by their frequency and frequency amplitudes up to the 4<sup>th</sup> harmonic.

Describing the exact interaction between tunnel resonance and the physical distance between microphones-mosquitoes in flight was not characterised with this setup, as the mosquito position is unconstrained. However additional development to understand the acoustic properties of the specific tunnel materials and geometries such as the analysis of calibration tones would be beneficial. A better understanding of the effects of position would help determine whether possible supplementary metrics such as frequency or amplitude variation, using standard deviation, could possibly be used in conjunction with mean frequencies and amplitudes.

# CHAPTER 3: DEVELOPING CONTROLLED MEASUREMENT APPROACHES



Portable semi-anechoic measurement chamber developed.

## 3.1 COVID impact statement

Development work undertaken in this chapter started from March 2021. Insectary access was still highly unpredictable and material shortages, whilst recovering, were still acute regarding microchips. Raspberry Pi Zero 2W units specifically were in extreme short supply, which directly affected assays relating to distance and angle since controllers were powered by these. A fault arose during testing requiring a replacement Raspberry Pi Zero 2W, however this could not be sourced

during this time. As a result, measurements for distance and angles were restricted, and data is presented in a preliminary manner.

Background noise could also not be mitigated in insectaries, due to building heating, ventilation and air conditioning (HVAC) systems running at a high (loud) level to meet mandated ventilation during high transmission COVID periods. This greatly impacted the approach taken to provide noise-free acoustic conditions, as creating low-noise insectary conditions became very challenging to produce.

The continued unpredictability of lockdowns resulted with an independent approach being taken for the remainder of the project, whereby minimal reliance on specific labs was designed into the methodologies outlined in this chapter. All equipment described was designed to be portable, whilst maintaining tightly controlled acoustic and environmental conditions, independently of a lab, for mosquito acoustic measurements.

## **3.2 The need for a controlled measurement space**

### **3.2.1 – THE COMPROMISE BETWEEN DESIGN SIMPLICITY, PRECISION AND ACCURACY**

Chapter 2 demonstrated how acoustic metrics could be measured and identified with simple but acoustically compromised acrylic flight tunnel designs. Whilst useful for refining the arena geometry for a potential field-ready device, the acoustic data these acrylic tunnels captured was compromised by their lack of acoustic controls (e.g. reflections, background noise, resonance etc).

In contrast to Chapter 2, this chapter aims to capture the sound wave made by mosquito wingbeat in an accurate manner. The specific interaction of the mosquito wingbeats within the reverberant tunnels meant that measured wingbeat frequency amplitudes may not have been representative of that produced by the mosquito alone, once they reached measurement microphones. Whilst the

influence of the tunnels would be consistent, meaning measurements made with them are *precise*, the unquantified attenuation/amplification effects means that measurements are not guaranteed to be *accurate*. To achieve accurate capture of mosquito wingbeats, their sounds must not be subjected to external changes as could be imposed by the acrylic tunnels. This key difference justifies developing an environment to enable controlled capture of mosquito wingbeats with minimal potential for alteration between the sound source and the measurement sensor.

Taking this approach will allow a gold-standard data-set to be collected, capturing with accuracy and precision, the wingbeat acoustics produced by mosquitoes under a variety of physiological conditions, whilst also providing tighter environmental control. Using this resource, it would be possible to investigate what differences, if any, can be identified for use in discrimination tasks, which will be covered in Chapters 4 and 5. We could then assess the persistence of such acoustic discriminators when recording flight sounds in suboptimal conditions, such as those in the compromised but more realistic acoustic tunnels developed and discussed in Chapter 2.

### 3.2.2 – ACOUSTIC CONTROL

Chapter 2 demonstrated that an approach of background noise compensation could effectively reduce the effects of background noise present in the acrylic tunnels. The simple flight arenas featured no sound attenuating measures, permitting ambient noise from the insectary to enter and resonate within the tunnel. A drawback of this approach is that every measurement required a period of ‘defined ambience’ to be identified manually during post-processing. This was used to generate the frequency spectra for background noise within the tunnels for each unique measurement, which was then subtracted from the manually defined flight burst frequency spectra. This meant that flight could be analysed in the frequency domain, but time-domain analysis would require further post-processing to perform background noise compensation at every time step of the microphones signal.

The original solution to this was to reduce ambient noise within the insectary, however this was not feasible due to the impacts of COVID as outlined in section 3.1. For this reason, it was decided that provision of acoustic control could not be provided by the facility, so the arena itself would have to be acoustically insulated. As such, our new design criterion was that a new measurement arena should provide *free-field* instead of diffuse acoustic conditions to capture mosquito flight without alteration or influence from the physical test environment, whilst also ensuring the measurement sensors were not subject to noise from external sources.

### 3.2.3 – ENVIRONMENTAL CONTROL

It is well established that environmental conditions not only affect acoustic transmission in general (British Standards Institute, 2011), but also the wing-beat frequency of mosquitoes (Staunton et al., 2019b). Key parameters to monitor and control are temperature and humidity which are typically set between 25-30°C and 60%-80% relative humidity in prior acoustic mosquito studies (Pantoja-Sánchez et al., 2022; Villarreal et al., 2017b). Due to the COVID restrictions discussed, insectary HVAC could not be relied on for environmental control so the flight space itself, independently of a specific insectary was required to be controlled and monitored.

Lighting is another factor that needs to be controlled, due to the influence of circadian rhythms on mosquito flight behaviour (Jones et al., 1967). This is set during mosquito rearing by controlling the scotophase during their development with timed insectary lighting.

Mosquitoes have also been shown to detect and react to human odour as they seek a host, identifying a blend of volatile organic compounds (VOCs) present in body odour (Showering et al., 2022) combined with other cues including carbon dioxide (Knols et al., 2010). During the measurements taken for Chapter 2, it was found that mosquitoes required external stimulation to initiate flight through tapping or

blowing, however this stimulus could greatly increase CO<sub>2</sub> and VOC from breath inside the measurement space. As it is known that these can influence mosquito behaviour, the proposed new chamber will need to hold these levels constant.

#### 3.2.4 – POSITION CONTROL

When a sound is measured from its source, the sound pressure level is correlated with the distance, as introduced in section 1.2.2. The diffuse conditions of the acrylic tunnels of Chapter 2, combined with untracked free flight meant that amplitudes measured could not be readily connected to mosquito position. As sound pressure level, and its variation, was seen to vary in the Chapter 2 tunnels (after averaging, and reduction of tunnel length: section 2.5), an improved controlled approach would be beneficial. Such an approach that allows for mosquito position to be described or directly controlled would greatly help to describe the frequency spectra and their respective amplitudes of the wingbeat.

#### 3.2.5 – AIM AND OBJECTIVES

##### **Chapter Aim**

This development chapter aims to establish a method to capture and describe the wing-beat acoustics of mosquitoes in an *accurate* and *repeatable* manner, whilst minimising dependencies on external controls afforded by typical entomology and acoustic lab environments.

##### **Chapter Objectives**

1. Design, construct and evaluate a novel measurement arena providing controlled acoustic & environmental conditions for wing-beat measurements of mosquitoes.
2. Design and develop methods and equipment for tethered measurement of mosquitoes whilst controlling their position within the arena

3. Design and develop methods and equipment for free flight measurement of mosquitoes within the arena
4. Establish a repeatable acoustic acquisition and processing workflow to describe mosquito wingbeat acoustics
5. Evaluate the effect of distance and angle on measured wingbeat acoustics
6. Propose and evaluate novel analysis approaches to capture and describe the wingbeat of mosquitoes

### **3.3        Developing the novel tools**

#### **3.3.1 – SEMI-ANECHOIC MEASUREMENT CHAMBER - FREE- FLIGHT**

Two approaches were taken for flight measurements, using tethered flight and free flight. The advantage offered by a tethered approach, was that it would allow for absolute control of mosquito position relative to the measurement microphone, however it would not be as representative and transferrable as a measurement series based on free-flight data. To retain the element of translation to a field device, the free-flight approach was designed around a novel free-field tunnel (figure 3.2), instead of a reverberant field.

A semi-anechoic chamber (figure 3.1) featuring two access doors was constructed from 3mm aluminium. The chamber was lined with sound attenuating foam on interior walls (RS Pro Melamine closed cell acoustic insulation, RS Components Ltd, UK) and doors (Polyurethane foam corrugated 50mm, Paulstra-Hutchinson, Levallois-Perret, FR). Both doors featured neoprene seals mounted to electronically assisted door close mechanisms to ensure tight closure. The same GRAS 46AE microphones as used in Chapter 2 were used, mounted on the LHS and RHS of the chamber, within the doors. External BNC connectors were mounted on the outside of the chamber, such that trailing wires for internal microphones did not need to be passed through the closed doors.

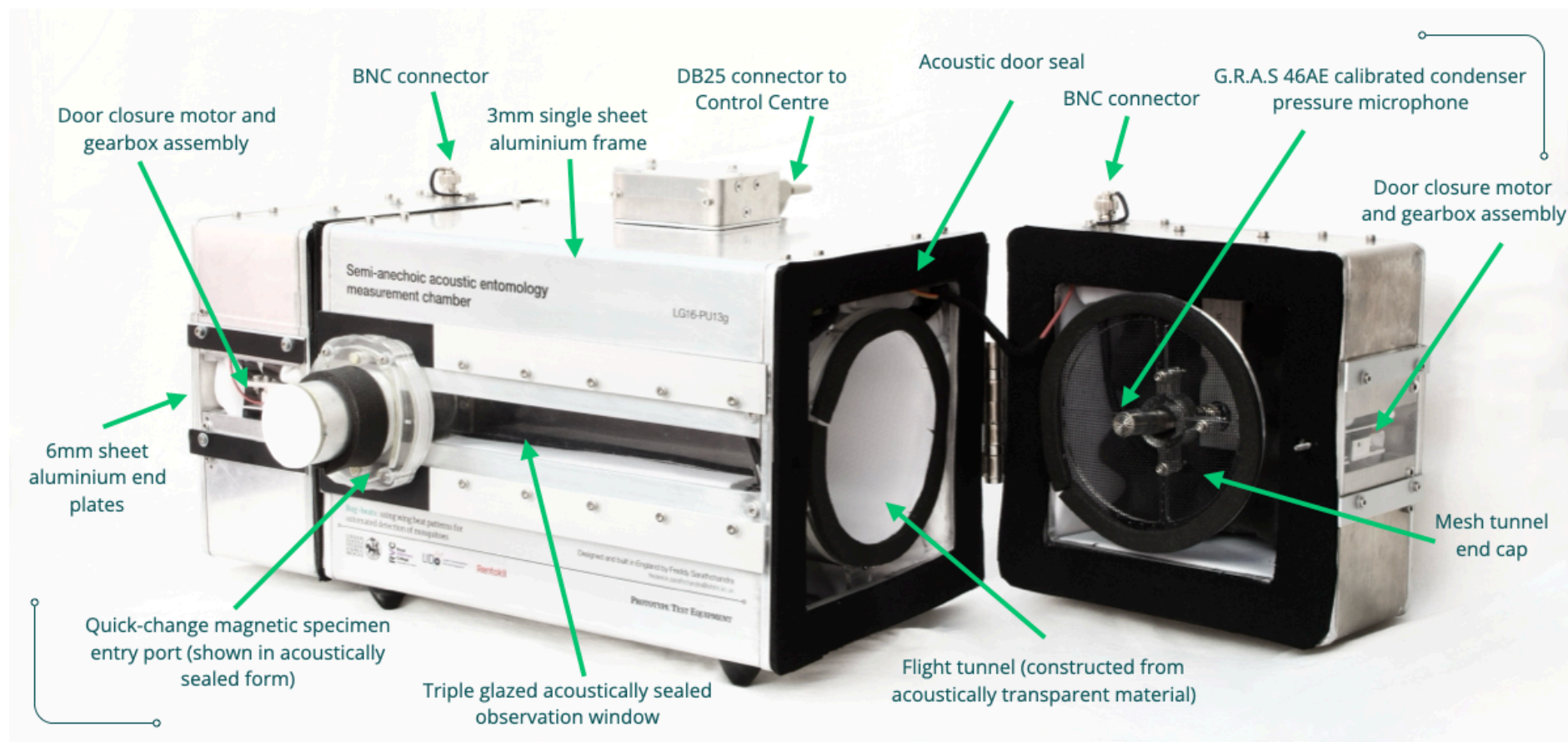


**Figure 3.1** – Semi-anechoic measurement chamber (shown with  $\text{\O}100$  tunnel installed inside)

For free-flight measurements, a new acoustically transparent flight tunnel concept was developed, whereby  $\text{\O}40$ ,  $\text{\O}76$  and  $\text{\O}100$  flight tunnels 300 mm in length were designed ( $\text{\O}76$  shown in figure 3.2). These comprised of an acrylic skeleton connected by aluminium tubes, which was lined with a specialised fabric, designed to be acoustically transparent (Acoustic cloth 2.0, Akustikstoff, Mörlenbach, DE). An observation window on the tunnel aligned with the chamber window to permitted flight to

remain visible during tests. The tunnel also featured a shaker system, which on demand could vibrate the tunnel to initiate flight of a mosquito at rest if required. The flight tunnels (figure 3.2) magnetically latched to the inside of the chamber, such that they could be quickly removed and swapped for different diameters or configurations as required.

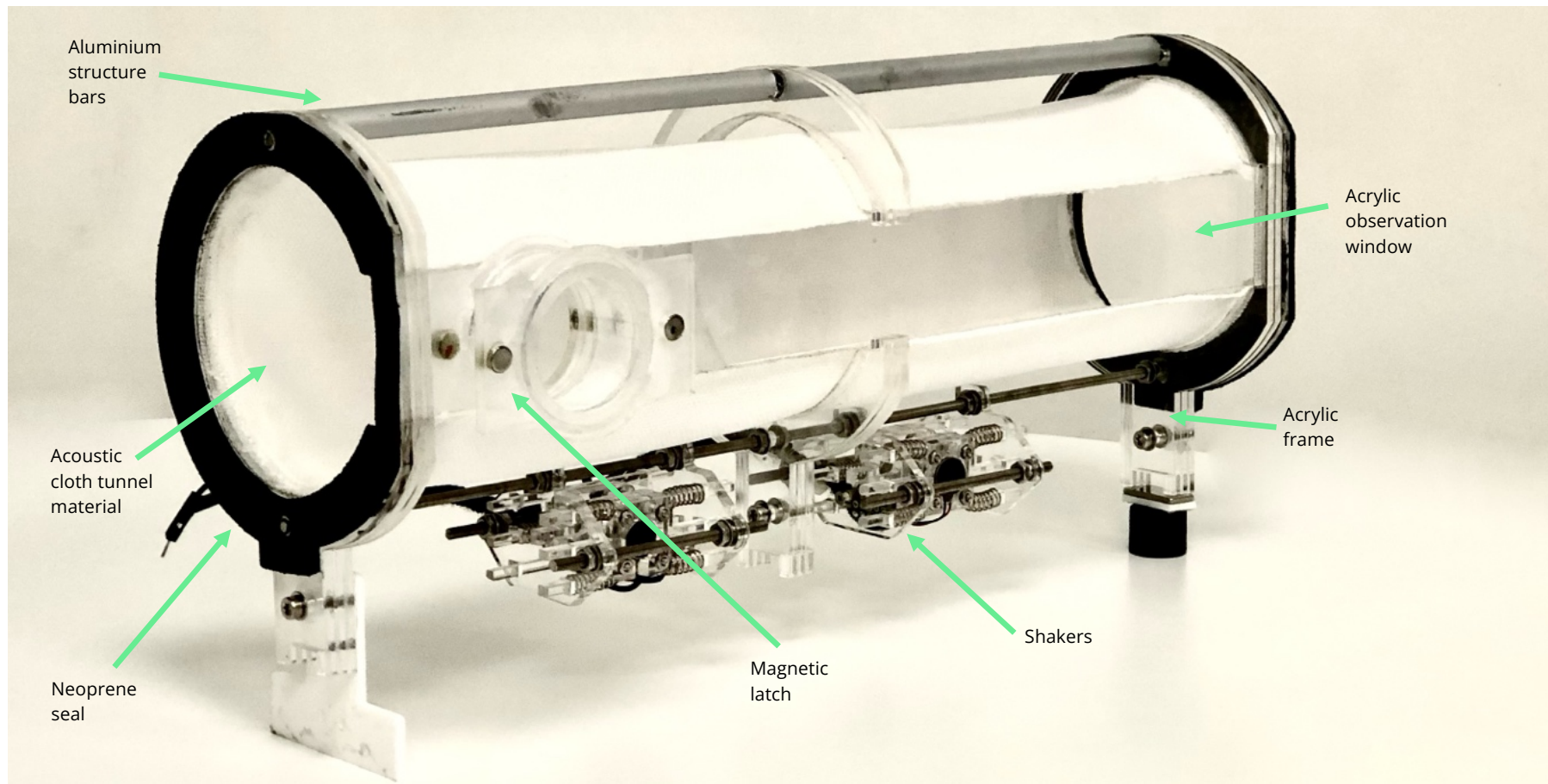
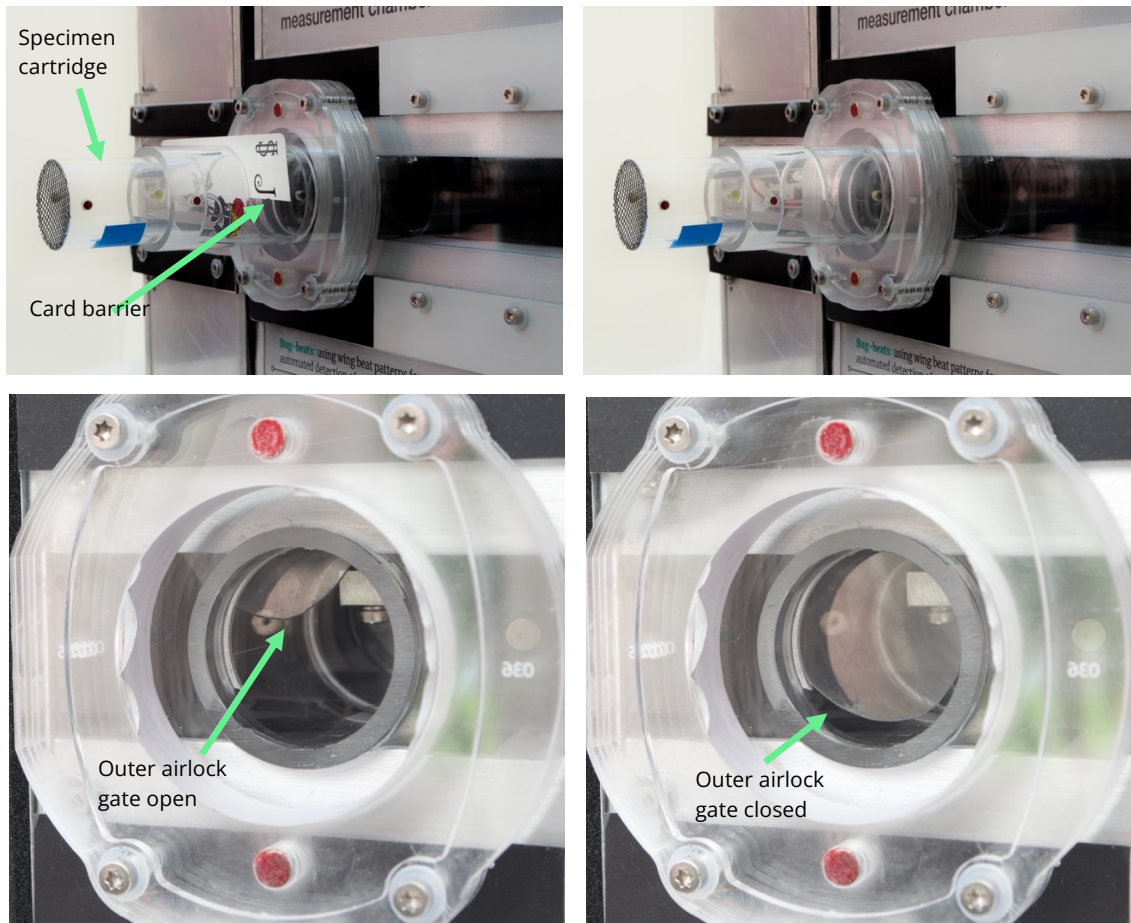


**Figure 3.2** – Ø76 acoustically transparent flight tunnel, with shakers



**Figures 3.3 (a-d)** – *clockwise from top left.* **a)** Specimen cartridge magnetically secures to chamber, with card barrier keeping mosquito out of chamber, **b)** card removed, allowing entry to “air lock”, **c)** outer “air lock” gate open, permitting entry of mosquito into “airlock”, **d)** outer “airlock” closed, securing mosquito between outer & inner “airlock”

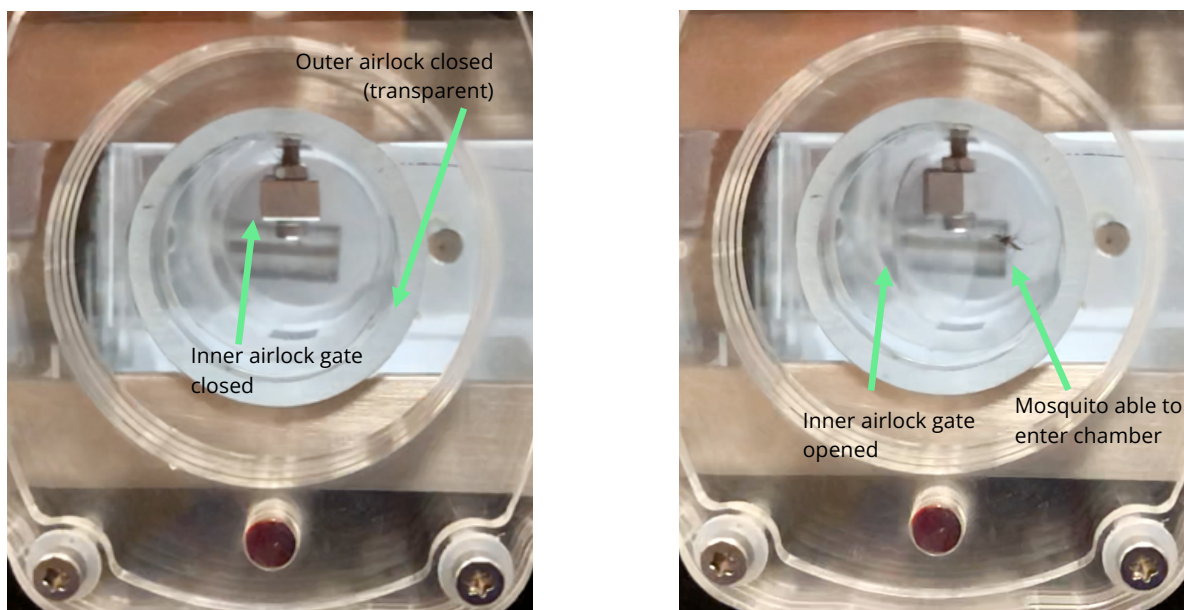


**Figure 3.4a (left), 3.4b (right)** – **a)** Specimen is inside airlock with both gates closed, **b)** inner airlock opened, permitting mosquito to enter chamber

The “airlock” system developed allowed mosquitos to be loaded and handled whilst minimising contact time. It consists of a two gate system (figures 3.3 – 3.4) that is controlled remotely using the Control Centre developed (figures 3.5, 3.6). The airlock minimises exposure of breath VOCs and CO<sub>2</sub> during trials as they are loaded into the chamber by robotising the initial stimulation required to initiate flight.

Instead of blowing or tapping the mosquito to start a measurement, the specimen cartridge containing the mosquito is loaded into the chamber side (figure 3.3a). The card is then removed manually (figure 3.3b), whilst the exterior airlock gate is open (figure 3.3d). The mosquito can then fly past the exterior airlock, and is prevented from entering the chamber by the closed interior airlock gate (figure 3.4a). The exterior gate can then be closed (figure 3.3d), securing the mosquito within the airlock. At this stage, the acoustic plug is secured over the chambers entry port (figure 3.8), such that the chamber interior remains insulated from ambient noise.



**Figure 3.5** –Control Centre allows monitoring of the chamber environmental sensors and displays status of chamber controls

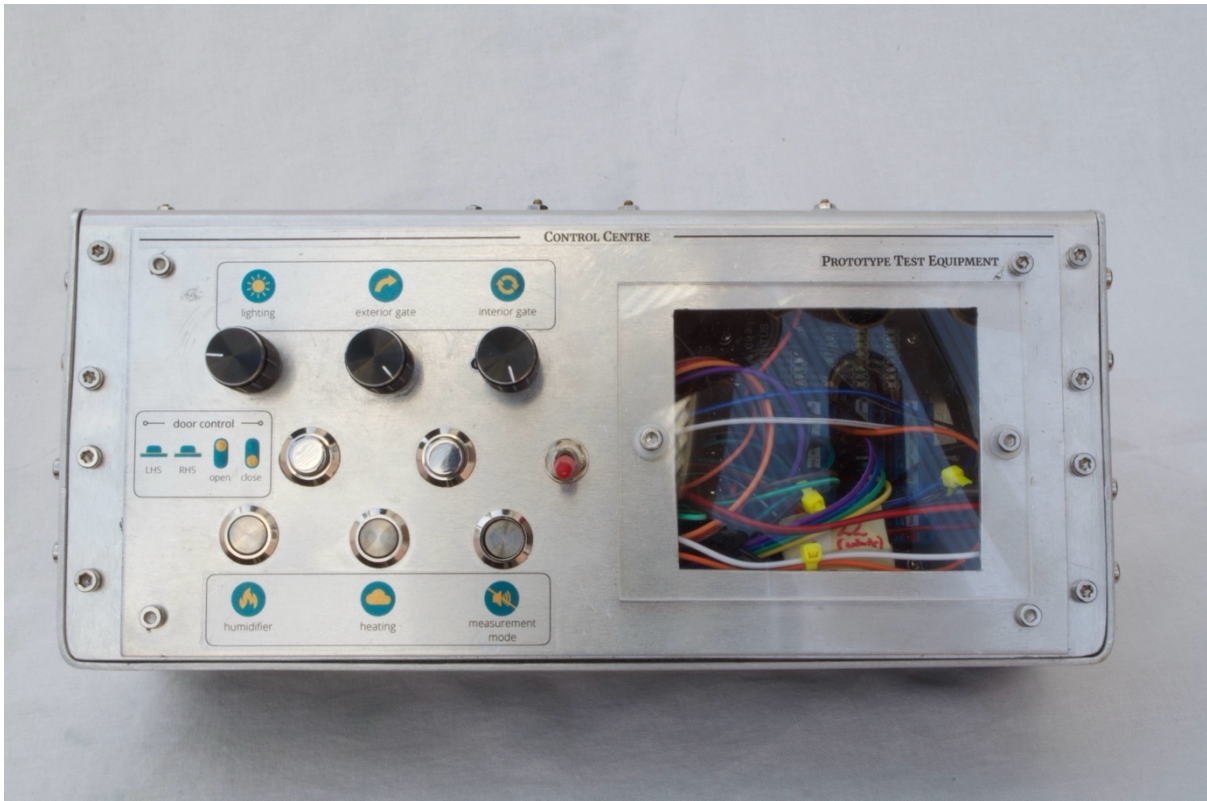


Figure 3.6 – Control Centre switchgear

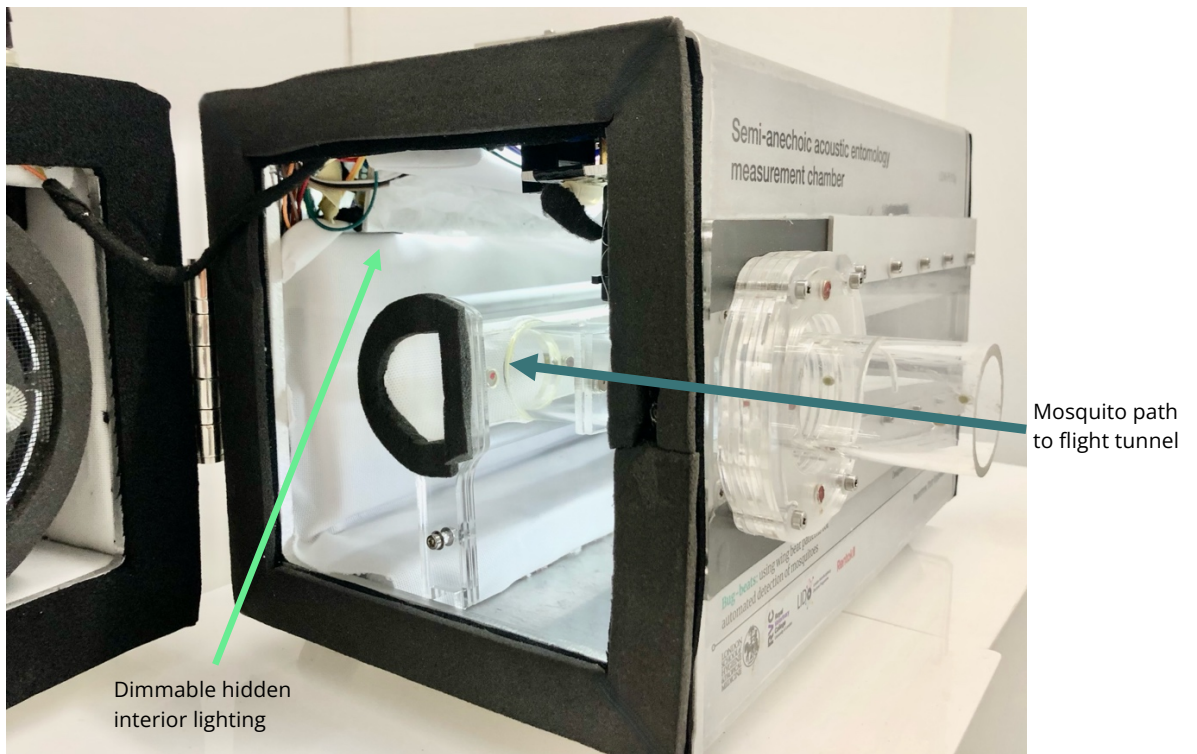
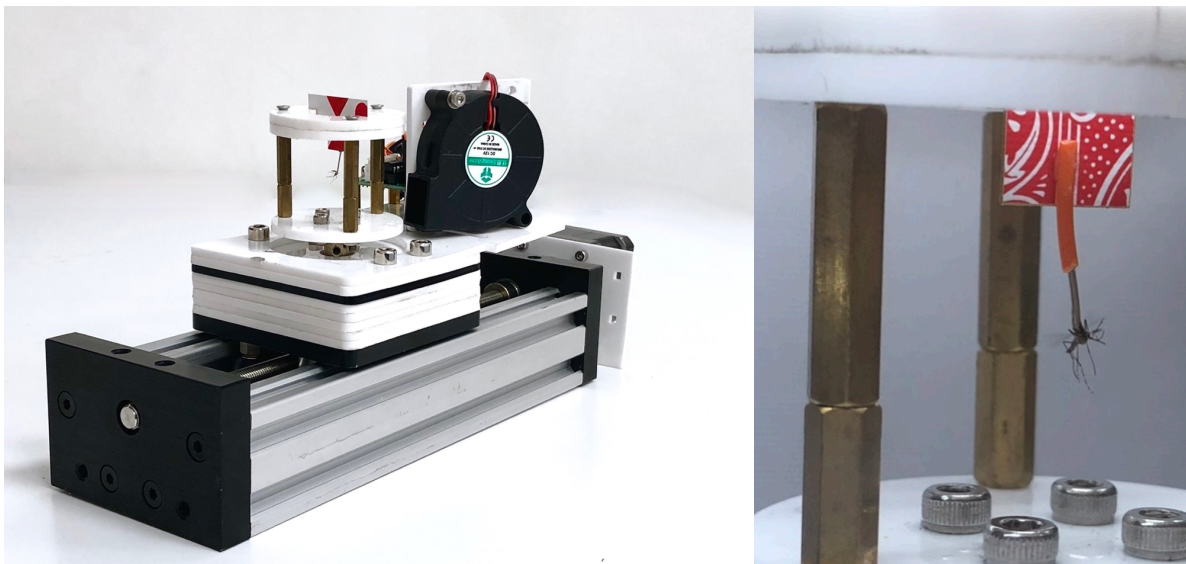


Figure 3.7 – Interior view showing mosquito entry to flight tunnel, following opening of interior “airlock” (Ø40 tunnel shown installed)



**Figure 3.8** – Exterior view showing acoustic plug in place, secured before opening interior airlock gate

### 3.3.2 – SEMI-ANECHOIC MEASUREMENT CHAMBER - TETHERED- FLIGHT



**Figure 3.9a (left), 3.9b (right)** – **a)** Linear actuator with rotary platform to allow 150 mm linear positioning of tethered mosquito combined with 360° rotation. **b)** Rotary cage with tethered mosquito

For conducting measurements with precise position control, the mosquito positioning tool was developed (figure 3.9a). It is swapped with the acoustically transparent flight tunnel (figure 3.10) and installed into the chamber in its place.

Tethering mosquitoes has been used across numerous studies to measure mosquito acoustics whilst keeping them in a fixed location. A wide range of tether types have been developed, with insect pins or human hair used as tethers, whilst glues have included Nailene glue or super glue (Cator et al., 2010; Villarreal et al., 2017b). Here, 24 awg solid core wire was used with a high-tack, non-toxic glue (TECHNOMELT PS 8668, Henkel AG & Co. KGaA, Düsseldorf, DE) to tether mosquitoes to a card placed within the rotary cage (figure 3.9b). Using solid core wire prevented twisting of the tethered mosquito, facilitated by the high contact surface area patch between the mosquito scutellum and the wire.

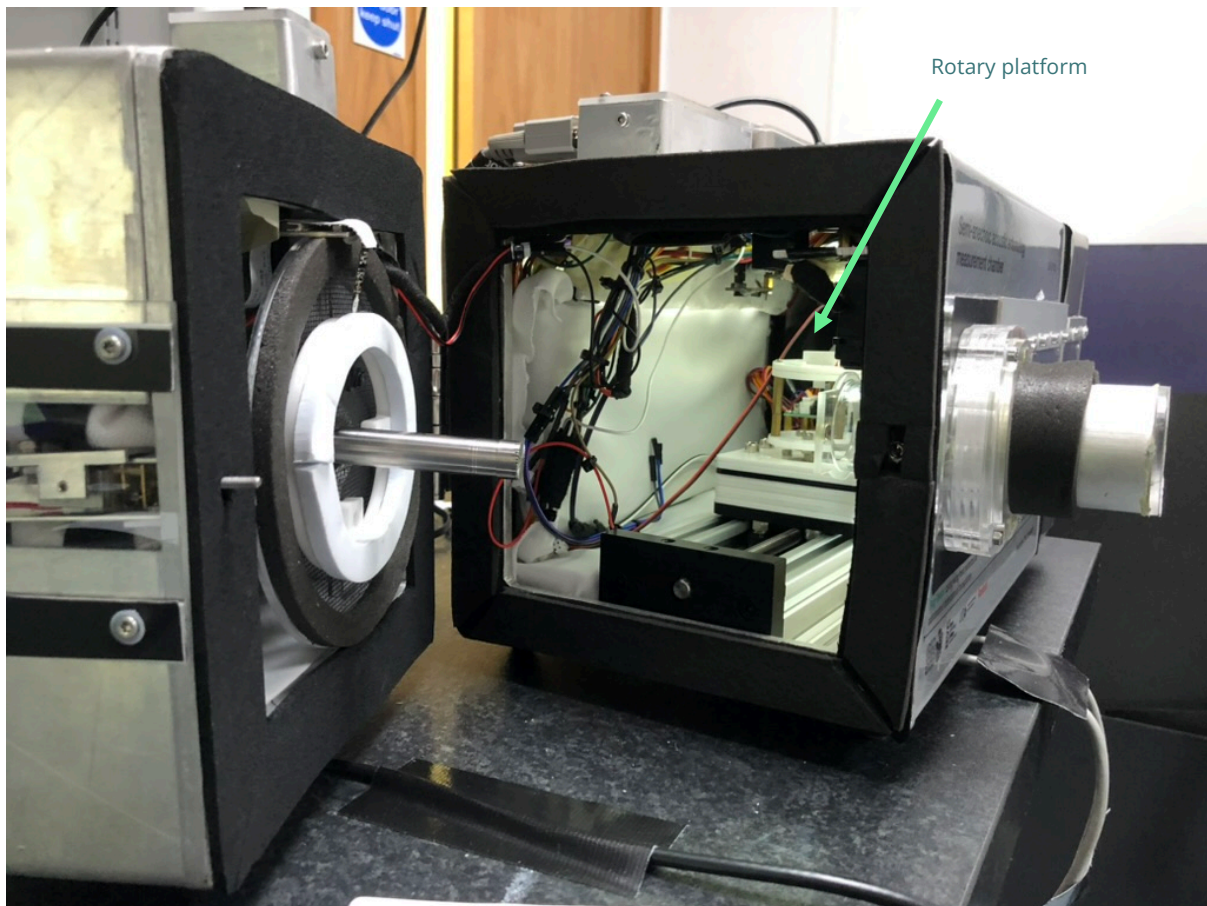


**Figure 3.10** - Mosquito positioning tool installed in the chamber



**Figure 3.11a (left), 3.11b (right) – a** , overview of the Position Controller, **b**) detail view of the PU13g-890 user interface for programming the distance and angle

A controller (Position Controller) was designed and developed, to control the mosquito distance and azimuth angle relative to the microphone (figures 3.10, 3.10b). This device allowed angle to be stepped in  $5^\circ$  increments, and distance to be set from 5mm to 120mm in 5mm increments, from the LHS microphone. All control is done remotely, with the chamber door closed. Figure 3.12 illustrates mosquito orientation relative to the microphone during distance measurements, and figure 3.13 illustrates angular frame of reference used for angle measurements.

The two control units developed (with internal Raspberry Pi devices) were adapted to run off a 12V battery pack such that the DC power source did not introduce 50 Hz mains interference. It was found that running the control units off a mains supply using a standard AC/DC switching power supply introduced electrical noise into the chamber, decreasing the signal-noise ratio of measurements.

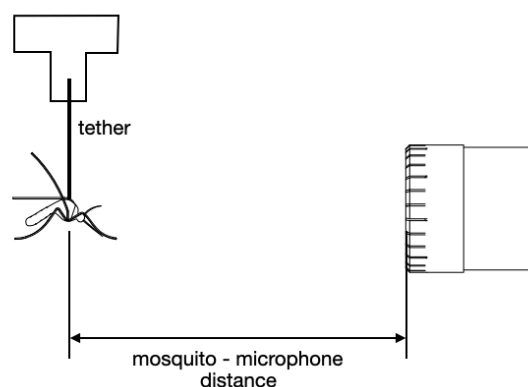


**Figure 3.12** – 5-120 mm distances measured (30 mm, side view shown).

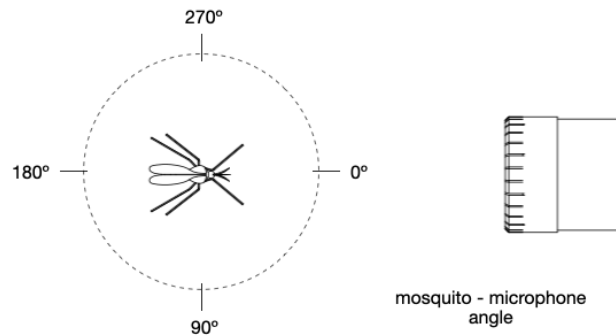


**Figure 3.13** – Angular reference frame used (30 mm, 0°, top view shown)

### 3.3.3 – VARIABLE ASPIRATOR VN-11B

In order to further minimise the effects of physical mosquito handling and damage identified during when using the previously developed aspirator (VN-11a, figure 2.10, section 2.3.2), due to its high airflow, a variable-speed aspirator was designed [VN-11b] (figure 3.14).



**Figure 3.14** – VN-11b Variable Aspirator



**Figure 3.15 (a-c)** – *left to right*. **a)** Detachable magnetic nozzle, **b)** nozzle removed with cartridge installed, **c)** VN-11b speed control dial and power button shown with screen to display fan power %

Using this device allowed for gentle & repeatable collection of mosquitoes from their cages, greatly minimising damage risk to mosquitoes and their wings during collection. This approach also eliminated exposure to breath VOCs which can occur with mouth aspiration techniques.

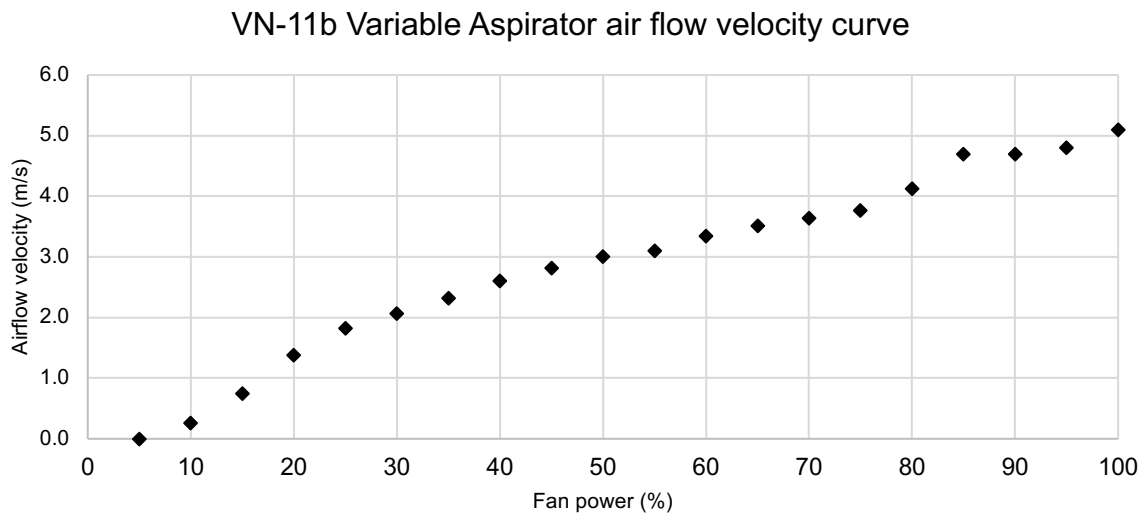


**Figure 3.16** - Performance curve for the VN-11b

A simple validation was undertaken using a hot-wire anemometer which measured airflow velocity at the aspirator nozzle, with a loaded specimen cartridge. Maximum airflow velocity was measured at 5.10 m/s at 100% fan power. Preliminary testing found an airflow of above 60-70% (3.34 – 3.64 m/s) to be sufficient to sample a mosquito at rest in a cloth sided rearing cage

## 3.3.4 – EQUIPMENT SUMMARY

The developed equipment described above met the design requirements necessary to conduct measurements of mosquitoes in free-flight or tethered conditions in a semi-anechoic arena whilst remaining transportable to any test facility or field site.

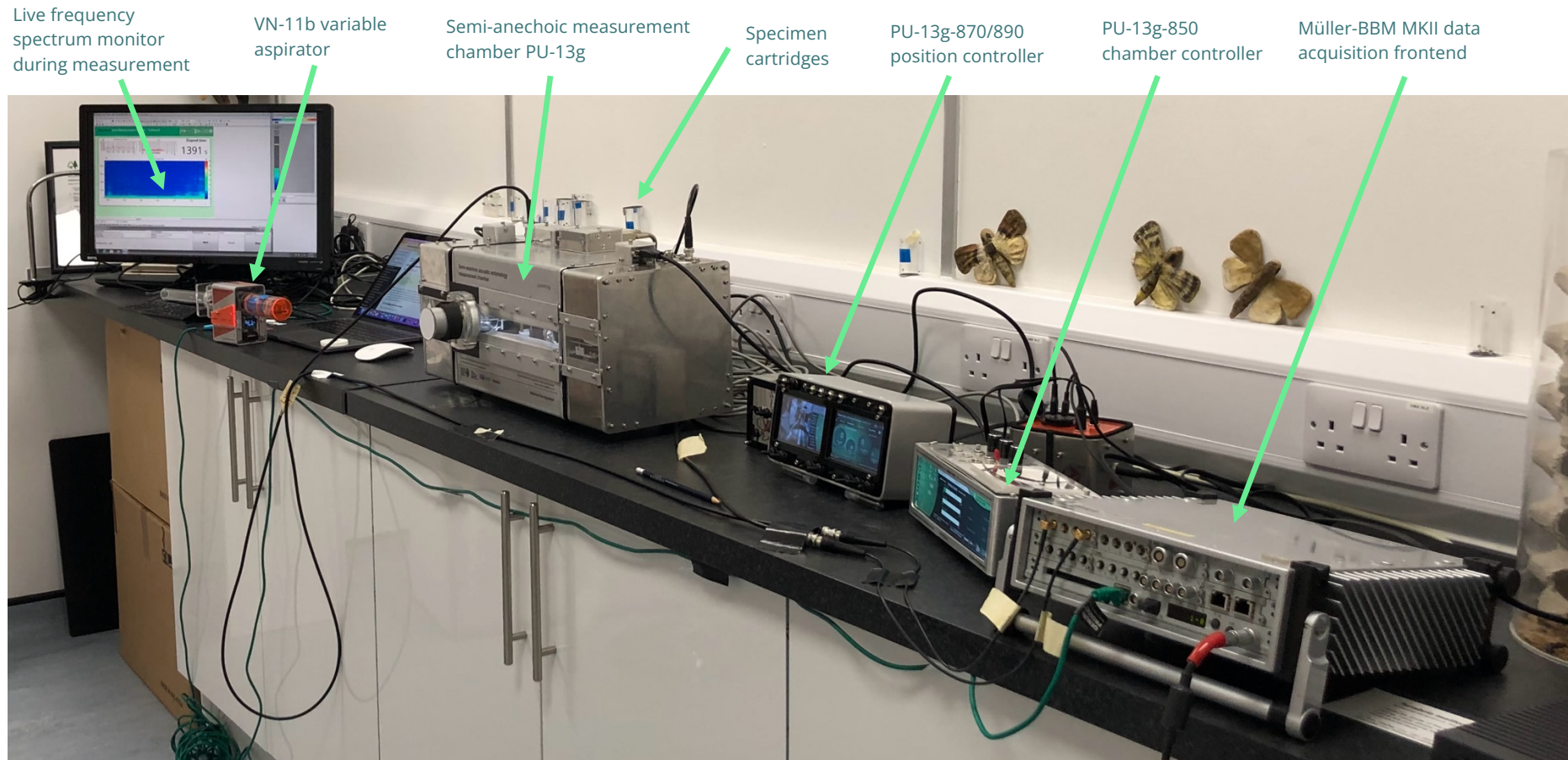


**Figure 3.17** – Overall equipment setup, for both free-flight and tethered measurements

## 3.4 Developing a tethered flight method

### 3.4.1 – AIRFLOW BASED TETHERING

Tethering requires mosquito anaesthesia, which is routinely performed using either CO<sub>2</sub> or ice (Attisano et al., 2015; Pantoja-Sánchez et al., 2022). With both approaches, a recovery time is needed before the mosquito can be used for a flight test, however the use of CO<sub>2</sub> has been demonstrated to alter flight behaviour of *Drosophila melanogaster* following exposures of only 5 minutes (Bartholomew et al., 2015). Given the ability of the VN-11b aspirator to create gentle airflows that can restrict motion (figure 3.16), an alternative approach was taken to mount insects to the tether that did not require anaesthesia.

Once a mosquito was collected, the specimen cartridge was removed from the aspirator. The cartridge was then placed directly over the aspirator entry port (figure 3.20[a]) and the aspirator was set to 50% power. This would cause the mosquito to be drawn into the cartridge lid mesh (ADFORS Saint-Gobain, Albion NY, USA) with the airflow sufficient (c.a 4.5 m/s) to prevent the mosquito from moving on this surface. The main cartridge body was then removed (figure 3.20[b]), providing access to mount the tether to the mosquito. Adhesive glue boards from an ultra-violet light trap (Rentokil-Initial PLC, Crawley, UK) were used as a source of tacky, non-toxic glue (TECHNOMELT PS 8668, Henkel AG & Co. KGaA, Düsseldorf, DE) applied to the tether. The tether itself was a strand of solid core 24 awg wire, affixed to a card with a cyanoacrylate based adhesive. With the mosquito held in place, the wire strand with a small sphere of fly paper glue at its base, was lowered onto the mosquito scutellum (figure 3.19, 3.20[c]) and the mosquito was installed into the positioning cage (figure 3.18)

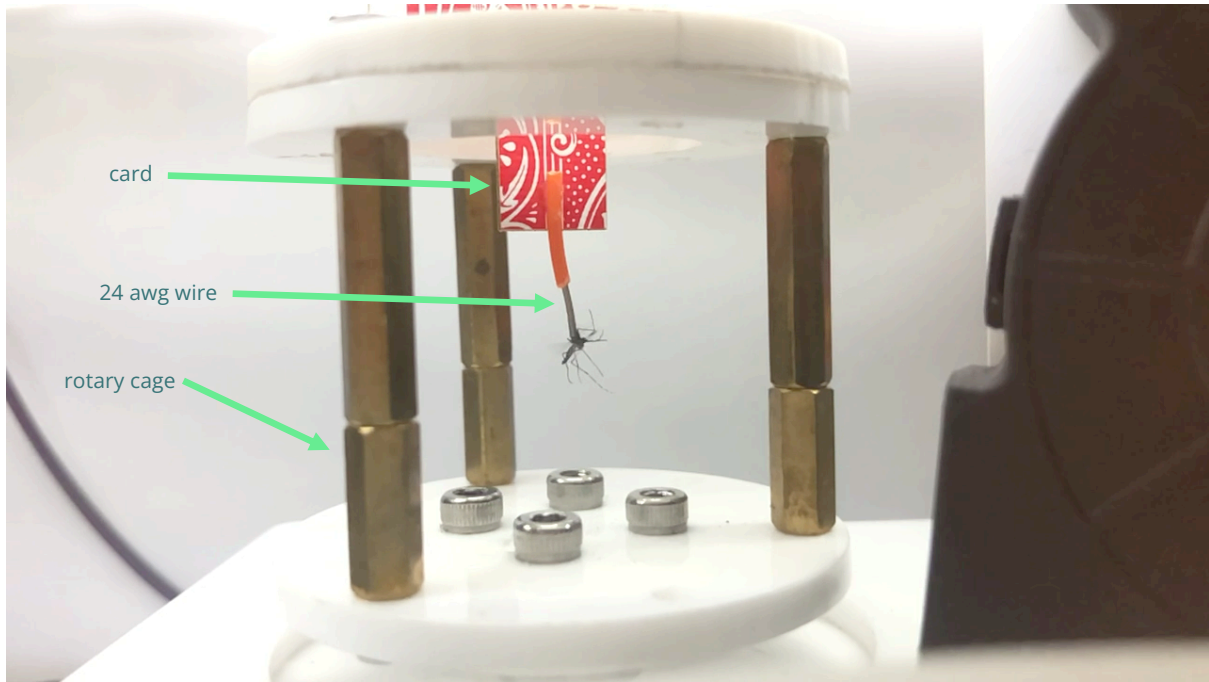


**Figure 3.18** – Mounting of a tethered mosquito



**Figure 3.19** – Detail view of tether position (*Aedes aegypti* female shown)

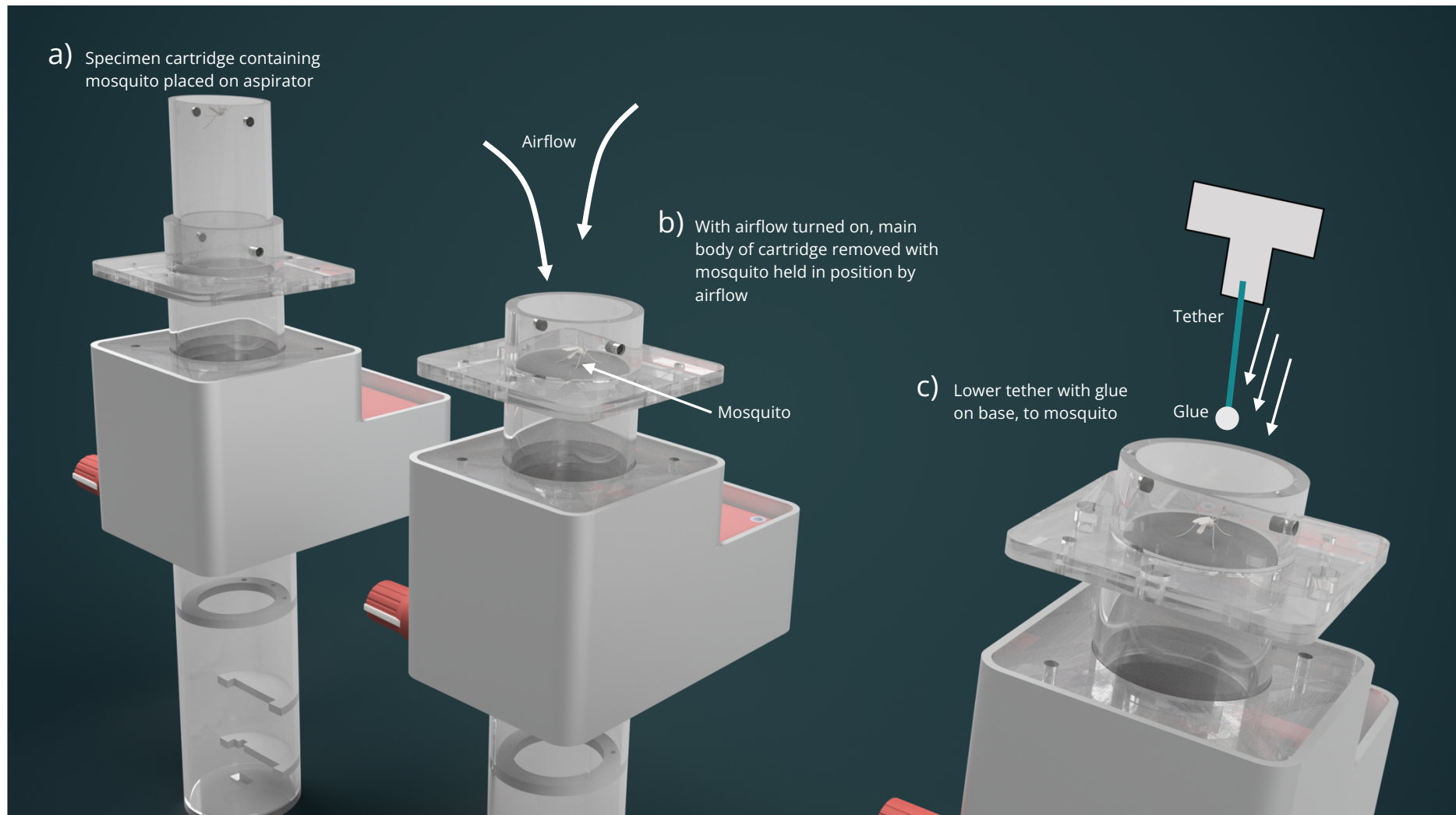


**Figure 3.20** – Three stages to the airflow mosquito tethering method

### 3.4.2 – PRELIMINARY EVALUATION OF THE EFFECT OF DISTANCE ON MOSQUITO ACOUSTICS

An investigation was undertaken using the positioning tool to evaluate the effect of distance on measured sound amplitudes of the frequency spectra produced by a tethered female *Ae. aegypti* mosquito. Ten measurement positions were evaluated per specimen between 5-120 mm in a randomised order, with a 20 second measurement taking place at each measurement distance. The chamber remained closed across all distance measurements, eliminating physical contact during mosquito repositioning. The mosquito angle relative to the microphone was kept at 0°, such that it was always oriented flying towards the measurement microphone.

Data were captured in the same manner as Chapter 2, using the MKII front end together with PAK 5.8 software suite. The GRAS 46AE measurement microphone was calibrated and its sensitivity verified at the start of every measurement day. Following data capture, a shared data processing workflow between PAK 5.8 and custom Python scripts using the `plotly` and `scipy` libraries allowed data to be visualised and analysed. A peak finder Python script was created to automatically detect frequency peaks to the 4<sup>th</sup> harmonic.

#### *Results of preliminary distance evaluation*

**Table 3.1**– Summary of frequency content across all distances measured

frequency	mean (Hz)	median (Hz)	standard deviation (Hz)	IQR (Hz)
fundamental	549.9	550.4	59.0	84.6
2nd harmonic	1096.7	1100.8	120.0	162.6
3rd harmonic	1653.2	1652.7	171.4	239.7
4th harmonic	2212.5	2214.8	237.0	314.2

Mean fundamental frequency across all mosquitoes measured (n=16) was 549.9 Hz (SD = 59.0 Hz). Amplitudes of fundamental and harmonics reduced with distance from the microphone (figure 3.22), with the fundamental remaining

highest across all distances. The order of amplitudes relative to each other for the fundamental and harmonics, was consistent, with the 3<sup>rd</sup> harmonic exhibiting a higher amplitude than the 2<sup>nd</sup> across all distances (figure 3.23c).

Figure 3.21 shows an example of initial spectrograms for a single mosquito measured across all 10 distances. The wingbeat frequency, harmonics and respective amplitudes are then identified with the peak identifier script, shown in figure 3.22.

Figures 3.23 shows the summarised amplitudes captured across all the tested distances. Amplitude of the fundamental and their harmonics are shown across the 10 evaluated distances.

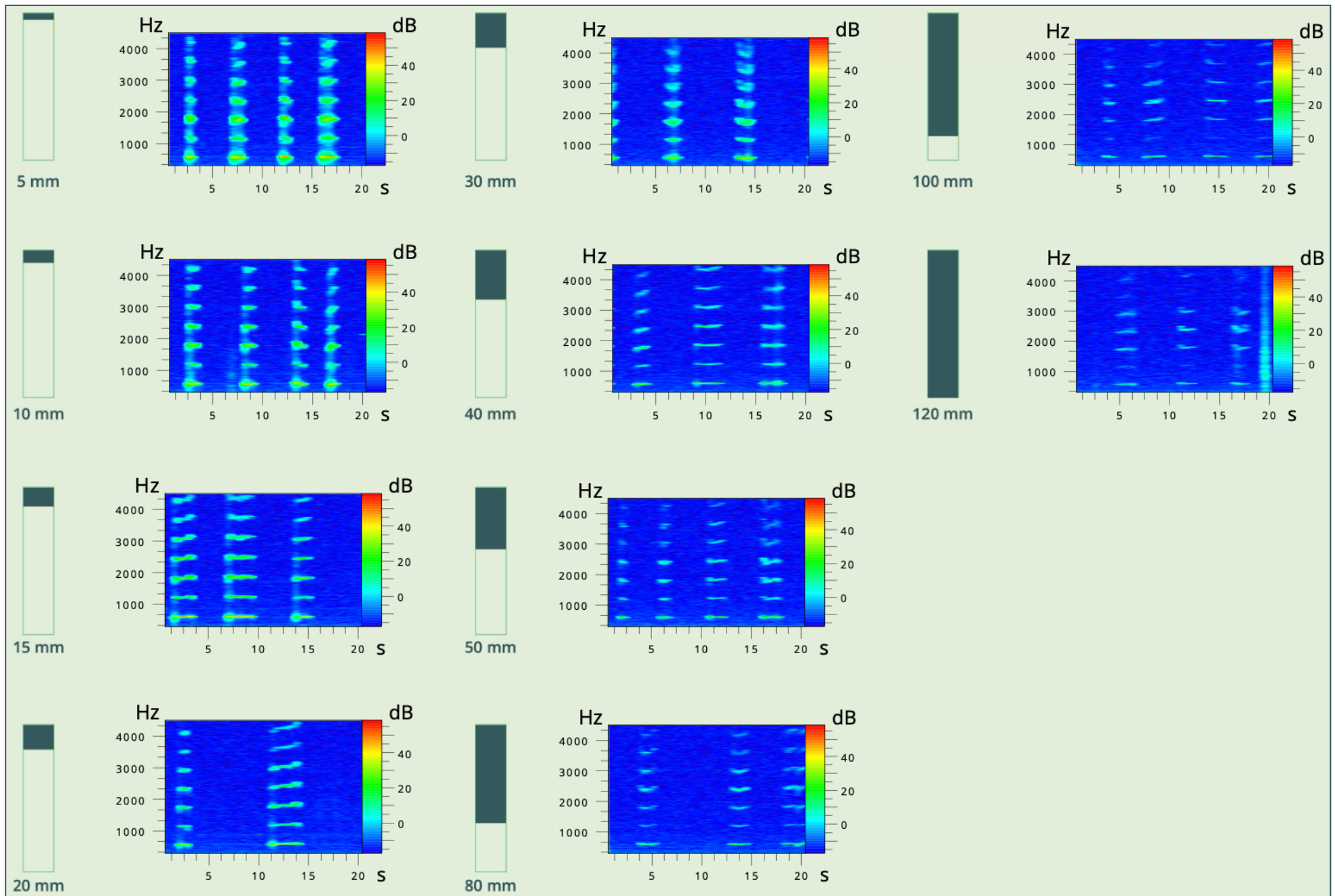
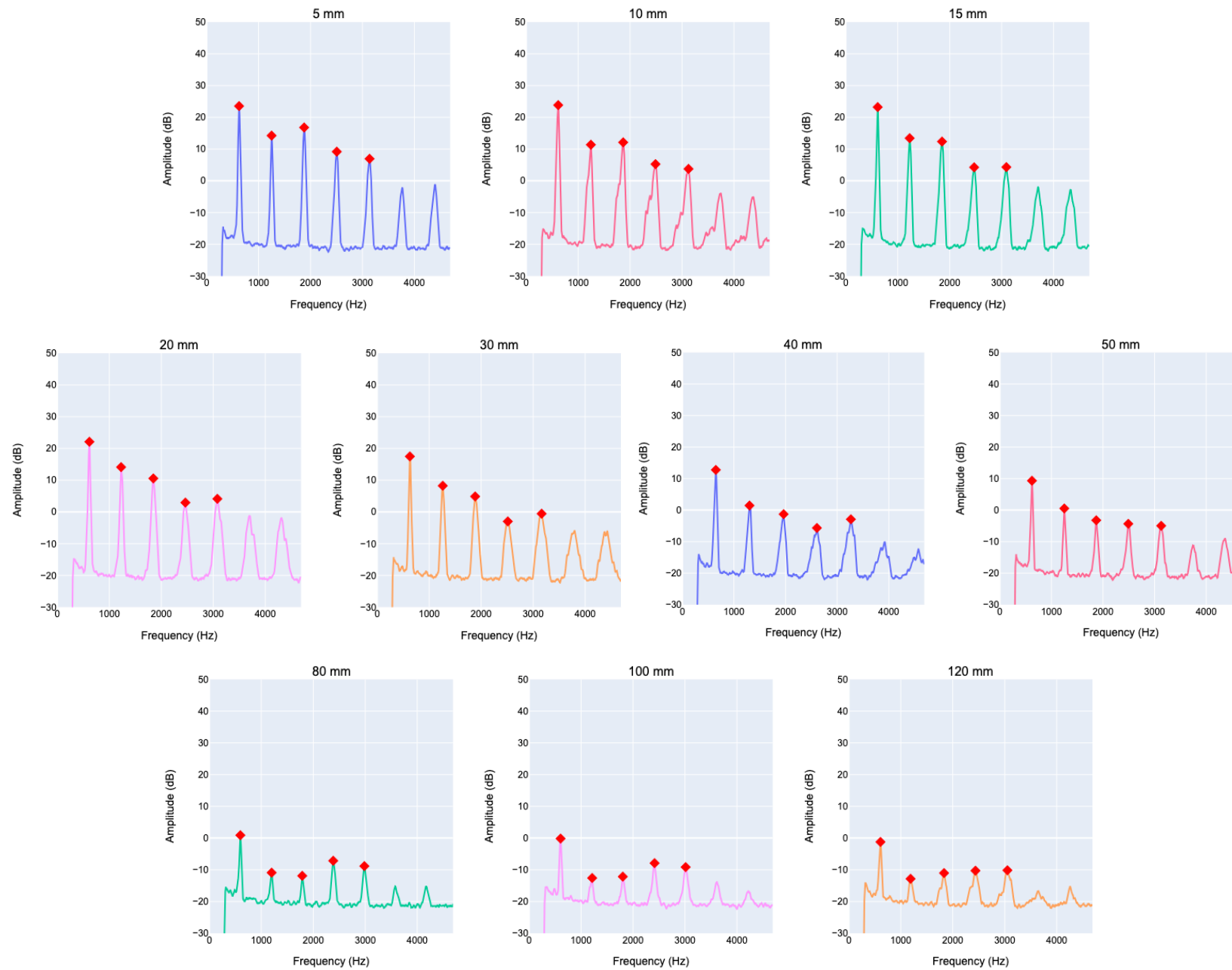
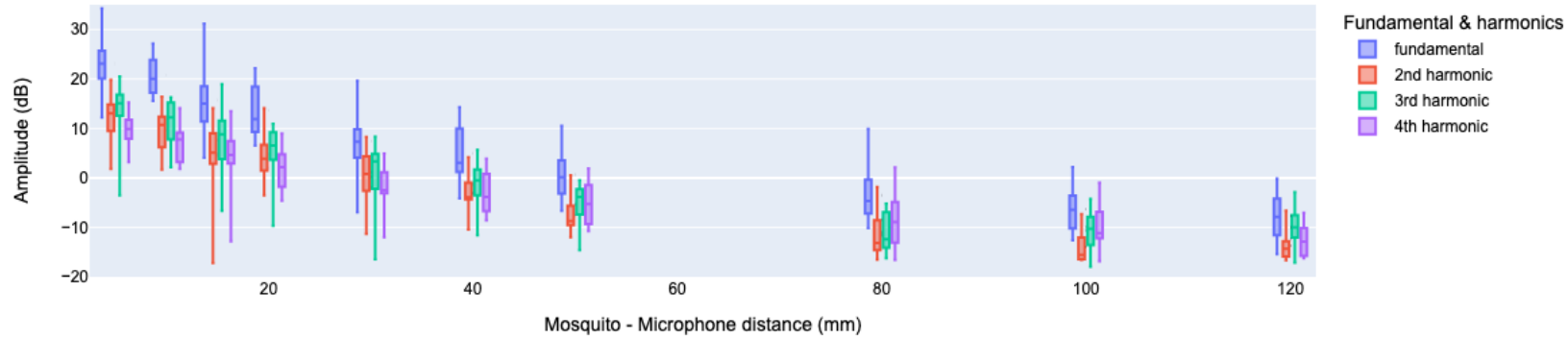


Figure 3.21 – Individual spectrograms for tethered *Ae. aegypti* at each measured distance (5-120mm)

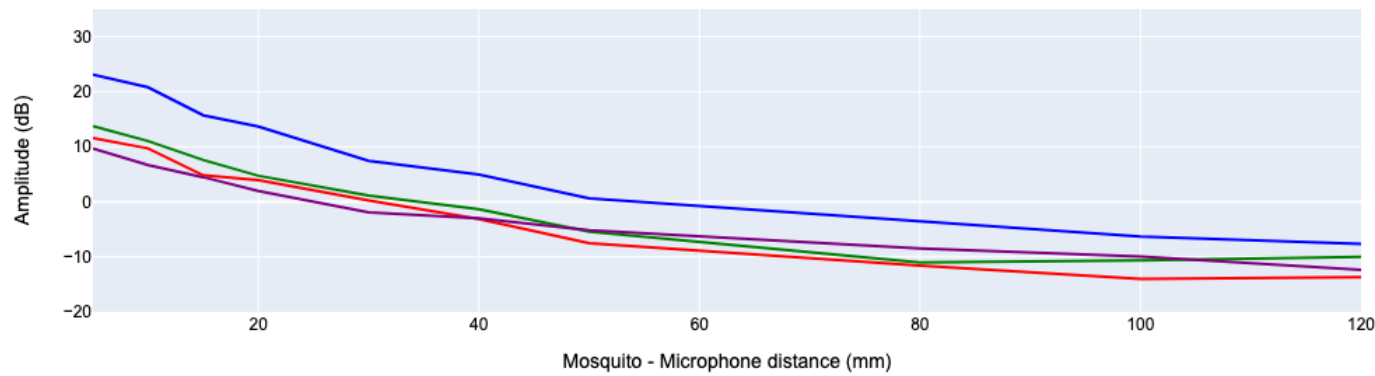


**Figure 3.22** -Example frequency spectra and amplitudes of tethered individual *Aedes aegypti* mosquito, with increasing microphone-mosquito distances. Automated peak finder script shows fundamental and harmonics and amplitudes identified.

Fundamental & harmonic amplitudes for *Aedes aegypti* by microphone distance : 5 mm to 120 mm



Mean amplitudes for *Aedes aegypti* by microphone distance : 5 mm to 120 mm



Fundamental & harmonic summarised amplitudes 5 mm to 120 mm

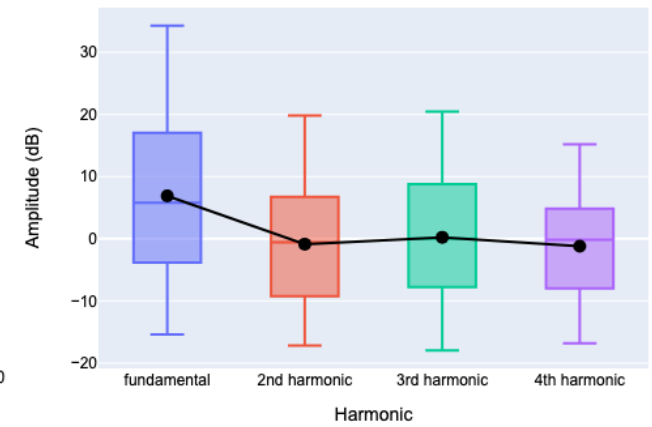


**Figure 3.23 (a-c)** - Summary of fundamental and harmonic amplitudes for tethered *Aedes aegypti* for 5-120 mm microphone-mosquito distances. *Top* (a) frequency amplitudes including spread, *bottom left* (b) means of frequency content, *bottom right* (c), summarised frequency content for all distances with mean amplitude line

### 3.4.3 – PRELIMINARY EVALUATION OF ANGLE ON MEASURED MOSQUITO ACOUSTICS

An investigation was undertaken using the positioning tool to evaluate the effect of angle on measured sound amplitudes of the frequency spectra produced by a tethered female *Aedes aegypti* mosquito. The developed apparatus permitted the microphone to mosquito angle to be changed in 30° increments from 0° to 330°. 12 measurement positions were evaluated per specimen in a randomised order, with a 20 second measurement taking place at each measurement distance.

The chamber remained closed across all distance and angle measurements, with all repositioning performed remotely via the Position Controller (figure 3.11). The mosquito angle relative to the microphone was checked at 0°, such that it was always oriented flying towards the measurement microphone, before repositioning the angle as required using the rotary posting tool. All angle measurements were taken at a distance of 30 mm from the microphone.

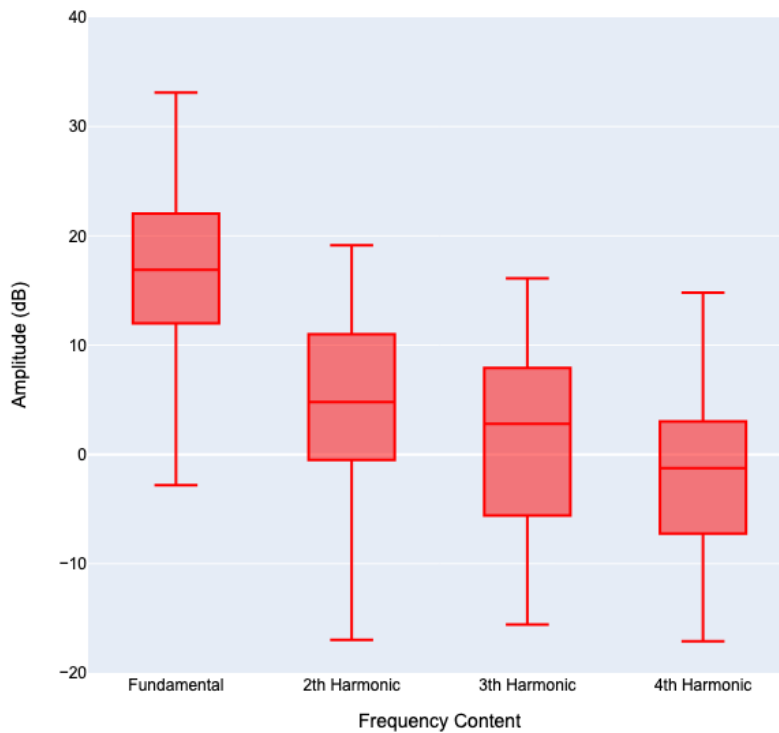
Data was captured in the same manner as section 3.4.2, with a further set of custom Python scripts being used for data comparison and visualisation using the Plotly and scipy libraries.

#### *Results of preliminary angle evaluation*

Table 3.2 shows the fundamental frequency and harmonics across all 12 angles measured.

**Table 3.2** – Summary of frequencies across all angles measured

Frequency	mean	median	standard deviation	IQR
fundamental	514.7	532.5	51.2	49.4
2nd harmonic	1053.0	1068.6	78.6	39.4
3rd harmonic	1616.3	1620.9	71.3	38.8
4th harmonic	2158.9	2161.7	85.7	42.1

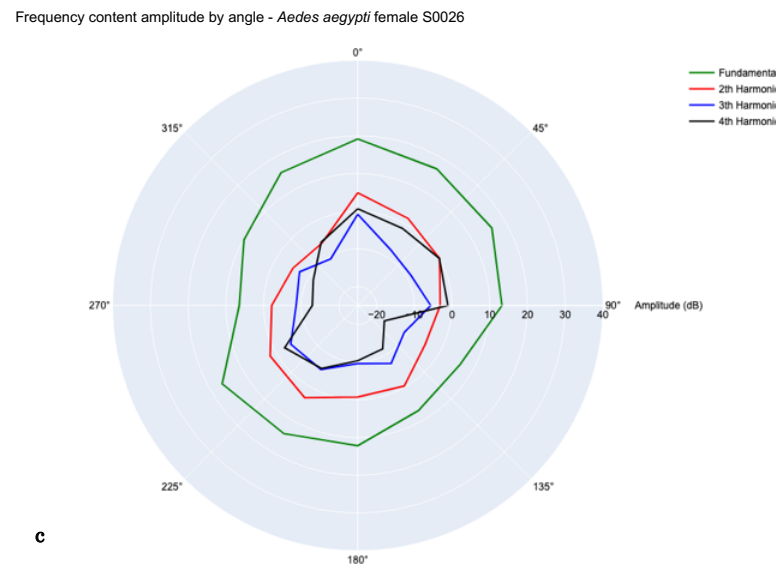
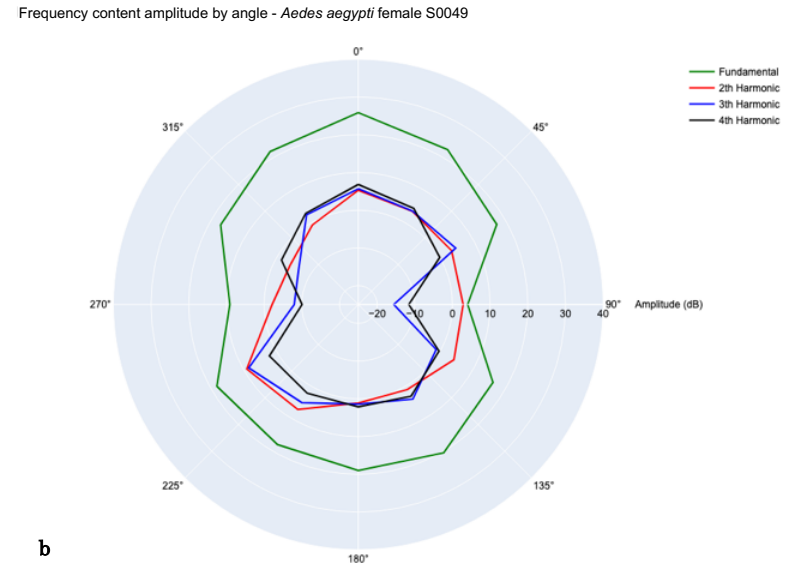
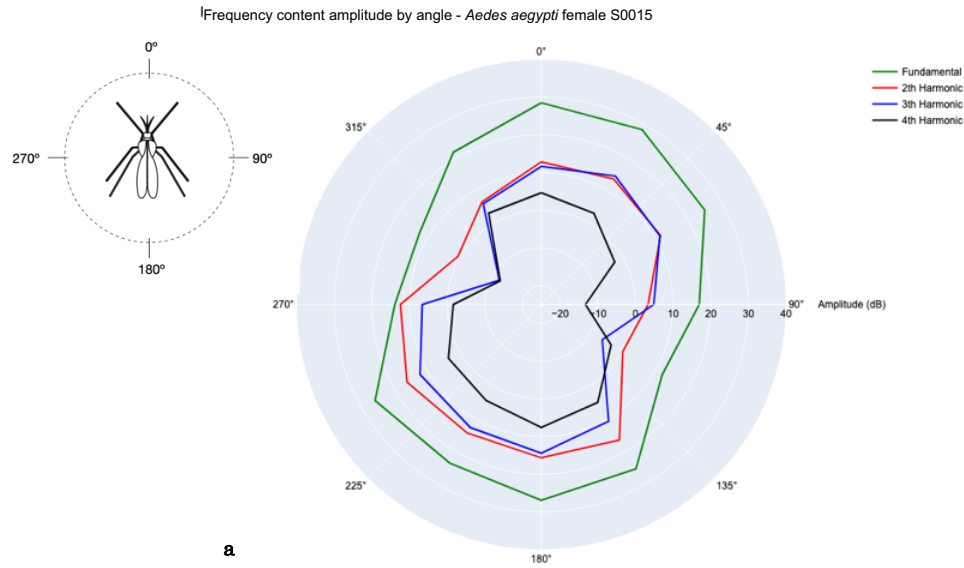


**Figures 3.24** – Summary of fundamental frequency and harmonic amplitudes across all measured angles

Figure 3.24 shows the combined amplitudes for the fundamental frequency and harmonics across all 12 angles measured, with corresponding frequency data in table 3.2.

Mean fundamental frequency across all individual measurements ( $n=60$ ) for all angles was 514.7 Hz (SD = 51.2 Hz) across all measured *Aedes aegypti* female mosquitoes ( $n=5$ ). Across all angles, the fundamental exhibited the highest mean amplitude of 16.7 dB (SD = 7.9 dB), and the 4<sup>th</sup> harmonic exhibited the lowest amplitude of -2.0 dB (SD = 7.2 dB).

Example radar plots of the amplitudes of the fundamental frequency and harmonics are shown in figure 3.25. These are for individual specimens, selected as examples with clear directivity patterns (3.25a, 3.25b) and less clear patterns (3.25c, 3.25d).



**Figures 3.25 a-d** – Measured fundamental and harmonic directivity patterns for four female individuals.

### 3.4.4 – DISCUSSION OF THE TETHERED DISTANCE AND ANGLE MEASUREMENTS

#### *Workflow*

The airflow tethering method successfully provided an asphyxiation-free approach to mosquito tethering. This permitted flight recording to take place without the risk of asphyxiation induced side-effects in the tethered mosquito. The semi-anechoic chamber provided a controlled acoustic sound-field, which greatly attenuated laboratory background noise. No background-noise compensation was required, with a 300 Hz high-pass filter being applied to all measurements to account for 50 Hz and (associate harmonics) mains interference.

#### *Flight tones - amplitudes*

Figure 3.23c illustrates a mean comparison of amplitudes of the fundamental and harmonics, which exhibits a differing ranking of amplitudes to that described using the acrylic tunnels. Here, the fundamental always features the highest amplitude, followed by the 3<sup>rd</sup> and then 2<sup>nd</sup> harmonic. In contrast, the measurements taken in the plastic tunnels in chapter 2 showed the 2<sup>nd</sup> or 3<sup>rd</sup> harmonics as having highest amplitude, and the fundamental was the lowest amplitude (figure 2.17). The differences between harmonic amplitudes under the tethered, semi-anechoic conditions here, was greater and therefore simpler to identify at closer distances (figure 3.23a).

The methodology of angle measurement used, was hindered by a slow setup time, and limitations with the adhesive. It was noted that during the measurements, the tacky and non-hardening nature of the tether adhesive used meant that the mosquito was able to twist along its tethered axis. As the mosquito angle was changed (which took c.a. 30-60s), the mosquito twisting resulted with inaccurate angular positioning. During rotation their visual environment would also change, as this was not uniform within the chamber, which may have caused the twisting

to occur as the mosquitoes would reorient their flight towards the same visual cue within the chamber.

This did not always occur however, allowing for measurements illustrated by figures 3.25a and 3.25b to be collected, which represent the characteristic dipole directionality which has been simulated for *Cx quinquefasciatus* (Bomphrey et al., 2022; Seo et al., 2020). However, figures 3.25c and 3.25d show less clear directivity patterns because the measurements were effectively averaged as the mosquito twisted in azimuth on the tether during recordings.

This simple description of mosquito fundamental and harmonic amplitudes varying with the angle of the observer microphone demonstrates empirically how physical factors can influence acoustic measurements. This result is also highly relevant to mating behaviour in swarms, where males locate females using their acoustic signature. From the wider perspective of obtaining repeatable acoustic descriptions, the angle must be controlled to ensure a repeatable relationship between the amplitude of fundamental and harmonics.

#### *Flight tones - frequencies*

The frequencies measured across all angles and distances featured mean fundamental frequencies at 594.9 Hz and 514.7 Hz respectively, with standard deviations of 59.0 Hz and 51.2 Hz. Frequencies were reflective of a 3s analysis period during the 20s measurement, that was manually selected from the individual spectrograms generated for each specimen (figure 3.21). As a result, frequency variation captured by the standard deviation represents variation between individuals, but it does not capture variation within individual mosquitoes.

### *Sound fields and measured quantities*

Using 5 - 120mm measurement distances, the sound field for the tethered measurements was within the near-field. This is for the fundamental frequency ranges previously described for the three species between 460 – 580 Hz (Chapter 2, table 2.3). At these frequencies, wavelengths are between 750 – 600 mm , using equation 3.1 (Serway, 2014).

(3.1)

$$\lambda = \frac{c}{f}$$

$\lambda$  = wavelength (m),  $c$  = speed of sound in medium (m/s) ,  $f$  = frequency (Hz)

Taking measurements in the near-field facilitates acquisition of high signal-noise ratio signals, as shown by the measurements captured earlier in this Chapter. However, accuracy in tethered mosquito positioning is required when working in the near-field to ensure that the mosquitoes are repeatably in the same location relative to the measurement microphone. This is due to the sound pressure level varying significantly by position in the near-field, in a manner that is more unpredictable than when in the far-field. In the far-field, expected sound pressure level will halve (6dB drop) by doubling distance (Brüel & Kjær, 1984).

A significant constraint in the development of the measurement arena, was portability, due to the COVID restrictions (section 3.1). The semi-anechoic measurement arena needed to be small enough to transport, and this meant that a chamber that could provide free-field conditions would require a mosquito – microphone distance of c.a. 750mm (at 580 Hz), which would not be feasible to transport. What the measurements here demonstrate however, is that the positional controller and tether method, facilitated accurate positioning of the tethered mosquitoes relative to the measurement microphones enabling consistent sound pressure levels to be captured for both the distance and angular measurements (sections 3.4.2, 3.4.3).

Another consideration of working in the near-field, was the acquisition of sound pressure, over particle velocity. As discussed in Chapter 1, particle velocity (vector quantity), has been used to describe insect flight tones in the literature in addition to sound pressure (scalar quantity). In the near-field, the relationship between sound pressure and particle velocity is  $90^\circ$  out of phase. Since sound pressure and particle velocity are related (equation 3.2), when they are  $90^\circ$  out of phase, this will have the effect when multiplied together, of giving a time-averaged sound intensity of zero (Brüel & Kjær, 1984).

(3.2)

$$\text{sound intensity} = \text{sound pressure} \times \text{particle velocity}$$

If exclusively particle velocity were to be measured in the near field, which is a reactive sound field, it would be expected that high particle velocities would be recorded, whilst their intensity would be very low. This is since the air particle vibration would be acting as a mass-spring system and *storing* energy rather than propagating it, as it otherwise would in the active far-field (Brüel & Kjær, 1986, 1984, 1982). Sound pressure on the other hand, would offer comparably lower levels in the near-field (Fernández Comesaña et al., 2014), which provides particle velocity approaches with a strong advantage. However in this specific use case, where background noise is already strongly attenuated by the semi-anechoic chamber, and mosquito position is accurately and repeatably controlled, the simplicity afforded by a sound pressure level measurement approach (in data acquisition and processing) justified its use as the basis for measurements.

The adopted approach using sound pressure level facilitates comparison between mosquitoes whilst under *constant* acoustic conditions. Since the focus of this study is to understand how physiology and morphology affect their acoustic profiles, this will be sufficient. However, to provide acoustic mosquito descriptions which are independent of their acoustic environment, would benefit from also capturing particle velocity.

### *Next steps*

The cause of variation in sound frequency and amplitude within individuals remains undescribed, however the tethering approach lends itself well to describing this in more detail. The reduction of frequency amplitude with distance has been demonstrated, whilst the effects of angle require further methodological refinement with the tether adhesive and changing visual environment to describe it in a more stable way.

Due to the semi-anechoic measurement environment, the measurements no longer require background compensation and a high signal-noise ratio is achieved by frequency descriptions, unlike with the acrylic tunnel-based measurements. This makes processing frequency domain measurements much simpler and time-domain analysis could also be feasible. When conducting comparative studies to explore the effects of morphology and physiology on mosquito acoustics, controlling for angle and distance is important.

## **3.5 The repeatability of tethered flight**

### 3.5.1 – THE ACOUSTIC PROFILE

Our acoustic analysis so far has described frequency and amplitude during a 3s segment of a 20s measurement. This should be expanded in future work to cover a longer measurement period so that temporal variation can be quantified. Since the fundamental frequency amplitude was found to change across the distance and angle measurements, it should be described how much these two metrics can vary by behaviour when the physical setup is held constant.

### 3.5.2 – WHY SHOULD FLIGHT EFFORT BE QUANTIFIED DURING A LONG TIME PERIOD MEASUREMENT?

Do mosquitoes maintain a constant flight tone? When the distance and angle measurements were taken, an assumption was made that the flight tones produced would be constant, across all the different positions measured. With this assumption, observed variation in amplitudes between distance and angles tested, was attributed exclusively to changing the position between the microphone and flapping wings. However, the assumption that the tethered mosquito will continually fly in the same way across all measurements of multiple angles or distances (which can take c.a 30 mins), may not be valid. It is known that for example tethered mosquitoes when flown to exhaustion exhibit alterations in their flight muscles with wingbeat frequency reductions reported (Johnson and Rowley, 1972). Flight exhaustion studies have also demonstrated how mosquitoes are capable of long flights, both in distance and time with 11 km flights lasting upwards of 6 hours reported for *Aedes japonicus* (Krupa et al., 2021).

To quantify potential changes in tethered flight tone across a longer period of time, longer measurements (800s) were recorded 30 mm away, and oriented 0° from the microphone. This served to evaluate the repeatability of using tethered mosquitoes during longer time-periods and to determine whether differences observed from distance and angle measurements were explained by the microphone positions relative to the mosquito, or by changes in the mosquito's behaviour.

Figure 3.26 shows the frequency content variation over time a much longer time period than used in section 3.4. The measured frequency varies continually over time. By analysing the tethered flight tone over a longer time period, it is clear that flight behaviour is not constant, producing different flight tones. Here, periodic rapid rises and slower declines in the wingbeat can be seen.

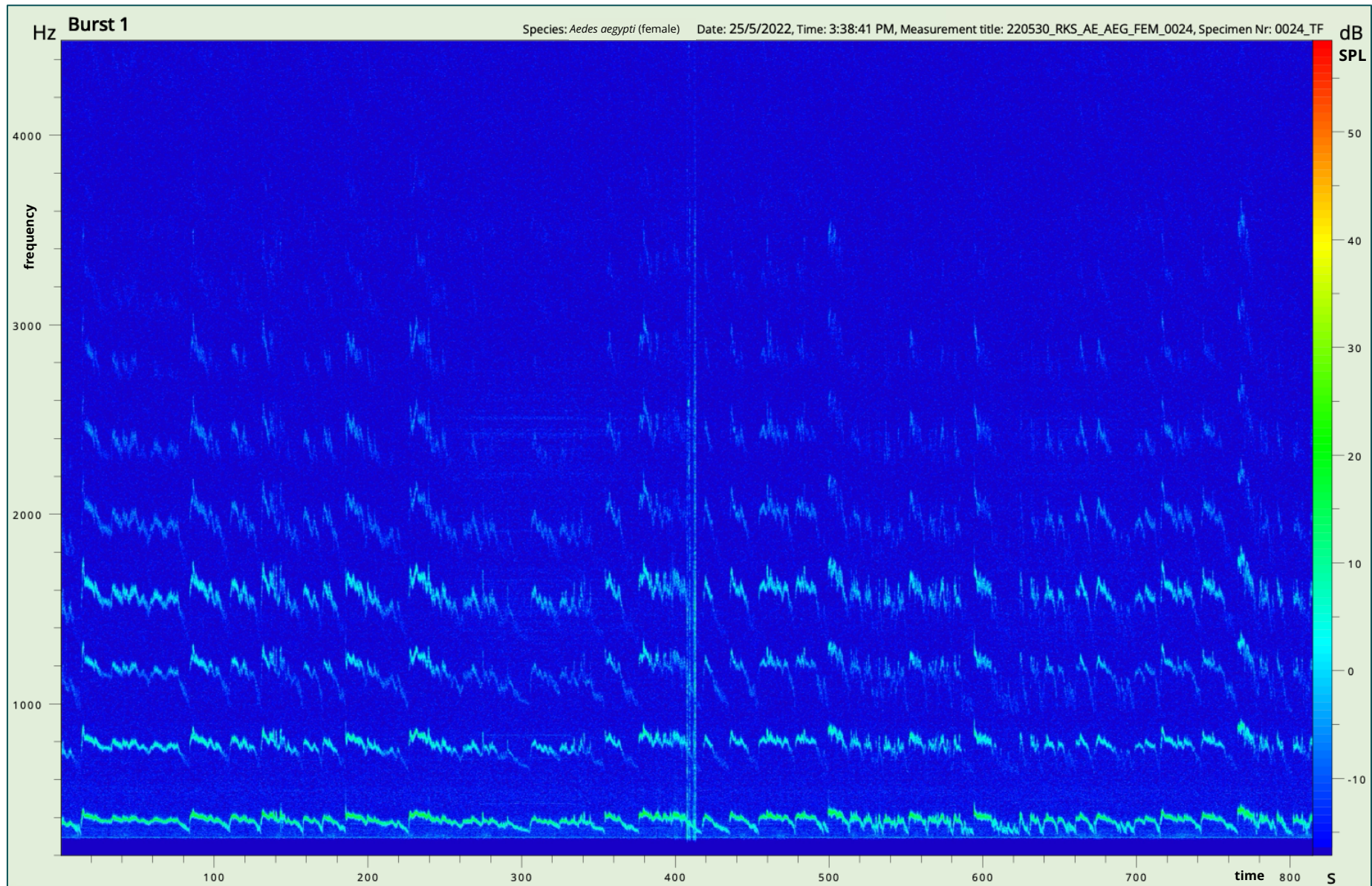
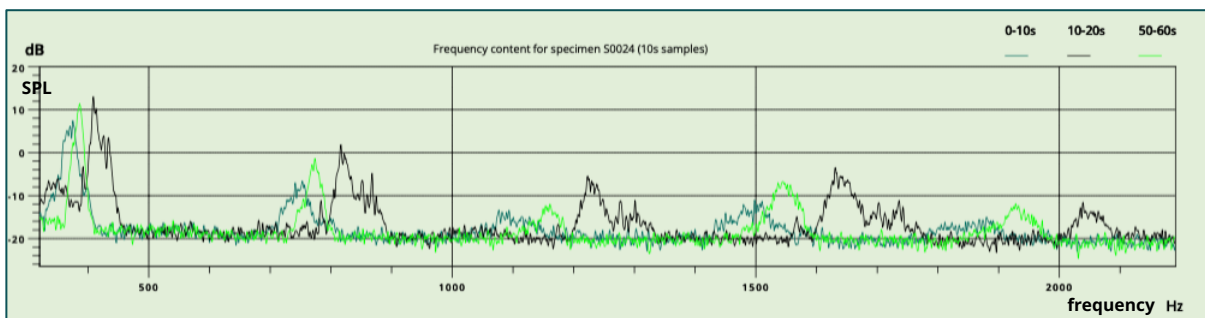


Figure 3.26 – 800s measurement of tethered *Aedes aegypti* female

This illustrates that there is a range in the wingbeat produced when tethered. One individual mosquito is able to produce a range of different fundamental frequencies at different respective amplitudes. This is further illustrated by figure 3.27, which shows snapshots of the frequency content captured during different 10s windows, for the 800s measurement shown in figure 3.26 of *Ae. aegypti*. Understanding the mechanisms that cause this variation, and specifically how to control and compensate for it, will be crucial for any future application that uses frequency and amplitude measurements for an identification application.



**Figure 3.27** – 10s frequency power spectra for *Aedes aegypti* female measurement (specimen represented in figure 3.35)

### 3.5.3 – DEVELOPMENT OF AN ANALYSIS APPROACH TO DESCRIBE THE VARIATION IN FUNDAMENTAL FLIGHT TONES

Flies of the genus' *Drosophila* and *Zaprionus* have been the subject of numerous acoustic studies, with temporal acoustic descriptions being made to describe aspects of their flight and copulation behaviours (Bennet-Clark, 1971; Bennet-Clark et al., 1980). Using frequency power spectra and simpler time-domain microphone throughput signals, acoustic profiles for multiple behaviours within each species were described. As pioneered by Bennet-Clark, connecting variation in acoustic profiles to their behaviours is useful, so a novel approach to expand on this approach was explored.

Figure 3.28 presents a novel approach to visualising frequency content of insect flight, over a longer time period. Unlike the 10s snapshot offered by figure 3.27, this approach presents the flight tone of a mosquito by tracking the variation of the fundamental frequency and fundamental frequency amplitude during an

entire flight measurement. This is achieved using a maximum amplitude tracker (PAK 5.8) with an applied bandpass filter, to identify the frequency of maximum amplitude (the fundamental) throughout a measurement duration. The bandpass filter passes frequencies within a broad frequency range expected to include the wingbeat frequency of species in question (400-800 Hz, used for female *Ae. aegypti*), and results with a description of wingbeat frequency variation over time.

This approach across a 500s measurement (figure 3.28) showed that the fundamental frequency for this individual of 389.6 Hz at 22.2 dB had a standard deviation of 18.66 Hz and 16.1 dB. What is also notable, is that the frequency and amplitude peaks, correspond, with increases in amplitude corresponding with increases in frequency.

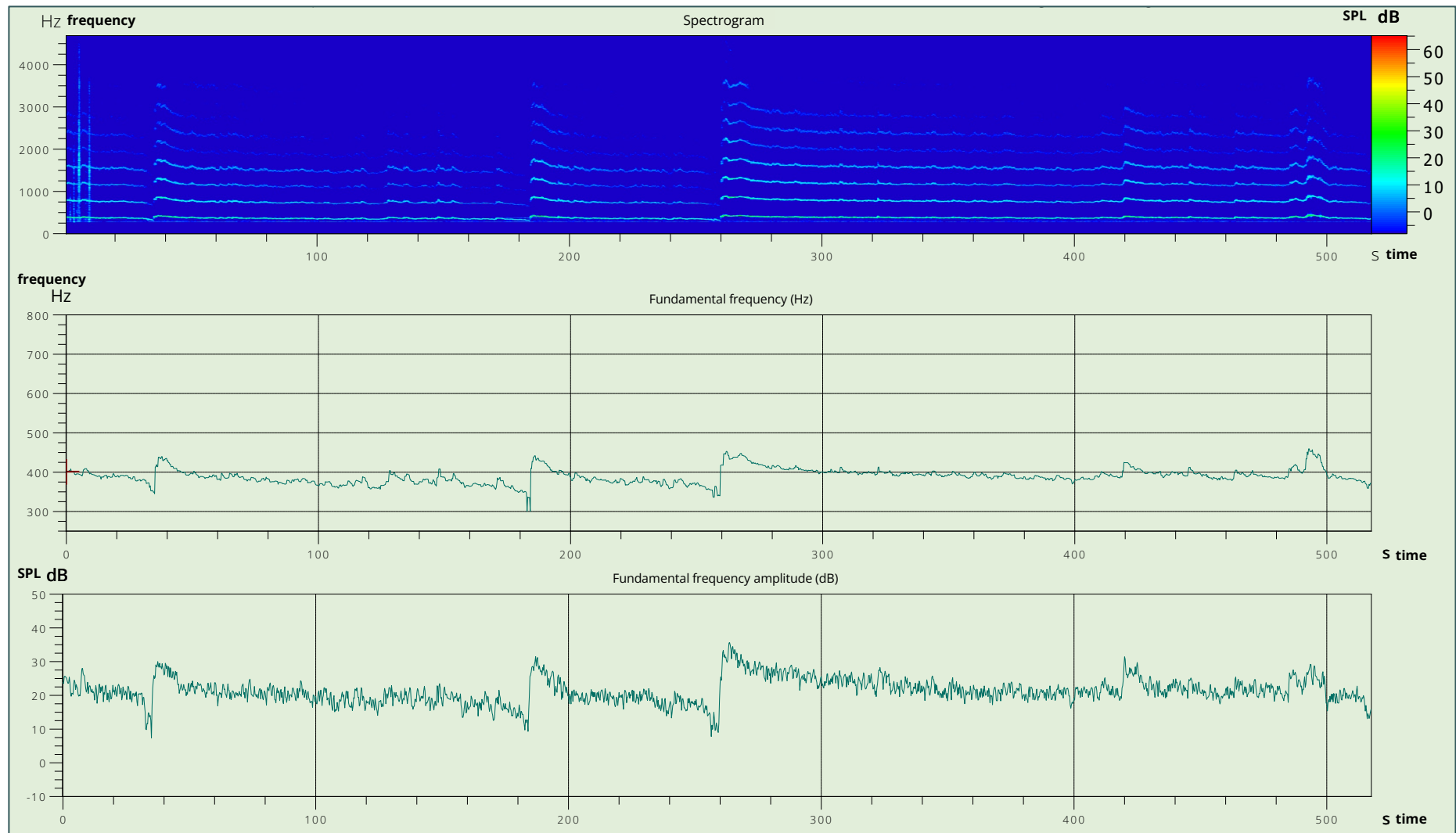


**Figure 3.28** –500s spectrogram with tracked fundamental frequency and frequency amplitude profile for tethered *Ae. aegypti*

To characterise this, the flight patterns illustrated by figure 3.28 have been described into four stages, These stages are defined here by the following patterns of change of the fundamental flight tone:

1. **Ramp** – the flight tone frequency rapidly increases, together with its amplitude increasing rapidly (figure 3.29)
2. **Constant flight** – the flight tone is steady, characterised by little variation in the frequency and amplitude (figure 3.30)
3. **Manoeuvres** – flight tone fluctuates, characterised by amplitude and frequency variation although changes not necessarily proportional to each other. (figure 3.31)
4. **Long constant flight** – flight tone is steady, but variation may be present in the frequency and amplitude. (figure 3.32)

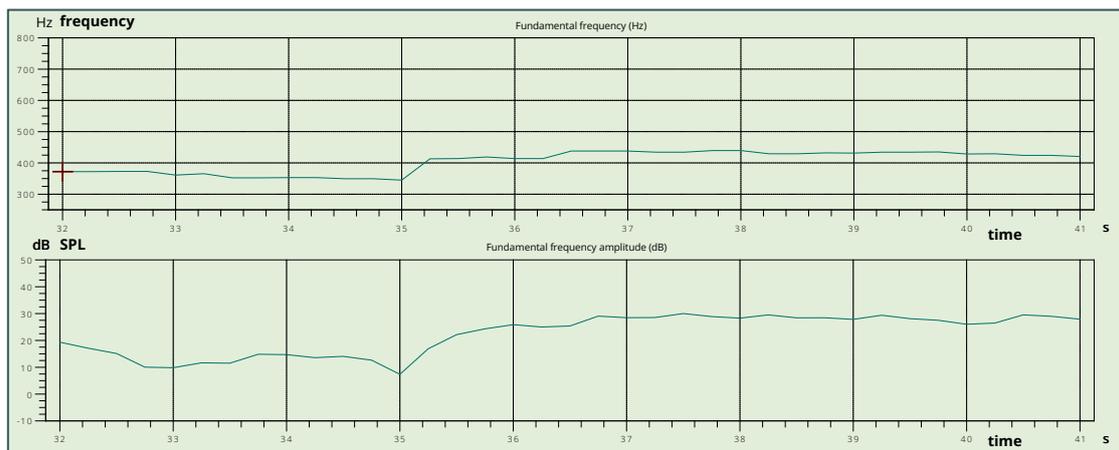


Figure 3.29 – “Ramp” frequency and frequency amplitude profile

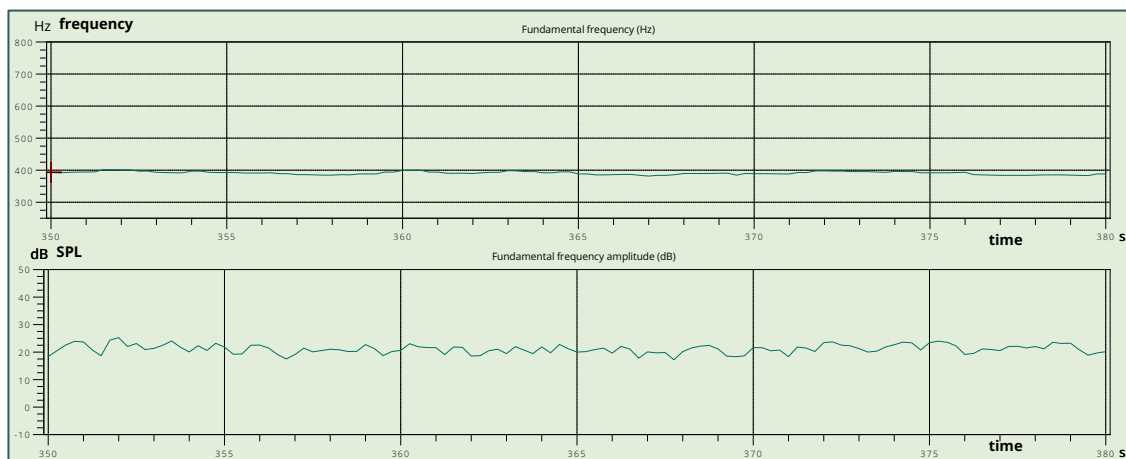


Figure 3.30 – “Constant” frequency and frequency amplitude profile

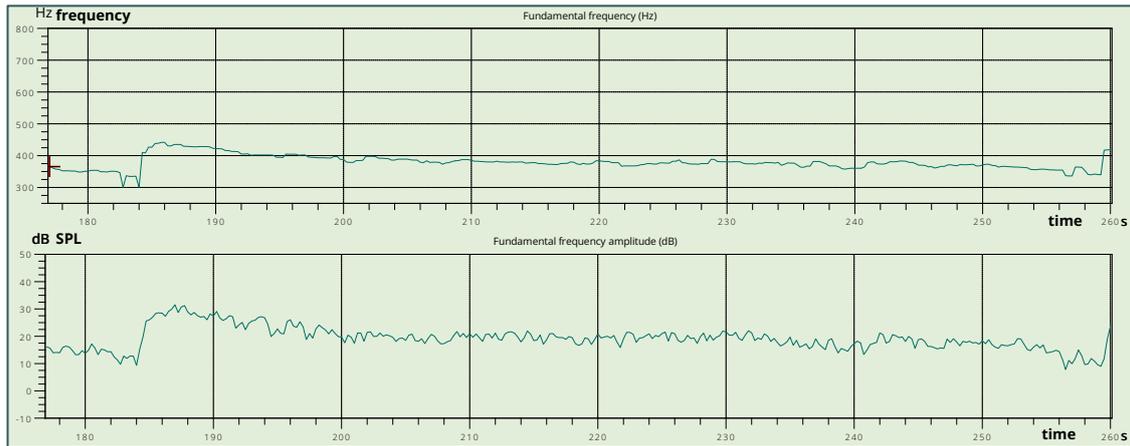


Figure 3.31 – “Flight manoeuvre” frequency and frequency amplitude profile

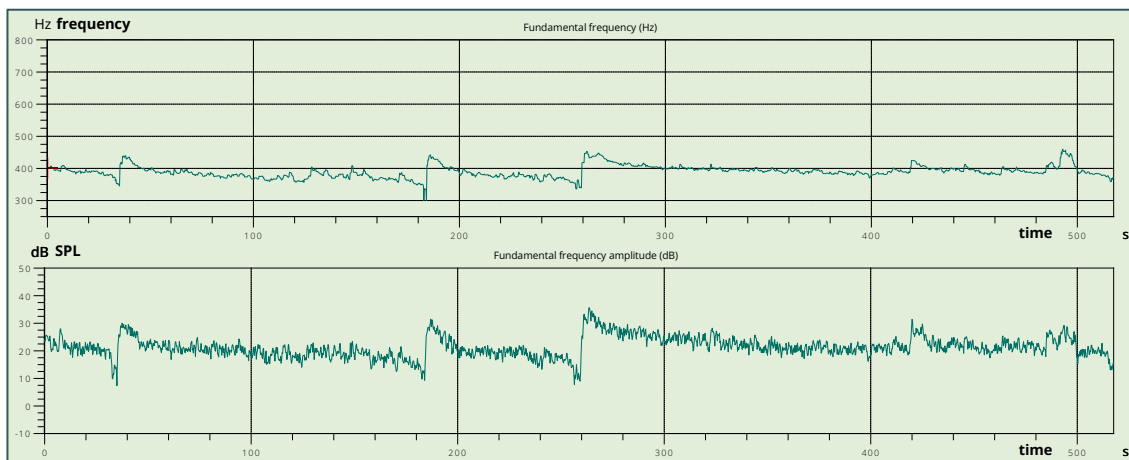


Figure 3.32 – “Long constant flight” frequency and frequency amplitude profile

A preliminary dataset ( $n=4$ ) of tethered *Aedes aegypti* females was collected with flight times of 300s. This was used to quantify the variation in fundamental frequency and frequency amplitude descriptions, by analysing different periods of the same individuals flight, that matched each of the four flight profiles.

Table 3.3 – Variation in described frequencies and frequency amplitudes by flight type

Flight type	Mean frequency (Hz)	Mean frequency std dev (Hz)	Mean frequency amplitude (dB)	Mean frequency amplitude std dev (dB)
Long constant flight	540.3	24.0	24.6	5.1
Flight manoeuvres	533.1	25.6	23.7	4.5
Ramp	531.2	30.9	22.3	4.9
Constant flight	549.3	<b>6.8</b>	26.1	<b>2.0</b>

Table 3.3 illustrates the impact of analysing mosquito flight tones during their different potential flight stages. Analyses that were conducted under the constant flight condition, featured the lowest variation for both frequency (6.8 Hz) and frequency amplitude (2.0 dB).

With the aim of conducting *repeatable* acoustic measurements, it is clear from this simple summary that analysis under controlled tethered conditions should be performed during periods of mosquito flight which are constant. This is much simpler to identify from the spectrogram of flight, when measurement periods are longer (>300s). Constant flight cannot be assumed however, so a manual identification of it must be performed for all measurements

#### 3.5.4 – DEVELOPMENT OF A VIBRATION-BASED MOSQUITO TETHER METRIC

As discussed in chapter 1, the cyclical contraction of mosquito thoracic flight muscles drives the wing flap which produces the wingbeat (Hedenström, 2014). The wingbeat sound arises from the generated pressure fluctuations on the wing surfaces (Clark, 2021) during the flapping of the wing. Since the indirect flight muscles produce thoracic deformations to drive the wing flap cycle, the possibility is raised for capturing inertial oscillations during tethered flight using an accelerometer, which may be a close correlate of the flight tone characteristics.

We explored the feasibility of an alternative method of describing the frequency spectra and their amplitudes that would be independent of the physical influence of distance and angle which we have now shown can have an unwanted influence on sound measurements. A high sensitivity, low mass (100mV/ms<sup>-2</sup>, 4.8g) uni-axial accelerometer (Brüel & Kjær 4508 B miniature CCLD piezoelectric accelerometer, Nærum Denmark) was mounted directly to the tether used in section 3.5, to assess whether this sensor could be used to describe mosquito acoustics through inertial vibrations (figure 3.33).

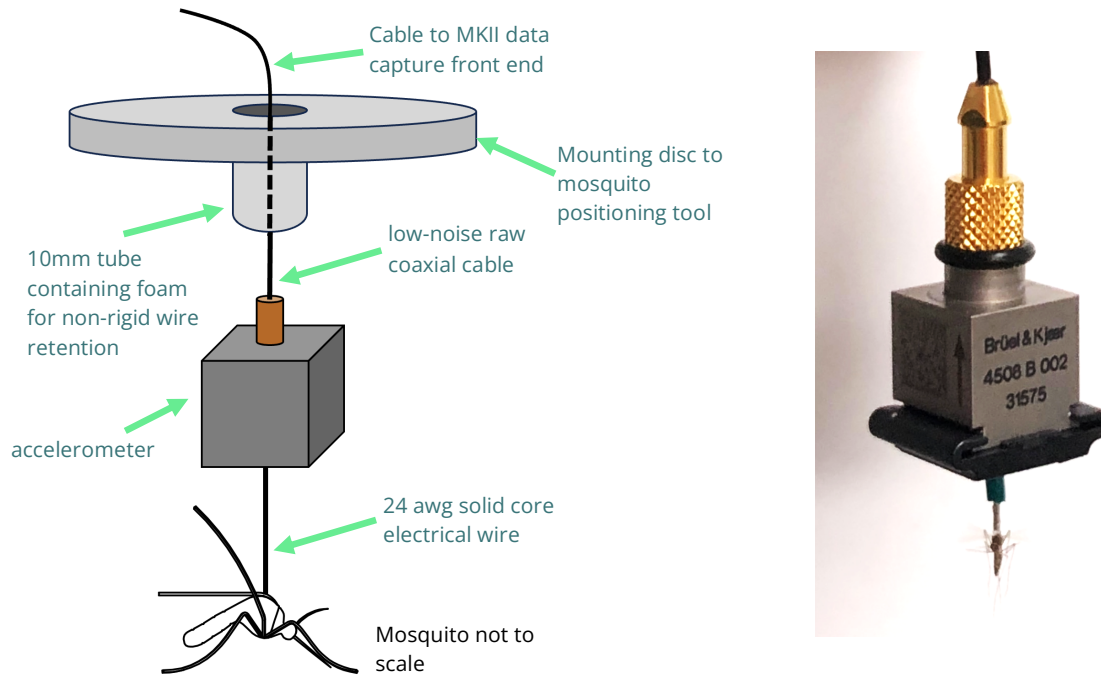


**Figure 3.33** – tethered accelerometer mounting diagram

Vibration can be measured through contact with the vibrating object (in this case the mosquito thorax) using an accelerometer, or by a non-contact method such as laser scanning vibrometry. Laser scanning vibrometers have been used within entomology and are an excellent method for describing wing or antenna resonant frequencies and displacements in mosquitoes and larger species including crickets (Göpfert et al., 1999b; Sarria-S et al., 2016). However, a significant disadvantage is that commercially available and calibrated solutions can be prohibitively expensive (c.a. £150k in 2016), and the measurement process cannot be deployed simply in the field.

It should be noted that despite the low mass of the small, titanium accelerometer selected for this experiment, the mass of the mosquito is vastly less than that of the accelerometer, so the dynamics of the system is expected to be dominated by the inherent physical properties of the measurement device. There is also expected to be an unquantified and variable damping effect from the “tacky” glue used to connect the mosquito to the metal wire tether. The amount of glue will vary, so the effect of damping will also vary. However, the intended aim of exploring this method for capturing mosquito vibration is to characterise flight effort changes

within a single measurement. If the mosquito flight kinematics are constant, the sound pressure level should also remain constant, but should a physical parameter such as microphone to mosquito distance be changed, the variation / constant level of vibration could be used to verify whether flight effort changed. This cross correlation would provide a novel, and simple metric to confirm whether observed changes in sound pressure level were therefore due to changes in flight effort, or due to different physical conditions between the mosquito and the microphone.

### Analysis

The analysis approach used to track the fundamental frequency of the microphone measurements in section 3.5.3, was adapted to analyse the outputs from the measurement microphone and accelerometer simultaneously. The fundamental frequency was tracked for both sensors. This dataset used *Ae. aegypti* (n=3, female) to assess whether accelerometry can be used to infer tethered flight acoustics. Mosquitoes were tethered at a 30 mm distance from the microphone, at a 0° angle (figure 3.34). All measurements were 1800s in length.

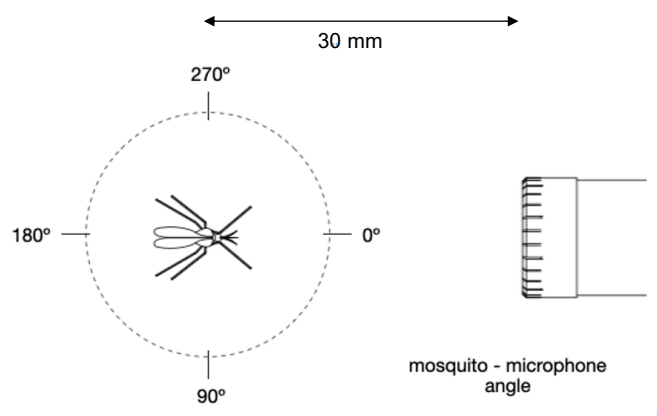


**Figure 3.34** – Tethered mosquito positioning relative to microphone mounting diagram

Figures 3.35 and 3.36 show an example measurement, with accelerometer data on the left, and microphone data on the right.

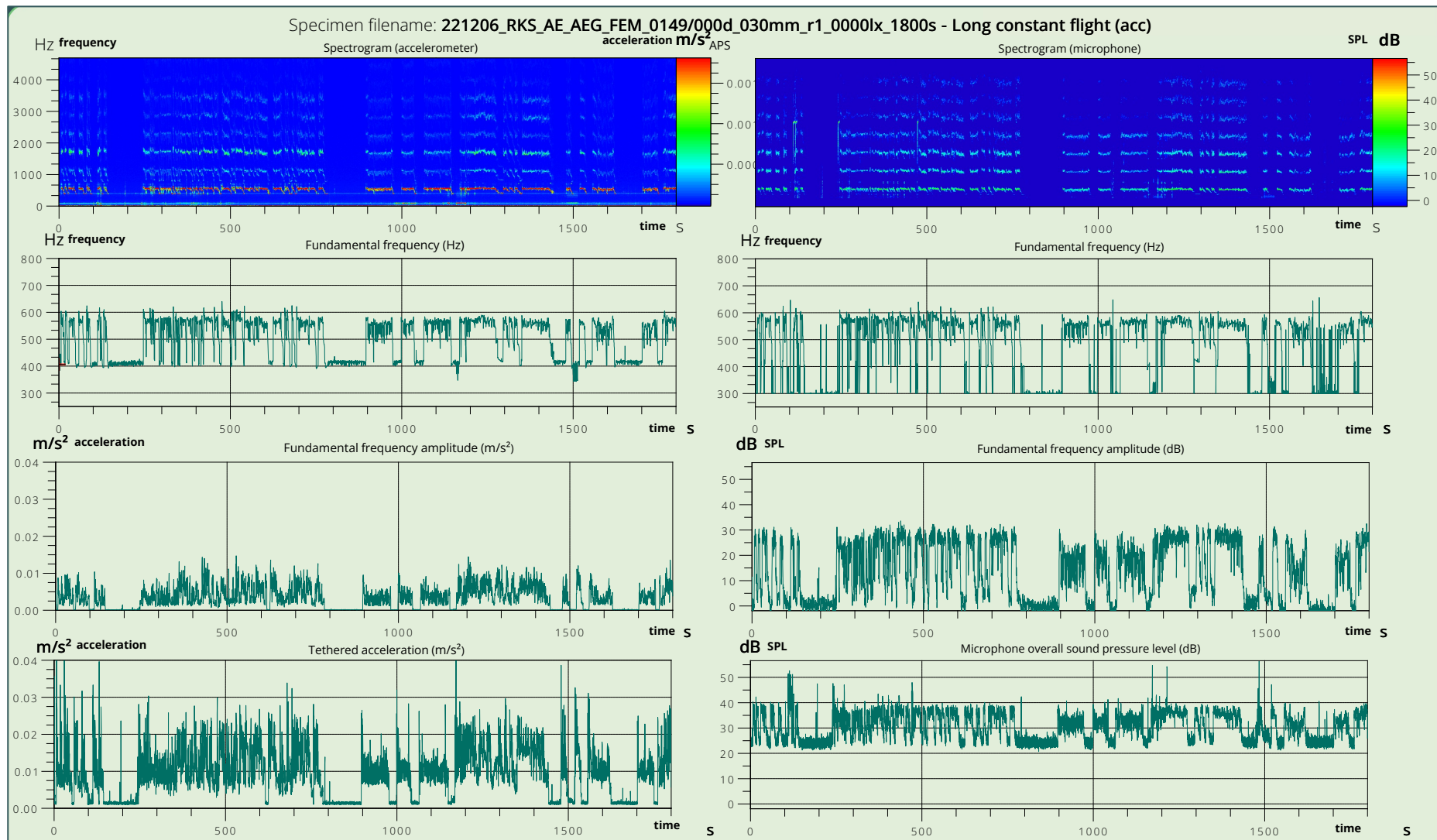


**Figure 3.35** – Example frequency data (1800s window) from accelerometer (left column) and microphone (right) for *Aedes aegypti*. Plotted content is: 1<sup>st</sup> row - spectrograms, 2<sup>nd</sup> row - frequency of maximum amplitude between 400-800 Hz (fundamental), 3<sup>rd</sup> row – amplitude of maximum frequency between 400-800 Hz, 4<sup>th</sup> row – sum level (acceleration or sound pressure level)

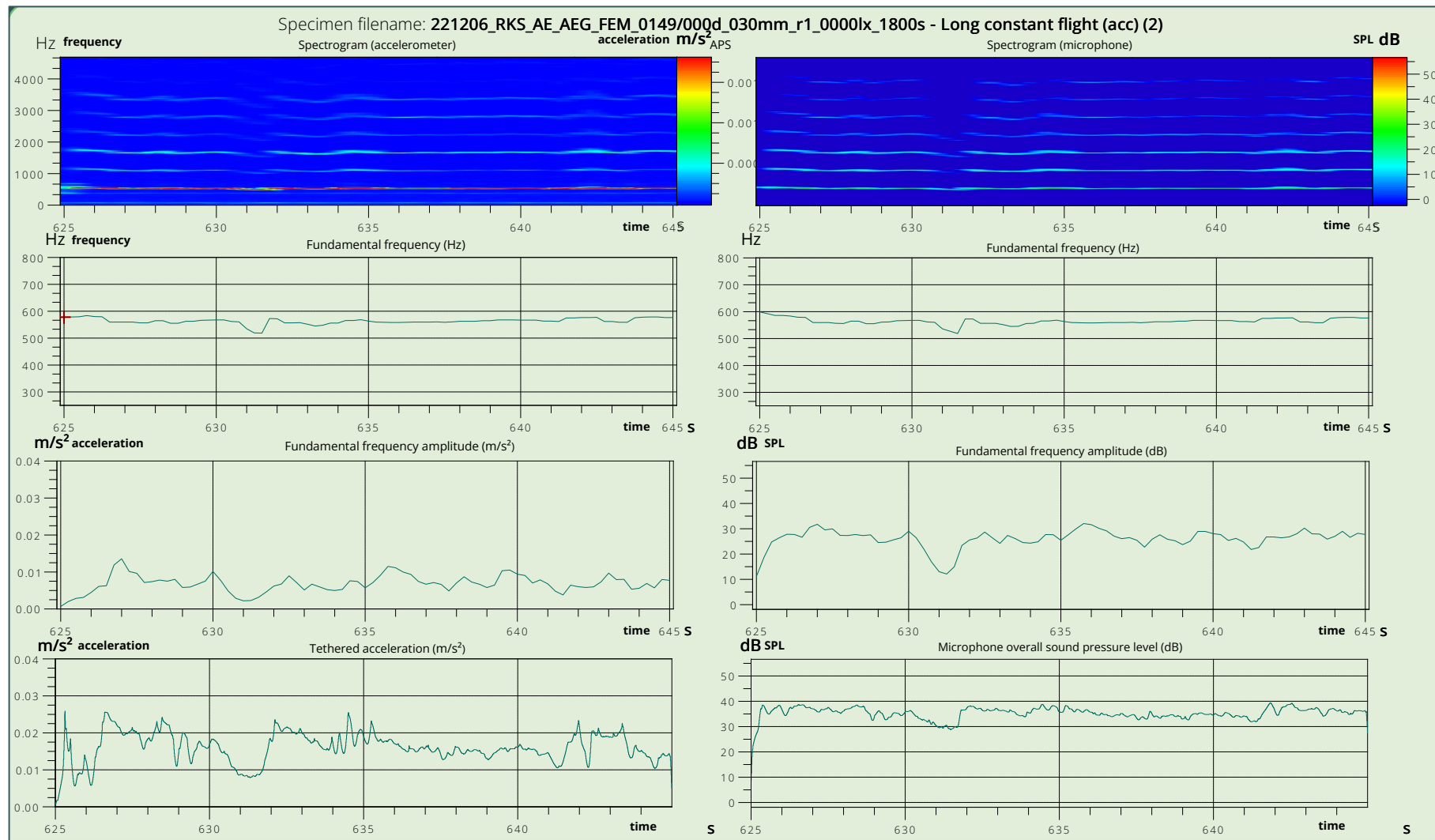


**Figure 3.36** – Example frequency data (20s window) from accelerometer (left column) and microphone (right) for *Ae. aegypti*. Plotted content is: 1<sup>st</sup> row - spectrograms, 2<sup>nd</sup> row - frequency of maximum amplitude between 400-800 Hz (fundamental), 3<sup>rd</sup> row – amplitude of maximum frequency between 400-800 Hz, 4<sup>th</sup> row – sum level (acceleration or sound pressure level)

Figure 3.35 shows the full 1800s measurement, whilst 3.36 shows a selected 20s segment. Data plotted in the first three rows follow post-processing of the acquired throughput signal (from either the microphone or accelerometer) to represent the frequencies using an FFT. The sum levels plotted on row 4 (raw throughput data from the accelerometer or microphone) have not been post-processed however. This means that the time resolution of the sum level data (row 4) is very high, whilst the time resolution of the frequency post-processed data is much lower due to the Nyquist sampling trade-off discussed in section 1.2.3.

To quantify the correlation between accelerometer and microphone amplitudes, unprocessed throughput data and frequency processed data were both analysed with custom Python scripts. The advantage of using the sum level, is that the unprocessed data remains at the original sampling rate (12 kHz) so there is a much larger data set to use in the measurement period. Using frequency amplitude data causes a much reduced number of data points, due to the application of the FFT.

#### *Time domain analysis*

To understand whether there was an identifiable, repeatable correlation between the amplitudes of sound pressure level and acceleration, a range of plots were generated by a first script, to plot acceleration with sound pressure levels (figure 3.37). Figure 3.37 uses data captured from a tethered *Ae. aegypti* shown on figures 3.35 and 3.36. The subfigures within figure 3.37 all use the total level data from the microphone and accelerometer without frequency analysis. Plots shown on the first column [a, d, g] plot sound pressure level against acceleration, with applied linear regressions. Second column plots [b, e, h] represent sound pressure level changes over time of the microphone, and third column plots [c, f, i] represent acceleration changes over time. Plotted rows feature different analysed time windows. First row plots [a, b, c] show the full 1800s, row 2 plots [d, e, f] show a 250s to 550s (300s) window, whilst row 3 plots [g, h, i] show a 0-60s window.

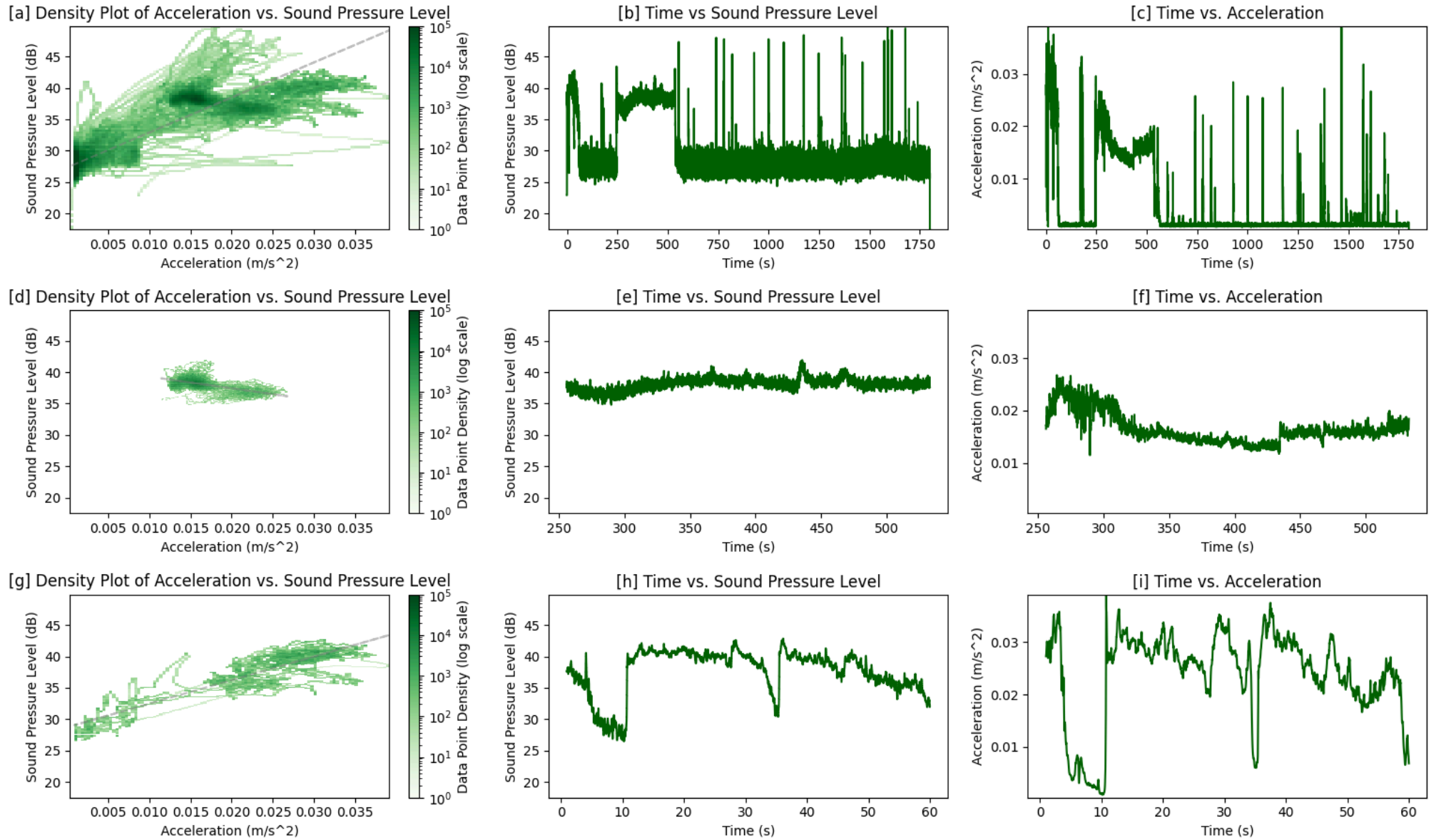


Figure 3.37. [a-i] -Example representations of tethered *Aedes aegypti* flight using sound pressure level (dB) and acceleration ( $m/s^2$ )based approaches

## Results – time domain

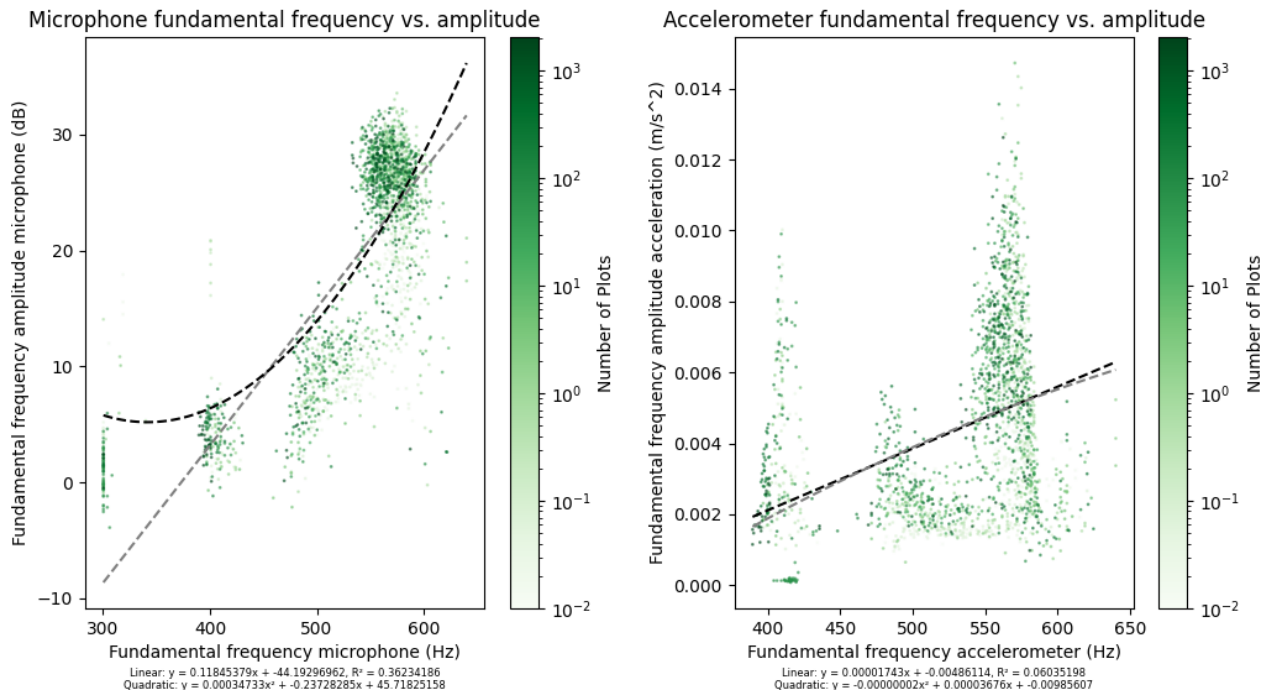
**Table 3.4** -  $R^2$  values for flight analysis lengths analysed using time-domain analysis (figure 3.37)

Analysis time	Flight type	Plot	$R^2$
1800s	Long flight	3.34.1	0.729
300s	Constant flight	3.34.4	0.482
60s	Manoeuvres	3.34.7	0.756

A stronger correlation ( $R^2 > 0.7$ ) was observed between the sound pressure level and accelerations for the long flight and manoeuvres analysed, whilst a weaker correlation shown ( $R^2 = 0.48$ ) for the constant flight period analysed. The constant flight, which exhibited a weaker correlation, featured less variation over time in sound pressure level and acceleration (figures 3.37[e], 3.37[f]) than the other flight types. This suggests that a linear correlation between sound pressure level and acceleration strengthens, when the range of amplitudes in an analysed period is greater. During these periods (figures 3.37[a], 3.37[g]), the tethered mosquito generated a wider range of amplitudes and vibration, however these cropped sections excluded extended periods of silence when the mosquito was not flapping.

## Frequency domain analysis

The second script investigated the correlation between frequency and amplitude, identified in the flight types of section 3.5.3. In the flight type examples figures (figures 3.29 – 3.32), it was seen that increases in frequency during a flight burst would have an associated amplitude increase. This Python script analyses the tracked fundamental during a selected flight burst and plots the fundamental against both accelerometer and microphone amplitudes (figures 3.38a,b). Linear and quadratic regressions were run to quantify any trends between measured frequency and frequency amplitude.



**Figures 3.38a left**, -Example comparison of frequency and frequency amplitude by sound pressure level (dB), **3.38b right**, acceleration (m/s<sup>2</sup>)

Mean fundamental frequencies (n=3) identified with the microphone and accelerometer were 528.9 Hz (SD 14.1 Hz) and 528.9 Hz (SD = 13.8 Hz). No strong linear or quadratic correlations ( $R^2 > 0.8$ ) were identified between the fundamental frequency and fundamental frequency amplitude measured for either the microphone ( $R^2 = 0.21$  linear,  $R^2 = 0.25$  quadratic) or accelerometer derived datasets ( $R^2 = 0.16$  linear,  $R^2 = 0.24$  quadratic).

**Table 3.5** -Mean fundamental frequency and amplitudes for tethered *Aedes aegypti* using accelerometer and microphone measurement data

	accelerometer	microphone	standard deviation accelerometer	standard deviation microphone
frequency (Hz)	528.4	528.9	13.8	14.1
level (dB or m/s <sup>2</sup> )	0.00521	23.9	0.00152	12.5

### *Discussion & conclusions from the accelerometer based tethering approach.*

The preliminary investigation has shown that an accelerometer based tethering approach can directly capture vibrations produced by a mosquito, despite the discrepancy in mass between the sensor and the subject. A proof-of-concept is

offered that demonstrates how this method of data-acquisition could be used to describe the fundamental frequency of mosquitoes during tethered flight.

Demonstrating the correlation of sound pressure levels recorded by a microphone, to acceleration amplitudes measured with an attached accelerometer is possible but not straightforward; unavoidable variation in adhesive size between tethered mosquitoes would render the acceleration value incomparable between individuals. However, if the flight type analysed is selected such that the characteristic peaks and troughs that occur during a manoeuvre are present, this approach may be able to signify repeatability of this flight type using acceleration.

With further analysis, it may be possible under this constant flight type, to describe the expected acceleration for an individual which could act as a potential measure of flight effort. This could be used as a supplementary metric during further studies, as it could help quantify flight effort, whilst other conditions (such as microphone position) change. This would simply allow for the effect of sound pressure level measurements to be explored, whilst retaining a supplementary metric to monitor the consistency of behaviour during a trial.

Relating the measured frequency to amplitudes of either acceleration or sound pressure level for this small dataset showed a weak correlation. Amplitudes of acceleration or sound pressure level appears to not be related to the fundamental frequency measured, although this is a small dataset. A more thorough investigation of this would be required to definitively investigate this relationship.

*Linear throughput cross correlation of accelerometer and microphone*

Figure 3.39 illustrates a different approach that can be taken to represent accelerometer and microphone data captured during tethered mosquito flight. Figures 3.37 and 3.38 used data from longer measurement times (60 -1800s), which lends itself well to high frequency resolution FFT analysis, and for comparison of amplitude ranges. Figure 3.39 represents much shorter time windows between 0.01s to 3s, which allows comparison of instantaneous time-domain sensor responses. To aid the visualisation of this, the microphone output has been plotted on a linear scale (Pa), unlike the previously used dB scale. The figures plot an “envelope curve” to represent the bounding envelope around the local maxima of the microphone / accelerometer raw throughputs, which for this analysis used the previous 8 data points. Since the raw throughput is used, both acceleration and microphone sound pressure level have been normalised.

Figures 3.39[a, b] show a flat normalised curve, which is expected as this time window represents a period of constant flight. The raw throughput however, clearly shows the pressure and acceleration fluctuations from the wingbeat, with the individual strokes visible. Due to the 12 kHz synchronised data acquisition for both the microphone and accelerometer, figures 3.39[c, d] clearly demonstrate that there is a minimal time lag between selected peaks (c.a. 0.001s). The 0.6s time window used in these figures, shows a complete flight burst, taking the tethered mosquito from rest, to flight, and back to rest. The peaks within this burst, which have been annotated, act as good references to compare the lag between the sound pressure level and acceleration metrics. Figures 3.39[e, f] represent the context of where the plots in figures 3.39[a-d] have been taken from. At this time scale, the envelope curve is not required for visualising peaks.

This short time window combination of tethered microphone and accelerometer data, helps to cross-correlate how the accelerometer can detect changes in acceleration which are captured with minimal time-lag in the microphone during tethered flight, with the presented method.

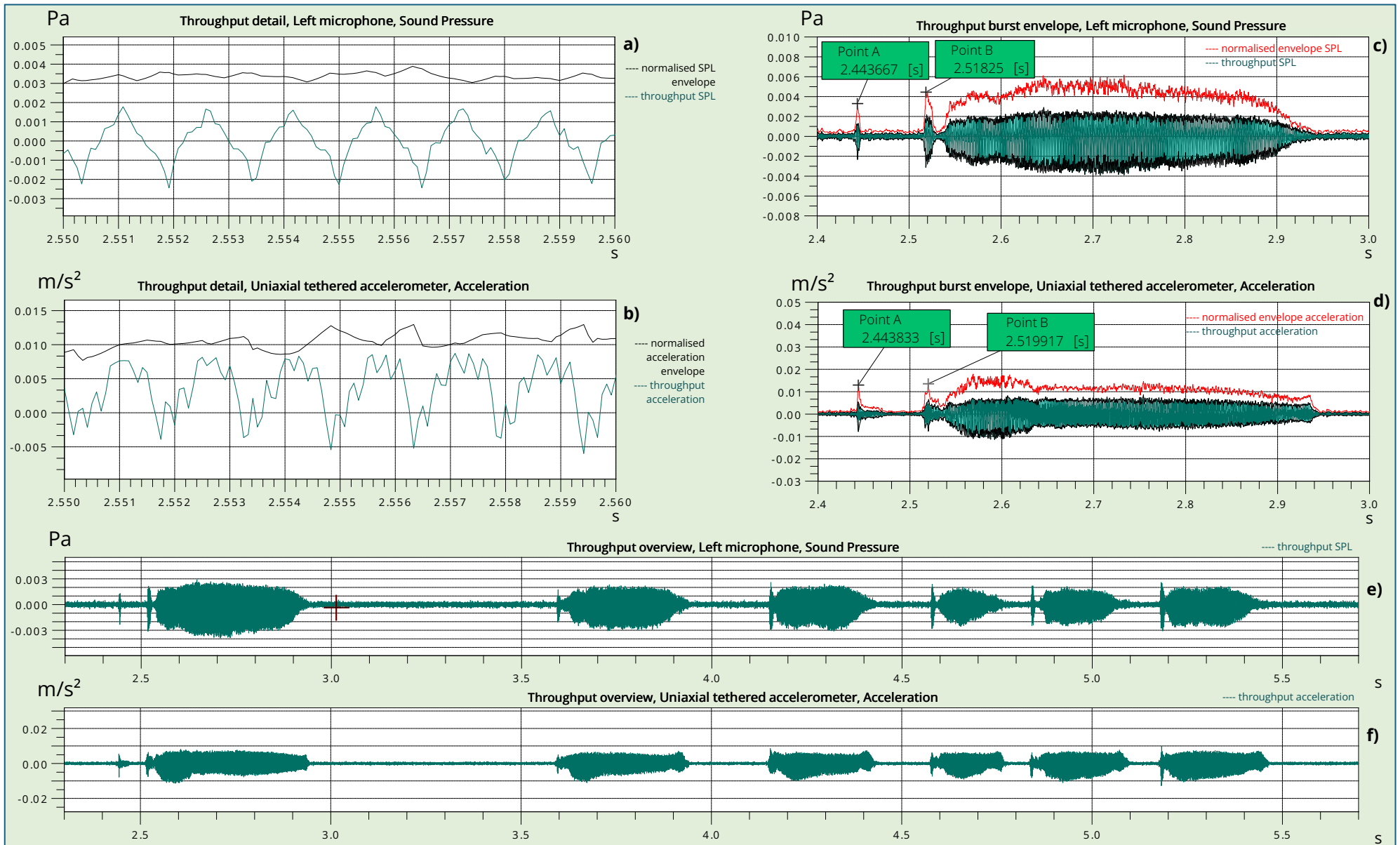


Figure 3.39. [a-f] -Detailed time domain (linear) representation of tethered *Aedes aegypti* flight using sound pressure level and acceleration based approaches

## 3.6 Developing a semi-anechoic free-flight method

### 3.6.1 – ASSESSMENT OF THE FREE-FLIGHT ANECHOIC FLIGHT TUNNEL

To validate the performance of the semi-anechoic free-flight tunnel, an initial comparison was conducted by measuring the flight profile of an individual mosquito (*Ae. aegypti*, female) under tethered, and free flight conditions. Free flight and tethered assessments were undertaken using the semi-anechoic chamber, and an additional measurement took place in the Ø80 acrylic tunnel described in Chapter 2, to demonstrate the effects of the two sound environments. This comparison is visualised by figure 3.40.

Further analysis was then undertaken using the data measured exclusively under semi-anechoic conditions. The analysis approach taken uses the concept of maximum amplitude frequency tracking, introduced in section 3.5. The feasibility was explored for tracking fundamental frequency and its amplitude under free-flight, instead of tethered flight.

Measurements and analysis are provided for an individual *Ae aegypti* female (14 days post emergence), to illustrate the differences between the two measurement styles more clearly. The individual was measured initially under free flight conditions for 300s, before being tethered (as per section 3.4-5) and re-measured using the tethered workflow. Individual flight bursts were identified from the spectrogram, and periods of constant flight were identified for further analysis. During these periods, the frequency and frequency amplitude datapoints were recorded for all flight bursts analysed.

A custom Python script using the `Plotly` library was written, to visualise the spread of the fundamental frequency and amplitude data for both measurement styles. Free-flight measurements used two microphones (LHS & RHS) whilst tethered flight used one microphone and one accelerometer.

## 3.6.2 – RESULTS OF ANECHOIC FREE-FLIGHT TUNNELS COMPARISON MEASUREMENTS

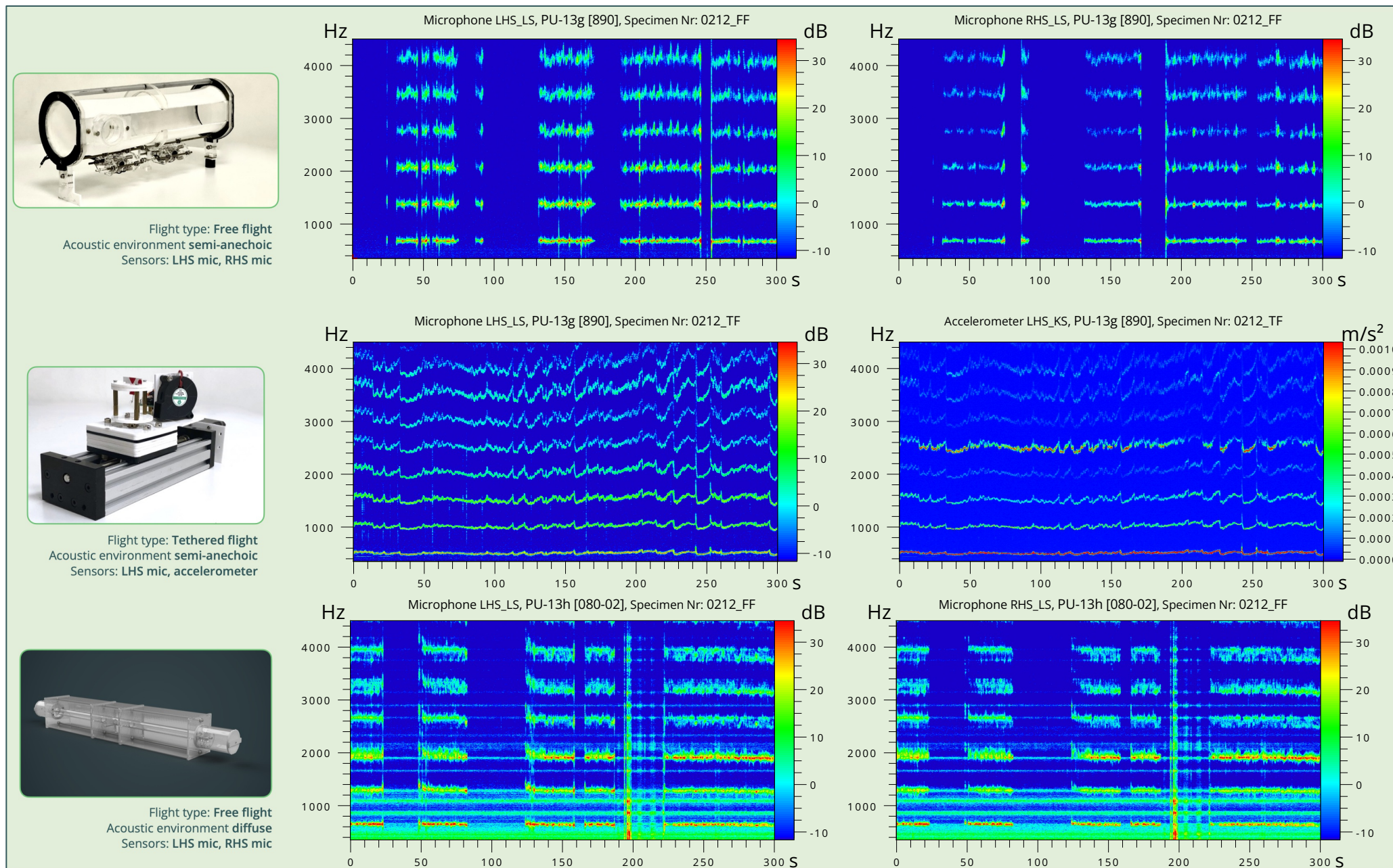


Figure 3.40 – Comparison of semi anechoic free flight, tethered flight, and reverberant free flight (Ø80) spectrograms

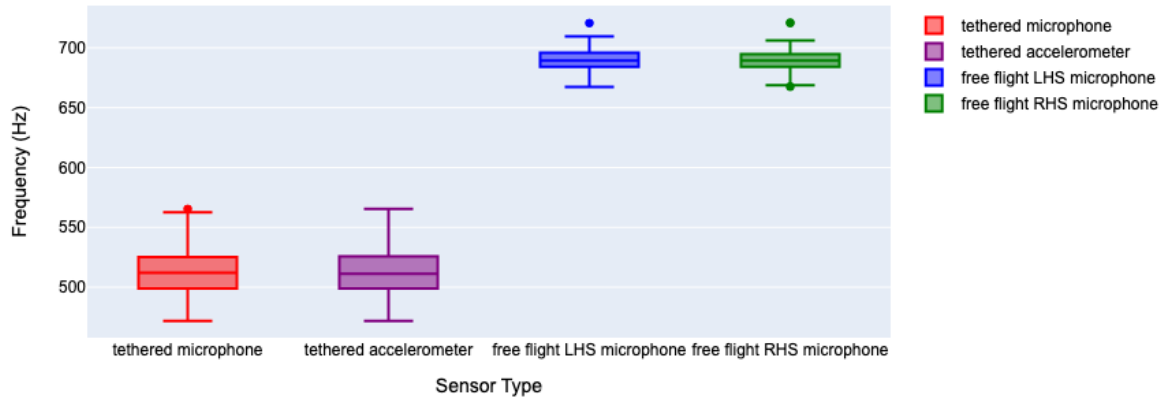


Figure 3.41 -Frequency comparison for individual *Aedes aegypti* under tethered and free-flight (anechoic) conditions

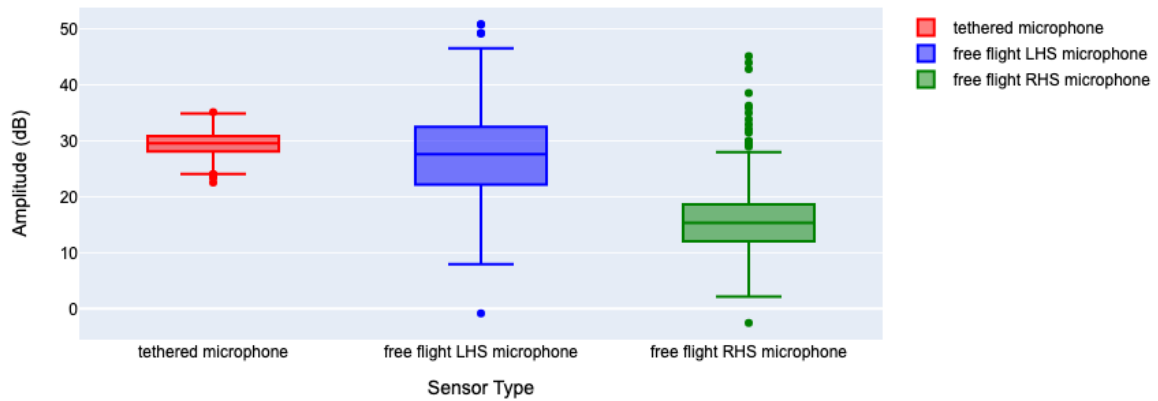


Figure 3.42 -Frequency amplitude comparison for individual *Aedes aegypti* under tethered and free-flight (anechoic) conditions

Table 3.6.– Fundamental frequency content for anechoic free-flight and tethered flight for individual *Aedes aegypti*

		Mean	Standard Deviation
Fundamental frequency (Hz)	Tethered microphone	512.6	18.1
	Tethered accelerometer	512.7	18.2
	Free flight LHS microphone	689.8	8.1
	Free flight RHS microphone	689.7	7.8
Fundamental frequency amplitude (dB)	Tethered microphone	29.5	2.0
	Free flight LHS microphone	27.1	8.6
	Free flight RHS microphone	16.0	6.5

Fundamental frequency and their respective amplitudes from the free-flight and tethered measurements were processed, as shown by table 3.6. Highest mean amplitude was for the tethered flight (29.5 dB) followed by free-flight on the LHS (27.1 dB) and RHS exhibiting the lowest (16.0 dB). Less than a 0.2 Hz difference

was registered between the two sensors used for both free flight and tethered measurements. Tethered mean fundamental frequency was 177.1 Hz below the mean fundamental measured for free-flight. Standard deviation of the fundamental frequency amplitude was higher for free flight than tethered flight (mean fundamental standard deviation free flight 7.9 dB, tethered flight 2.0 dB).

### 3.6.3 – DISCUSSION OF ANECHOIC FREE FLIGHT TUNNEL MEASUREMENTS

The semi-anechoic free flight equipment developed offers another method to describe mosquito acoustics, which allows more natural flight behaviour than that afforded by a tethered approach. The uncontrolled mosquito-microphone distance results with a greater standard deviation in fundamental frequency amplitudes across both measurement microphones, when compared with the tethered measurement. For the free flight, the LHS mean fundamental amplitude was higher than the RHS, which is reflected in the spectrogram. This can be simply explained as free flight allowed the mosquito up to 300 mm between it and a microphone, whilst tethered measurements were always fixed at 30 mm. The exact distance during free flight was random, and with this setup, uncontrolled.

The fundamental frequency during tethered flight featured more variation than free flight, reflected by the higher standard deviation (18.1 Hz tethered flight, 7.9 Hz free flight). Inspection of the spectrogram (figure 3.40) shows continuous flight across the 300s tethered measurement, but with a varying fundamental. Conversely, free flight measurements, while not continuous across the 300s, produced a much more consistent flight tone. The mean frequency during tethered flight was lower than the mean during free flight, which corresponds with comparable investigations exploring the differences with free flight and tethered mosquito acoustics (Pantoja-Sánchez et al., 2019b). However, the tethered measurement exhibited lower variation in its amplitude of the fundamental (2.0dB tethered vs 8.6 & 6.5 dB free flight).

Both approaches offer pros and cons, with the free flight approach lending itself to capturing flight representative of the field, whilst tethered flight offers control of microphone distance and hence sound pressure level amplitude. Frequency descriptions made using the tethered approach were shown to have high frequency variation, however the analysis approach was not selective, unlike those taken in previous sections where the *flight types* were selected. The flight types could also be described for free-flight measurements, however this would necessitate a tracking system to be implemented, such as video tracking (Muijres et al., 2023). Therefore a more practical analysis approach using the equipment already developed, would be to instead use tethered flight. Constant flight regions should be specifically selected from measurements, to reduce the standard deviation presented in this section that arose from combined analysis of all flight types.

## 3.7 Chapter summary

### 3.7.1 – CONTROLLING MOSQUITO ACOUSTIC MEASUREMENTS

This chapter has presented a series of preliminary investigations conducted to validate the efficacy of different approaches to capturing the flight sounds of mosquitoes. The theme throughout, was to describe how to obtain metrics that describe flight sounds *repeatably*, such that these could be next applied to explore the effects of physiological factors within mosquitoes in future work. The semi-anechoic chamber designed for taking precision measurements was a success, showing very low-noise and no influence of ambient sounds. This substantially improved signal quality and decreased post processing time.

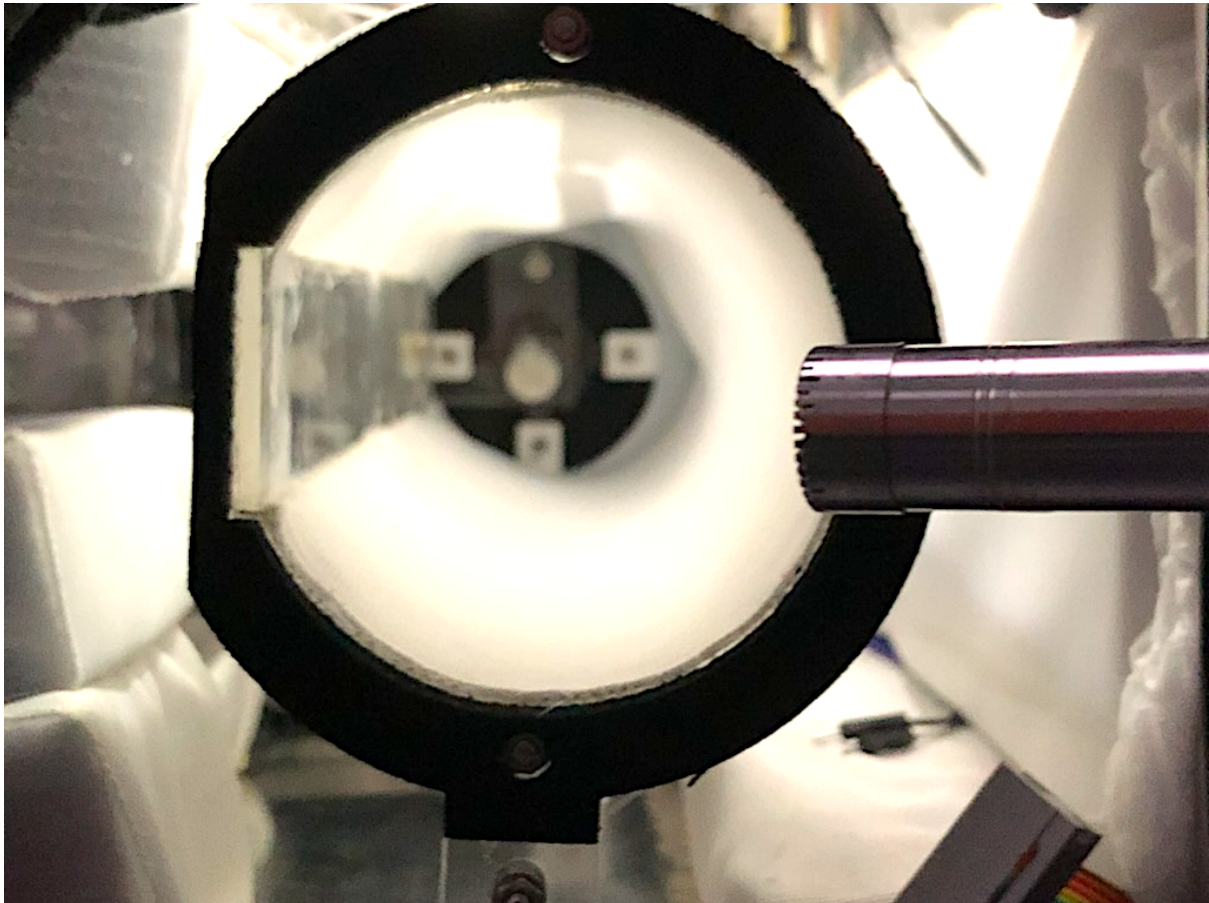
The fundamental frequency of the wingbeat under the tethered semi-anechoic conditions afforded by the developed measurement chamber featured the highest amplitude with measured *Ae. aegypti* mosquitoes. It was shown that amplitude across the fundamental and 2<sup>nd</sup> to 4<sup>th</sup> harmonics reduces with distance from a

measurement microphone, and the angle from which the acoustic emission is observed with a microphone affects their amplitudes as well. A novel tethering approach was shown to capture mosquito flight acoustics through vibration, although in its current form the metric cannot be used to compare flight effort between mosquitoes. It may, with further work, be used to illustrate changes in an individual's flight effort within a measurement, and it can capture the frequency spectra accurately.

Increasing measurement times from 20s to 300s revealed behavioural variation in mosquito flight tones, and a bandpass maximum amplitude tracker that exploits the ultra-low noise environment of the measurement chamber allowed for the fundamental to be tracked during longer flight bursts. Tethered flight demonstrated low fundamental frequency amplitude variation, however these recordings featured higher frequency variation. Free-flight measurements exhibited lower fundamental frequency variation but higher amplitude variation.

Controlled measurements can use the fundamental frequency as a measurement metric, but the acoustic workflow should also ensure *variation* is captured and described. This can be achieved using the standard deviation of the fundamental frequency and its respective amplitude over sufficient timescales.

# CHAPTER 4: FLIGHT TYPE AND SPECIES COMPARISONS



Interior view of the semi-anechoic flight tunnel

## 4.1 Introduction

### 4.1.1 - UNDERSTANDING FREE FLIGHT AND TETHERED ACOUSTICS

Developing an understanding of free flight would facilitate the efficient translation of findings into a field acoustic mosquito surveillance approach, since this is the most realistic mode of flight that would be used. However as discussed in Chapter 3, there are advantages to using a tethered approach in the context of the

laboratory studies. The tethered approach offers known positional control between the mosquito and measurement microphone which makes subsequent analysis using sound pressure level feasible without tracking mosquito position, as would be required under free flight. It also reduces complex flight tones arising from changes in flight position (League et al., 2022). The tethered approach developed in Chapter 3 was simpler to set up, as free flight measurements particularly needed external stimulation to initiate flight (using fans, or shakers built into the flight tunnel). A disadvantage however, is that tethering can alter the wingbeat, although there is no clear consensus on the extent of this, as introduced in section 1.2.2.

It has been hypothesised that differences in tethering effects within the literature could be attributed to the non-standardisation of tethering approaches used across different studies (Villarreal et al., 2017b). Glues, tethers, and knockout methods are variable between studies and could each affect the way mosquitoes fly when tethered. The airflow tethering method developed for this project (Chapter 3) would compound this, as the glue and restraining method both are new. The arena developed for free flight comparison is also novel, whereby the acoustically transparent flight tunnel concept allows for resonance-free measurements to be taken.

Therefore, a specific free and tethered flight comparison would be of value to describe how the specific tethering approach developed, compares with the novel free flight arena developed. This could then serve as a guide, to determine which approach should be used for further laboratory investigations of factors that affect mosquito acoustics.

#### 4.1.2 – MOSQUITO SPECIES

Chapter 2 conducted a preliminary assessment between female *Cx. quinquefasciatus*, *An. gambiae* and *Ae. aegypti* under free flight, reverberant conditions provided by the Ø80mm tunnel design. Conversely, the semi-anechoic chamber developed in Chapter 3 permits measurement without these acoustic compromises. Accordingly, it is of great interest to conduct a more thorough comparison between the same three species, to evaluate the differences observed under semi-anechoic conditions.

#### 4.1.3 – AIMS AND OBJECTIVES

As the literature provides conflicting accounts of the effects of tethering when compared to free flight, quantifying the differences between the two measurement approaches developed here will allow for the translatability of the two approaches to be determined. This will enable an understanding of how tethered results could be used in a free-flight chamber that might inform a simple design for acoustic mosquito identification device suitable for use in the field.

A dataset will be collected to compare wingbeat acoustics across the three species assessed in Chapter 2: *Ae. aegypti*, *An. gambiae* and *Cx. quinquefasciatus*.

### **Chapter Aim**

The aim of this chapter is to investigate the measured wingbeat acoustics of mosquitoes using the tethered and free-flight approaches developed in Chapter 3. The null hypothesis evaluated is that there are no differences in the wingbeat frequency between the two flight modes. This chapter will also evaluate free flight acoustics across three species by validation of the null hypothesis that there is no difference between their wingbeat frequencies.

## Chapter Objectives

- Describe the wingbeat acoustic profiles with the semi-anechoic developed methods and workflows of Chapter 3, under tethered and free flight with *Ae. aegypti* female mosquitoes, using the same individuals for both measurement conditions.
- Describe and compare the wingbeat acoustic profiles for individual *Ae. aegypti* mosquitoes when measured twice separated by a 30 minute interval.
- Describe and compare the semi-anechoic free-flight wingbeat profiles of *Ae. aegypti*, *An. gambiae* and *Cx. quinquefasciatus*

## 4.2 Materials and methods

### 4.2.1 – EXPERIMENTAL DESIGN: FREE FLIGHT VS TETHERED FLIGHT

A Latin square design was used to evaluate how the flight mode (tethered or free-flight) affects the flight of an individual mosquito (appendix A1). Female *Ae. aegypti* mosquitoes (n = 30), non-blood fed and all between 14-30 days post emergence were measured twice each, in the following three possible combinations (n=60):

- 1<sup>st</sup> free-flight, 2<sup>nd</sup> tethered (n=20)
- 1<sup>st</sup> tethered, 2<sup>nd</sup> tethered (n=20)
- 1<sup>st</sup> free-flight, 2<sup>nd</sup> free-flight (n=20)

Measurements were then taken in a randomised order, which could be three combinations of tethered and free-flight. The only measurement combination not evaluated was tethered first, followed by free-flight as, once mosquitoes were tethered, the tether could not be removed. The effect of recording mosquito flight

twice was accounted for in the design by the repetition of tethered and free flight measurements twice, in addition to the tethered and free flight combination.

Statistical analysis was conducted using a linear mixed effect model. This allowed the significance of order, and flight type and their interaction to be evaluated whilst accounting for the repeated measures encountered by using the same specimen for two measurements. Null hypotheses evaluated were:

1. There is no significant difference between free flight or tethered conditions.
2. Order of measurement does not result with a significant difference.
3. There is no significant interaction effect between measurement order and flight type.

The primary outcome measurement metrics used to test the null hypotheses were the sensor mean fundamental frequency and its standard deviation during the flight burst periods analysed. Both measurement scenarios used two sensors, with two microphones (LHS & RHS) used for free-flight measurements, whilst a single microphone and accelerometer were used for tethered measurements. All tethered measurements were conducted at a 30mm distance from the microphone at a 0° angle.

Using the tethered measurements also permitted for analysis of frequency amplitudes. Acceleration and sound pressure levels of the fundamental frequency were described using the LHS microphone and tether accelerometer. A one-way ANOVA was used to evaluate of the effect of measurement order on observed tethered amplitudes and their amplitude standard deviations. Free flight measurements could not be used for amplitude descriptions since the position of mosquitoes relative to the measurement microphones during free-flight was not characterised. Prior to the one-way ANOVA proceeding, a normality test of residuals based on the Shapiro-Wilkes test was performed to validate normal distribution of the data to be analysed, and a logarithmic data transform applied if required.

#### 4.2.2 – EXPERIMENTAL DESIGN: FREE FLIGHT SPECIES COMPARISON

Free flight measurements were taken for the three species individually within the semi-anechoic chamber, with each species cohort reared in parallel with each other. To compensate for their differing diel rhythms (Wilke et al., 2023), measurements were taken to coincide with each species specific active time. *Ae. aegypti* measurements were taken during corresponding day hours, whilst *Cx. quinquefasciatus* & *An. gambiae* measurements were taken outside these hours, as defined by the photophase used during their rearing. Measurements taken were 1800s in duration, and analysis followed the approach in section 4.2.3.

The three species were analysed against each other using a one-way ANOVA with Tukey HSD post hoc analyses ( $P < 0.05$ ). This was performed using the mean fundamental frequency of the LHS and RHS microphones for each measurement, which was the defined primary outcome metric. The standard deviation of the fundamental frequency for each analysed sample was used as a secondary measurement metric, which was also calculated from the mean of the LHS and RHS microphones. Prior to the one-way ANOVA proceeding, a normality test of residuals based on the Shapiro-Wilkes test was performed to validate the normal distribution of the data to be analysed.

#### 4.2.3 – MOSQUITO REARING AND HANDLING

*Ae. aegypti*, *An. gambiae* and *Cx. quinquefasciatus* were reared as described in section 2.3.3, with each species kept in separate rearing cages. Mosquitoes were 14-30 days post emergence and non-blood fed. This age group was selected as it was found to reliably fly under both free flight and tethered conditions with little external stimulation required. This grouping also matches the oldest age group evaluated by the study of Staunton et al. (2019b). Handling and tethering followed the airflow tether technique described in section 3.1.1

#### 4.2.4 - ACOUSTIC SETUP

All measurement apparatus were kept in the same insectary as the adult mosquito cages, to ensure constant humidity and temperature for the mosquitoes between their rearing cage to test arena. Acoustic equipment calibration followed the same method described in section 2.3.3. All measurements were taken at insectary conditions of 60% humidity at 29°C. To ensure silence within the anechoic chamber, the insectary humidifier was turned off and its 3 phase power supply was isolated from the humidifier to reduce 50 Hz mains interference. Internal sensors within the chamber would monitor the humidity and temperature.

##### *Free flight*

For free flight measurements, the Ø76 acoustically transparent flight tunnel (figure 3.2) was installed into the semi-anechoic chamber. Free flight measurements used two measurement microphones (section 3.3.1), and mosquitoes were introduced to the chamber via the airlock system (section 3.3.1).

##### *Tethered*

For tethered measurements, the positional controller (section 3.3.2, figure 3.8a) was installed into the chamber, and tethered mosquitoes were positioned within the semi-anechoic chamber. The position of the mosquito was set to 0° and 30 mm from the measurement microphone. Tethered measurements used a single microphone and a tether mounted accelerometer as detailed in section 3.3.2. Before commencing the recording, the direction of the mosquito was verified again to 0°, to ensure that it was oriented facing the microphone, as required. If the bead of glue used to tether the mosquitoes was too small, it could twist and change its orientation. In these instances, the specimen was discarded as its direction would not be constant throughout the measurement. Following the measurement, the mosquito direction was inspected, to ensure that its direction had not changed with respect to the microphone, otherwise the measurement was discarded.

### *Free flight to tether flight mode hardware changeover*

Swapping the flight type apparatus within the semi-anechoic chamber (positional controller for tethered, acoustically transparent tunnel for free flight) took c.a 1-2 minutes to perform. To avoid recalibrating the two measurement microphones and accelerometer, these three sensors were calibrated initially at the start of a test day, and were kept connected throughout all measurements, regardless of tethered or free flight.

#### 4.2.5 – ANALYSIS WORKFLOW

Using PAK 5.8 analysis templates, the spectrograms were individually generated for each specimen (example appendix figure A2). Each flight measurement was inspected, and a region of constant flight was identified, to a maximum of 10s. The frequency spectra and their respective amplitudes were generated in a second template (example appendix figure A3), which analysed the standard deviations of frequency and amplitudes for both microphone and accelerometer measurements (table 4.1).

The second measurement report would generate four metrics (table 4.1) for both the microphone and accelerometer sensors, with microphone fundamental frequency and amplitude defined as the primary outcomes.

**Table 4.1** – Acoustic metrics (and labels) used for analysis of tethered mosquito flight

	<b>Microphone</b>	<b>Accelerometer</b>
1. Fundamental frequency (Hz)	M1	A1
2. Fundamental frequency amplitude (dB)	M2	A2
3. Fundamental frequency standard deviation (Hz)	M3	A3
4. Fundamental frequency amplitude standard deviation (dB)	M4	A4

A measurement time of 300s for the free flight and tether comparison investigation was used, as the original 1800s measurement time would not permit enough replicates to be completed per test day. As outlined in Chapter 3, stable parts of

mosquito flight (constant flight burst) were manually selected from all spectrograms to identify the fundamental frequency.

Free flight measurements used the two microphones on the LHS and RHS of the chamber, and the fundamental frequency was identified from their combined means. This approach was also used for tethered measurements, using the means of the LHS microphone and the tethered accelerometer. Amplitude assessments were undertaken for exclusively tethered mosquitoes, using both the LHS microphone and the accelerometer acceleration.

## 4.3 Results

### 4.3.1 – TETHERING VS FREE FLIGHT

#### *Fundamental frequency – flight type*

Estimated marginal mean fundamental frequency under tethered flight was reported at 600.7 Hz (SE = 9.90 Hz) and 618.3 Hz (SE = 9.90 Hz) under free flight (figure 4.1). There was not a statistically significant difference detected between the fundamental frequencies measured under tethered and free-flight conditions ( $df = 44.5$ ,  $F = 2.416$ ,  $p = 0.126$ ).

#### *Fundamental frequency – order*

There was no statistically significant difference detected between the fundamental frequencies by measurement order ( $df = 32.41$ ,  $F = 1.391$ ,  $p = 0.247$ ). Estimated marginal means of fundamental frequency were 613.9 Hz (SE = 8.95 Hz) for first measurements, and 605.06 Hz (SE = 8.95 Hz) for second measurements (figure 4.1).

#### *Fundamental frequency – flight type and order interaction*

No significant effects were detected between the interaction of flight order and flight type ( $df = 30.49$ ,  $F = 3.327$ ,  $p = 0.078$ ). Estimated marginal means during free flight were 629.7 Hz (SE = 9.79 Hz) for first measurements, and 606.8 Hz (SE = 12.6 Hz) for second measurements. Estimated marginal means during tethered flight were 598.1 Hz (SE = 12.6 Hz) for first measurements, and 603.4 Hz (SE = 9.8 Hz) for second measurements (figure 4.2).

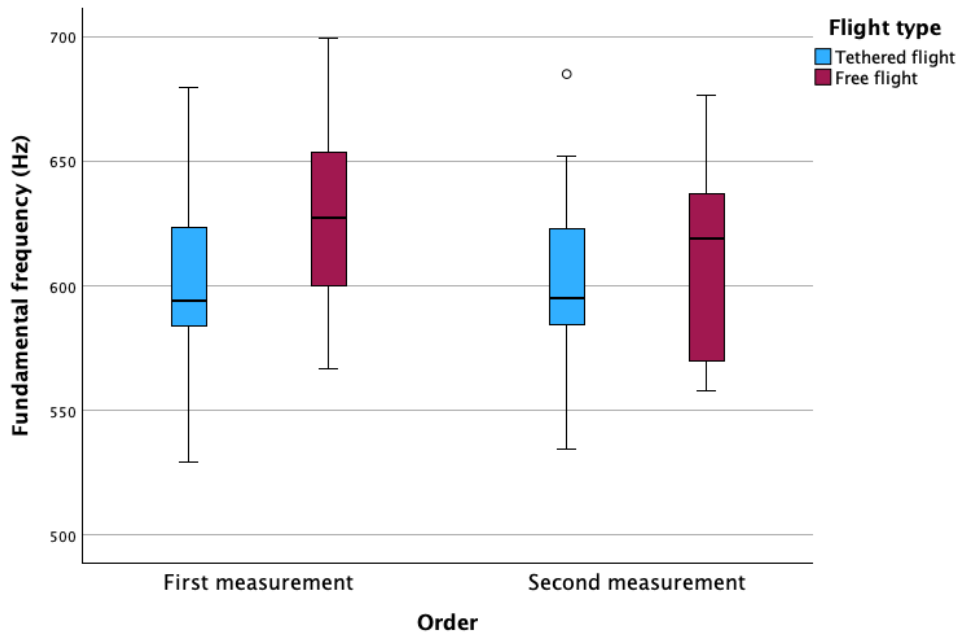


**Figure 4.1** – Fundamental frequencies by order for tethered and free flight measurements. Outliers represented by circle

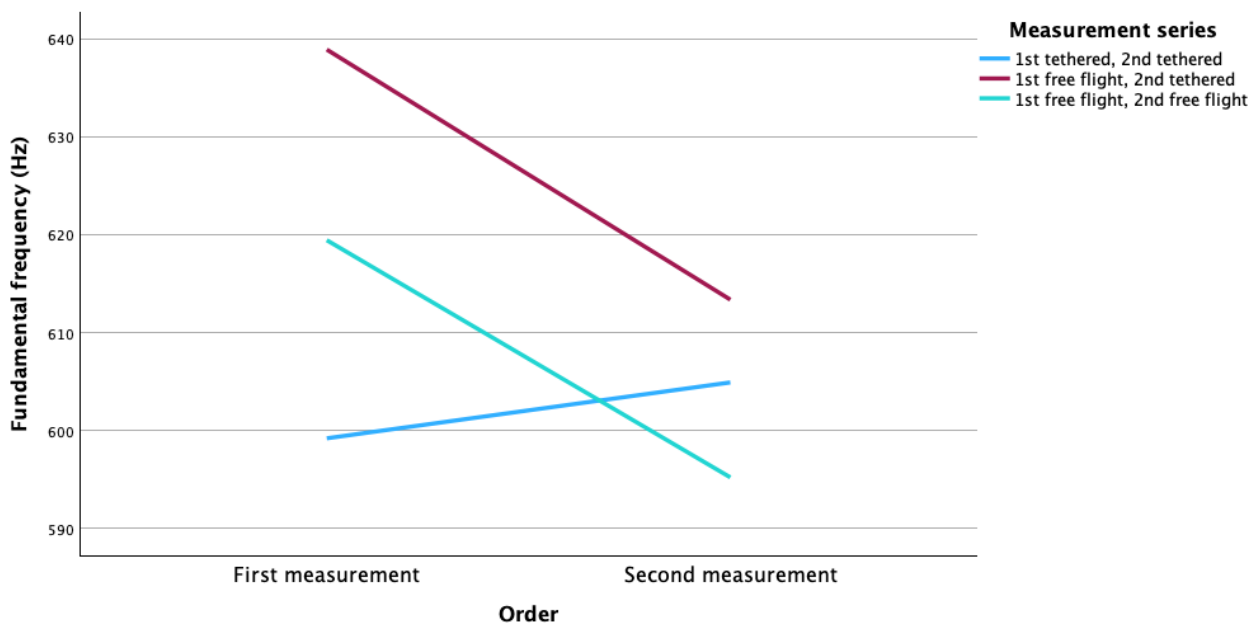


**Figure 4.2** – Mean fundamental frequencies by order for the three flight type combinations

### *Fundamental frequency standard deviation – flight type*

Estimated marginal means of the fundamental frequency standard deviation was at 10.09 Hz (SE 2.27 Hz) under free-flight conditions, and 8.73 Hz (SE = 2.27 Hz) under tethered conditions. No significant difference was detected between the flight types ( $df = 49.95$ ,  $F = 0.186$ ,  $p = 0.667$ ).

### *Fundamental frequency standard deviation – order*

Estimated marginal means of the fundamental frequency standard deviation was at 12.73 Hz (SE = 2.17 Hz) for first measurements, and 6.09 Hz (SE = 2.17 Hz) for second measurements (figure 4.3). A significant difference is reported between the measurement orders, (df = 33.85,  $F = 5.512$ ,  $p = 0.025$ ).

### *Fundamental frequency standard deviation – flight type and order interaction*

No significant effects were detected for the interaction of flight type and measurement order (df = 40.48,  $F = 0.569$ ,  $p = 0.455$ ). Estimated marginal means during free flight were 12.3 Hz (SE = 2.49 Hz) for first measurements, and 7.86 Hz (SE = 3.51 Hz) for second measurements. Estimated marginal means during tethered flight were 13.1 Hz (SE = 3.51 Hz) for first measurements, and 4.3 Hz (SE = 2.549 Hz) for second measurements (figure 4.4).

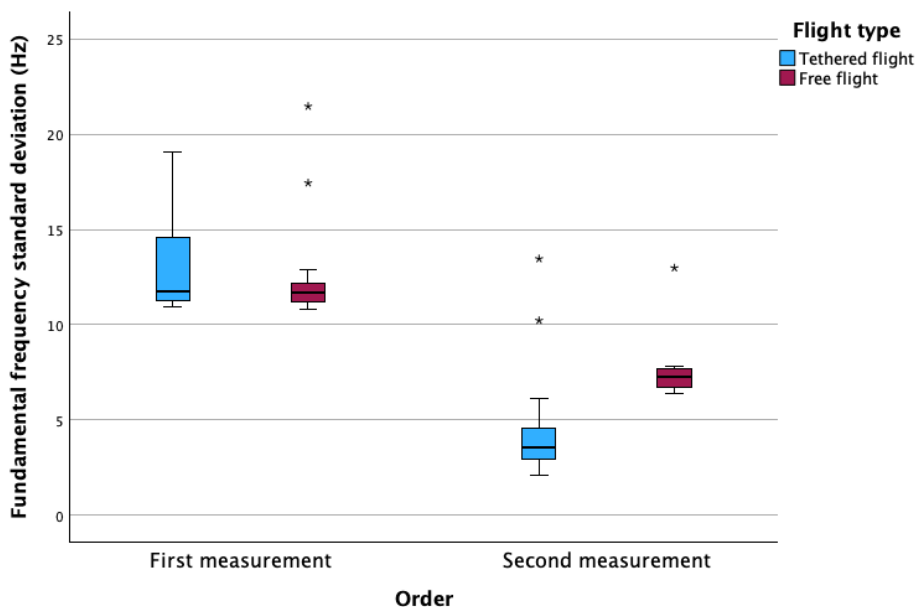


**Figure 4.3** – Fundamental frequency standard deviations by order for tethered and free flight measurements. Outliers represented by asterisks

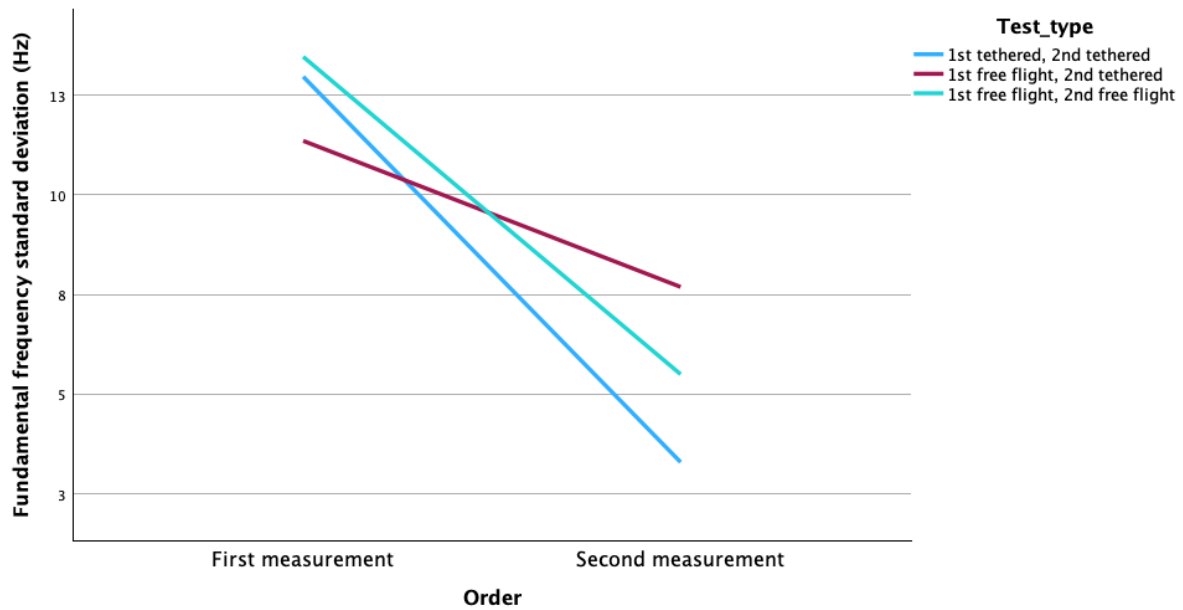


**Figure 4.4** – Mean fundamental frequency standard deviations by order for the three flight type combinations

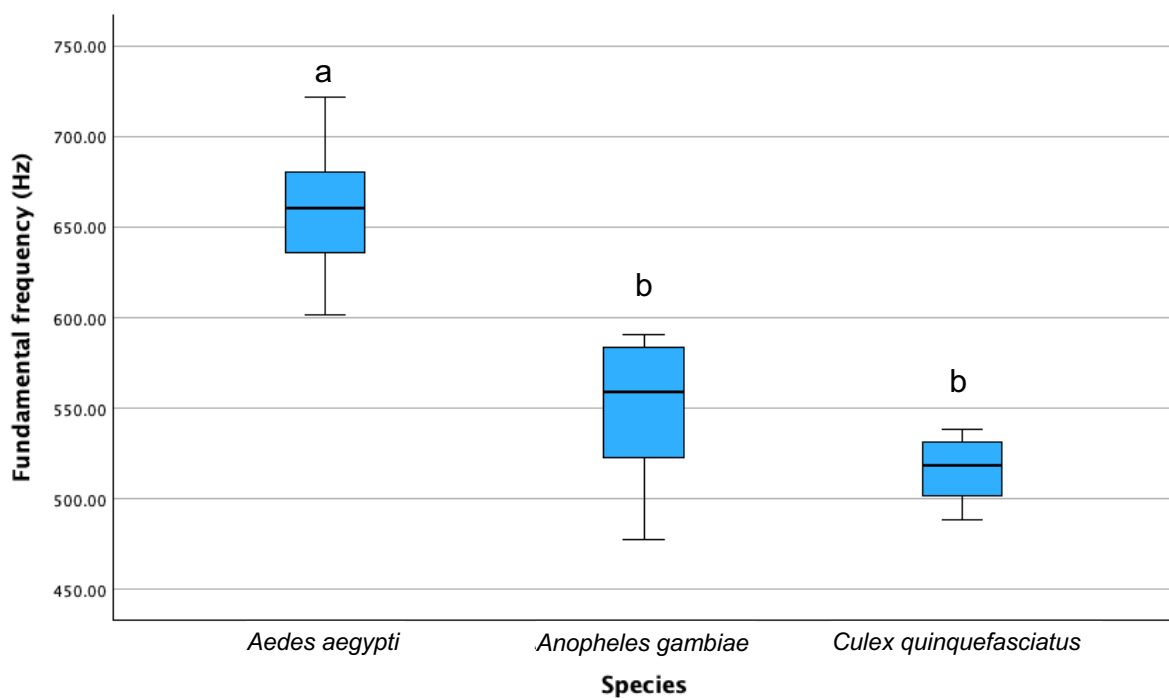
#### *Fundamental frequency amplitude metrics – tethered order comparison*

Female tethered *Ae. aegypti* mosquitoes ( $n = 10$ ) were measured twice, at 30 min intervals. No significant effect was detected across all microphone and accelerometer derived amplitude metrics, between first and second tethered measurements. Mean fundamental frequency sound pressure level was detected at 27.4 dB (SE = 1.963 dB) for first measurements and 26.6 dB (SE = 1.963 dB) for second measurements ( $df = 1$ ,  $F = 0.081$ ,  $p = 0.779$ ). Mean fundamental frequency acceleration was detected at 0.00262  $m/s^2$  (SE = 0.0007  $m/s^2$ ) for first measurements and 0.00243  $m/s^2$  (SE = 0.0007  $m/s^2$ ) for second measurements ( $df = 1$ ,  $F = 0.036$ ,  $p = 0.852$ ).

Mean fundamental frequency standard deviation of sound pressure level was detected at 1.54 dB (SE = 0.23) for first measurements and 1.27 dB (SE = 0.23) for second measurements ( $df = 1$ ,  $F = 0.707$ ,  $p = 0.412$ ). Mean fundamental frequency standard deviation of acceleration was reported at 0.0007  $m/s^2$  (SE = 0.0002  $m/s^2$ ) for first measurements and 0.0006  $m/s^2$  (SE = 0.0002  $m/s^2$ ) for second measurements ( $df = 1$ ,  $F = 0.060$ ,  $p = 0.809$ ).

## 4.3.2 – FREE FLIGHT SPECIES COMPARISON

Female *Ae. aegypti* (n = 10), *An. gambiae* (n = 10), and *Cx. quinquefasciatus* (n = 10) mosquitoes were measured in the semi anechoic chamber under free-flight conditions. Mosquitoes were not blood fed and between 0-8 days post emergence when measured individually.

*Fundamental frequency*

**Figure 4.5** – Mean free flight fundamental frequencies by species. Letters above the boxplots indicate which groups differ significantly from one another (One way ANOVA with Tukey post-hoc analyses  $P < 0.05$ )

Mean fundamental frequency for *Ae. aegypti* is detected at 661.4 Hz (SE = 10.1 Hz), 547.9 Hz (SE = 10.1 Hz) for *An. gambiae* and 516.9 Hz (SE = 10.1 Hz) for *Cx. quinquefasciatus* (figure 4.5). Differences detected between *An. gambiae* or *Cx. quinquefasciatus*, versus *Ae. aegypti* were significant ( $F = 56.832$ ,  $p < 0.001$ ).

### Fundamental frequency standard deviation

Mean fundamental frequency standard deviation measured across the 10s analysis window, for *Ae. aegypti* is reported at 3.84 Hz (SE 0.38 Hz), 9.04 Hz (SE = 0.38 Hz) for *An. gambiae* and 3.97 Hz (SE = 0.38 Hz) for *Cx. quinquefasciatus* (figure 4.6). A statistically significant difference was detected between *Ae. aegypti* or *Cx. quinquefasciatus*, versus *An. gambiae* ( $F = 62.41$ ,  $p < 0.001$ ).

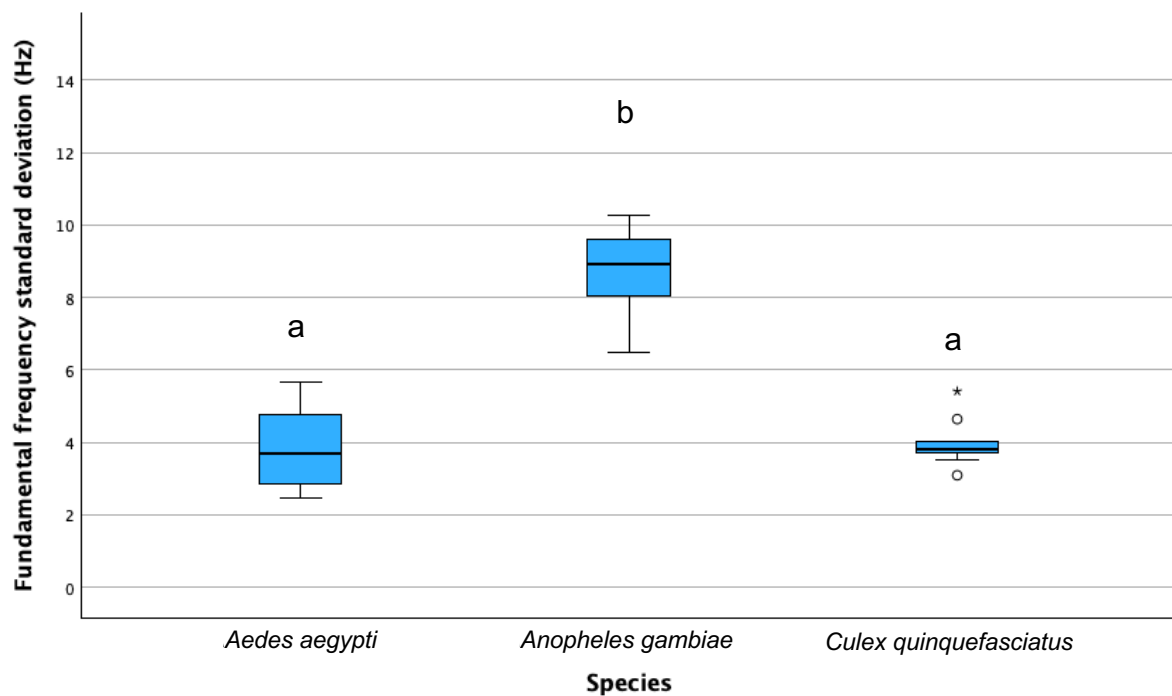


**Figure 4.6** – Mean free flight fundamental frequency standard deviation by species. Letters above the boxplots indicate which groups differ significantly from one another (One way ANOVA with Tukey post-hoc analyses  $P < 0.05$ )

## 4.4 Harmonic convergence – an example

### 4.4.1 – HARMONIC CONVERGENCE OF FLIGHT TONES

During the measurement series of section. 4.3, which focussed on capturing and describing the free-flight acoustics of *Ae. aegypti*, *An. gambiae* and *Cx. quinquefasciatus* females, an incidental copulation event was captured in free flight for a male and female *Cx. quinquefasciatus*. Due to the difficulties in initiating this flight behaviour on demand, this was not planned as a measurement series, however the data captured are presented for this event as the uniquely high signal-noise ratio of the semi-anechoic free-flight chamber allows simple comparison to prior tethered and free-flight descriptions.

It is well documented that during courtship between male and female mosquitoes, there is a modulation of flight tone that occurs between the two sexes. Males typically exhibit higher fundamental frequencies than their female counterparts, which has been validated across mosquito genera. The higher wingbeat frequencies produced by males than females has been described extensively (Lauren J Cator et al., 2009b; League et al., 2022; Villarreal et al., 2017b). However, during courtship, a flight tone modulation has been reported whereby a period of “frequency-matching behaviour” occurs where wing-beat frequencies of the two sexes converge on a nearest shared harmonic (Warren et al., 2009a). Earlier studies describing this harmonic convergence behaviour used methods involving tethered specimens, whereby either the of two sexes were tethered, with one specimen moved past a stationary partner to record the harmonic convergence effect record the harmonic convergence effect (Lauren J Cator et al., 2009b). Variations to this approach swapped one flight partner with an artificial tone played through an earbud style headphone at a level deemed comparable to mosquito flight, to further investigate the harmonic convergence effect (Cator and Zanti, 2016).

These experiments are performed under tethered or semi-tethered conditions, mostly using microphones as the chosen sensors. This is due to the harmonic convergence effect requiring examination of the behaviour changes that occur over time when two mosquitoes are in close physical proximity to each other, which is simplest to perform with tethered mosquitoes and microphones. However, an increasing number of studies have devised approaches to capture the acoustics of more natural swarming behaviour (Garcia Castillo et al., 2021; Simões et al., 2016a). These are more challenging to set up though, requiring more extensive acoustic arenas and more microphones to capture free-flight swarming tones.

#### 4.4.2 –RESULTS

A male and female *Cx. quinquefasciatus*, both 7 days post emergence, were concurrently released into the Ø76 semi-anechoic flight tunnel. Both sexes flew within the free flight tunnel, with a copulation event occurring at 260s (figures 4.7 – 4.10). Free flight was recorded for a total of 900s, with post copulation flight occurring for both males and females. Pre-copulation fundamental frequencies were recorded at 855.5 Hz (male) and 468.8 Hz (female). During the copulation event, the fundamental frequency of the male increased, as visible on the spectrograms (figure 4.7 - 4.9), with the frequency spectra calculated during this frequency change period exhibiting a lower peak combined with the additional frequencies (figures 4.7).

During copulation, amplitude of the female's fundamental frequency remained louder (25.2 dB) than the male's fundamental frequency amplitude (13.9 dB). At this time, both mosquitoes were recorded at an unspecified position relative to the measurement microphones. Post copulation tones for the female returned to 468.8 Hz, whilst the male was recorded at 832.0 Hz. Both males and females were recorded in free flight after the copulation event, with the male flying uninterrupted for over 300s, whilst the female exhibited resting behaviour. Following the cessation of flight from the male, the female recommenced flight, at which point it demonstrated an intermittent flight pattern up to 900s (figure 4.10).

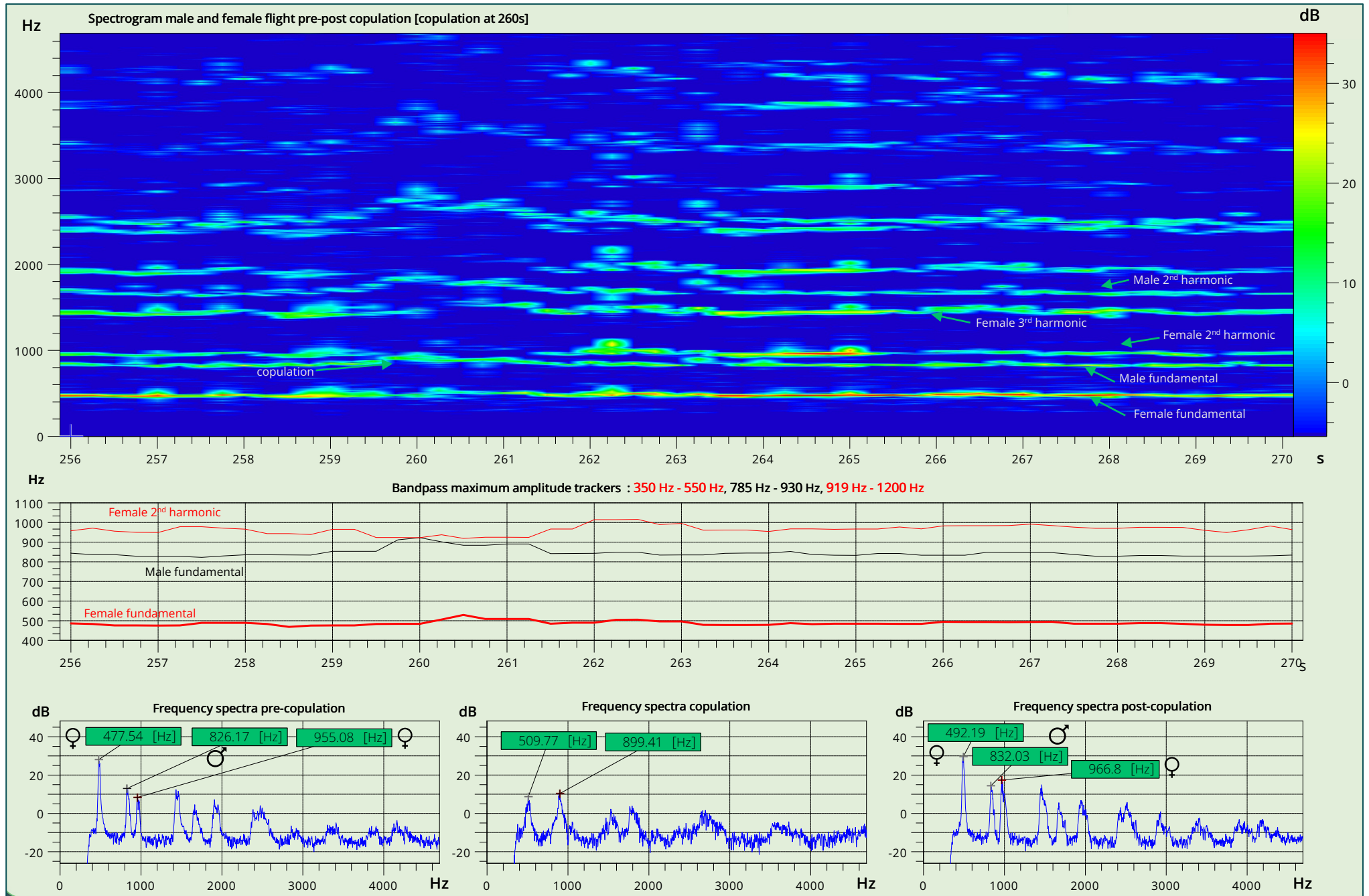


**Figure 4.7** – Labeled spectrograms and frequency spectra before, during and after copulation for *Culex quinquefasciatus*

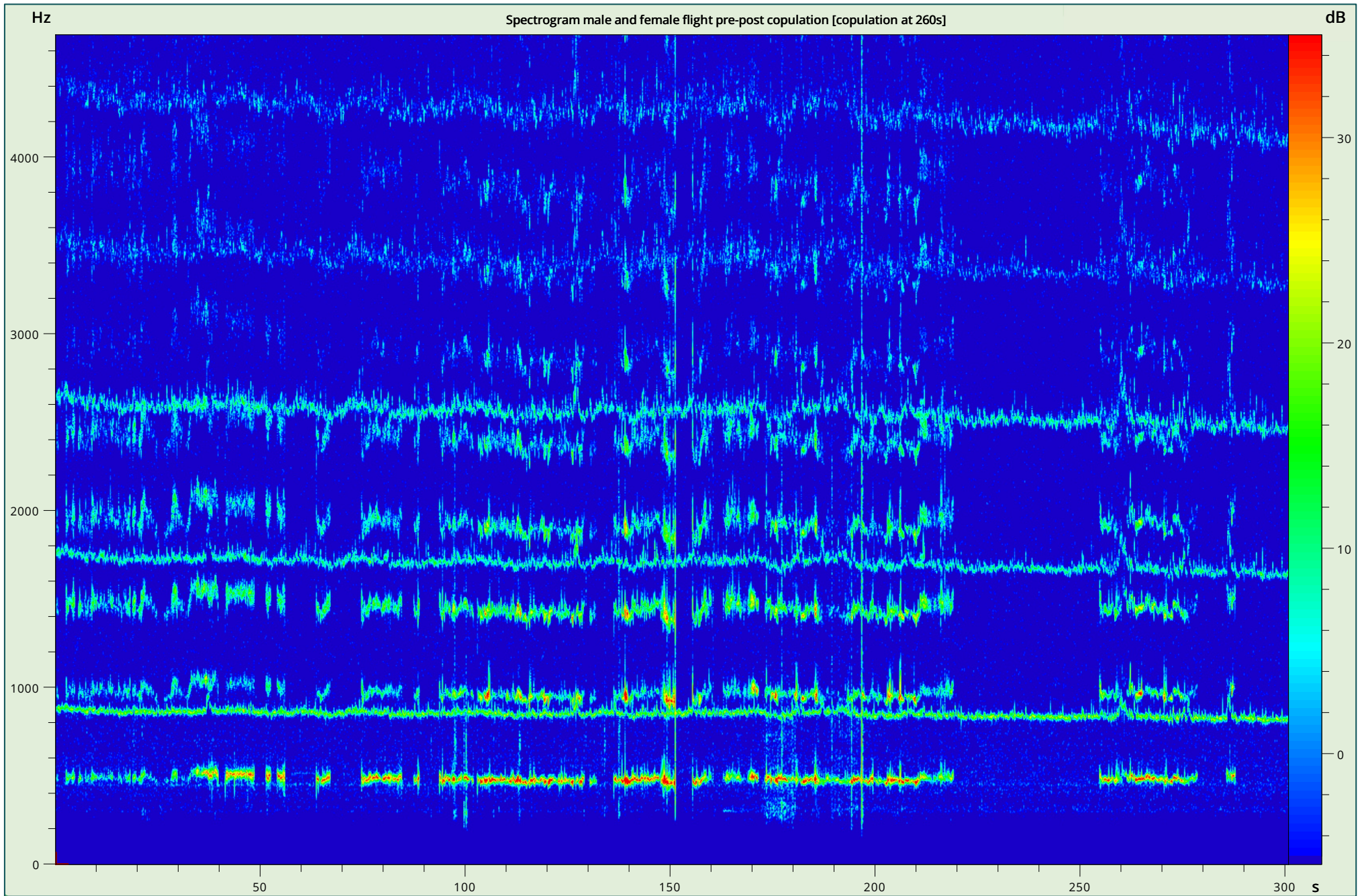


**Figure 4.8** – Detailed 300s spectrogram before, during and after copulation for *Culex quinquefasciatus*

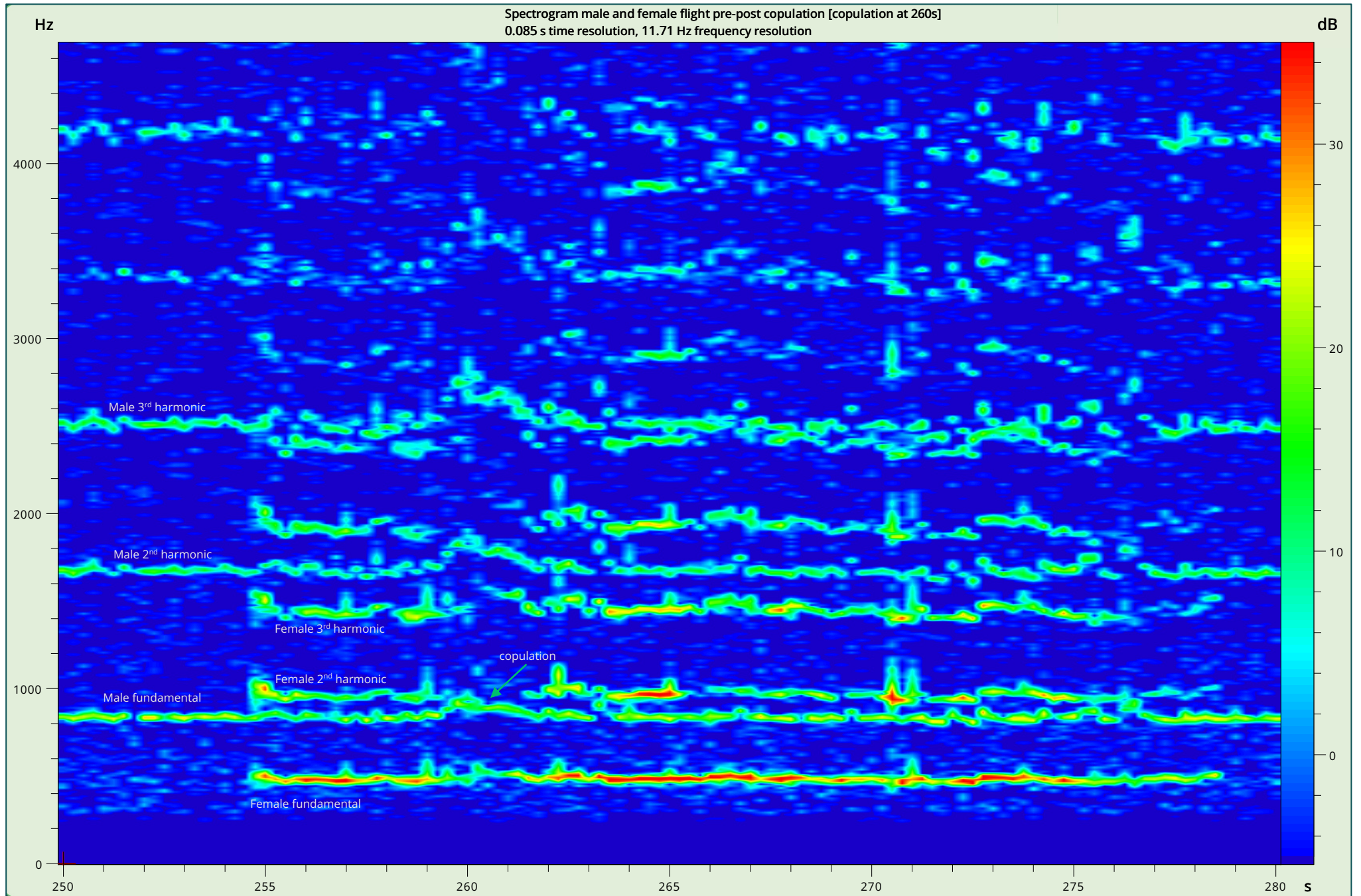


**Figure 4.9** – Detailed spectrogram during copulation for *Culex quinquefasciatus* (0.085s time resolution at 11.71 Hz frequency resolution)

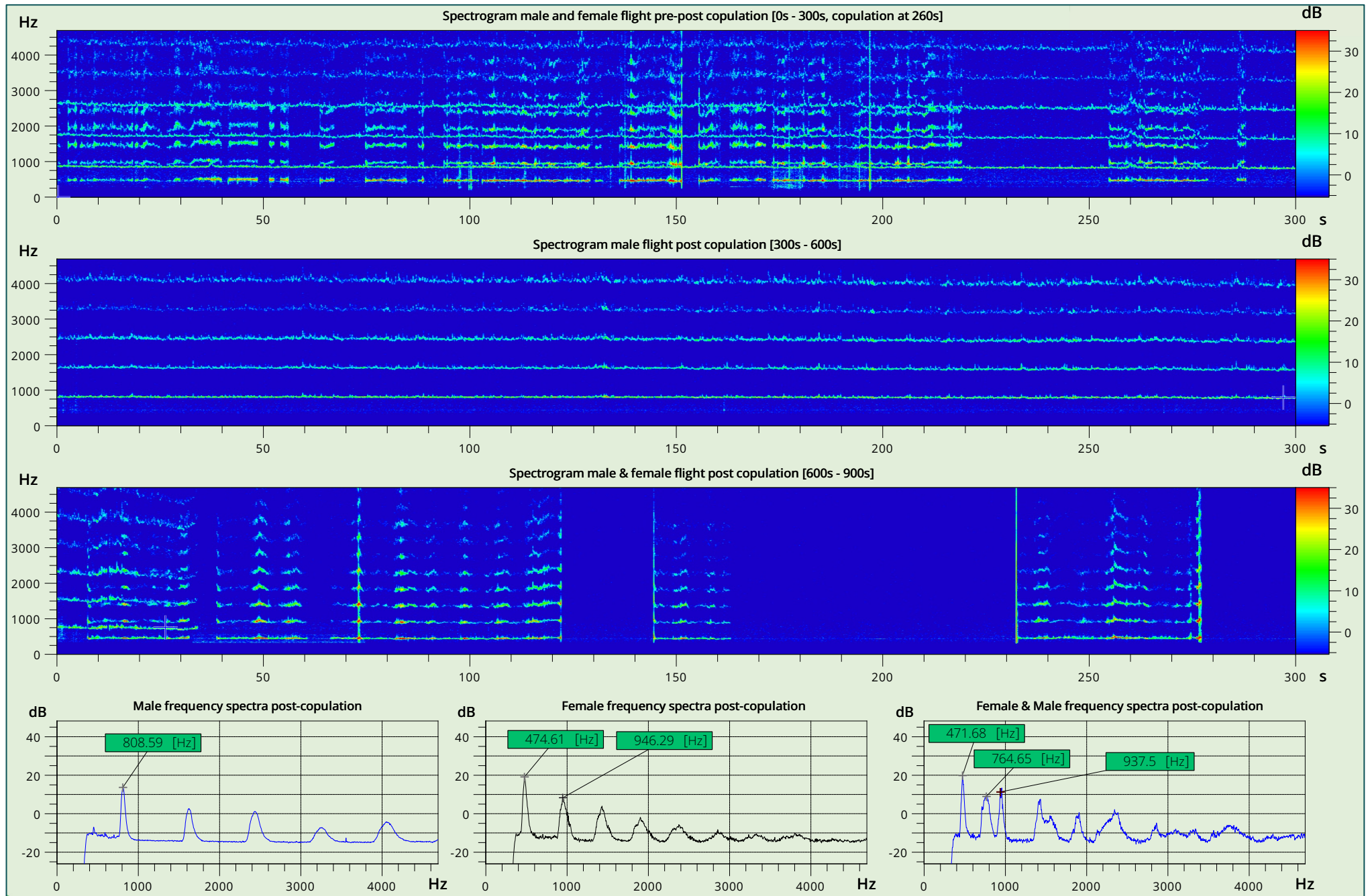


Figure 4.10 – 0s - 900s spectrograms (labelled) before, during and after copulation for *Culex quinquefasciatus*

## 4.5 Discussion

### 4.5.1 – TETHERED VS FREE FLIGHT

The investigation to compare the wing beat frequency under tethered and free flight conditions demonstrated that the mean fundamental frequency of the *Ae. aegypti* mosquitoes was lower during tethered flight than free flight (figure 4.1), but this was not statistically significant. As discussed in the introduction of this chapter, the literature features comparisons of free flight and tethered flight that both support and reject the hypothesis that there is no significant difference in fundamental flight tone between the two measurement approaches. The findings presented here, for this specific tethered and free flight methodology support the results of Villarreal et al. (2017b), which also described no significant differences in fundamental frequency between free flight and tethered approaches. The comparison conducted by Villarreal et al is also comparable to the results presented here, as *Ae. aegypti* was used, and their experimental design used a similar repeated measures setup whereby the same individuals were also evaluated under both flight conditions.

Conversely, the study of Pantoja-Sánchez et al. (2019), used *Anopheles darlingi* and reported a significant difference in fundamental frequency, with the frequency observed to be lower when tethered. Whilst the fundamental frequency means reported in this experiment were also lower when tethered, the difference here was not detected as statistically significant.

The present study enabled a direct comparison between the two methodologies which provides a valuable addition to the available knowledge base where conflicting results are presently found in the literature. For the specific methodology and equipment developed here, there is now a stronger justification for using a tethered approach over free flight, at least for describing the wingbeat frequency of *Ae. aegypti*. The tethered approach allows for controlled measurement

and simple acquisition of wingbeat frequency and its amplitude using sound pressure levels. Free-flight approaches cannot generate this amplitude data without additional data processing steps to track and describe mosquito position relative to the measurement microphones. However, the tethered approach does lose the temporal patterns present in free flight, which was illustrated and compared by figure 3.40. For this reason, a tethered approach should only focus on constant flight regions, when conducting controlled acoustic comparisons. This will be feasible and useful when investigating morphology and physiology effects, but a free-flight approach would also be beneficial in future work where more acoustic patterns could be described within this temporal data.

The measurement order demonstrated no significant effect on fundamental frequencies (figure 4.2), however there was a significant effect observed for the standard deviation of the fundamental frequencies. This was across all tested combinations of tethered and free flight approaches (figure 4.1). The observed reduction in standard deviation of the fundamental frequency (figure 3) for the analysed flight bursts could demonstrate a possible stabilisation of flight, from within the initial 300s measurement window to the subsequent second measurement which was after a 30 minute pause. Whilst the fundamental frequency identified was not significantly different between orders, the reduction in its variation within the measurement windows analysed could have implications for the repeatability of an automated approach for identifying mosquitoes based on being able to obtain a more stable signal.

The measurement order, when tethered demonstrated no significant effect in reported amplitudes for both acceleration and sound pressure level. This simple description demonstrates the stability of the measured mosquito flight tones under tethered conditions. It also demonstrates that the vibration-based metrics can complement the descriptions provided by a microphone, and can be used for further tethered assessments.

Describing the effect of order, using the fundamental frequency, has helped to provide a better understanding of the stability of mosquito flight. The utility of this description is that it demonstrates that the fundamental frequency when under both flight conditions is comparable, so further studies can potentially be designed using whichever is more appropriate and feasible for what is being evaluated. The order investigation also demonstrates the validity of using a repeated measures style of experimental design, since the fundamental frequency was not significantly different following the 30 min pause in recordings under both flight conditions. This could allow expansion in future work of the preliminary experiments using plastic flight tunnels or multiple tethered distance and angles (Chapter 2), which used the same mosquitoes under differing geometric arenas and measurement setups.

#### 4.5.2 – FREE FLIGHT SPECIES COMPARISON

Using the fundamental frequency demonstrated that when the three species were evaluated in free flight, only the frequencies of *An. gambiae* and *Cx. quinquefasciatus* were not significantly different from each other (figure 4.5). An interpretation of this finding could be that use of this metric would permit identification of the species which demonstrated significant differences. However, with the current methodology, this is not proposed as realistic outcome. The variation in wing beat frequency measured presents a frequency overlap that would make identification based purely on the fundamental frequency challenging. This overlap has been discussed by Kim et al. (2021) where their pairwise comparison of 26 mosquito species in free flight found overlaps of fundamental frequency with at least one other species. To overcome this, it was suggested by Kim et al. (2021) that a multivariate approach should be taken to incorporate different metrics to supplement the fundamental frequency, such as time, or measurement location. However, the variation in the fundamental frequency during the analysed window, as described by its standard deviation in the presented data here, could provide another acoustic metric for a multivariate analysis strategy.

A major advantage that the presented microphone-based free flight measurement approach offers over contemporary optical methods, is that measurement duration is not restricted, whilst optical methods can only acquire wingbeat data during the short duration that the mosquito in flight passes through a light beam (section 1.2.1). Using a microphone-based approach allows the variation in much longer measurements (c.a. 10s) to be described and potentially used as a supplementary acoustic metric, which optical approaches would not be able to exploit.

The presented data demonstrated that under free flight, variation (standard deviation) in the wingbeat frequency of *An. gambiae* was significantly different to that of *Ae. aegypti* and *Cx. quinquefasciatus*. However, when solely using the fundamental frequency metric, there was not a significant difference between *An. gambiae* and *Cx. quinquefasciatus*. Therefore, by using a combination of the fundamental frequency and its variation, a novel *acoustic* multivariate acoustic approach could increase the efficacy of future developed mosquito identification methods.

The lower standard deviations of *Ae. aegypti* and *Cx. quinquefasciatus* (figure 4.6) can be explained by observation of their spectrograms (figure 4.11). The flight bursts for these two species are longer and more stable, than those of *An. gambiae*. This resulted with their analysed periods of flight being much more stable, than those used for *An. gambiae*, which exhibited the additional frequency content associated with flight manoeuvres rather than constant flight (as described in Chapter 3). This difference in flight behaviour represented by the fundamental frequency standard deviation, could potentially be used for mosquito identification, in addition to the wingbeat fundamental frequency metric.

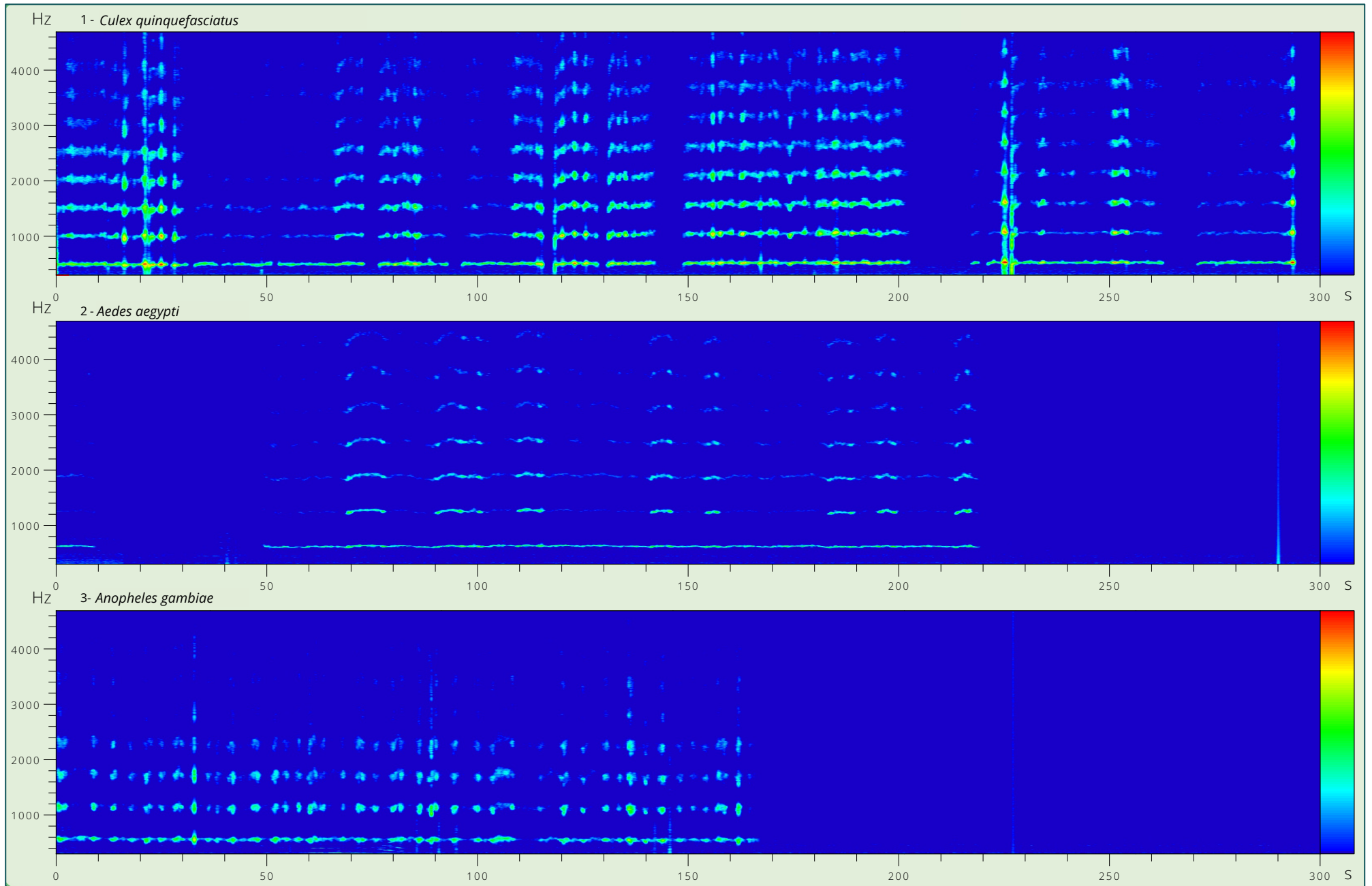


**Figure 4.11** – Spectrogram comparison of *Cx. quinquefasciatus*, *Ae. aegypti* and *An. gambiae*

### 4.5.3 – HARMONIC CONVERGENCE

The single measurement presented provides an illustration of the free-flight tones produced by the male and female *Cx. quinquefasciatus* mosquito before, during and after copulation. The flight tones produced by the female remain steady and constant, and the same can be said for the flight tones produced by the male. There is a clear increase in frequency at the point of copulation reported (figure 4.), which complements the prior acoustic descriptions of *Cx. quinquefasciatus* (Ingham, 2017; Simões et al., 2016b).

Rapid Frequency Modulation (RFM) has been proposed as a behaviour that males of *Cx. quinquefasciatus* exhibit during copulation, whereby a steep increase in wing-beat frequency is followed by a rapid modulation in the lead up to copula formation (Simões et al., 2016b). This behaviour is reported for both males and females, however in the presented dataset this can only be observed in the male. The female exhibits a different behaviour, whereby during the period of RFM in the male, the female fundamental remains constant, yet its amplitude reduces.

Of interest are also the harmonics, which attenuate to an extent that make them no longer visible to background levels. To counteract the Nyquist time-frequency resolution trade-off, the blocksize has been modified in figure 4.9 to increase time resolution such that this specific behaviour could be visualised with greater clarity. With the presented 0.085s time resolution, it is clear that the female fundamental frequency remained constant throughout the copulation interaction. The steep increase in male frequency can be clearly observed however, with the harmonics of the males confirming this.

Following the copulation event, an extended period of male flight was observed, at a constant flight tone, and female flight was also reported at a constant fundamental flight tone.

The logistical challenges of setting up this specific measurement, prevent in its current design capture of a larger dataset, however the RFM acoustic pattern can be observed and potentially used to identify copulation events in environments where this may be a useful metric to identify through mosquito acoustics.

## 4.6 Chapter summary

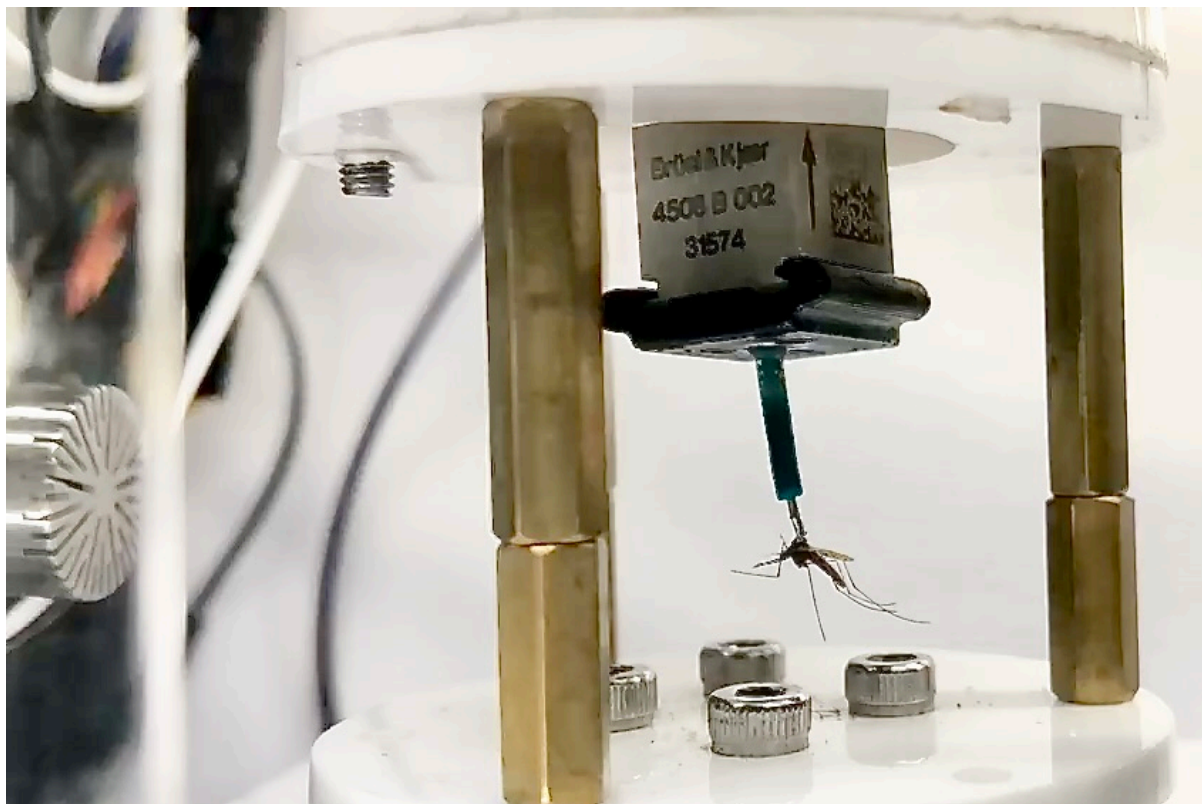
The effect of tethering compared to free flight has been discussed in the literature, however it has been demonstrated that for the developed methods here, with *Ae. aegypti*, there was not a significant difference in the fundamental frequency measured. It would be a useful exercise for future work to perform these descriptions for *An. gambiae* and *Cx. quinquefasciatus*, as well as for additional species to be investigated in the future. This established that a tethered approach to describe wingbeat frequency can be used in further laboratory acoustic descriptions that may benefit from the extra control this approach offers over a free flight approach.

Demonstrating that there was no significant frequency difference when conducting two measurements 30 minutes apart, suggests future work can be performed with a time pause. This would allow future experiments that require repeated use of individuals to be conducted. Examples of these could include experiments exploring the effect of changing angle, distance or tunnel geometry as proposed in Chapters 2 & 3, to be conducted.

The microphone-based approach allowed for copulation events to be captured, which would not be feasible using optical approaches. Whilst capturing this behaviour was an incidental finding, it has demonstrated another benefit of using microphones over light beam-break optical approaches. Microphones allow longer time period events to be captured which optical approaches would not be able to perform, when both male and female mosquitoes are in free flight.

The utility of using the standard deviation of fundamental frequency during an analysed 10s flight burst has also been demonstrated. This was also possible due to the microphone-based measurement and the semi-anechoic chamber designed, since the flight tone could be captured and analysed across this entire period. The fundamental frequency standard deviation metric indicated significant differences between species which otherwise featured no significant differences between their fundamental frequencies. This opens the possibility of establishing an acoustic multivariate approach. Such an approach could use a combination of acoustic metrics, including fundamental frequency and its variation over time, as described by the standard deviation here, to support acoustic classification.

# CHAPTER 5: PHYSIOLOGICAL EFFECTS ON MOSQUITO ACOUSTICS



Tethered mosquito inside the measurement chamber with accelerometer and microphone sensors

## 5.1 Introduction

### 5.1.1 - EXPLORING PHYSIOLOGY WITH THE TETHERED APPROACH

In Chapter 4, the free flight assessment between *Ae. aegypti*, *Cx. quinquefasciatus* and *An. gambiae* demonstrated that significant differences in flight tone could be identified between *Ae. aegypti* and either *An. gambiae* or *Cx. quinquefasciatus* (figure 4.5). However by also using the standard deviation of the fundamental frequency across its analysis period, differences in the stability of the fundamental

could be used to establish a significant difference between *An. gambiae* and the other two species (figure 4.6). What was not investigated further in Chapter 4 however, was the utility of sound pressure level amplitude metrics. The free flight and tethered flight comparison investigation demonstrated that alongside the fundamental frequency being repeatable (figure 4.1), its amplitude also did not exhibit significant differences, indicating it was also a stable metric over a 30 minute interval. This greater set of acoustic metrics that the tethered approach provides over a free flight approach, therefore makes it an excellent choice when investigating the acoustics of mosquitoes beyond species differences. Since these metrics go beyond the wingbeat frequency, their acoustic descriptions may reveal differences in their wingbeat acoustics that are simpler to identify than a wingbeat frequency exclusive approach.

### 5.1.2 –SELECTION OF PHYSIOLOGY TO INVESTIGATE

As introduced in section 1.2.2, a significant body of research has been accrued to understand the role acoustics plays with mosquito behaviours. These have included but are not limited to the acoustic effects of: male-female interactions (Cator and Zanti, 2016), age (Park et al., 2023), size and temperature (Staunton et al., 2019b). These have primarily used the fundamental frequency as the primary measurement metric, whereas the tethered approach developed can go beyond describing flight acoustics exclusively with this metric.

However, despite the literature containing acoustic assessments of many possible mosquito physiological states (section 1.2.2), a limitation arises since methods followed are not the same. There is no unified protocol for measuring the mosquito wingbeat (Villarreal et al., 2017b), which makes comparing results from across multiple physiological state studies more challenging. This is compounded when physiological state effects are validated across differing species, making it more challenging to understand expected acoustic effects.

What would therefore be of great utility would be to conduct a controlled but broad investigation, that allows comparison of physiological states whilst also using multiple mosquito species of interest. Section 1.2.4 introduced factors that are of interest to describe from the perspective of *vector control*, which included species, age and blood meals. The effects of blood meals, and age are two factors well suited for this investigation with a tethered approach, across the same three species evaluated in Chapter 2 (*Ae. aegypti*, *An. gambiae* and *Cx. quinquefasciatus*).

### *Age*

When considering the effect of age on mosquito acoustics, the study of Staunton et al. (2019b) was already referenced, whereby three age groupings were investigated for their effect on the wingbeat frequency for *Ae. aegypti* at 1, 2 and 3 weeks post emergence. It was noted that 3 weeks was a little longer than the typical lifespan of *Ae. aegypti* in the field, however testing of the extreme age scenario was done to stress any potential age effects (Staunton et al., 2019b). The same three groupings of age were (with post-hoc analysis) evaluated in a more recent study of Park et al. (2023), where lifecycle stages were also evaluated with the wingbeat frequency.

### *Blood meal*

Unlike prior work on connecting mosquito wing-beat frequencies to their age, far less attention has been paid to exploring how a blood meal affects mosquito acoustics. The aforementioned investigation of Park et al. (2023) did not explicitly evaluate the effect of a blood meal, but post-blood meal mosquitoes were measured for their wingbeat frequency during their period of digestion 3 days post blood meal. The number of blood meals would also be a useful metric to describe acoustically if possible. If a mosquito has fed twice, it is more likely to be a vector as it would have had twice as many opportunities to collect infected blood, than an individual that has fed once. The effect, if any, would therefore be of great interest to describe using wingbeat acoustics.

### 5.1.3 – AIMS AND OBJECTIVES

As more focus in the literature is turning to the potential of exploiting the wingbeat frequency of mosquitoes for surveillance through multiple capturing methods (infra-red, ultrasonic, acoustic sensors), the work proposed in this chapter will explore how acoustic descriptions measured with the novel tethered methodology (Chapter 3), compare to previous research using two physiological effects: *blood meal* and *age*. Expanding the acoustic description from exclusively wing-beat frequency, to cover its sound pressure level amplitude and variation will introduce simple yet novel metrics to supplement the existing literature on the physiological effects on mosquito flight acoustics.

Tethered flight will allow the flight types discussed in Chapter 3 to be identified, and frequency descriptions can be made during periods of *constant flight*. This is to capture the most stable part of tethered flight, which as discussed in Chapter 3 was the closest match to the temporal patterns of free-flight. As this chapter will also use the accelerometer tethering approach of Chapter 3, further validation of the accelerometer can also be undertaken to evaluate accelerometer performance using a larger dataset.

### Chapter Aim

The aim of this chapter is to describe how the acoustics of a mosquito are affected by its physiological factors of age and number of blood meals, We will use the approach and novel equipment designed for tethered flight detailed in Chapter 3. The null hypothesis is that neither age nor bloodmeal number affect the fundamental frequency or amplitude of a mosquito wingbeat. The measurements performed will also generate a good data set to further evaluate the capabilities of using the accelerometer to capture wingbeat acoustic descriptions, when compared to a microphone. The following objectives will facilitate the evaluation of the null hypotheses.

## Chapter Objectives

- Describe the effect, if any, of age on fundamental frequency and its amplitude for tethered *Ae. aegypti*, *An. gambiae* and *Cx. quinquefasciatus* in three age classes (0-7 days post emergence, 7-14 days post emergence & 14-30 days post emergence)
- Describe the effect, if any, of blood meals on the fundamental frequency and its amplitude, for tethered *Ae. aegypti*, *An. gambiae* and *Cx. quinquefasciatus*.
- Determine the differences in wingbeat frequency metrics captured and described by the microphone and accelerometer during tethering.

## 5.2 Materials and methods

### 5.2.1 – MOSQUITO REARING AND HANDLING

*Ae. aegypti*, *An. gambiae* and *Cx. quinquefasciatus* were reared following the protocol described in section 2.3.3. Specific changes for age and bloodmeal assays are described below.

Adult mosquito handling was performed exclusively using the variable aspirator (section 3.3.3). Individual females for testing, were identified within the rearing cages and aspirated into the specimen containers with a maximum fan power of 60% to ensure minimal damage to the specimen. The mosquito was then allowed to rest for a 5-minute period in the specimen container, before tethering.

Tethering to the accelerometer was carried out as outlined in Chapter 3. The individual mosquito was tethered using the VN-30 aspirator, such that it was suspended below the accelerometer. At this stage, its flight was checked to ensure that wings were not impeded, or that the glue was not constraining wing motion. The individual could then be loaded into the semi-anechoic chamber, where the

mosquito positioning tool was set to a distance of 30 mm from the measurement microphone at a 0° angle, as specified in Chapter 3.

### *Age rearing*

The three genera were grouped into 3 age categories based of their post-emergence ages in days. For each species, colonies were maintained concurrently for all three ages, which were 0-7 days, 7-14 days and 14-30 days. Due to rearing capacity limitations, the three species were not concurrently tested across all three age groups. As a result, a direct species comparison was not conducted with this dataset.

For each species, 10 individuals from each age category were measured. Mosquitoes were not blood fed, prior to testing. It was also found during the development of this protocol that *An. gambiae* exhibited poor flight when tethered 14-30 days post emergence, so this species was only evaluated at 0-7 days and 7-14 days post emergence.

### *Bloodmeal rearing*

*An. gambiae* and *Cx. quinquefasciatus* were prepared with three treatments to assess bloodmeal effects: no bloodmeal, one bloodmeal and two bloodmeals. Donated human blood was used, delivered to mosquito rearing cages via an insect blood feeding apparatus (Hemotek PS6A220, Hemotek Ltd UK). Blood was placed in 3 ml aluminium reservoirs, which were heated to 35°C by the Hemotek system. A Parafilm membrane (Amcor, Zürich CH) was stretched over the aluminium reservoirs, and after a heating time of 30 minutes, were placed on the top of mosquito cages for direct membrane feeding. Mosquitoes were allowed to blood feed for 2 hours, before removing the reservoirs from the rearing cages.

Following first bloodmeals, an egg cup was placed within the rearing cages to facilitate egg laying. Second bloodmeals were then delivered at least 5 days after

the first blood meal. Due to rearing facility challenges, the second blood meal for *Ae. aegypti* could not be tested, which is why this treatment is omitted from the analysis.

The bloodmeal groups were concurrently reared within a species, but as with the age rearing, the three species were not reared concurrently due to rearing capacity limitations. Accordingly, cross species effects are not investigated. During the development of this protocol, it was found that tethered flight was not possible for freshly blood fed individuals, so the approach of Park et al. (2023) was followed to allow a digestion period post-bloodmeal of 3 days before conducting tests, using a membrane blood feeder with screened human blood.

Individuals for testing were selected such that on test days, the no bloodmeal and single bloodmeal individuals were 7-14 days post emergence. Individuals that received two bloodmeals were 14-30 days post emergence. Post emergence, mosquitoes were split into three cages: no bloodmeal, one bloodmeal and two bloodmeals.

### 5.2.2 – ACOUSTIC SETUP

The tethered method described in section 4.2.3 was followed, with a single microphone and accelerometer used to capture mosquito wingbeats within the semi-anechoic chamber. Measurement length was set to 1800s. This long measurement time was used, to allow the mosquito to initiate its own flight, rather than use tapping or blowing to start flight which could disrupt the orientation of the mosquito relative to the measurement microphone (due to the tacky glue used as discussed in section 3.4.4).

### 5.2.3 – ANALYSIS WORKFLOW

The analysis workflow followed is outlined in section 4.2.4. The acoustic measurement metrics used for analysis are shown below for reference in table 5.1.

**Table 5.1** – Acoustic metrics (and labels) used for analysis of tethered mosquito flight

	Microphone	Accelerometer
5. Fundamental frequency (Hz)	M1	A1
6. Fundamental frequency amplitude (dB)	M2	A2
7. Fundamental frequency standard deviation (Hz)	M3	A3
8. Fundamental frequency amplitude standard deviation (dB)	M4	A4

### 5.2.4 – STATISTICAL ANALYSES & DATA VISUALISATION

#### *Age and blood meals*

For each species we independently assessed at two variables, age or blood meals, and sought to detect the differences within each, using the acoustic metrics (table 5.1).

**Table 5.2** – Overview of experiments and treatments investigating mosquito age and blood meal effects

Experiment	Treatment	<i>Aedes aegypti</i>	<i>Anopheles gambiae</i>	<i>Culex quinquefasciatus</i>
Blood meal	No blood meal	n = 10	n = 10	n = 10
	1 blood meal	n = 10	n = 10	n = 10
	2 blood meals	n = 0	n = 10	n = 10
Age	0-7 days post emergence	n = 10	n = 10	n = 10
	7-14 days post emergence	n = 10	n = 10	n = 10
	14-30 days post emergence	n = 10	n = 0	n = 10

The measurement metrics were exported from the measurement reports created in PAK 5.8 (Müller-BBM VibroAkustik Systeme, Planegg, Germany) to a .csv file format, which was subsequently analysed using IBM SPSS Statistics 29.0.1.0

(IBM Corp, New York, USA). Treatments (number of blood meals, or age group) within each group (blood meals or age), were compared against the others within its respective species. Null hypotheses tested for the age experiment, were that there was no significant difference in acoustic metrics between age groups. For the blood meal group, null hypotheses evaluated were that there was no significant difference in acoustic metrics between the three blood meal treatments.

Both data sets were analysed using a two-way ANOVA with Tukey HSD post hoc analyses ( $P < 0.05$ ) for each measurement metric combined with species. The microphone fundamental frequency and its amplitude were set as the primary outcome variables throughout the analyses presented here. The remaining metrics were defined as secondary outcomes, listed in table 5.2. Prior to the two-way ANOVA proceeding, a normality test of residuals based on the Shapiro-Wilkes test was performed to validate normal distribution of the data to be analysed, and a logarithmic data transform applied if required. To examine species-specific effects, where statistically significant differences were identified in primary outcome metrics, a one-way ANOVA was conducted on specific species groups.

#### *Microphone and accelerometer tethered performance*

To evaluate the performance of the tethered accelerometer, the frequency metrics (fundamental frequency [M1 & A1], and fundamental frequency standard deviation [M3 & A3]) derived from both sensors were evaluated. The null hypothesis tested was that there was no significant difference between the fundamental frequency or fundamental frequency standard deviation obtained from the accelerometer and microphone.

Two paired-samples T-tests were undertaken using the fundamental frequency of the microphone and accelerometer [M1 & A1], and the fundamental frequency standard deviation [M3 & A3]. This analysis was undertaken across all measured age groups and species ( $n = 180$ ).

## 5.3 Results

### 5.3.1 – EFFECT OF AGE

Eight individual groupings (n=10) across the three species were measured and analysed using eight metrics:

#### *Aedes aegypti*

- 0-7 days post emergence
- 7-14 days post emergence
- 14-30 days post emergence

#### *Anopheles gambiae*

- 0-7 days post emergence
- 7-14 days post emergence

#### *Culex quinquefasciatus*

- 0-7 days post emergence
- 7-14 days post emergence
- 14-30 days post emergence

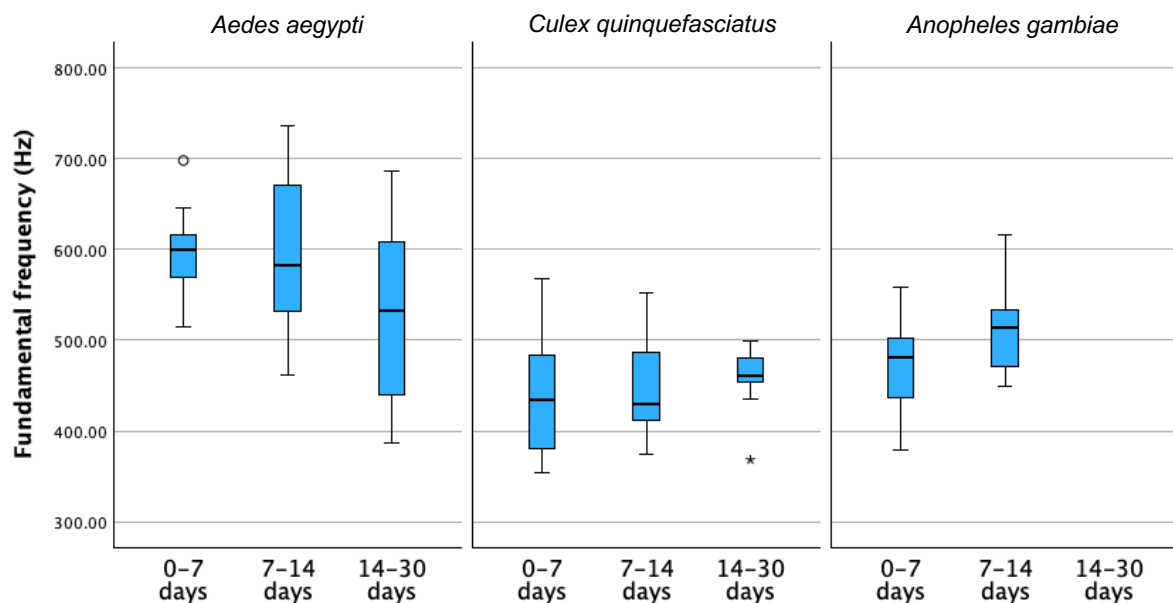


Figure 5.1 – Microphone wing-beat frequencies measured by age and species, box and whisker plots

Using the fundamental frequency recorded by the microphone [M1], no significant interaction was found between species and age ( $df = 3$ ,  $F = 2.092$ ,  $p = 0.109$ ), or age groups individually ( $df = 2$ ,  $F = 1.189$ ,  $p = 0.310$ ). Summarised frequencies are represented in figure 5.2, and shown in table 5.3

**Table 5.3** – Overview of microphone fundamental frequencies [M1] by age and species

Experiment	Treatment	Fundamental frequency microphone [M1] (Hz)		
		<i>Aedes aegypti</i>	<i>Anopheles gambiae</i>	<i>Culex quinquefasciatus</i>
Age	0-7 days post emergence	600.2 (SD = 50.6)	475.7 (SD = 53.3)	436.5 (SD = 67.6)
	7-14 days post emergence	588.5 (SD = 70.3)	509.1 (SD = 51.3)	450.1 (SD = 56.5)
	14-30 days post emergence	532.0 (SD = 100.0)	-	458.4 (SD = 37.2)

Using the fundamental frequency amplitude of the microphone [M2], no significant interaction was found between species and age ( $df = 3$ ,  $F = 2.055$ ,  $p = 0.114$ ). Age groups demonstrated a significant difference across all species collectively ( $df = 2$ ,  $F = 5.424$ ,  $p = 0.006$ ). A subsequent one-way ANOVA was applied to identify the effect of age groups within each species. A significant difference was detected for *Ae. aegypti* between the 0-7 day & 14-30 day groups (mean difference 8.92 dB, SE = 2.00 dB,  $p < 0.001$ ) and between the 7-14 day & 14-30 day groups (mean difference 4.98 dB, SE = 2.00 dB,  $p = 0.048$ ) shown on figure 5.2.

**Table 5.4** – Overview of microphone fundamental frequency amplitudes [M2] by age and species

Experiment	Treatment	Fundamental frequency microphone amplitude [M2] (dB)		
		<i>Aedes aegypti</i>	<i>Anopheles gambiae</i>	<i>Culex quinquefasciatus</i>
Age	0-7 days post emergence	26.9 (SD = 4.1)	22.8 (SD = 7.0)	25.7 (SD = 7.1)
	7-14 days post emergence	22.91 (SD = 3.8)	24.22 (SD = 3.3)	21.7 (SD = 5.8)
	14-30 days post emergence	17.93 (SD = 5.3)	-	21.7 (SD = 5.6)

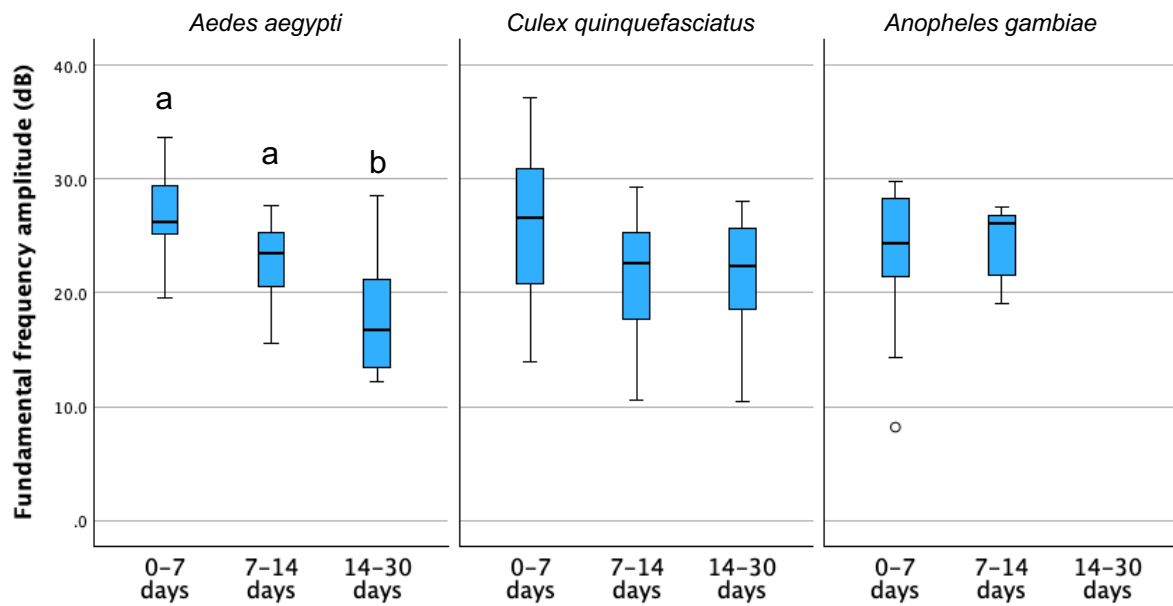


**Figure 5.2** – Microphone wing-beat frequencies amplitudes measured by age and species, box and whisker plots. Letters above the boxplots indicate which groups differ significantly from one another (One way ANOVA with Tukey post-hoc analyses  $P < 0.05$ ). Outliers represented by circles.

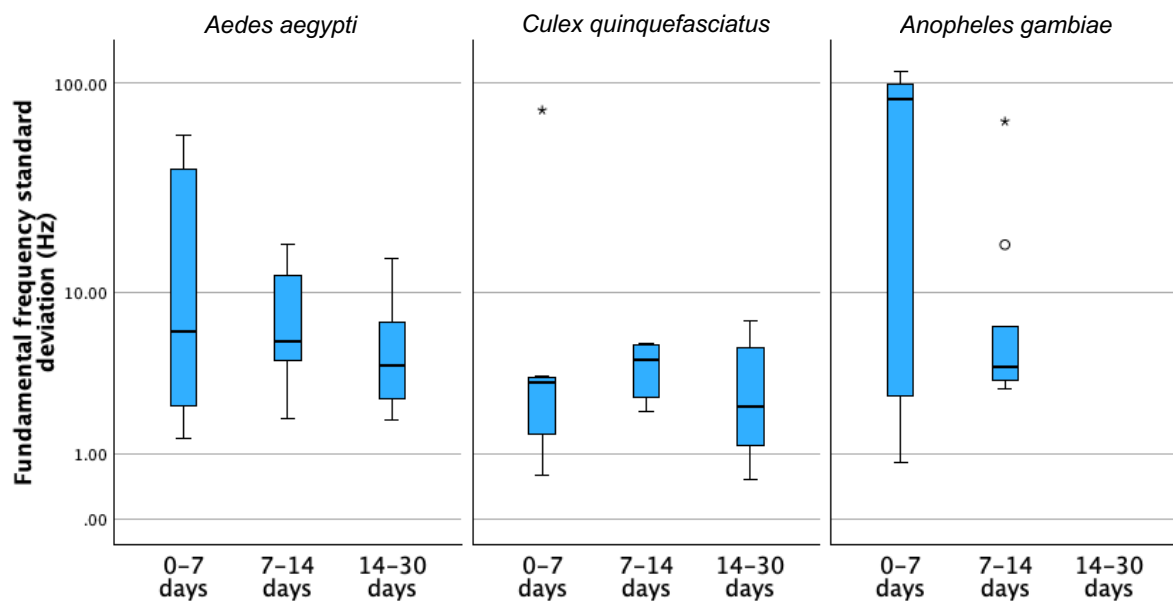


**Figure 5.3** – Microphone wing-beat frequencies standard deviations, measured by age and species, box and whisker plots. Outliers represented by circles and asterisks.

For the remaining six metrics evaluated, two were microphone derived (fundamental frequency standard deviation [M3], fundamental frequency amplitude standard deviation [M4]), and the remaining four were accelerometer derived. For the fundamental frequency standard deviation [M3] (figure 5.3), no

significant effect of combined age and species interaction is detected ( $df = 3$ ,  $F = 2.185$ ,  $p = 0.097$ ) and no significant effect is detected for exclusively age ( $df = 2$ ,  $F = 1.982$ ,  $p = 0.145$ ). Using the [M4] fundamental frequency amplitude standard deviation metric, no effect is detected between the interaction of species and age ( $df = 3$ ,  $F = 1.174$ ,  $p = 0.326$ ), or age ( $df = 2$ ,  $F = 2.210$ ,  $p = 0.117$ ). Across the remaining accelerometer-based measurement metrics [A1-A4], no significant interactions were detected between species and age or age.

### 5.3.2 – EFFECT OF BLOODMEALS

Eight individual groupings ( $n=10$ ) across the three species were measured and analysed using the 8 measurement metrics. Post-blood meal mosquitoes were left for a minimum of 48 hours with access to an oviposition site within their cages.

#### *Aedes aegypti*

- No blood
- 1 blood meal

#### *Anopheles gambiae*

- No blood
- 1 blood meal
- 2 blood meals

#### *Culex quinquefasciatus*

- No blood
- 1 blood meal
- 2 blood meals

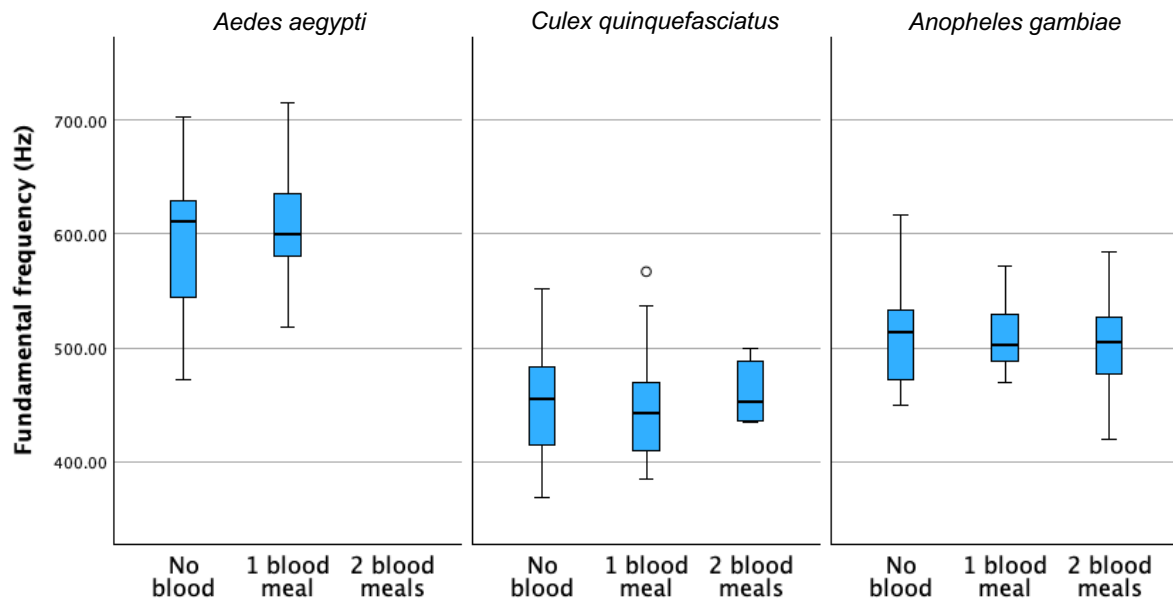


**Figure 5.4** – Microphone wing-beat frequencies measured by blood meals and species, box and whisker plots. Outliers represented by circles

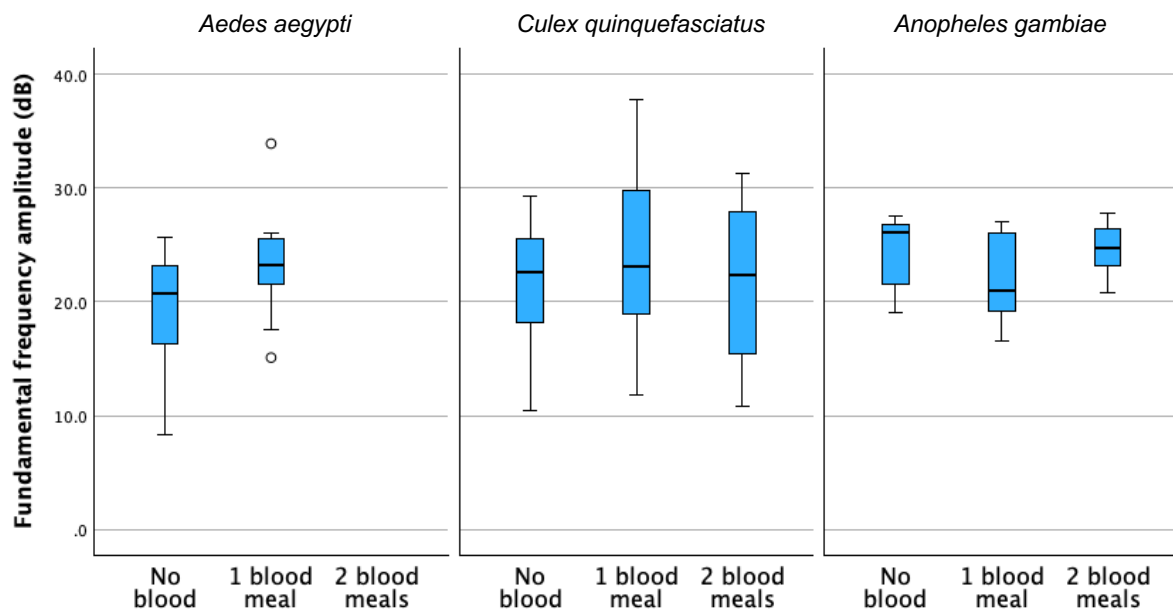


**Figure 5.5** – Microphone wing-beat frequencies amplitudes measured by blood meals and species, box and whisker plots. Outliers represented by circles

Using the fundamental frequency of the microphone [M1] (figure 5.4, table 5.5), no significant interaction was found between species and blood meals ( $df = 3$ ,  $F = 0.298$ ,  $p = 0.827$ ), or blood meal groups individually ( $df = 2$ ,  $F = 0.011$ ,  $p = 0.989$ ) whilst the effect between the three species without blood meals was found to be significant ( $df = 2$ ,  $F = 60.903$ ,  $p < 0.001$ ).

**Table 5.5** – Overview of microphone fundamental frequencies [M1] by blood meals

Experiment	Treatment	Fundamental frequency microphone [M1] (Hz)		
		<i>Aedes aegypti</i>	<i>Anopheles gambiae</i>	<i>Culex quinquefasciatus</i>
Blood meal	No blood meal	594.5 (SD = 50.6)	509.5 (SD = 51.3)	454.3 (SD = 46.7)
	1 blood meal	604.2 (SD = 56.3)	511.3 (SD = 32.0)	448.0 (SD = 47.8)
	2 blood meals	-	507.3 (SD = 42.4)	460.3 (SD = 24.4)

Using the fundamental frequency amplitude of the microphone (figure 5.5, table 5.6) [M2], no significant interaction was found between blood meals and species ( $df = 3$ ,  $F = 1.530$ ,  $p = 0.212$ ), blood meal groups individually ( $df = 2$ ,  $F = 0.529$ ,  $p = 0.591$ ) or species individually ( $df = 2$ ,  $F = 0.813$ ,  $p = 0.447$ ).

**Table 5.6** – Overview of microphone fundamental frequencies [M1] by blood meals

Experiment	Treatment	Fundamental frequency microphone amplitude [M2] (dB)		
		<i>Aedes aegypti</i>	<i>Anopheles gambiae</i>	<i>Culex quinquefasciatus</i>
Blood meal	No blood meal	19.62 (SD = 5.26)	24.22 (SD = 3.33)	21.69 (SD = 5.56)
	1 blood meal	23.30 (SD = 5.12)	21.91 (SD = 3.73)	24.24 (SD = 6.95)
	2 blood meals		23.55 (SD = 3.26)	21.70 (SD = 6.93)

For the remaining six metrics used, two were microphone derived (fundamental frequency standard deviation [M3], fundamental frequency amplitude standard deviation [M4]) with the remaining four accelerometer derived. No effect of blood meal and species interaction is detected for the fundamental frequency standard deviation [M3] ( $df = 3$ ,  $F = 1.345$ ,  $p = 0.265$ ), or for the effect of blood meals ( $df = 2$ ,  $F = 0.608$ ,  $p = 0.546$ ), whilst an effect is reported with species ( $df = 2$ ,  $F = 17.256$ ,  $p < 0.001$ ). This species-specific effect was further investigated with a one-way ANOVA, with a significant interaction reported only between *Cx. quinquefasciatus* (mean fundamental frequency standard deviation [M3] = 2.93 Hz, SE = 0.30) and *An. gambiae* ( $p < 0.001$ ) (mean fundamental frequency standard deviation [M3] = 9.48 Hz, SE = 12.84).

Using the [M4] fundamental frequency amplitude standard deviation metric, no effect is reported between the interaction of species and blood meal ( $df = 3$ ,  $F = 0.036$ ,  $p = 0.991$ ), blood meal ( $df = 2$ ,  $F = 0.006$ ,  $p = 0.994$ ) or species ( $df = 2$ ,  $F = 3.558$ ,  $p = 0.032$ ). Across the remaining accelerometer-based measurement metrics [A1-A4], no significant interactions were found between species and blood meal or blood meal individually.

### 5.3.3 – ACCELEROMETER VS MICROPHONE PERFORMANCE

Accelerometer and microphone performance during tethered flight was evaluated through comparison of fundamental frequency and fundamental frequency standard deviation measured through both approaches across tethered *Ae. aegypti*, *Cx. quinquefasciatus* and *An. gambiae* mosquitoes ( $n = 180$ ). Comparison of fundamental frequency demonstrated no significant difference between the two measurement approaches, with a paired samples T-test demonstrating a mean difference of 6.72 Hz (SD 56.54 Hz) between approaches (two-sided  $p = 0.112$ ) with a correlation of 0.782.

Fundamental frequency standard deviation descriptions demonstrated a mean difference of 1.13 Hz (SD 9.73 Hz) between measurement approaches, with no significant difference reported (two-sided  $p = 0.120$ ) with a correlation of 0.919.

## 5.4 Discussion

### 5.4.1 – EFFECTS OF AGE

Starting with *Ae. aegypti*, this species had its fundamental frequency described with the same age groupings by Staunton et al. (2019b), however their observed increase in wingbeat frequency was not found here. Earlier works of Costello (1974) reported an increase and plateauing of the fundamental frequencies with increasing age, which was not observed here and Park et al. (2023) conducted a similar age assessment, which detected significant differences between the youngest and oldest mosquito tested.

Here, the fundamental frequency was described with a tethered methodology, unlike the free flight approach of Staunton et al. (2019b) and Park et al. (2023). Whilst this result does not confirm prior comparable work, it should be considered that the analyses were confined to the constant flight type, with the extreme peaks that were seen during flight manoeuvres (Chapter 3) removed.

Therefore, the differences observed may be due to the smaller range of frequency content captured by the analysis approach used here. Using periods of stable flight also allowed a fine frequency resolution to be achieved, with every mosquito wingbeat frequency description featuring a 0.73 Hz frequency resolution afforded by the 1.4s block size at the selected 12 kHz sampling rate. This is a key differentiation from prior work, as this was only achievable with the stability of the tethered approach, combined with the specific FFT parameters chosen.

Age was also shown to have no significant effect on the wing beat frequency of tethered *Cx. quinquefasciatus* or *An. gambiae* mosquitoes evaluated. The effect of age on the fundamental frequency of *Cx. quinquefasciatus* has not been the subject of previous studies for direct comparison, however in the same vein as previous work performed on *Ae. aegypti* it was hypothesised here that there may be a

connection between age groups and the fundamental frequency (Park et al., 2023; Staunton et al., 2019b). For *Cx. quinquefasciatus*, the role of acoustics has however been more extensively explored for its role in harmonic convergence between males and females (Warren et al., 2009b), with comparable behaviour exhibited by *Ae. aegypti*.

From all the age groups evaluated across the three species, the only primary outcome metric that demonstrated a significant difference by age was the fundamental frequency amplitude of *Ae. aegypti*, showing a reduction in amplitude with increasing age (figure 5.2). This reduction was not combined with a change in fundamental frequency however, and this was not observed for the *Cx. quinquefasciatus* or *An. gambiae*.

Whilst no effect is detected on how increasing age influences wing-beat frequency, the stability of *Cx. quinquefasciatus* measurements must also be noted. Throughout the age measurements, it exhibited the lowest fundamental frequency standard deviation during tethered flight (Figure 5.3). This may prove to be a useful metric to consider when distinguishing species that may otherwise feature fundamental frequencies with overlapping ranges. The reasons for this stability may lie with imposed restrictions in the tether mount, or there may be an advantage for producing a stable flight tone such as for courtship behaviour which is known to actively use the wingbeat (Cator and Zanti, 2016; Warren et al., 2009a).

The effect of age on the fundamental frequency of *An. gambiae* has also not been explicitly explored, however its fundamental frequency has been investigated extensively previously for its role in harmonic convergence during mating behaviour (e.g Pennetier et al., 2010; Potamitis and Rigakis, 2016) as with *Cx. quinquefasciatus*. The female fundamental frequency of *An. gambiae* was reported between 460-467 Hz when tethered by Pennetier et al., which closely matches the mean reported here of 475.7 Hz at 0-7 days. Whilst an increase was observed between the two age groups evaluated here, this was not statistically

significant. This increase in wingbeat frequency however, matches the previously discussed findings of Staunton et al. for *Ae. aegypti*. It would be of great interest to further connect these reported acoustic changes with a greater understanding of the physical changes to mosquitoes as they age, such as their wing size, condition and overall body size as these have also been shown to impact their wingbeat frequency (Park et al., 2023; Staunton et al., 2019b). A deeper understanding of this connection may reveal why differences observed were not statistically significant here.

#### 5.4.2 – EFFECTS OF BLOOD FEEDING

The specific behaviour being evaluated here, is the effect of *blood-feeding history*. This is different than evaluating the effect of a freshly ingested bloodmeal which, would result with a significant body mass change that could accordingly change mosquito wing kinematics and acoustics. Here, blood feeding after a digestion period, showed no significant effect on the fundamental frequency for the three species evaluated across all bloodmeal numbers evaluated.

A factor to consider in this method, is the rest time allowed following bloodmeals. This was chosen such that the mosquitoes would be entering their oviposition physiological state during the measurements (Agyapong et al., 2014). No egg cups were provided before completion of a first bloodmeal measurement, in order to maintain this physiological state for the first blood meal measurements. This was to encourage the natural flight behaviour that would follow as mosquitoes search for an oviposition site. A post-bloodmeal rest period of three days was used by Park et al. (2023) in their study which also examined oviposition acoustics, and their investigation, using *Ae. aegypti* exclusively, demonstrated a decrease in wingbeat frequency with age. However this did not separate non-blood fed and blood fed mosquitoes in the older group. As no differences were detected here, the null hypothesis is confirmed for all species, that bloodmeals do not significantly affect the wingbeat frequency.

### 5.4.3 – COMPARISON OF MICROPHONE AND ACCELEROMETER METRICS

A frequency comparison between the accelerometer and microphone allowed for an evaluation of the accelerometer for measuring frequencies. No significant difference was detected between the two sensors for the fundamental frequency and fundamental frequency standard deviation metrics, confirming the viability of using a direct vibration capture method to describe tethered mosquito flight acoustics.

The advantages of the accelerometer approach over a scanning laser vibrometer are sensor size, robustness and cost. As this measurement occurred in the semi-anechoic chamber, direct line of sight was not always possible, which would complicate the use of the vibrometer. Cost was also a major factor, with the calibrated accelerometer approach offering frequency descriptions of the mosquito roughly 100x cheaper than commercially available scanning laser vibrometers.

The mass loading effect of the accelerometer however, is a significant drawback, that prevents its use for capturing *accurate* acceleration readings. In its present configuration, the acceleration values cannot be compared between specimens, whereas a laser vibrometer solution will provide accurate acceleration data which can be readily compared between specimens. However the intended application of the acceleration data here is not to compare data between specimens, but to provide a secondary metric of “flight effort” during each measurement. This is such that changes in sound pressure level (if any) can be connected to changes in their environment (e.g microphone-mosquito distance) or flight behaviour when tethered. It is for this specific use-case, that the simpler accelerometer could yield a novel manner of verifying sound pressure level derived acoustic metrics for each measurement.

From a practical perspective, *Cx. quinquefasciatus* was the simplest to mount using this tethering method, owing to the comparatively larger scutellum area which was used for gluing (figure 5.6). The same tether wire gauge (22 AWG) was

used for all species to keep the transfer of vibration to the accelerometer constant; however, the tether process could be refined by exploring the efficacy of a thinner wire gauge.



**Figures 5.6** – *Cx. quinquefasciatus* (left) and *An. gambiae* (right) tethered,

## 5.5 Chapter summary

This chapter evaluated how the novel tethered approach could be used to describe the effects of age and blood meals on the wingbeat acoustics of *Ae. aegypti*, *An. gambiae* and *Cx. quinquefasciatus*. Three age categories were evaluated between 0-30 days post emergence, with only the amplitude of *Ae. aegypti* reducing with age. No significant differences in the fundamental frequency for age or blood meals were found across all three species evaluated.

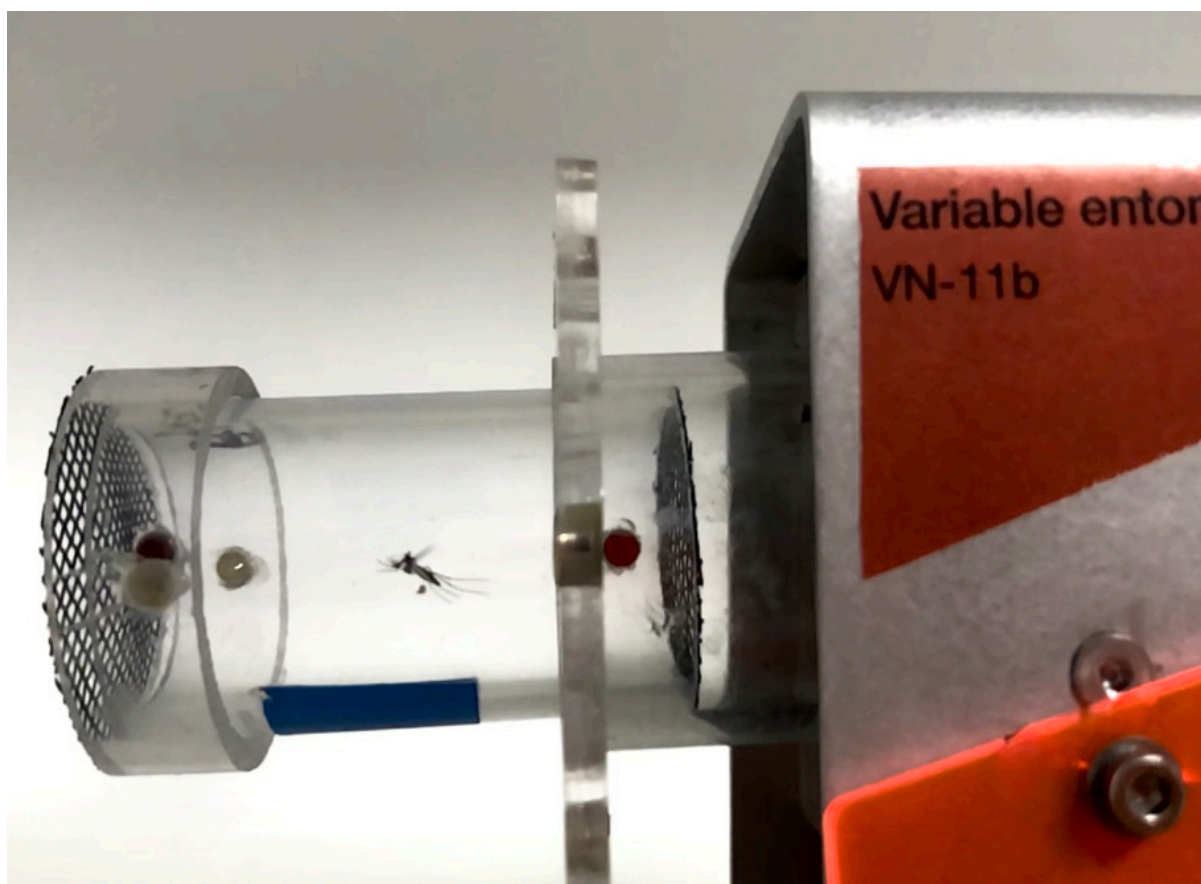
The null hypotheses that neither age nor bloodmeals affect the fundamental frequency or amplitude of a mosquito wing-beat can therefore be accepted.

This measurement series also permitted an evaluation of the accelerometer-based tethering technique. 180 mosquitoes across the three species were compared using

both microphone- and accelerometer-derived fundamental frequencies with no significant difference detected between the frequencies described by the sensors. This dataset validates the suitability of directly tethered accelerometers to describe the fundamental frequencies of a tethered mosquito.

An accelerometer-based tethering technique should therefore be considered as a viable and potentially more reliable, replicable, and cost-effective method to record the fundamental frequencies of these and other species in future laboratory studies and field applications.

## CHAPTER 6: GENERAL DISCUSSION



Mosquito in free flight within specimen cartridge, following controlled aspiration from rearing cages

### 6.1 Summary

#### 6.1.1 –METHODS, DEVICES, ACOUSTIC RECORDINGS & FREQUENCY ANALYSIS

The source of the flight tone of a mosquito are its flapping wings during flight, and **Chapters 2** and **3** focussed on developing optimised spaces to capture these sounds. Two distinctly different approaches to flight arena designs were taken which focussed on either design simplicity (plastic tunnels) or accuracy & precision (semi-anechoic chamber). Whilst the outputs of both approaches were acoustic descriptions of mosquito wingbeats, the clarity and reproducibility of the flight tones captured were markedly different.

Preliminary measurements in **Chapter 2** demonstrated that the diameter of reverberant plastic tunnels was linked to the signal-noise ratio for measured wingbeat acoustics. Reductions in tunnel diameters resulted with increased signal-noise ratios. However, due to the lack of sound attenuating materials in these designs, a background noise removal script was required to identify wingbeat frequency spectra amongst the background noise present. Using this tool, a species comparison conducted established significant differences in the fundamental frequencies of *Aedes aegypti* or *Anopheles gambiae* with *Culex quinquefasciatus*. This was based off a short analysis time window, since the background noise compensation script, however. Interestingly, for descriptions made in the plastic tunnels, the fundamental frequency was not detected as the frequency of highest amplitude within the wingbeat.

Since the overall focus of this thesis was to capture and interpret the sounds generated by mosquitoes under controlled conditions, no further work was undertaken using plastic tunnels. Instead, all further studies were conducted using the bespoke semi-anechoic chamber developed in **Chapter 3** to obtain more controlled mosquito acoustic measurements. This chamber, together with its calibrated microphones and data acquisition method, enabled measurements to be captured with a uniquely high signal-noise ratio, whilst also permitting long time period measurements. This setup also permitted wingbeat measurements using both tethered specimens and in those in free flight. Tethered flight exhibited far more temporal variation than free-flight, so subsequent tethered flight analyses were defined into four flight types. The most stable flight type (constant flight) was chosen for the acoustic descriptions of **Chapters 4 and 5**.

To ensure repeatability, novel supporting laboratory handling equipment were designed and realised. This included a variable airflow aspirator and its accessory specimen cartridges. These ensured mosquitoes were always handled in a gentle manner, whilst minimally exposing mosquitoes to human odour. The cartridge system enabled efficient throughput of mosquitoes from rearing cages to measurement arenas.

A comparison of free flight and tethered flight is presented in **Chapter 4**. The literature contains conflicting accounts on the effects of tethering on the wingbeat frequency, so this was assessed using *Aedes aegypti* under both conditions. Despite an excellent signal-noise ratio, no significant difference was seen in the fundamental frequency of *Ae. aegypti* in tethered and free flight. This gave more confidence in using the tethered approach to conduct controlled measurements for assessing physiological effects in **Chapter 5**. **Chapter 4** also provided an initial frequency assessment under free flight for the three species, with *Ae. aegypti* demonstrating a significantly different fundamental frequency than *Culex quinquefasciatus* and *Anopheles gambiae*. This was different to the detected species differences in wingbeat frequency when using the reverberant plastic tunnels.

**Chapter 5** examined in further detail the acoustics of the three species, using the tighter control offered by a tethered approach. Experiments were conducted to investigate the effects of age, and blood meals for *Ae. aegypti*, *Cx. quinquefasciatus* and *An. gambiae*, using the controlled tethered approach. Blood meals and age were not correlated with a significant difference in the fundamental frequency in any of the species.

## 6.2 Measurement approaches

### 6.2.1 – DESIGN TRADE-OFFS DURING DEVELOPMENT OF MEASUREMENT SPACES

The initial plastic tunnels, which were of acrylic construction, allowed the capture of mosquito flight tones under free flight, however measurements were compromised. Whilst tunnels allowed sampled mosquitoes to fly freely, their lack of acoustic insulation resulted with measurements exhibiting varying and uncontrolled signal-noise ratios, due to high background noise levels in the test facilities. The implications of this are that, whilst it is more realistic to use simple geometries like these in an ideal end goal application, the compromises in signal

clarity meant that the repeatability of measurements could not be easily controlled.

This is reflected in section 2.4, with figure 2.13 illustrating this design compromise in both the spectrograms and averaged frequency spectra for each tunnel, where the varying background noise level and signal to noise ratio can be seen. The purpose of the preliminary investigation into the effect of tunnel diameter was to provide an evidence base to determine the dimensions of an idealised flight arena. This would permit long flight bursts to obtain higher frequency resolution according to the Nyquist sampling theorem (Shannon, 1949). However, the measurements of *Ae. aegypti* within the four tunnels demonstrated that before assessing the impact of geometry on flight bursts, accounting for and overcoming the varying signal-noise ratios would be required. This was explored in section 2.4, whereby a simple approach to background noise compensation was undertaken for each flight burst analysed. It should be noted that this approach required the manual identification of flight bursts and periods of no flight.

Should the mosquito wingbeat acoustics be integrated into a future method of detection within a resonant tunnel format, such as those explored in section 2.4, a method of differentiating periods of flight and no flight would be required. For each time-step of potential flight, a corresponding period of no flight could be compensated for to identify the flight burst. However, this will need to consider the flight type analysed, which was only revealed by the longer time period measurements enabled by the semi-anechoic chamber in **Chapters 3,4 and 5**.

The preliminary dataset captured in section 2.6 showed that whilst the different species could have their wingbeats captured using an Ø80 tunnel diameter arena, the lack of positional control prevented use of an amplitude metric since distance relative to the microphones was untracked. This was enabled in the subsequent measurements under semi-anechoic conditions, without any background noise compensation needing to be performed as previously mentioned. With a tightly controlled acoustic environment, using the positional manipulator developed in

section 3.4.2, a clear description could be made for *Ae. aegypti* to describe its frequency and amplitude content in relation to angle and distance from the measurement microphone.

For reference, the acoustic properties of winged insects have been described both from measurements (Sueur et al., 2005) as well as from simulations (Bomphrey et al., 2022; Seo et al., 2020). They have been described as a dipole Gutin-like sound, which whilst initially used to describe the aeroacoustics of an aircraft propeller (Gutin, 1936), have been applied to aeroacoustic simulations of mosquito flight sounds (Bomphrey et al., 2022), where this connection was described. The dipole nature of the mosquito acoustic emission was measured and appears to correspond with the simulated patterns made for *Cx. quinquefasciatus* (Seo et al., 2020) however with differing amplitudes and fundamental frequencies for the tested *Ae. aegypti*. What is useful to consider from the perspective of a device design, is that the angular position of the mosquito relative to the measurement microphone will influence the amplitude measured. This is in addition to the distance from the measurement microphone, which also exhibited a reduction in amplitude by distance (section 3.5.2), similar to that described by Seo et al. (2020) for *Cx. quinquefasciatus*. The preliminary descriptions can also be compared to the descriptions of Arthur *et al* (2014), who conducted extensive measurements of *Ae. aegypti* by distance and angle. The general amplitudes recorded here are lower than that of Arthur *et al*, however the amplitude reduction with distance also corresponds to their presented descriptions.

Given the highly directional nature of mosquito flight tones, their frequency content and respective amplitudes should be connected to the orientation of the mosquito relative to the microphones. Any proposed application of monitoring mosquitoes using their wingbeat under free flight, would have varying uncontrolled distances and angles during their flight. Accordingly, flight sounds should be captured for analysis using shorter time periods, such that variation from the changing mosquito position relative to the measurement sensors, can be captured and described.

This effect of position with unconstrained free flight could not be tracked within the scope of this project, although free flight positional tracking of mosquitoes in flight has been performed with apparatus developed to analyse their flight patterns during swarming or host-seeking around bednets e.g. Jones et al.2021. If a method of tracking could be combined with the free flight measurements taken, it would be of great interest to connect the flight types describe of section 3.5 (e.g. constant flight, ramp, manoeuvres), with a more precise descriptions of the motions being performed to create these varying flight profiles. Tracking would also allow connection of amplitude with distance, which would be useful to compare with the tethered positional controller explored in section 3.4.

#### 6.2.2 – LONGER TIME-PERIOD MEASUREMENTS

The variation in wingbeat frequency displayed during tethered flight has been visualised and accounted for by different approaches, such as the generation of frequency histograms (Arthur et al., 2014c), or manual selection of 5 or 10s stable flight bursts for analysis (Simões et al., 2016a). Here, by using measurement times of up to 30 minutes, periods of stable flight could be readily captured. This approach allowed all tethered measurements to use exclusively the periods of stable flight. When conducting analysis on free flight mosquitoes however, stable flight could also be analysed but without the positional control relative to the measurement microphone. It is worth noting that identifying stable flight periods when measured under free flight conditions would not be possible with a single optical sensor approach as a wingbeat signal only occurs as their light beam is broken. Instead, more complex designs that employ multiple optical sensor arrangements within a flight tunnel (T.-H. Ouyang et al., 2015) may feasibly produce comparable longer time period wingbeat data as the acoustic data presented. The simple analysis in section 3.5.3 demonstrated how the pattern of flight that is analysed greatly affects the standard deviation of the signal, with periods of “constant flight” featuring a standard deviation of 6.8 Hz, whilst the

“ramp” flight types exhibited a greater standard deviation of their fundamental frequency of 30.9 Hz.

The implications of this, are that utilisation of the fundamental frequency as a metric to describe mosquito species or associated physiology, should also be based upon an understanding of its flight type at the time of data capture. This approach would allow for a more controlled understanding of the what the captured acoustic data represents, in relation to the mosquito behaviour.

In the potential application of using the wingbeat profiles for identification, it would be useful to gather the longest recording of a mosquito flight burst as possible. In relation to the reverberant tunnels, this is the main justification for suggesting the implementation of a dynamic method of background noise compensation for each time step. The ideal end result should permit the traces of flight bursts captured in the semi-anechoic chamber to be comparable to a proposed resonant (acrylic) setup. This approach would allow identification to occur during the most stable parts of mosquito flight, by having the capacity to identify this flight type from a long time period measurement.

It would then be of interest to conduct a reverberant and semi-anechoic free flight comparison, to further understand the differences in described wingbeat frequencies obtained for the two species comparison conducted. As these results were not intended to be compared, the mosquitoes were reared at different times, so a controlled assessment would be vital to compare the acoustic descriptions possible from these methods.

### 6.2.3 – CONSIDERATIONS OF TETHERED AND FREE FLIGHT APPROACHES

The approaches evaluated in this thesis for measuring mosquito acoustics feature their own advantages and disadvantages. However, it is helpful to consider the

application and intended use of the data when presenting this discussion on their respective merits.

The tethered approach allowed for controlled, and repeatable measurements to be made. The investigation comparing tethered versus free flight for *Ae. aegypti* found no significant effect between the fundamental frequencies. Accordingly, the tethered method was selected for subsequent data capture due to its simplicity in capturing the sound profiles of mosquitoes, from its fixed position allowing repeatable measurements and straightforward analysis.

However, any automated future device would not use mosquitoes in tethered flight, so the free flight approach is far more translatable from the perspective of a device design. The benefit of the developed method, using both tethered and free flight acoustics, is that it has established a simple workflow to explore physiological factors influencing mosquito wingbeat acoustics. Under controlled conditions (tethered), if any effect was found, they could be validated simply under free flight conditions, which would illustrate whether these effects could be identified in a free flight field surveillance device.

During semi-anechoic free flight, a significant difference was determined between *Cx. quinquefasciatus* or *An. gambiae* and *Ae. aegypti* with their fundamental frequencies. However use of this metric as the sole measurement metric was not sufficient to differentiate between *Cx. quinquefasciatus* and *An. gambiae*. This is where, potential supplementary metrics could be developed to describe the expected variation under each of the flight types of section 3.5.3. The data presented is preliminary, for a much smaller sample of specimens that that used in Chapters 4 and 5.

Expansion of the data processing workflow to generate acoustic descriptions for all flight types (not just constant flight), across all the treatments and replicates may facilitate novel ways for differentiating species or treatments. As the flight time analysed was manually selected, expansion to cover multiple flight types in

addition to the constant flight type used would be prohibitively time consuming (if manual). It should be noted that this is a common problem with other acoustic approaches taken, with even optical machine learning based approaches sometimes requiring a manual process of flight burst selection following acquisition for model training (T. H. Ouyang et al., 2015). Overcoming this hurdle is important, to counteract the more general phenomenon when implementing machine learning approaches of ensuring that training data is representative of data used during field classification (Ackerman et al., 2021).

#### 6.2.4 – FURTHER DEVELOPMENT OF ACCELEROMETER-BASED MEASUREMENTS

The accelerometer measurement approach demonstrated that during tethered measurements of mosquitoes, their fundamental frequency can be effectively captured through vibration of the tether. This novel approach for capturing the mosquito wingbeat is much less susceptible to background noise, providing that the measurement space is mechanically isolated. This advantage allowed for collection of noise-free data, comparable in signal quality, with proposed optical methods of capturing wingbeats (Batista et al., 2011a; de Nadai et al., 2021). Like optical methods (when tethered), use of an accelerometer permits the wingbeat to be captured over a long time period (for as long as the mosquito flies) as well.

The drawback of using accelerometers to describe mosquito wingbeats using the developed method, is that amplitudes of acceleration cannot be readily compared between specimens due to the varying size and damping effects of the applied tether adhesive. Whilst amplitude can be used to monitor changes within a measurement, comparing reductions or increases in amplitude across specimens is not feasible. The adhesive used remained flexible, but the crude adhesive application method caused its size to vary between specimens (figure 6.1). As a result, this would provide a different damping effect, changing the vibration transferred to the tether and into the accelerometer, accordingly.



**Figure 6.1** – Two *Cx. quinquefasciatus* tethered specimens featuring varying adhesive sizes

The utility of the accelerometer-based measurements, beyond its superior resistance to background noise over microphones, was that it offered a method of describing changes in flight effort during a tethered measurement. This could have great utility when conducting repeated measures style recordings of tethered mosquitoes, for example in the distance and angular measurements of section 3.4.3. Here, multiple measurements of a unique specimen were taken whilst changing the geometric properties of the measurement space (e.g. distance / angle of microphone relative to mosquito), so having a method of monitoring flight effort between all geometric conditions would be useful to understand whether observed differences from microphones were exclusively due to changes in the measurement setup (distance / angles) rather than due to changes in the mosquito flight effort. This was particularly relevant to the measurement arena setup developed here, as the small, portable nature of the semi-anechoic chamber prevented the use of large sensor arrays that have been developed in other studies to capture the sound field or wing kinematics across multiple angles / distances simultaneously (Arthur et al., 2014c; Bompfrey et al., 2017b).

## 6.3 Application to vector control

### 6.3.1 – INTEGRATING THE ACOUSTIC DESCRIPTIONS INTO VECTOR SURVEILLANCE

Any integration into a future automated acoustic identification tool would require substantial work to overcome the effects of background noise. In an idealised, scenario where this is possible, the results presented here help provide an initial indication that separating *Ae. aegypti* from *Cx. quinquefasciatus* or *An. gambiae* could be possible using their fundamental frequency. Whilst separately identifying *Cx. quinquefasciatus* and *An. gambiae* using the fundamental frequency was not possible with the presented results under free flight, from the perspective of vector surveillance, being able to separate *Ae. aegypti* would still be of great utility. In the field, control measures differ greatly depending upon the biting behaviour of the mosquito, with *Ae. aegypti* being predominantly day active, whereas *An. gambiae* is active from dawn to dusk. Therefore, being able to understand the populations of these two species would allow appropriate control measures to be implemented that are targeted for day or night biting (e.g. indoor residual spraying, larviciding or insecticide-treated bednets).

With finer understanding of the species making up local mosquito populations, the efficacy of control measures could be increased as species specific approaches can be used at the right time. Collection of live entomological data is challenging, either by larval or adult collections, so the results presented here are encouraging to justify the further development of automated approaches to identifying free flight adults.

Understanding whether mosquitoes have blood fed is a metric routinely collected during studies that use molecular methods of identification (Salako et al., 2019), as this metric allows for a better understanding of the feeding activity patterns of mosquitoes in sampled areas. The presented data did not show any acoustic differences between blood fed and non blood fed mosquitoes, which would indicate

that it would not be feasible to identify this metric from acoustic measurements alone. However, an alternative approach, could be to instead adapt the location of sampling whereby acoustic identification of mosquitoes takes place at locations frequented post-blood meal, such as at oviposition sites. There are two ways that the egg laying behaviour of mosquitoes is used for mosquito surveillance, through specific trap designs known as gravid or ovitraps. Ovitrap allow mosquitoes (mostly *Aedes*) to egg lay on a substrate, whilst allowing the mosquito to subsequently fly away, requiring subsequent collection and inspection of the eggs for identification. Gravid traps on the other hand capture the mosquito (mostly *Culex*), and are used particularly during xenomonitoring, whereby pathogen load surveillance is conducted by either dissection or molecular analysis of sampled mosquitoes (e.g. for lymphatic filariasis) (Cameron and Ramesh, 2021; Djiappi-Tchamen et al., 2022a, 2022b; Irish et al., 2015; Ortega-Morales et al., 2018).

These trap types are used both for surveillance and control (Day, 2016; Suman, 2019), with a significant advantage they offer being the targeting of gravid female mosquitoes. This feature of their design would make these traps ideal arenas for acoustic detection that could allow sampling of previously blood fed - and therefore more likely to be carrying a pathogen - ovipositing females. By incorporating acoustic surveillance in these trap types, acoustic analysis exclusively be on gravid mosquitoes, so it would not be necessary to extract specific acoustic patterns to identify mosquitoes as blood fed, since this was demonstrated to not be acoustically identifiable in **Chapter 4** across the species tested.

Gravid mosquitoes utilise odour cues in the water, present from grasses and conspecific larvae (Day, 2016; Mwingira et al., 2020; Suman, 2019). Using an understanding of these odour cues, in combination with an acoustic monitoring approach may provide an alternative method of field identification to overcome the identification barriers between species, such as that presented between *Cx. quinquefasciatus* and *An. gambiae* which exhibited fundamental frequencies which overlapped in **Chapter 4**.

Incorporating location into a multi-variate approach to acoustic detection would be a useful feature when considering a future surveillance approach. This could help overcome the barriers caused by overlapping fundamental frequencies which have thus far hindered widescale adoption of a successful, commercially available, and viable surveillance solution.

### 6.3.2 – FLIGHT PATTERNS AND SURVEILLANCE TOOL DESIGN

Flight patterns were discussed in **Chapter 3**, whereby acoustic identification within the entirety of this project focussed exclusively on periods of constant flight. This was the significant advantage offered by the microphone approach, as it allowed these periods within extended measurements of mosquito flight to be readily (albeit manually within this project scope) identified for frequency analysis.

Beyond the scope of the results presented here, it may be useful to explore how a flight type identification could be used in an aforementioned multi-variate identification approach. A more extensive process of time domain flight type characterisation could expand upon the descriptions illustrated in section 3.5.3, for *Ae. aegypti*. This could be similar in approach (examining longer time period acoustic behaviour) to the work done for characterising acoustic harmonic convergence behaviour between males and female mosquitoes (Lauren J. Cator et al., 2009; Warren et al., 2009b).

Understanding changes in acoustic behaviour over time, could be helpful to reveal the root cause for the significant differences observed in the fundamental frequency standard deviations between the three species whilst under free flight in section 5.3.2. Here, it was observed that under free flight, *An. gambiae* exhibited the highest standard deviation during analysed flight bursts, whilst *Ae. aegypti* exhibited the lowest. Adapted from figure 4.11 presented in **Chapter 4**, figure 6.2

illustrates a free flight fundamental frequency comparison between the three species.

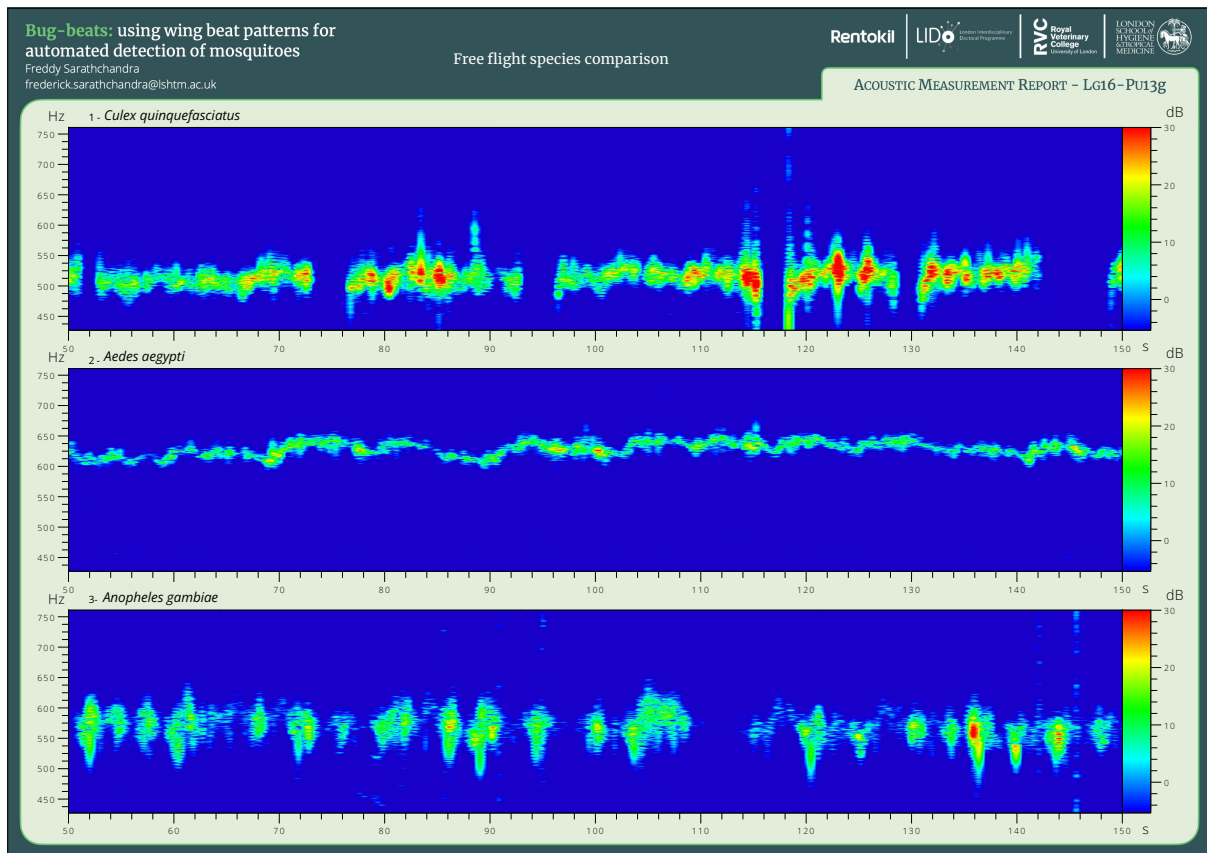


**Figure 6.2** – From top to bottom, fundamental frequency spectrograms under semi-anechoic free flight for *Cx. quinquefasciatus*, *Ae. aegypti* and *An. gambiae*

In this figure 6.2, differences between the spread of fundamentals between the species can be seen during their free flight, which would cause the varying standard deviations reported in **Chapter 4**. *Ae. aegypti* demonstrates the most continuous and narrowband fundamental frequency spectrogram (lowest fundamental frequency standard deviation), whilst *An. gambiae* consists of a much more broken fundamental frequency flight spectrogram (highest fundamental frequency standard deviation). Production of the *Cx. quinquefasciatus* wingbeat frequency appears more continuous than the more intermittently generated *An. gambiae* wingbeat, but it shows more frequency variation than *Ae. aegypti*.

Whilst the standard deviation of the fundamental frequency (during an analysis period) captured part of these differences, any future measurement series

undertaken for the application of detection could expand on the differences in flight behaviour within free flight demonstrated here. Flight burst time, in combination with frequency variation within each burst for example, could yield further metrics that when used in conjunction with the simple fundamental frequency, may strengthen the capabilities of a multi-variate acoustic identification approach.

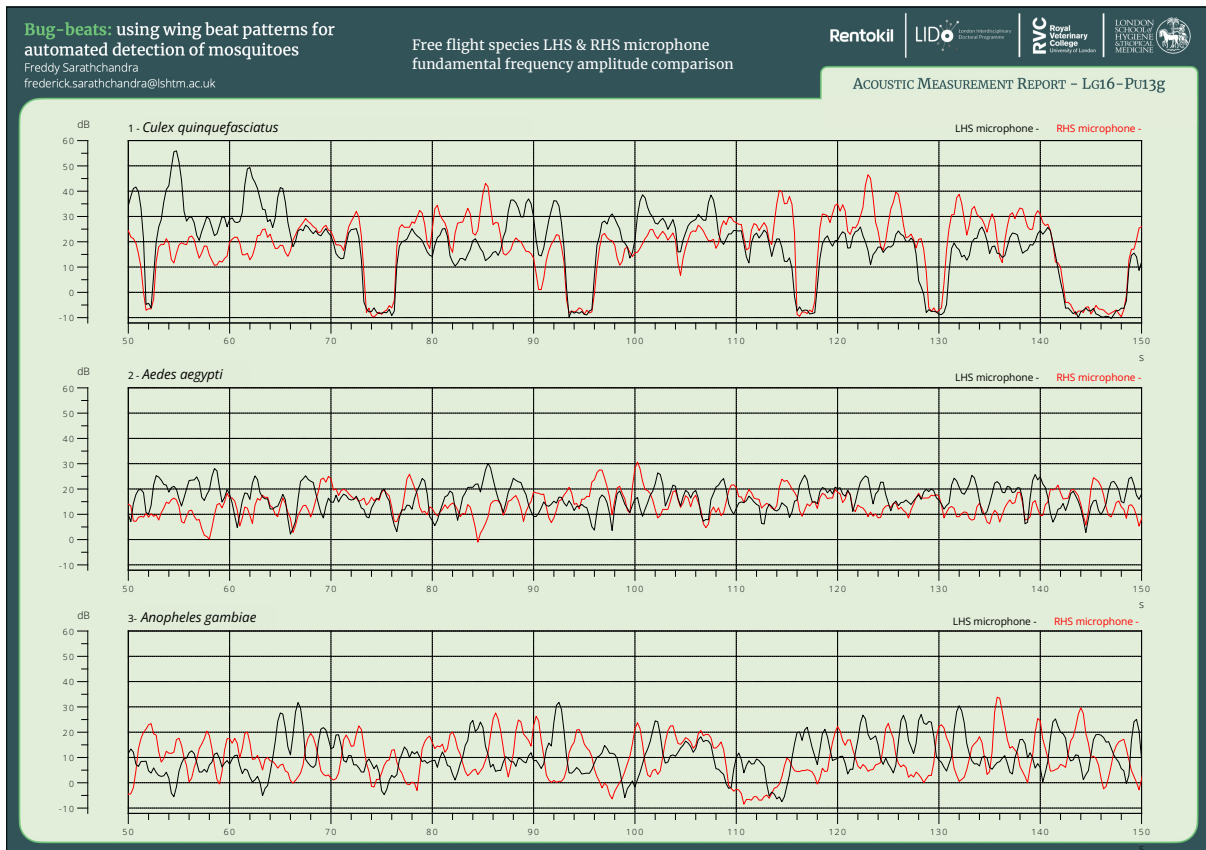


**Figure 6.3** – From top to bottom, fundamental frequency amplitudes under semi-anechoic free flight for *Cx. quinquefasciatus*, *Ae. aegypti* and *An. gambiae*

Expansion of the spectrogram in figure 6.2 is illustrated by a fundamental frequency amplitude tracker in figure 6.3. This plots the LHS and RHS microphone amplitudes of the maximum frequency detected within a frequency band corresponding to the expected wingbeat frequencies of the three species (450-750 Hz), within a 100s measurement window. Here, the amplitude of the fundamental frequency is shown over time, for both LHS and RHS microphones. This figure illustrates how the amplitude of the fundamental frequency changes as the mosquito flies through the flight tunnel. Comparing data between the LHS

and RHS was not conducted in the presented analyses of Chapters 4 and 5, but this figure shows how amplitudes of this data could be explored further. In **Chapter 3**, the amplitude of mosquito flight whilst tethered was used as a metric, however due to the untracked nature of free flight within the tunnels, amplitude was not used for analyses conducted in **Chapter 4**. Figure 6.3 shows that for all three species, the amplitudes of the fundamental for the LHS and RHS microphones can be seen crossing over. Points on the plot where the amplitudes cross, would occur when the amplitudes recorded by both the LHS and RHS microphones are equal, which could be where the mosquito is in a central position within the tunnel, allowing amplitude-based tracking.

This frequency amplitude can also be related to the angular radar plots (figures 3.23, 6.4) of **Chapter 3**, whereby the amplitude of the fundamental and harmonics and were shown to change their amplitudes with angle. If this preliminary dataset collected were to be expanded across multiple genera and with further replicates, it could help develop an understanding for what amplitudes are to be expected within free flight by varying distances and angles. It could be inferred that when the mosquito is flying along the tunnel length, and is at a central position, the amplitude of the LHS and RHS microphones should be equal. This would need confirmation that the amplitude at  $0^\circ$  and  $180^\circ$  are comparable though, as if there is an amplitude difference then the moment where the LHS and RHS amplitudes are equal would not correspond to an exactly central position.

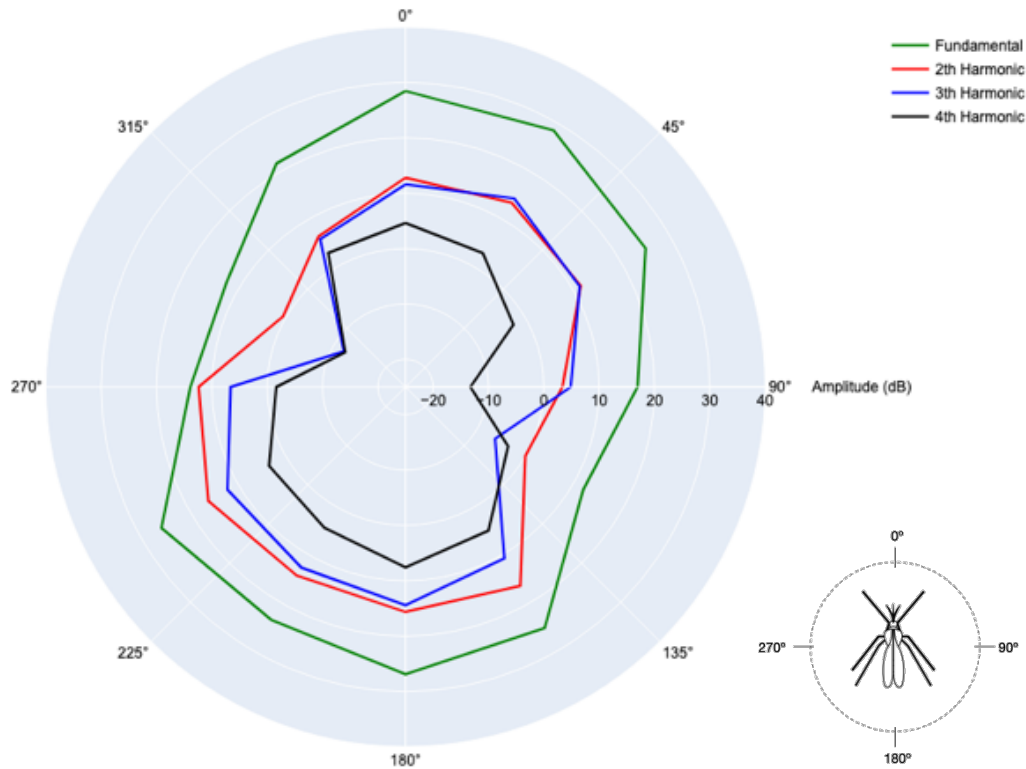


**Figure 6.4**– Radar plot showing amplitude of fundamental and harmonics by angle relative to microphone from Chapter 3 (selected from figure 3.24)

A deeper understanding of expected amplitudes by angle could also help illustrate flight manoeuvres such as direction changes. The radar plot (figure 6.4) demonstrates a reduction in amplitude at the 90° and 270° positions, which also occurs at harmonics. At multiple angles, if the amplitude relationships between the harmonics can be described robustly for the three species with the angular positioning tool, it would be of interest to explore the feasibility of identifying these during free flight. Direction changes along the tunnel length can be seen as points of inflection on figure 6.3. Therefore, at these points we would expect the amplitude of harmonics to change from the pattern observed when traveling along an axis towards or away from the microphone (0° and 180°), to those observed from the side of the mosquito (as it travels along an axis defined by 90° and 270°).

### 6.3.3 –ACOUSTIC PHYSIOLOGICAL STATE IDENTIFICATION & VECTOR SURVEILLANCE

#### *Blood fed and gravid mosquitoes*

As mentioned in the previous sections 6.3.1 and 6.3.2, blood fed mosquitoes could not be identified exclusively from their fundamental frequency, however a future detection application based around a gravid trap could infer the gravid status of a mosquito should a female acoustic profile be detected at an oviposition site. When post blood meal measurements were undertaken (**Chapter 5**), mosquitoes which were fed a single blood meal, were not permitted to oviposit to encourage flight behaviour. However it would be of interest to expand the longer time domain recordings (figure 6.2) to identify whether different oviposition behaviours that are unique to different species can be acoustically identified. For example, there are a number of different mosquito oviposition behaviours that have been characterised by distinctive flight patterns that may be acoustically identifiable. Once an oviposition site is selected by the mosquito its behaviour changes to egg-deposition. This approach varies between species, with examples including skip oviposition where egg batches are scattered between sites, or egg-brooding whereby females actively guard their eggs (Day, 2016).

Other mosquito species (*Sabethes albiprivus*) which oviposit in tree holes, have been reported to exhibit a sequence of rapid “up-and-down” motions in their flights before egg laying, using a catapult action (Vieira et al., 2020). Their “up-and-down” flight pattern described during this mosquito’s unique oviposition flight pattern, may yield a spectrogram quite comparable to that of *An. gambiae* in figure 6.2. This spectrogram shows how a similar flight motion was observed during *An. gambiae* free flight which produced the wider range of frequencies around the fundamental, with also a modulating amplitude over time. The incidental finding reported in section 4.4.2, demonstrates how longer time period measurements can capture mosquito behaviour such as the copulation event and the associated frequency matching of this, and it would be of interest to compare against egg-deposition behaviours.

A better understanding the physiological state of a mosquito is of importance to their control, especially as the toolkit available for controlling mosquitoes is expanding to target a greater range of their lifecycle stages (Benelli et al., 2016). Applying the developed acoustic methods to identification of ovipositing mosquitoes would be of interest for future work, as the acoustics of this key part of a mosquito's lifecycle remains an understudied area in comparison to other stages such as mating. Ovitrap and gravid traps are routinely in use for surveillance and can be used as a control strategy (Barrera et al., 2014; Johnson et al., 2016), however understanding the population of gravid females with an automated approach could greatly facilitate control efforts of mosquito populations.

### *Mosquito age*

The utility of knowing the age of mosquitoes, is to obtain a better understanding of their vectorial capacity (Johnson et al., 2020b). As mosquitoes get older, the likelihood of them blood-feeding, acquiring a pathogen, ovipositing and then being able to transmit a pathogen increases (following completion of the extrinsic incubation period). This dynamic of age can also be affected by insecticide resistance, whereby mosquito susceptibility to insecticides has been demonstrated to be correlated to age (Rajatileka et al., 2011). Characterising the age of mosquito populations can also provide evidence to understand the epidemiological impacts of vector control approaches (Johnson et al., 2020b). However deriving age information for epidemiological impact assessment, exclusively from the fundamental frequency of a mosquito wingbeat with the presented data was not possible with the presented analysis.

Targeted application of measurement arenas by physiological state could support overcoming this issue, to describe mosquito populations better without a direct acoustic age-grading capability. Whilst it may not be possible with the presented acoustic metrics to distinguish ages, measurement arenas could be designed to attract specific mosquito genera and physiological states, where their ages can be

indirectly inferred. As mentioned previously regarding ovitraps and gravid traps, which attract exclusively gravid females, a design that measures the acoustic profile of these mosquitoes can infer, that these are not young and nulliparous.

Host-seeking females, which can be nulliparous or parous (so a wider age range) could be detected with a with a different design approach. Traps which are odour and carbon dioxide baited, such as baited CDC light traps can lure mosquitoes seeking bloodmeals (Yan et al., 2021). Exploring the acoustic impact of parity, would be of interest for a host-seeking trap as this could be used as a potential indicator of mosquito age across the wider potential range it would attract, if this could be acoustically distinguished.

Over an extended period of time, a varied approach that samples acoustic data from multiple trap design types such as ovitraps, gravid traps or host-seeking traps, could allow automated acquisition of mosquito population data. These could exploit descriptions that use fundamental frequency and its standard deviation as presented in Chapters 4 and 5. By the collection of mosquito acoustics targeted to specific to physiological states through trap design, it may be feasible to improve understanding of mosquito population dynamics as numbers that are host-seeking or blood fed could be potentially accounted for across the three genera.

This proposed multi-trap approach to using mosquito wingbeats for vector surveillance will only be feasible once wingbeats can be collected and processed in the field with the same level of clarity as the semi-anechoic chamber. This would require extensive engineering and design effort to obtain a comparably high signal-noise-ratio wingbeat description, with a field device.

## 6.4 Conclusions

Describing mosquito acoustics can be undertaken in a number of ways, with different arenas and sensors able to capture the flight sounds of the mosquito wingbeat throughout the literature. Development of a series of devices and methods in this project focused on obtaining flight descriptions that would be applicable to the detection of mosquitoes in the field using their acoustic signatures. Alongside this, however, was the goal of obtaining measurements of the best possible quality in highly controlled conditions. This dual approach enables exploration of what aspects of physiology it may be feasible to identify acoustically.

Initial arenas were kept simple with known compromise in their design. They were of acrylic pipe construction and allowed mosquitoes in free flight to be sampled within a reverberant acoustic space. Whilst this was undertaken due to the challenges of completing research under COVID-19 lockdowns, this exercise in measuring mosquito acoustics in a simple arena demonstrated that, with suitable *post hoc* background noise compensation, the mosquito flight tone could be described, even within a reverberant environment. It also demonstrated how the diameter of cylindrical flight chambers affects the signal-to-noise ratio of the measured wingbeat, with smaller diameters offering superior performance than their larger diameter counterparts. The complexity of implementing a background noise compensation method, meant that longer time period measurements were more difficult to conduct, and for this project it was decided that it would be more beneficial to attenuate background noise through refinement of the measurement arena instead.

The multiple tunnel diameter approach taken for *Ae. aegypti* should be expanded across the different genera tested, as it would be of great use to define through measurement, which tunnel diameter results with a signal to noise ratio of the wingbeat whilst permitting long stable flight patterns. Using the Ø80 tunnel,

which was the best compromise in providing sustained flight with a reasonable signal to noise ratio for *Ae. aegypti*, the different fundamental frequencies of the three genera could also be described by their fundamental frequencies.

The semi-anechoic chamber developed allowed for much more controlled and thorough acoustic descriptions to be made of mosquitoes both under tethered and free flight conditions. Measurements up to 30 minutes in duration could be taken, and these revealed how during tethered flight, there were characteristic periods in mosquito flight with some regions being more stable in frequency content than others. From the perspective of repeatability, it was defined that only the stable parts of mosquito flight were to be used for comparative measurements, which was only possible by using the 30-minute measurements.

The unique positioning setup designed allowed the effects of angle and distance to be explored for a tethered mosquito, and a dipole sound-field was described, in correlation with prior simulation and measurement studies. This was achieved with the novel semi-anechoic chamber which remained portable, such that measurements could continue at multiple test labs ensuring data collection continued amongst the ongoing uncertainty from COVID-19 lab access restrictions.

Using a tethered approach in combination with an accelerometer, demonstrated that the vibration captured from a solid core wire tether was able to describe fundamental frequencies that were comparable to those captured by a microphone. This novel approach to capturing mosquito wingbeats using direct vibration capture through a tether, may support efforts in sampling mosquito flight tones that are less prone to interference from background noise. This is often cited as a drawback of microphone sampling of wingbeats over optical methods. The benefit of the accelerometer is that it could offer a method of describing flight effort, to act as more of a quality control metric to ensure mosquito flight tones are constant during repeated measures style measurements. This would allow a more in-depth use of the positioning device developed, to describe the effect of distance and angle

across a range of genera, to build on the preliminary dataset compiled for *Ae. aegypti*.

In semi-anechoic free flight, *Ae. aegypti* demonstrated a fundamental frequency that was significantly different from measured *Cx. quinquefasciatus* or *An. gambiae*. However, distinguishing the latter two species from each other was more challenging due to their frequency overlap. What this also demonstrated though was that more metrics in addition to the fundamental frequency could support efforts for acoustic identification, and the variation within a flight tone, which was described here using the standard deviation during an analysed sample, proved to be useful. This can only be described by long time period measurements afforded by microphones, in an arena that provides a high signal to noise ratio. The standard deviation of the fundamental frequency was significantly different for *An. gambiae* from the other two genera, and this is simple to see in a flight trace (figure 6.2). When observed, *An. gambiae* flight is less stable than *Ae. aegypti* which can be seen on flight traces and described by its standard deviation of fundamental frequency.

It would be of great interest to explore how other mosquito behaviours, which cause distinguishable flight patterns can be described with a wider suite of acoustic metrics to build on the commonly used fundamental frequency. This approach has been covered extensively in the literature for courtship behaviour, but ovipositioning acoustics could open a new domain and area whereby useful data on mosquito populations could be collected for integration into existing vector control strategies.

Building upon the free flight investigation, an assessment of mosquito physiology was conducted across the three genera under the more tightly controlled conditions afforded by the tethered setup. Using fundamental frequency and its standard deviation as the primary measurement outcomes, no differences were reported by age or blood feeds for the three genera. This demonstrates that, for tethered specimens, it would not be possible to discriminate between these

physiological states using exclusively these two measurement metrics. One option, of several, might be to add further data, such as time of day, to be incorporated into future multi-variate models use a measured wingbeat sounds.

A comparison was also undertaken between the two semi-anechoic flight conditions tested, to describe how different mosquito acoustics were under free flight and anechoic conditions. No significant difference in fundamental frequency or its standard deviation was reported between both approaches, confirming the validity of using both approaches for obtaining these metrics. This however was only conducted on *Ae. aegypti* and should be repeated for the other two genera.

In summary, the work conducted within this project demonstrated that mosquito acoustics must be captured and processed in a manner that is appropriate for the mosquito being sampled. However, if both sampling and processing methods can create a long, clean signal, their wingbeat sounds in flight offer a rich source of information that can improve our understanding of populations in the field.

# REFERENCES

- Abeyasinghe, R.R., Galappaththy, G.N.L., Smith Gueye, C., Kahn, J.G., Feachem, R.G.A., 2012. Malaria Control and Elimination in Sri Lanka: Documenting Progress and Success Factors in a Conflict Setting. *PLoS One* 7, e43162. <https://doi.org/10.1371/journal.pone.0043162>
- Ackerman, S., Raz, O., Zalmanovici, M., Zlotnick, A., 2021. Automatically detecting data drift in machine learning classifiers.
- Agyapong, J., Chabi, J., Ablorde, A., Kartey, W.D., Osei, J.H.N., De Souza, D.K., Dadzie, S., Boakye, D.A., Ohta, N., Hadi, M.P., Suzuki, T., 2014. Ovipositional Behavior of *Anopheles gambiae* Mosquitoes. *Trop Med Health* 42, 187–190. <https://doi.org/10.2149/tmh.2014-13>
- Aldersley, A., Champneys, A., Homer, M., Robert, D., 2014. Time-frequency composition of mosquito flight tones obtained using Hilbert spectral analysis. *J Acoust Soc Am* 136, 1982–1989. <https://doi.org/10.1121/1.4895689>
- Arthur, B.J., Emr, K.S., Wyttenbach, R.A., Hoy, R.R., 2014a. Mosquito (*Aedes aegypti*) flight tones: Frequency, harmonicity, spherical spreading, and phase relationships. *J Acoust Soc Am* 135, 933–941. <https://doi.org/10.1121/1.4861233>
- Attisano, A., Murphy, J.T., Vickers, A., Moore, P.J., 2015. A simple flight mill for the study of tethered flight in insects. *Journal of Visualized Experiments* 2015, 53377. <https://doi.org/10.3791/53377>
- Azam, F.B., Carney, R.M., Kariev, S., Nallan, K., Subramanian, M., Sampath, G., Kumar, A., Chellappan, S., 2023. Classifying stages in the gonotrophic cycle of mosquitoes from images using computer vision techniques. *Sci Rep* 13, 22130. <https://doi.org/10.1038/s41598-023-47266-7>
- Azil, A.H., Li, M., Williams, C.R., 2011. Dengue vector surveillance programs: A review of methodological diversity in some endemic and epidemic countries. *Asia Pac J Public Health*. <https://doi.org/10.1177/1010539511426595>
- Barrera, R., Amador, M., Acevedo, V., Caban, B., Felix, G., Mackay, A.J., 2014. Use of the CDC Autocidal Gravid Ovitrap to Control and Prevent Outbreaks of *Aedes aegypti* (Diptera: Culicidae). *J Med Entomol* 51, 145–154. <https://doi.org/10.1603/ME13096>
- Bartholomew, N.R., Burdett, J.M., Vandenbrooks, J.M., Quinlan, M.C., Call, G.B., 2015. Impaired climbing and flight behaviour in *Drosophila melanogaster* following carbon dioxide anaesthesia OPEN. <https://doi.org/10.1038/srep15298>
- Batista, G.E.A.P.A., Hao, Y., Keogh, E., Mafra-Neto, A., 2011a. Towards Automatic Classification on Flying Insects Using Inexpensive Sensors, in: 2011 10th International Conference on Machine Learning and Applications and Workshops. IEEE, pp. 364–369. <https://doi.org/10.1109/ICMLA.2011.145>
- Beier, J.C., Keating, J., Githure, J.I., Macdonald, M.B., Impoinvil, D.E., Novak, R.J., 2008. Integrated vector management for malaria control. *Malar J* 7, S4. <https://doi.org/10.1186/1475-2875-7-S1-S4>

- Belton, P., Costello, R.A., 1979. Flight sounds of the females of some mosquitoes of western Canada. *Entomol Exp Appl* 26, 105–114.  
<https://doi.org/10.1111/j.1570-7458.1979.tb02904.x>
- Benelli, G., Jeffries, C.L., Walker, T., 2016. Biological control of mosquito vectors: Past, present, and future. *Insects*.  
<https://doi.org/10.3390/insects7040052>
- Bennet-Clark, H.C., 1984. A Particle Velocity Microphone for the Song of Small Insects and Other Acoustic Measurements. *Journal of Experimental Biology* 108, 459–464. <https://doi.org/10.1242/jeb.108.1.459>
- Bennet-Clark, H.C., 1971. Acoustics of Insect Song. *Nature* 234, 255–259.  
<https://doi.org/10.1038/234255a0>
- Bennet-Clark, H.C., Leroy, Y., Tsacas, L., 1980. Species and sex-specific songs and courtship behaviour in the genus *Zaprionus* (Diptera-*Drosophilidae*). *Anim Behav* 28, 230–255. [https://doi.org/10.1016/S0003-3472\(80\)80027-3](https://doi.org/10.1016/S0003-3472(80)80027-3)
- Bomphrey, R.J., Nakata, T., Phillips, N., Walker, S.M., 2017a. Smart wing rotation and trailing-edge vortices enable high frequency mosquito flight. *Nature* 544, 92–95. <https://doi.org/10.1038/nature21727>
- Bomphrey, R.J., Nakata, T., Simões, P., Walker, S.M., Russell, I.J., 2022. Auditory sensory range of male mosquitoes for the detection of female flight sound. <https://doi.org/10.1098/rsif.2022.0285>
- British Standards Institute, 2011. Acoustics — Determination of sound power levels and sound energy levels of noise sources using sound pressure — Engineering methods for an essentially free field over a reflecting plane (ISO 3744:2010).
- Brogdon, W.G., 1994. Measurement of flight tone differences between female *Aedes aegypti* and *A.albopictus* (Diptera: Culicidae). *J Med Entomol*.  
<https://doi.org/10.1093/jmedent/31.5.700>
- Brüel & Kjær, 1986. *Sound Intensity*. Brüel & Kjær, Nærum.
- Brüel & Kjær, 1984. *Measuring Sound*, 1st ed. Brüel & Kjær, Nærum.
- Brüel & Kjær, 1982. *Measuring Vibration*. Brüel & Kjær, Nærum.  
<https://doi.org/10.1177/002029408201500101>
- Cameron, M.M., Ramesh, A., 2021. The use of molecular xenomonitoring for surveillance of mosquito-borne diseases. *Philosophical Transactions of the Royal Society B: Biological Sciences* 376, 20190816.  
<https://doi.org/10.1098/rstb.2019.0816>
- Castillo, J.S., Bellantuono, A.J., DeGennaro, M., 2023. Building a Uniport Olfactometer to Assess Mosquito Responses to Odors. *Cold Spring Harb Protoc* 2023, pdb.prot108174. <https://doi.org/10.1101/pdb.prot108174>
- Cator, Lauren J., Arthur, B.J., Harrington, L.C., Hoy, R.R., 2009. Harmonic Convergence in the Love Songs of the Dengue Vector Mosquito. *Science* (1979) 323, 1077–1079. <https://doi.org/10.1126/science.1166541>
- Cator, L.J., Arthur, B.J., Ponlawat, A., Harrington, L.C., 2011. Behavioral observations and sound recordings of free-flight mating swarms of *Ae. aegypti* (Diptera: Culicidae) in Thailand. *J Med Entomol* 48, 941–946.  
<https://doi.org/10.1603/ME11019>
- Cator, L.J., Ng’habi, K.R., Hoy, R.R., Harrington, L.C., 2010. Sizing up a mate: variation in production and response to acoustic signals in *Anopheles gambiae*. <https://doi.org/10.1093/beheco/arq087>

- Cator, L.J., Zanti, Z., 2016. Size, sounds and sex: interactions between body size and harmonic convergence signals determine mating success in *Aedes aegypti*. *Parasit Vectors* 9, 1–11. <https://doi.org/10.1186/s13071-016-1914-6>
- Chan, A., Chiang, L.P., Hapuarachchi, H.C., Tan, C.H., Pang, S.C., Lee, R., Lee, K.S., Ng, L.C., Lam-Phua, S.G., 2014. DNA barcoding: complementing morphological identification of mosquito species in Singapore. *Parasites & Vectors* 7. <https://doi.org/10.1186/S13071-014-0569-4>
- Chang, A.Y., Parrales, M.E., Jimenez, J., Sobieszczyk, M.E., Hammer, S.M., Copenhaver, D.J., Kulkarni, R.P., 2009. Combining Google Earth and GIS mapping technologies in a dengue surveillance system for developing countries. *Int J Health Geogr* 8, 49. <https://doi.org/10.1186/1476-072X-8-49>
- Clark, C.J., 2021. Ways that Animal Wings Produce Sound. *Integr Comp Biol* 61, 696–709. <https://doi.org/10.1093/icb/icab008>
- Clements, A.N., 1999. The Biology of Mosquitoes, Volume 2, Sensory Reception and Behaviour, in: *The Biology of Mosquitoes, Volume 2, Sensory Reception and Behaviour*. CABI Publishing, Wallingford, pp. 480–551.
- Costello, R.A., 1974. Effects of environmental and physiological factors on the acoustic behaviour of *Aedes aegypti* (L.) (Diptera: Culicidae).
- Dahmana, H., Mediannikov, O., 2020. Mosquito-Borne Diseases Emergence/Resurgence and How to Effectively Control It Biologically. *Pathogens* 9, 310. <https://doi.org/10.3390/pathogens9040310>
- Day, J., 2016. Mosquito Oviposition Behavior and Vector Control. *Insects* 7, 65. <https://doi.org/10.3390/insects7040065>
- de Nadai, B.L., Maletzke, A.G., Corbi, J.J., Batista, G.E.A.P.A., Reiskind, M.H., 2021. The impact of body size on *Aedes [Stegomyia] aegypti* wingbeat frequency: implications for mosquito identification. *Med Vet Entomol* 35, 617–624. <https://doi.org/10.1111/MVE.12540>
- Djiappi-Tchamen, B., Nana-Ndjangwo, M.S., Nchoutpouen, E., Makoudjou, I., Ngangue-Siewe, I.N., Talipouo, A., Mayi, M.P.A., Awono-Ambene, P., Wondji, C., Tchuinkam, T., Antonio-Nkondjio, C., 2022. *Aedes* Mosquito Surveillance Using Ovitraps, Sweep Nets, and Biogent Traps in the City of Yaoundé, Cameroon. *Insects* 13, 793. <https://doi.org/10.3390/insects13090793>
- Duhrkopf, R.E., Hartberg, W.K., 1992. Differences in male mating response and female flight sounds in *Aedes aegypti* and *Ae. albopictus* (Diptera: Culicidae). *J Med Entomol*. <https://doi.org/10.1093/jmedent/29.5.796>
- ECDC, 2018. Epidemiological update: West Nile virus transmission season in Europe, 2018 [WWW Document]. European Centre for Disease Prevention and Control. URL <https://www.ecdc.europa.eu/en/news-events/epidemiological-update-west-nile-virus-transmission-season-europe-2018> (accessed 7.23.20).
- Farnworth, E.G., 1972. Effects of ambient temperature, humidity, and age on wing-beat frequency of *Periplaneta* species. *J. Insect Physiol* 18, 827–839.
- Fernández Comesaña, D., Tijs, E., De Bree, H.-E., 2014. Exploring the properties of acoustic particle velocity sensors for near-field noise source localisation applications, in: *Forum Acusticum*. <https://doi.org/10.13140/2.1.4296.6406>
- Franklinos, L.H. V, Jones, K.E., Redding, D.W., Abubakar, I., 2019. The effect of global change on mosquito-borne disease. *Lancet Infect Dis* 19, e302–e312. [https://doi.org/10.1016/S1473-3099\(19\)30161-6](https://doi.org/10.1016/S1473-3099(19)30161-6)

- Garcia Castillo, S.S., Pritts, K.S., Krishnan, R.S., Harrington, L.C., League, G.P., 2021. Harmonic convergence coordinates swarm mating by enhancing mate detection in the malaria mosquito *Anopheles gambiae*. *Sci Rep* 11, 24102. <https://doi.org/10.1038/s41598-021-03236-5>
- Garjito, T.A., Susanti, L., Mujiyono, M., Prihatin, M.T., Susilo, D., Nugroho, S.S., Mujiyanto, M., Wigati, R.A., Satoto, T.B.T., Manguin, S., Gavotte, L., Frutos, R., 2021. Assessment of Mosquito Collection Methods for Dengue Surveillance. *Front Med (Lausanne)* 8, 685926. <https://doi.org/10.3389/FMED.2021.685926/BIBTEX>
- Garrett-Jones, C., 1964a. Prognosis for Interruption of Malaria Transmission Through Assessment of the Mosquito's Vectorial Capacity. *Nature* 204, 1173–1175. <https://doi.org/10.1038/2041173a0>
- Garrett-Jones, C., 1964b. The human blood index of malaria vectors in relation to epidemiological assessment. *Bull World Health Organ* 30, 241–61.
- Golding, N., Wilson, A.L., Moyes, C.L., Cano, J., Pigott, D.M., Velayudhan, R., Brooker, S.J., Smith, D.L., Hay, S.I., Lindsay, S.W., 2015. Integrating vector control across diseases. *BMC Med* 13, 249–249. <https://doi.org/10.1186/s12916-015-0491-4>
- González-Pérez, M.I., Faulhaber, B., Aranda, C., Williams, M., Villalonga, P., Silva, M., Costa Osório, H., Encarnaçao, J., Talavera, S., Busquets, N., 2024. Field evaluation of an automated mosquito surveillance system which classifies *Aedes* and *Culex* mosquitoes by genus and sex. *Parasit Vectors* 17, 97. <https://doi.org/10.1186/s13071-024-06177-w>
- Göpfert, M.C., Briegel, H., Robert, D., 1999a. Mosquito hearing: Sound-induced antennal vibrations in male and female *Aedes aegypti*. *Journal of Experimental Biology* 202, 2727–2738.
- Göpfert, M.C., Robert, D., 2000. Nanometre-range acoustic sensitivity in male and female mosquitoes. *Proceedings of the Royal Society B: Biological Sciences* 267, 453–457. <https://doi.org/10.1098/rspb.2000.1021>
- GRAS Sound & Vibration, 2024. G.R.A.S 46AE specifications [WWW Document]. URL [https://www.grasacoustics.com/products/measurement-microphone-sets/product/ss\\_export/pdf2?product\\_id=140](https://www.grasacoustics.com/products/measurement-microphone-sets/product/ss_export/pdf2?product_id=140) (accessed 3.9.24).
- Grobbelaar, A.A., Weyer, J., Moolla, N., Jansen van Vuren, P., Moises, F., Paweska, J.T., 2016. Resurgence of Yellow Fever in Angola, 2015–2016. *Emerg Infect Dis* 22, 1854–1855. <https://doi.org/10.3201/eid2210.160818>
- Gullan, P.J., Cranston, P.S., 2014. *The insects : an outline of entomology*.
- Gutin, L., 1936. Uber das Schallfeld einer rotierenden Luftschraube. *Physikalische Zeitschrift der Sowjetunion* 9.
- Hammond, A., Galizi, R., Kyrou, K., Simoni, A., Siniscalchi, C., Katsanos, D., Gribble, M., Baker, D., Marois, E., Russell, S., Burt, A., Windbichler, N., Crisanti, A., Nolan, T., 2016. A CRISPR-Cas9 gene drive system targeting female reproduction in the malaria mosquito vector *Anopheles gambiae*. *Nat Biotechnol* 34, 78–83. <https://doi.org/10.1038/nbt.3439>
- Hardy, J.L., Houk, E.J., Kramer, L.D., Reeves, W.C., 1983. Intrinsic Factors Affecting Vector Competence of Mosquitoes for Arboviruses. *Annu Rev Entomol* 28, 229–262. <https://doi.org/10.1146/annurev.en.28.010183.001305>
- Harrison, R.E., Brown, M.R., Strand, M.R., 2021. Whole blood and blood components from vertebrates differentially affect egg formation in three

- species of anautogenous mosquitoes. *Parasit Vectors* 14, 119.  
<https://doi.org/10.1186/s13071-021-04594-9>
- Hedenström, A., 2014. How Insect Flight Steering Muscles Work. *PLoS Biol* 12, e1001822. <https://doi.org/10.1371/journal.pbio.1001822>
- Hoffmann, A.A., Iturbe-Ormaetxe, I., Callahan, A.G., Phillips, B.L., Billington, K., Axford, J.K., Montgomery, B., Turley, A.P., O'Neill, S.L., 2014. Stability of the wMel Wolbachia Infection following invasion into *Aedes aegypti* populations. *PLoS Negl Trop Dis* 8, e3115–e3115.  
<https://doi.org/10.1371/journal.pntd.0003115>
- Ingham, R., 2017. Physiological mechanisms underlying male *Culex quinquefasciatus* acoustic mating behaviour. University of Brighton.
- Irish, S.R., Stevens, W.M.B., Derua, Y.A., Walker, T., Cameron, M.M., 2015. Comparison of methods for xenomonitoring in vectors of lymphatic filariasis in northeastern Tanzania. *American Journal of Tropical Medicine and Hygiene* 93, 983–989. <https://doi.org/10.4269/ajtmh.15-0234>
- Johnson, B.G., Rowley, W.A., 1972. Ultrastructural changes in *Culex tarsalis* flight muscle associated with exhaustive flight. *J Insect Physiol* 18, 2391–2399. [https://doi.org/10.1016/0022-1910\(72\)90183-7](https://doi.org/10.1016/0022-1910(72)90183-7)
- Johnson, B.J., Hugo, L.E., Churcher, T.S., Ong, O.T.W., Devine, G.J., 2020a. Mosquito Age Grading and Vector-Control Programmes. *Trends Parasitol* 36, 39–51. <https://doi.org/10.1016/j.pt.2019.10.011>
- Johnson, B.J., Hurst, T., Quoc, H.L., Unlu, I., Freebairn, C., Faraji, A., Ritchie, S.A., 2016. Field Comparisons of the Gravid *Aedes* Trap (GAT) and BG-Sentinel Trap for Monitoring *Aedes albopictus* (Diptera: Culicidae) Populations and Notes on Indoor GAT Collections in Vietnam. *J Med Entomol* tjw166. <https://doi.org/10.1093/jme/tjw166>
- Johnson, B.J., Manby, R., Devine, G.J., 2022. The Use of Automated Traps to Assess the Efficacy of Insecticide Barrier Treatments Against Abundant Mosquitoes in Remote Environments. *J Med Entomol* 59, 384–389.  
<https://doi.org/10.1093/jme/tjab178>
- Johnson, B.J., Ritchie, S.A., Fonseca, D.M., 2017. The State of the Art of Lethal Oviposition Trap-Based Mass Interventions for Arboviral Control. *Insects (Basel, Switzerland)* 8, 5. <https://doi.org/10.3390/insects8010005>
- Jones, J., Murray, G.P.D., McCall, P.J., 2021. A minimal 3D model of mosquito flight behaviour around the human baited bed net. *Malar J* 20.  
<https://doi.org/10.1186/s12936-020-03546-5>
- Jones, M.D.R., Hill, M., Hope, A.M., 1967. The circadian flight activity of the mosquito *Anopheles gambiae*: phase setting by the light regime. *J. Exp. Biol* 47, 503–511.
- Kilpatrick, A.M., Pape, W.J., 2013. Predicting Human West Nile Virus Infections With Mosquito Surveillance Data. *Am J Epidemiol* 178, 829–835.  
<https://doi.org/10.1093/aje/kwt046>
- Kim, D., DeBriere, T.J., Cherukumalli, S., White, G.S., Burkett-Cadena, N.D., 2021. Infrared light sensors permit rapid recording of wingbeat frequency and bioacoustic species identification of mosquitoes. *Sci Rep* 11, 10042.  
<https://doi.org/10.1038/s41598-021-89644-z>
- Kimani, T., Schelling, E., Bett, B., Ngigi, M., Randolph, T., Fuhrmann, S., 2016. Public Health Benefits from Livestock Rift Valley Fever Control: A

- Simulation of Two Epidemics in Kenya. *Ecohealth* 13, 729–742.  
<https://doi.org/10.1007/s10393-016-1192-y>
- Kiskin, I., Cobb, A.D., Wang, L., Roberts, S., 2020. HumBug Zooniverse: a crowd-sourced acoustic mosquito dataset. ICASSP, IEEE International Conference on Acoustics, Speech and Signal Processing - Proceedings 2020-May, 916–920.
- Kittichai, V., Kaewthamasorn, M., Samung, Y., Jomtarak, R., Naing, K.M., Tongloy, T., Chuwongin, S., Boonsang, S., 2023. Automatic identification of medically important mosquitoes using embedded learning approach-based image-retrieval system. *Sci Rep* 13, 10609. <https://doi.org/10.1038/s41598-023-37574-3>
- Kittichai, V., Pongsakul, T., Chumchuen, K., Samung, Y., Sriwichai, P., Phatthamolrat, N., Tongloy, T., Jaksukam, K., Chuwongin, S., Boonsang, S., 2021. Deep learning approaches for challenging species and gender identification of mosquito vectors. *Sci Rep* 11, 4838.  
<https://doi.org/10.1038/s41598-021-84219-4>
- Knols, B., Takken, W., Smallegange, R., 2010. Olfaction in vector-host interactions, Olfaction in vector-host interactions. Brill | Wageningen Academic. <https://doi.org/10.3920/978-90-8686-698-4>
- Kothera, L., Byrd, B., Savage, H.M., 2017. Duplex Real-Time PCR Assay Distinguishes *Aedes aegypti* From *Ae. albopictus* (Diptera: Culicidae) Using DNA From Sonicated First-Instar Larvae. *J Med Entomol* 54, 1567–1572.  
<https://doi.org/10.1093/jme/tjx125>
- Kouassi, B.L., Edi, C., Ouattara, A.F., Ekra, A.K., Bellai, L.G., Gouaméné, J., Kacou, Y.A.K., Kouamé, J.K.I., Béké, A.H.O., Yokoli, F.N., Gbalegba, C.G.N., Tia, E., Yapo, R.M., Konan, L.Y., N'Tamon, R.N., Akre, M.A., Koffi, A.A., Tanoh, A.M., Zinzindohoué, P., Kouadio, B., Yepassis-Zembrou, P.L., Belemvire, A., Irish, S.R., Cissé, N.G., Flatley, C., Chabi, J., 2023. Entomological monitoring data driving decision-making for appropriate and sustainable malaria vector control in Côte d'Ivoire. *Malar J* 22, 1–15.  
<https://doi.org/10.1186/S12936-023-04439-Z/FIGURES/9>
- Kramer, L.D., Ciota, A.T., 2015. Dissecting vectorial capacity for mosquito-borne viruses. *Curr Opin Virol* 15, 112–118.  
<https://doi.org/10.1016/j.coviro.2015.10.003>
- Krupa, E., Gréhal, A.-L., Esnault, J., Bender, C., Mathieu, B., 2021. Laboratory Evaluation of Flight Capacities of *Aedes japonicus* (Diptera: Culicidae) Using a Flight Mill Device. *Journal of Insect Science* 21.  
<https://doi.org/10.1093/jisesa/ieab093>
- Kyu, H.H., Abate, D., Abate, K.H., Abay, S.M., Murray, C.J.L., 2018. Global, regional, and national disability-adjusted life-years (DALYs) for 359 diseases and injuries and healthy life expectancy (HALE) for 195 countries and territories, 1990–2017: a systematic analysis for the Global Burden of Disease Study 2017. *The Lancet* 392, 1859–1922.  
[https://doi.org/10.1016/S0140-6736\(18\)32335-3](https://doi.org/10.1016/S0140-6736(18)32335-3)
- Lahondère, C., Vinauger, C., Liaw, J.E., Tobin, K.K.S., Joiner, J.M., Riffell, J.A., 2023. Effect of Temperature on Mosquito Olfaction. *Integr Comp Biol* 63, 356–367. <https://doi.org/10.1093/icb/icad066>

- Lambrechts, L., Paaijmans, K.P., Fansiri, T., Carrington, L.B., Kramer, L.D., Thomas, M.B., Scott, T.W., 2011. Impact of daily temperature fluctuations on dengue virus transmission by *Aedes aegypti*. *Proceedings of the National Academy of Sciences* 108, 7460–7465. <https://doi.org/10.1073/pnas.1101377108>
- Landois Hermann, 1867. Die Ton- und Stimmapparate der Insecten : in anatomisch-physiologischer und akustischer Beziehung /, Die Ton- und Stimmapparate der Insecten : in anatomisch-physiologischer und akustischer Beziehung. W. Engelmann, Leipzig : <https://doi.org/10.5962/bhl.title.104946>
- League, G.P., Alfonso-Parra, C., Pantoja-Sánchez, H., Harrington, L.C., 2022. Acoustic-Related Mating Behavior in Tethered and Free-Flying Mosquitoes. *Cold Spring Harb Protoc* 2022, 456–461. <https://doi.org/10.1101/pdb.top107667>
- Levenbook, L., Williams, C.M., 1956. Mitochondria in the flight muscles of insects. *J Gen Physiol* 39, 497–512. <https://doi.org/10.1085/jgp.39.4.497>
- Li, Y., Kamara, F., Zhou, G., Puthiyakunnon, S., Li, C., Liu, Y., Zhou, Y., Yao, L., Yan, G., Chen, X.-G., 2014. Urbanization Increases *Aedes albopictus* Larval Habitats and Accelerates Mosquito Development and Survivorship. *PLoS Negl Trop Dis* 8, e3301. <https://doi.org/10.1371/journal.pntd.0003301>
- Li, Y., Zilli, D., Chan, H., Kiskin, I., Sinka, M., Roberts, S., Willis, K., 2017. Mosquito detection with low-cost smartphones: data acquisition for malaria research.
- MacDonald, G., 1957. *The epidemiology and control of malaria*. Oxford University Press, New York, NY.
- Mesaros, A., Heittola, T., Benetos, E., Foster, P., Lagrange, M., Virtanen, T., Plumbley, M.D., 2018. Fast mosquito acoustic detection with field cup recordings: an initial investigation. *IEEE/ACM Trans Audio Speech Lang Process* 26, 379–393. <https://doi.org/10.1109/TASLP.2017.2778423>
- Microflown Technologies, 2024. The acoustic particle velocity sensor [WWW Document]. URL <https://www.microflown.com/products/acoustic-particle-velocity-sensors> (accessed 3.9.24).
- Mitchell, S.N., Catteruccia, F., 2017. Anopheline reproductive biology: Impacts on vectorial capacity and potential avenues for malaria control. *Cold Spring Harb Perspect Med* 7, 14. <https://doi.org/10.1101/cshperspect.a025593>
- Montoya, J.P., Pantoja-Sánchez, H., Gomez, S., Avila, F.W., Alfonso-Parra, C., 2021. Flight tone characterisation of the south american malaria vector *Anopheles darlingi* (Diptera: Culicidae). *Mem Inst Oswaldo Cruz* 116. <https://doi.org/10.1590/0074-02760200497>
- Moore, A., Miller, J.R., Tabashnik, B.E., Gage, S.H., 1986. Automated Identification of Flying Insects by Analysis of Wingbeat Frequencies. *J Econ Entomol.* <https://doi.org/10.1093/jee/79.6.1703>
- Moore, A., Miller, R.H., 2002. Automated Identification of Optically Sensed Aphid (Homoptera: Aphidae) Wingbeat Waveforms, *Ann. Entomol. Soc. Am.*
- Muijres, F.T., Chang, S.W., Van Veen, W.G., Spitzen, J., Biemans, B.T., Koehl, M.A.R., Dudley, R., 2017. Escaping blood-fed malaria mosquitoes minimize tactile detection without compromising on take-off speed. *Journal of Experimental Biology* 220, 3751–3762. <https://doi.org/10.1242/jeb.163402>

- Muijres, F.T., Dickerson, A.K., Pieters, R., 2023. Designing a Generic Videography Experiment for Studying Mosquito Behavior. Cold Spring Harb Protoc 2023, pdb.prot107926. <https://doi.org/10.1101/pdb.prot107926>
- Mukundarajan, H., Hol, F.J.H., Castillo, E.A., Newby, C., Prakash, M., 2017a. Using mobile phones as acoustic sensors for high-throughput mosquito surveillance. *Elife* 6, 1–26. <https://doi.org/10.7554/eLife.27854>
- Müller BBM VibroAkustik Systeme, 2024. Müller BBM MKII [WWW Document].
- Mwingira, V.S., Spitzen, J., Mboera, L.E.G., Torres-Estrada, J.L., Takken, W., 2020. The Influence of Larval Stage and Density on Oviposition Site-Selection Behavior of the Afrotropical Malaria Mosquito *Anopheles coluzzii* (Diptera: Culicidae). *J Med Entomol* 57, 657–666. <https://doi.org/10.1093/jme/tjz172>
- National Instruments, 2019. Acquiring an Analog Signal, National Instruments. Austin, TX.
- Nayar, J.K.; Sauerman Jr., D.M., 1972. Flight performance and fuel utilization as a function of age in female *Aedes taeniorhynchus*. *Isr J Entomol* VII, 27–35.
- Novoseltsev, V.N., Michalski, A.I., Novoseltseva, J.A., Yashin, A.I., Carey, J.R., Ellis, A.M., 2012. An age-structured extension to the vectorial capacity model. *PLoS One* 7. <https://doi.org/10.1371/journal.pone.0039479>
- Ohm, J.R., Baldini, F., Barreaux, P., Lefevre, T., Lynch, P.A., Suh, E., Whitehead, S.A., Thomas, M.B., 2018. Rethinking the extrinsic incubation period of malaria parasites. *Parasit Vectors* 11, 1–9. <https://doi.org/10.1186/S13071-018-2761-4/FIGURES/3>
- Omucheni, D.L., Kaduki, K.A., Mukabana, W.R., 2023. Identification of three medically important mosquito species using Raman spectroscopy. *Journal of Raman Spectroscopy* 54, 512–523. <https://doi.org/10.1002/JRS.6516>
- Ortega-Morales, A.I., Moreno-García, M., González-Acosta, C., Correa-Morales, F., 2018. Mosquito Surveillance in Mexico: The Use of Ovitraps for *Aedes aegypti*, *Ae. albopictus*, and Non-Target Species. *Florida Entomologist* 101, 623. <https://doi.org/10.1653/024.101.0425>
- Oshana, R., 2006. DSP Software Development Techniques for Embedded and Real-Time Systems. Elsevier. <https://doi.org/10.1016/B978-0-7506-7759-2.X5000-5>
- Ouyang, T.H., Yang, E.C., Jiang, J.A., Lin, T. Te, 2015. Mosquito vector monitoring system based on optical wingbeat classification. *Comput Electron Agric* 118, 47–55. <https://doi.org/10.1016/j.compag.2015.08.021>
- Ouyang, T.-H., Yang, E.-C., Jiang, J.-A., Lin, T.-T., 2015. Mosquito vector monitoring system based on optical wingbeat classification. *Comput Electron Agric* 118, 47–55. <https://doi.org/10.1016/j.compag.2015.08.021>
- Paaijmans, K.P., Blanford, S., Bell, A.S., Blanford, J.I., Read, A.F., Thomas, M.B., 2010. Influence of climate on malaria transmission depends on daily temperature variation. *Proc Natl Acad Sci U S A* 107, 15135–9. <https://doi.org/10.1073/pnas.1006422107>
- PAHO, 2017. Number of reported cases of chikungunya fever in the Americas, by country or territory 2017 (to week noted). Cumulative cases [WWW Document]. *Epidemiol Weekly*. URL

- <https://www.paho.org/hq/dmdocuments/2017/2017-dec-22-phe-CHIKV-cases-ew-51.pdf> (accessed 7.23.20).
- Pantoja-Sánchez, H., Gomez, S., Velez, V., Avila, F.W., Alfonso-Parra, C., 2019a. Precopulatory acoustic interactions of the New World malaria vector *Anopheles albimanus* (Diptera: Culicidae). *Parasit Vectors* 12. <https://doi.org/10.1186/s13071-019-3648-8>
- Pantoja-Sánchez, H., League, G.P., Harrington, L.C., Alfonso-Parra, C., 2022. Recording and Analysis of Mosquito Acoustic-Related Mating Behavior. *Cold Spring Harb Protoc* 2022, 506–513. <https://doi.org/10.1101/pdb.prot107989>
- Park, D., Bowles, J., McKenzie, B., Narayanan, H.V., Prakash, M., Blagburn, B., Starkey, L., Zohdy, S., 2020. An investigation of *Dirofilaria immitis* infection and its effects on mosquito wingbeat frequencies. *Vet Parasitol* 283. <https://doi.org/10.1016/j.vetpar.2020.109112>
- Park, D., Bowles, J., Norrid, K., Dobson, F.S., Abebe, A., Narayanan, H.V., Prakash, M., Blagburn, B., Starkey, L., Zohdy, S., 2023. Effect of age on wingbeat frequency of *Aedes aegypti* and potential application for age estimation of mosquitoes. *Med Vet Entomol* 37, 491–498. <https://doi.org/10.1111/mve.12647>
- Pascual, M., Dobson, A.P., Bouma, M.J., 2009. Underestimating malaria risk under variable temperatures. *Proc Natl Acad Sci U S A* 106, 13645–6. <https://doi.org/10.1073/pnas.0906909106>
- Pennetier, C., Warren, B., Dabiré, K.R., Russell, I.J., Gibson, G., 2010a. “Singing on the Wing” as a Mechanism for Species Recognition in the Malarial Mosquito *Anopheles gambiae*. *Current Biology* 20, 131–136. <https://doi.org/10.1016/j.cub.2009.11.040>
- Potamitis, I., Rigakis, I., 2016. Measuring the fundamental frequency and the harmonic properties of the wingbeat of a large number of mosquitoes in flight using 2D optoacoustic sensors. *Applied Acoustics* 109, 54–60. <https://doi.org/10.1016/j.apacoust.2016.03.005>
- Protopopoff, N., Mosha, J.F., Lukole, E., Charlwood, J.D., Wright, A., Mwalimu, C.D., Manjurano, A., Mosha, F.W., Kisinza, W., Kleinschmidt, I., Rowland, M., 2018. Effectiveness of a long-lasting piperonyl butoxide-treated insecticidal net and indoor residual spray interventions, separately and together, against malaria transmitted by pyrethroid-resistant mosquitoes: a cluster, randomised controlled, two-by-two factorial design trial. *The Lancet* 391, 1577–1588. [https://doi.org/10.1016/S0140-6736\(18\)30427-6](https://doi.org/10.1016/S0140-6736(18)30427-6)
- Quan, T.M., Thao, T.T.N., Duy, N.M., Nhat, T.M., Clapham, H., 2020. Estimates of the global burden of Japanese encephalitis and the impact of vaccination from 2000-2015. *Elife* 9. <https://doi.org/10.7554/eLife.51027>
- Rajatileka, S., Burhani, J., Ranson, H., 2011. Mosquito age and susceptibility to insecticides. *Trans R Soc Trop Med Hyg* 105, 247–253. <https://doi.org/10.1016/j.trstmh.2011.01.009>
- Reeves, L.E., Burkett-Cadena, N.D., 2023. Mosquito Blood Meal Analysis. *Cold Spring Harb Protoc*. <https://doi.org/10.1101/pdb.top107706>
- Roth, G.A., Abate, D., Abate, K.H., Abay, S.M., 2018. Global, regional, and national age-sex-specific mortality for 282 causes of death in 195 countries and territories, 1980–2017: a systematic analysis for the Global Burden of

- Disease Study 2017. *The Lancet* 392, 1736–1788.  
[https://doi.org/10.1016/S0140-6736\(18\)32203-7](https://doi.org/10.1016/S0140-6736(18)32203-7)
- Rueda, L.M., Debboun, M., 2019. Taxonomy, Identification, and Biology of Mosquitoes, in: *Mosquitoes, Communities, and Public Health in Texas*. Elsevier Inc., pp. 3–7. <https://doi.org/10.1016/B978-0-12-814545-6.00001-8>
- Rund, S.S.C., Labb, L.F., Benefiel, O.M., Duffield, G.E., 2020. Artificial light at night increases *Aedes aegypti* mosquito biting behavior with implications for arboviral disease transmission. *American Journal of Tropical Medicine and Hygiene* 103, 2450–2452. <https://doi.org/10.4269/ajtmh.20-0885>
- Russell, C.B., Hunter, F.F., 2010. A Modified Centers for Disease Control and Prevention Gravid Trap for Easier Mosquito Collection. *J Am Mosq Control Assoc* 26, 119–120. <https://doi.org/10.2987/09-5905.1>
- Salako, A.S., Ossè, R., Padonou, G.G., Dagnon, F., Aikpon, R., Kpanou, C., Sagbohan, H., Sovi, A., Sèzonlin, M., Akogbeto, M.C., 2019. Population Dynamics of *Anopheles gambiae* s.l. and *Culex quinquefasciatus* in Rural and Urban Settings Before an Indoor Residual Spraying Campaign in Northern Benin. *Vector Borne and Zoonotic Diseases* 19, 674. <https://doi.org/10.1089/VBZ.2018.2409>
- Santos, D.A.A., Rodrigues, J.J.P.C., Furtado, V., Saleem, K., Korotaev, V., 2019a. Automated electronic approaches for detecting disease vectors mosquitoes through the wing-beat frequency. *J Clean Prod* 217, 767–775. <https://doi.org/10.1016/j.jclepro.2019.01.187>
- Sarathchandra, F., 2015. *The Low Cost Mosquito Trap*. University of Bath.
- Sarria-S, F.A., Buxton, K., Jonsson, T., Montealegre-Z, F., 2016. Wing mechanics, vibrational and acoustic communication in a new bush-cricket species of the genus *Copiphora* (Orthoptera: Tettigoniidae) from Colombia. *Zoologischer Anzeiger - A Journal of Comparative Zoology* 263, 55–65. <https://doi.org/10.1016/J.JCZ.2016.04.008>
- Seixas, G., Paul, R.E.L., Pires, B., Alves, G., de Jesus, A., Silva, A.-C., Devine, G.J., Sousa, C.A., 2019. An evaluation of efficacy of the auto-dissemination technique as a tool for *Aedes aegypti* control in Madeira, Portugal. *Parasit Vectors* 12, 202–202. <https://doi.org/10.1186/s13071-019-3454-3>
- Seo, J.H., Hedrick, T.L., Mittal, R., 2020. Mechanism and scaling of wing tone generation in mosquitoes. *Bioinspir Biomim* 15. <https://doi.org/10.1088/1748-3190/ab54fc>
- Serway, R.A., 2014. *Physics for scientists and engineers*, 9th ed., Internat... ed. Brooks/Cole Cengage Learning, Australia ;
- Shannon, C.E., 1949. Communication in the Presence of Noise. *Proceedings of the IRE* 37, 10–21. <https://doi.org/10.1109/JRPROC.1949.232969>
- Showering, A., Martinez, J., Benavente, E.D., Gezan, S.A., Jones, R.T., Oke, C., Tytheridge, S., Pretorius, E., Scott, D., Allen, R.L., D'Alessandro, U., Lindsay, S.W., Armour, J.A.L., Pickett, J., Logan, J.G., 2022. Skin microbiome alters attractiveness to *Anopheles* mosquitoes. *BMC Microbiol* 22. <https://doi.org/10.1186/s12866-022-02502-4>
- Sikaala, C.H., Killeen, G.F., Chanda, J., Chinula, D., Miller, J.M., Russell, T.L., Seyoum, A., 2013. Evaluation of alternative mosquito sampling methods for malaria vectors in Lowland South - East Zambia. *Parasit Vectors* 6, 91. <https://doi.org/10.1186/1756-3305-6-91>

- Simões, P.M.V., Ingham, R.A., Gibson, G., Russell, I.J., 2016a. A role for acoustic distortion in novel rapid frequency modulation behaviour in free-flying male mosquitoes. *Journal of Experimental Biology* 219, 2039–2047. <https://doi.org/10.1242/jeb.135293>
- Sivagnaname, N., Gunasekaran, K., 2012. Need for an efficient adult trap for the surveillance of dengue vectors. *Indian Journal of Medical Research* 136, 739–749.
- Smith, D.L., McKenzie, F.E., 2004. Statics and dynamics of malaria infection in *Anopheles* mosquitoes. *Malar J*. <https://doi.org/10.1186/1475-2875-3-13>
- Smith, D.L., Perkins, T.A., Reiner, R.C., Barker, C.M., Niu, T., Chaves, L.F., Ellis, A.M., George, D.B., Le Menach, A., Pulliam, J.R.C., Bisanzio, D., Buckee, C., Chiyaka, C., Cummings, D.A.T., Garcia, A.J., Gatton, M.L., Gething, P.W., Hartley, D.M., Johnston, G., Klein, E.Y., Michael, E., Lloyd, A.L., Pigott, D.M., Reisen, W.K., Ruktanonchai, N., Singh, B.K., Stoller, J., Tatem, A.J., Kitron, U., Godfray, H.C.J., Cohen, J.M., Hay, S.I., Scott, T.W., 2014. Recasting the theory of mosquito-borne pathogen transmission dynamics and control. *Trans R Soc Trop Med Hyg* 108, 185–197. <https://doi.org/10.1093/trstmh/tru026>
- Somerville, A.G.T., Gleave, K., Jones, C.M., Reimer, L.J., 2019a. The consequences of *Brugia malayi* infection on the flight and energy resources of *Aedes aegypti* mosquitoes. *Sci Rep* 9, 18449. <https://doi.org/10.1038/s41598-019-54819-2>
- Sotavalta, O., 1952a. Flight-tone and wing-stroke frequency of insects and the dynamics of insect flight. *Nature* 170, 1057–1058. <https://doi.org/10.1038/1701057a0>
- Sotavalta, O., 1952b. The essential factor regulating the wing-stroke frequency of insects in wing mutilation and loading experiments and in experiments at subatmospheric pressure, in: *Annales Zoologici Societatis Zoologicae Botanicae Fennicae “Vanamo” Tom. 15.*
- Sougoufara, S., Diédhiou, S.M., Doucouré, S., Diagne, N., Sembène, P.M., Harry, M., Trape, J.-F., Sokhna, C., Ndiath, M.O., 2014. Biting by *Anopheles funestus* in broad daylight after use of long-lasting insecticidal nets: a new challenge to malaria elimination. *Malar J* 13, 125. <https://doi.org/10.1186/1475-2875-13-125>
- Spitzen, J., Takken, W., 2018. Keeping track of mosquitoes: A review of tools to track, record and analyse mosquito flight. *Parasit Vectors* 11. <https://doi.org/10.1186/s13071-018-2735-6>
- Staunton, K.M., Usher, L., Prachar, T., Ritchie, S.A., Snoad, N., Johnson, B.J., 2019a. A novel methodology for recording wing beat frequencies of untethered male and female *Aedes aegypti*. *J Am Mosq Control Assoc* 35, 169–177.
- Sueur, J., Tuck, E.J., Robert, D., 2005. Sound radiation around a flying fly. Citation: *The Journal of the Acoustical Society of America* 118, 530. <https://doi.org/10.1121/1.1932227>
- Suman, D.S., 2019. Evaluation of enhanced oviposition attractant formulations against *Aedes* and *Culex* vector mosquitoes in urban and semi-urban areas. *Parasitol Res* 118, 743–750. <https://doi.org/10.1007/s00436-019-06228-7>

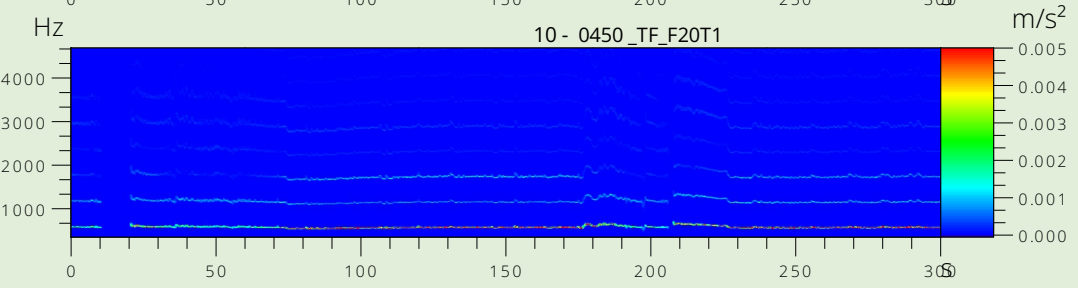
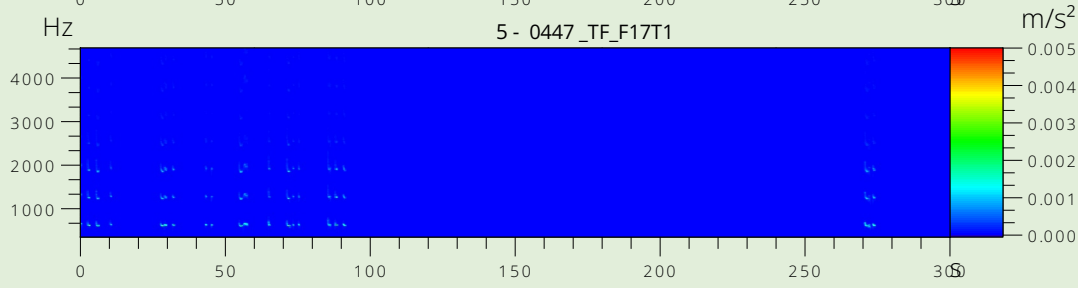
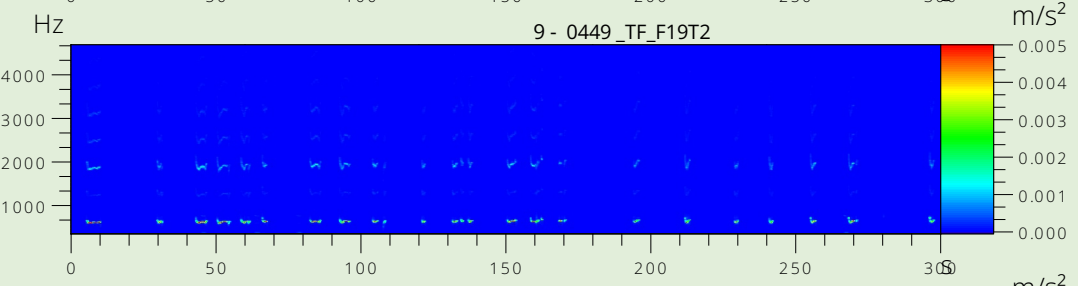
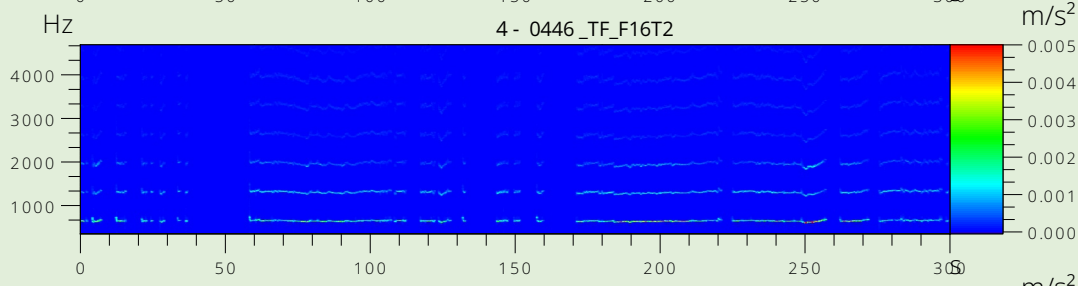
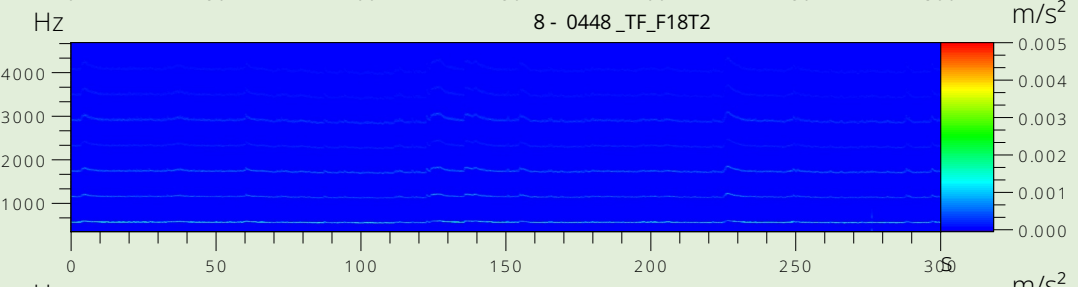
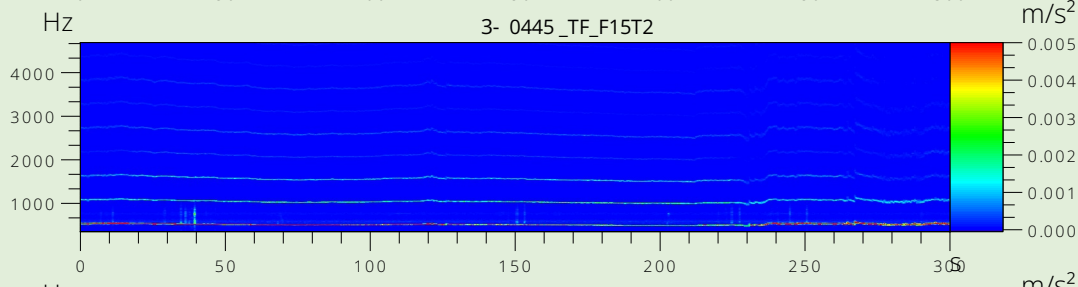
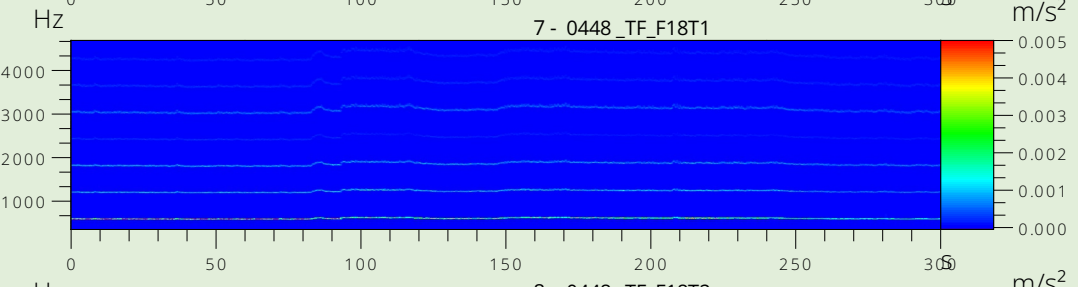
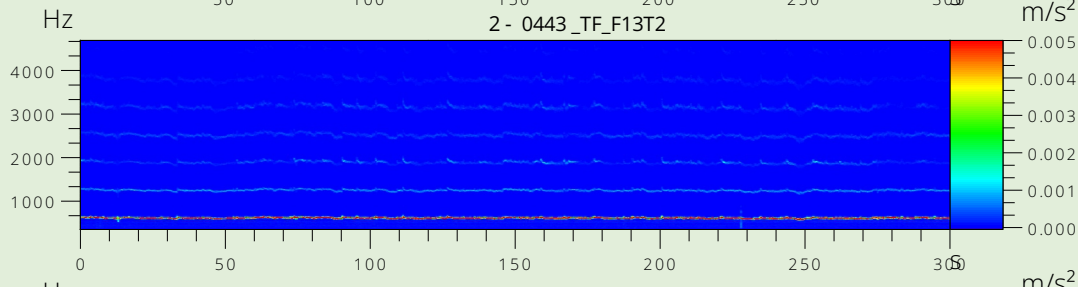
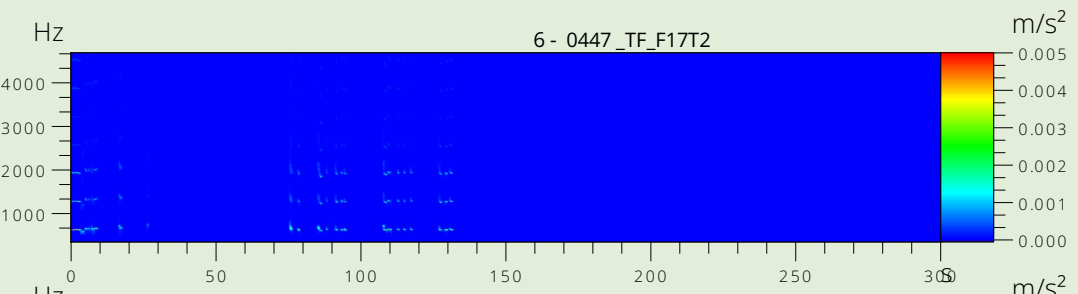
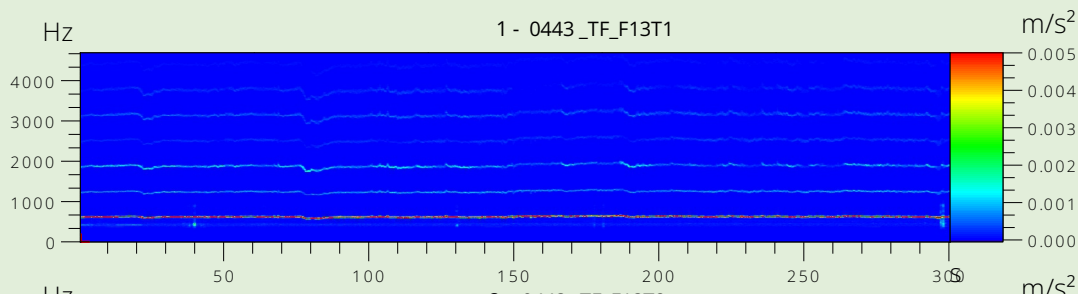
- Texas Instruments, 2024. Texas Instruments ADS1013 Datasheet [WWW Document]. URL <https://www.ti.com/product/ADS1013> (accessed 3.10.24).
- Tong Qiu, Y., Spitzen, J., Smallegange, R.C., Knols -9789086866267, B.G.J., 2007. Monitoring systems for adult insect pests and disease vectors. Wageningen Academic.
- Tripet, F., Dolo, G., Traoré, S., Lanzaro, G.C., 2004. The “wingbeat hypothesis” of reproductive isolation between members of the *Anopheles gambiae* complex (Diptera: Culicidae) does not fly. *J Med Entomol* 41, 375–384. <https://doi.org/10.1603/0022-2585-41.3.375>
- Trujillano, F., Jimenez Garay, G., Alatrística-Salas, H., Byrne, I., Nunez-del-Prado, M., Chan, K., Manrique, E., Johnson, E., Apollinaire, N., Kouame Kouakou, P., Oumbouke, W.A., Tiono, A.B., Guelbeogo, M.W., Lines, J., Carrasco-Escobar, G., Fornace, K., 2023. Mapping Malaria Vector Habitats in West Africa: Drone Imagery and Deep Learning Analysis for Targeted Vector Surveillance. *Remote Sens (Basel)* 15, 2775. <https://doi.org/10.3390/rs15112775>
- Vasconcelos, D., Nunes, N., Ribeiro, M., Prandi, C., Rogers, A., 2019. LOCOMOBIS: A low-cost acoustic-based sensing system to monitor and classify mosquitoes, in: 2019 16th IEEE Annual Consumer Communications and Networking Conference, CCNC 2019. <https://doi.org/10.1109/CCNC.2019.8651767>
- Vazquez-Prokopec, G.M., Montgomery, B.L., Horne, P., Clennon, J.A., Ritchie, S.A., 2017. Combining contact tracing with targeted indoor residual spraying significantly reduces dengue transmission. *Sci Adv* 3, e1602024–e1602024. <https://doi.org/10.1126/sciadv.1602024>
- Vieira, G., Bersot, M.I.L., Pereira, G.R., de Abreu, F.V.S., Nascimento-Pereira, A.C., Neves, M.S.A.S., Rosa-Freitas, M.G., Motta, M.A., Lourenço-de-Oliveira, R., 2020. High Speed Video Documentation of the Mosquito *Sabethes albiprivus* Egg-Catapulting Oviposition Behavior (Diptera: Culicidae). *Neotrop Entomol* 49, 662–667. <https://doi.org/10.1007/s13744-020-00782-x>
- Villarreal, Susa.M., Winokur, O., Harrington, L., 2017a. The impact of temperature and body size on fundamental flight tone variation in the mosquito vector *Aedes aegypti* (Diptera: Culicidae): Implications for acoustic lures. *J Med Entomol* 54, 1116–1121. <https://doi.org/10.1093/jme/tjx079>
- Vinauger, C., Riffell, J.A., 2023. Tethered Preparation for the Analysis of Mosquito Visual-Motor Responses Using Modular Visual Displays. *Cold Spring Harb Protoc* 2023, 679–684. <https://doi.org/10.1101/pdb.prot108179>
- Walker, M., Chandrasegaran, K., Vinauger, C., Robert, M.A., Childs, L.M., 2021. Modeling the effects of *Aedes aegypti*'s larval environment on adult body mass at emergence. *PLoS Comput Biol* 17, e1009102. <https://doi.org/10.1371/journal.pcbi.1009102>
- Walker, T., 2020. Sampling, ID & incrimination of Culicine mosquitoes. London.
- Wang, R., Hu, C., Fu, X., Long, T., Zeng, T., 2017. Micro-Doppler measurement of insect wing-beat frequencies with W-band coherent radar. *Sci Rep* 7, 1396. <https://doi.org/10.1038/s41598-017-01616-4>

- Warren, B., Gibson, G., Russell, I.J., 2009a. Sex Recognition through Midflight Mating Duets in *Culex* Mosquitoes Is Mediated by Acoustic Distortion. *Current Biology* 19, 485–491. <https://doi.org/10.1016/j.cub.2009.01.059>
- West, R.G., Mathias, D.R., Day, J.F., Boohene, C.K., Unnasch, T.R., Burkett-Cadena, N.D., 2020. Vectorial Capacity of *Culiseta melanura* (Diptera: Culicidae) Changes Seasonally and Is Related to Epizootic Transmission of Eastern Equine Encephalitis Virus in Central Florida. *Front Ecol Evol* 8. <https://doi.org/10.3389/fevo.2020.00270>
- Wilke, A.B.B., Mhlanga, A., Kummer, A.G., Vasquez, C., Moreno, M., Petrie, W.D., Rodriguez, A., Vitek, C., Hamer, G.L., Mutebi, J.-P., Ajelli, M., 2023. Diel activity patterns of vector mosquito species in the urban environment: Implications for vector control strategies. *PLoS Negl Trop Dis* 17, e0011074. <https://doi.org/10.1371/journal.pntd.0011074>
- World Health Organization, 2023. World malaria report 2023. WHO, Geneva.
- World Health Organization, 2020a. Multisectoral Approach to the Prevention and Control of Vector-Borne Diseases: A conceptual framework.
- World Health Organization, 2017. Global vector control response 2017–2030. Geneva.
- World Health Organization, 2009. Dengue Guidelines for Diagnosis, Treatment, Prevention and Control, in: World Health Organization. Geneva, pp. 1–144.
- World Health Organization, 1975a. Manual on Practical Entomology in Malaria. Geneva. <https://doi.org/10.1017/CBO9781107415324.004>
- Wu, V.Y., Chen, B., Christofferson, R., Ebel, G., Fagre, A.C., Gallichotte, E.N., Sweeny, A.R., Carlson, C.J., Ryan, S.J., 2022. A minimum data standard for vector competence experiments. *Sci Data* 9, 634. <https://doi.org/10.1038/s41597-022-01741-4>
- Yan, J., Gangoso, L., Ruiz, S., Soriguer, R., Figuerola, J., Martínez-de la Puente, J., 2021. Understanding host utilization by mosquitoes: determinants, challenges and future directions. *Biol Rev Camb Philos Soc* 96, 1367–1385. <https://doi.org/10.1111/brv.12706>
- Yin, M.S., Haddawy, P., Ziemer, T., Wetjen, F., Supratak, A., Chiamsakul, K., Siritanakorn, W., Chantanalertvilai, T., Sriwichai, P., Sa-ngamuang, C., 2023. A deep learning-based pipeline for mosquito detection and classification from wingbeat sounds. *Multimed Tools Appl* 82, 5189–5205. <https://doi.org/10.1007/s11042-022-13367-0>
- Zheng, X., Zhang, D., Li, Y., Yang, C., Wu, Y., Liang, X., Liang, Y., Pan, X., Hu, L., Sun, Q., Wang, X., Wei, Y., Zhu, J., Qian, W., Yan, Z., Parker, A.G., Gilles, J.R.L., Bourtzis, K., Bouyer, J., Tang, M., Zheng, B., Yu, J., Liu, J., Zhuang, J., Hu, Zhigang, Zhang, M., Gong, J.-T., Hong, X.-Y., Zhang, Z., Lin, L., Liu, Q., Hu, Zhiyong, Wu, Z., Baton, L.A., Hoffmann, A.A., Xi, Z., 2019. Incompatible and sterile insect techniques combined eliminate mosquitoes. *Nature (London)* 572, 56–61. <https://doi.org/10.1038/s41586-019-1407-9>

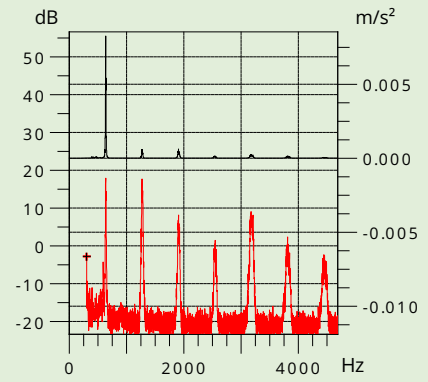
## A1. Free flight – tether Latin Square (Chapter 4)

The following Latin Square design was followed to test n=30 mosquitoes under both tethered and free flight conditions.

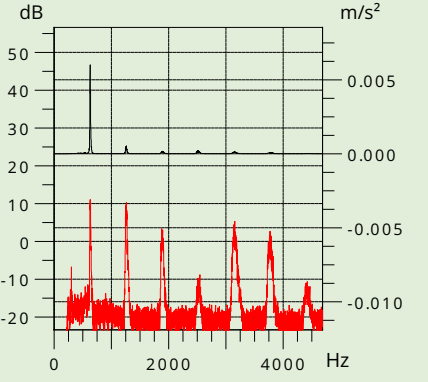
Specimen Nr	F Nr	1 <sup>st</sup> flight mode	Trial 1 start time	2 <sup>nd</sup> flight mode	Trial 2 start time
S0431	F1	Tether	09:00	Tether	09:30
S0432	F2	Tether	09.45	Tether	10.15
S0433	F3	Free flight	10.45	Free flight	11.15
S0434	F4	Free flight	11:00	Free flight	11.30
S0435	F5	Free flight	11.15	Tether	11.45
S0436	F6	Tether	12:00	Tether	12.15
S0437	F7	Free flight	14:00	Free flight	14.30
S0438	F8	Free flight	14.15	Tether	14.45
S0439	F9	Free flight	15.15	Tether	15.45
Day 1 end					
S0440	F10	Free flight	08:30	Free flight	09:00
S0441	F11	Free flight	09:30	Free flight	10:00
S0442	F12	Free flight	10:30	Tether	11:00
S0443	F13	Tether	11:30	Tether	12:00
S0444	F14	Free flight	12:30	Free flight	13:00
S0445	F15	Free flight	13:00	Tether	13:30
S0446	F16	Free flight	14:00	Tether	14:30
S0447	F17	Tether	15:00	Tether	15:30
S0448	F18	Tether	16:00	Tether	16:30
Day 2 end					
S0449	F19	Free flight	08:30	Tether	09:00
S0450	F20	Tether	09:30	Tether	10:00
S0451	F21	Free flight	10:30	Free flight	11:00
S0452	F22	Free flight	11:30	Tether	12:00
S0453	F23	Free flight	12:30	Tether	13:00
S0454	F24	Tether	13:00	Tether	13:30
S0455	F25	Tether	14:00	Tether	14:30
S0456	F26	Free flight	15:00	Free flight	15:30
S0457	F27	Free flight	16:00	Free flight	16:30
Day 3 end					
S0458	F28	Free flight	08:30	Free flight	09:00
S0459	F29	Free flight	09:30	Tether	10:00
S0460	F30	Tether	10:30	Tether	11:00



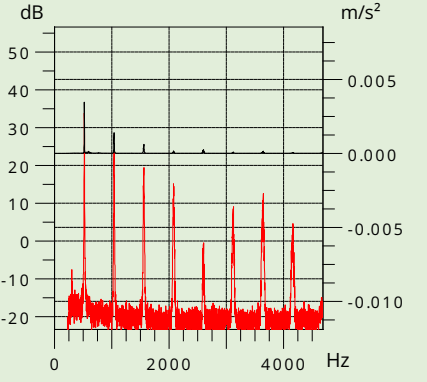
**1** Species: *Aedes aegypti* (female), Specimen Nr: 0443\_TF\_F13T1  
Body height: 3.3 mm, Body width: 1.4 mm  
Blood fed: No, Sugar fed: Yes, Post emergence age; 24 days



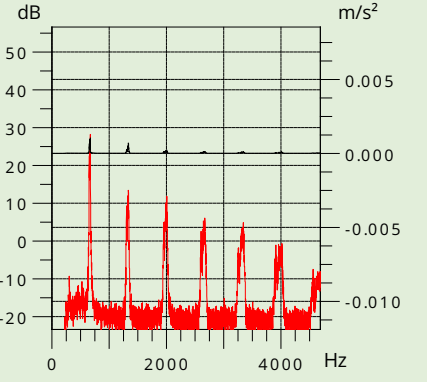
**2** Species: *Aedes aegypti* (female), Specimen Nr: 0443\_TF\_F13T2  
Body height: 3.3 mm, Body width: 1.4 mm  
Blood fed: No, Sugar fed: Yes, Post emergence age; 24 days



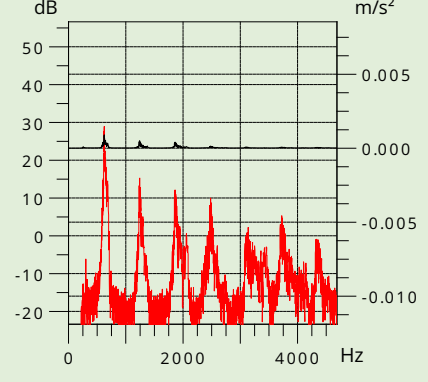
**3** Species: *Aedes aegypti* (female), Specimen Nr: 0445\_TF\_F15T2  
Body height: 3.5 mm, Body width: 1.6 mm  
Blood fed: No, Sugar fed: Yes, Post emergence age; 24 days



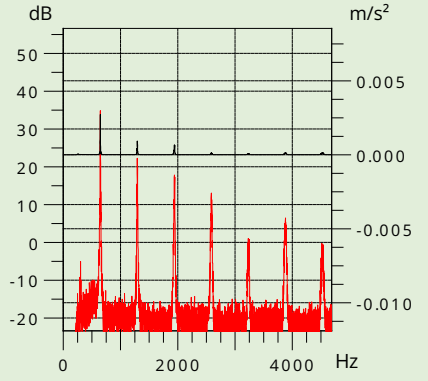
**4** Species: *Aedes aegypti* (female), Specimen Nr: 0446\_TF\_F16T2  
Body height: 3.7 mm, Body width: 1.6 mm  
Blood fed: No, Sugar fed: Yes, Post emergence age; 24 days



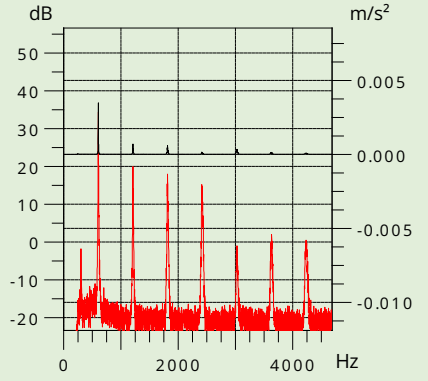
**5** Species: *Aedes aegypti* (female), Specimen Nr: 0447\_TF\_F17T1  
Body height: 3.7 mm, Body width: 1.4 mm  
Blood fed: No, Sugar fed: Yes, Post emergence age; 24 days



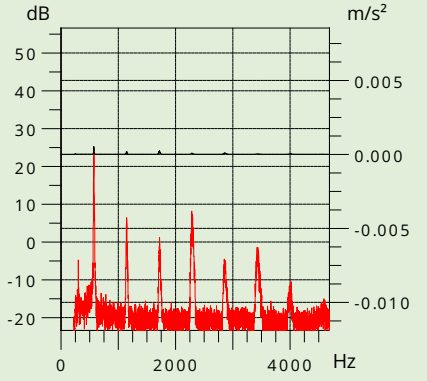
**6** Species: *Aedes aegypti* (female), Specimen Nr: 0447\_TF\_F17T2  
Body height: 3.7 mm, Body width: 1.4 mm  
Blood fed: No, Sugar fed: Yes, Post emergence age; 24 days



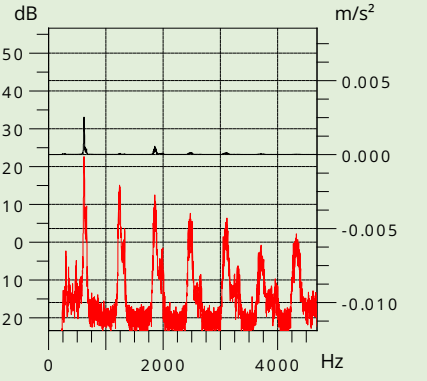
**7** Species: *Aedes aegypti* (female), Specimen Nr: 0448\_TF\_F18T1  
Body height: 3.9 mm, Body width: 1.6 mm  
Blood fed: No, Sugar fed: Yes, Post emergence age; 24 days



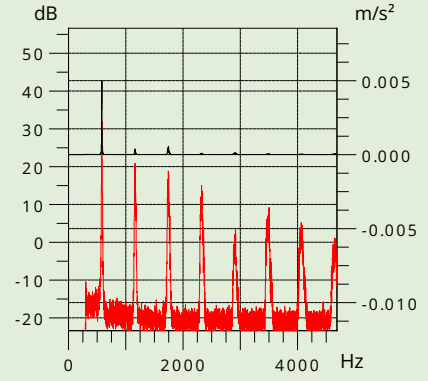
**8** Species: *Aedes aegypti* (female), Specimen Nr: 0448\_TF\_F18T2  
Body height: 3.9 mm, Body width: 1.6 mm  
Blood fed: No, Sugar fed: Yes, Post emergence age; 24 days



**9** Species: *Aedes aegypti* (female), Specimen Nr: 0449\_TF\_F19T2  
Body height: 3.7 mm, Body width: 1.4 mm  
Blood fed: No, Sugar fed: Yes, Post emergence age; 25 days



**10** Species: *Aedes aegypti* (female), Specimen Nr: 0450\_TF\_F20T1  
Body height: 3.7 mm, Body width: 1.6 mm  
Blood fed: No, Sugar fed: Yes, Post emergence age; 25 days

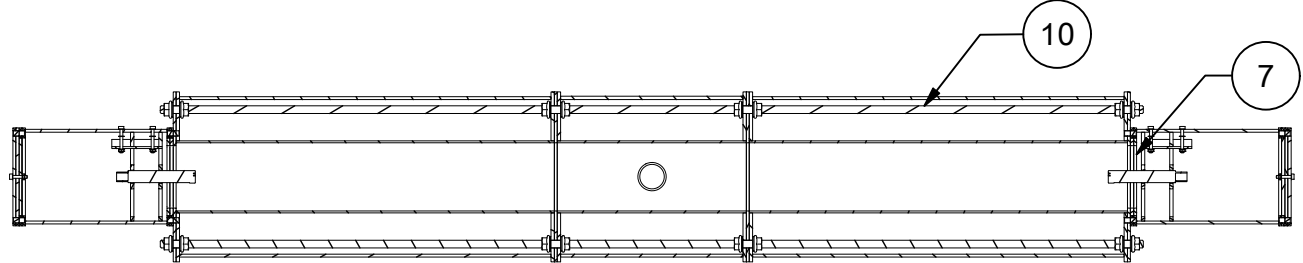
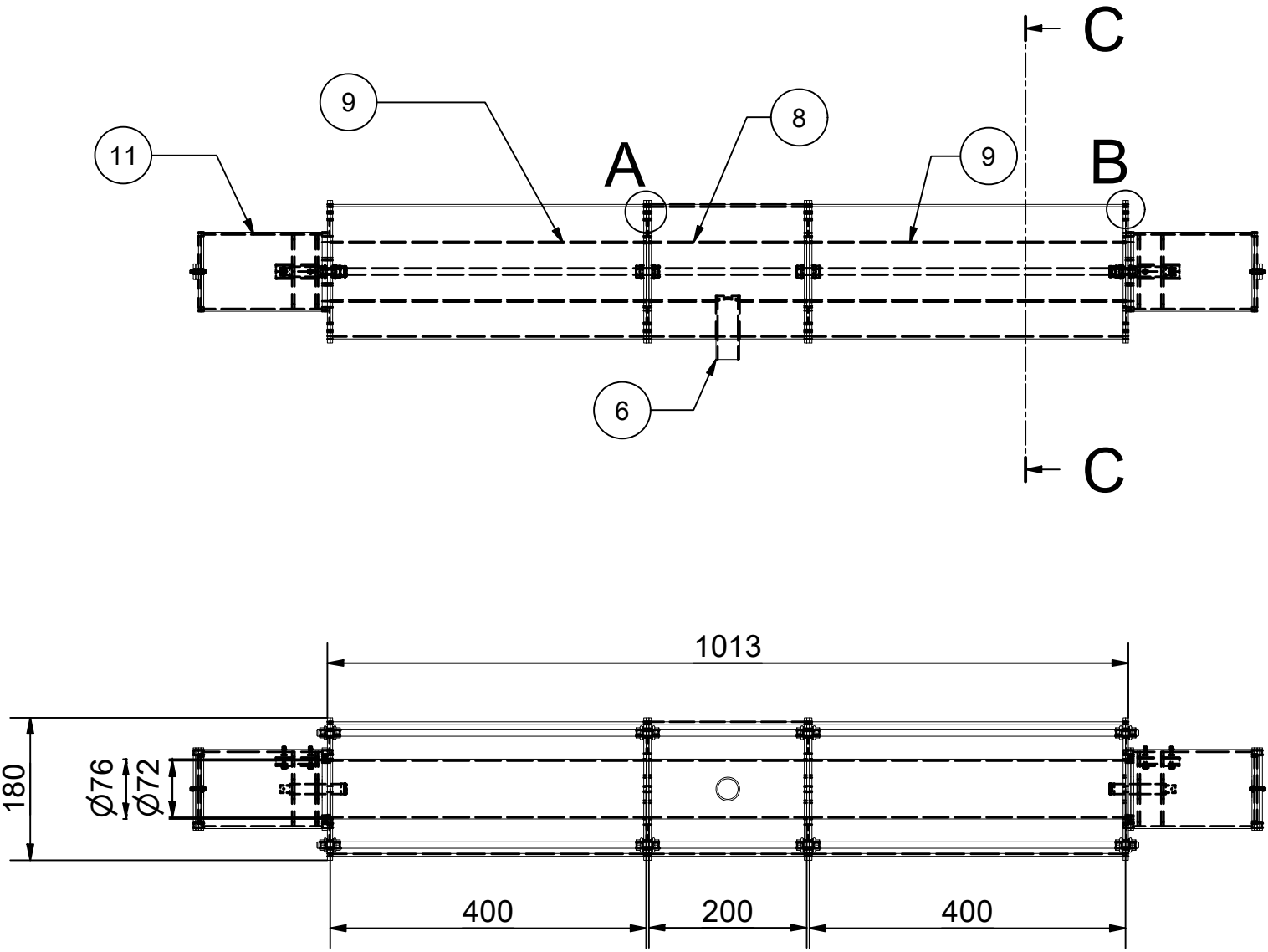


**Tethered flight - Frequency Content**

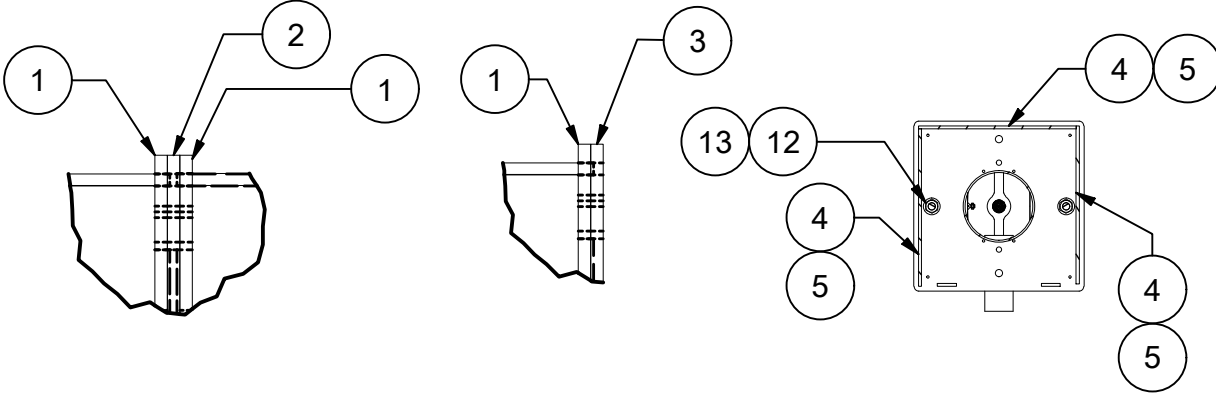
Plot Nr	Specimen Nr	Species	Blood fed	Sugar fed	Post-emergence age (days)	Body width (mm)	Body height (mm)	Fundamental frequency mic (Hz)	Fundamental frequency mic amplitude (dB(lin))	Fundamental frequency acc (Hz)	Fundamental frequency acc amplitude (m/s <sup>2</sup> )	Fundamental frequency mic std dev (Hz)	Fundamental frequency mic amplitude std dev (dB(lin))	Fundamental frequency acc std dev (Hz)	Fundamental frequency acc amplitude std dev (m/s <sup>2</sup> )
1	0443_TF_F13T1	<i>Aedes aegypti</i>	No	Yes	24	1.4	3.3	634.28	17.9	634.28	0.008261	2.78	-0.4	2.38	0.002634
2	0443_TF_F13T2	<i>Aedes aegypti</i>	No	Yes	24	1.4	3.3	627.69	11.1	627.69	0.006	3.5	-0.8	3.69	0.001486
3	0445_TF_F15T2	<i>Aedes aegypti</i>	No	Yes	24	1.6	3.5	520.02	33.8	520.02	0.003462	1.4	-2.2	1.4	0.000885
4	0446_TF_F16T2	<i>Aedes aegypti</i>	No	Yes	24	1.6	3.7	668.7	28.2	668.7	0.001047	5.61	-1.2	6.58	0.000469
5	0447_TF_F17T1	<i>Aedes aegypti</i>	No	Yes	24	1.4	3.7	621.83	28.9	621.83	0.000904	21.45	3.4	30.63	0.000478
6	0447_TF_F17T2	<i>Aedes aegypti</i>	No	Yes	24	1.4	3.7	646.73	34.8	646.73	0.002722	1.14	-1.6	1.14	0.000841
7	0448_TF_F18T1	<i>Aedes aegypti</i>	No	Yes	24	1.6	3.9	604.98	34.4	604.98	0.003483	0.71	-1.8	0.74	0.000613
8	0448_TF_F18T2	<i>Aedes aegypti</i>	No	Yes	24	1.6	3.9	572.75	24.8	572.75	0.000534	2.44	-1.7	2.42	0.000131
9	0449_TF_F19T2	<i>Aedes aegypti</i>	No	Yes	25	1.4	3.7	618.16	22.6	618.16	0.002528	18.79	3.2	16.8	0.002128
10	0450_TF_F20T1	<i>Aedes aegypti</i>	No	Yes	25	1.6	3.7	582.28	32.0	582.28	0.005011	3.4	-0.8	3.22	0.001853

NOTE: DRAWING ILLUSTRATED WITH NOMINAL 3.3MM SHEET ACRYLIC!

D-D ( 1:8 )



A ( 1:2 )    B ( 1:2 )    C-C ( 1:8 )

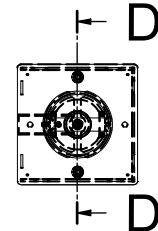
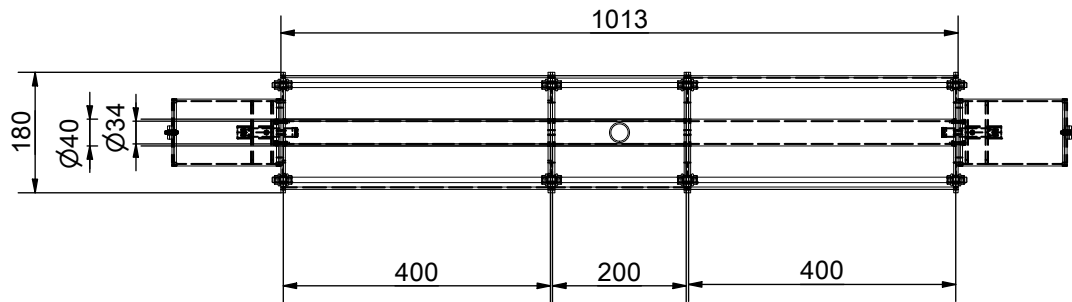
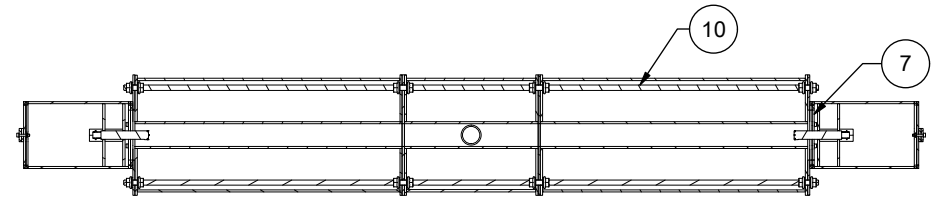
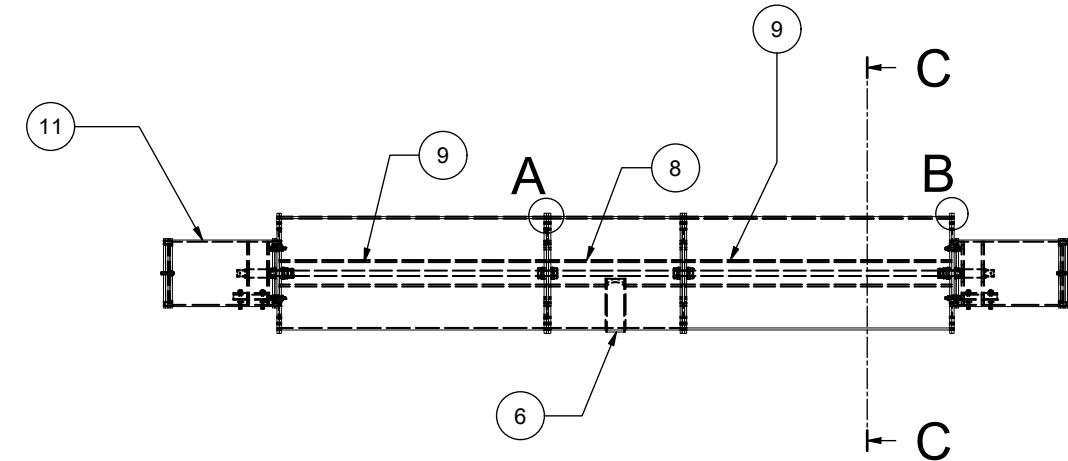


ITEM	QTY	PART NUMBER	DESCRIPTION
13	16	-	M8 WASHER
12	16	-	M8 FLANGED NUT
11	2	LG16_PU_13_PU13f_810	CAPSULE ASSY
10	2	LG16_PU_13_PU13f_401	M8 THREADED BAR 1040
9	2	LG16_PU_13_PU13f_102	76ODTUBE 400
8	1	LG16_PU_13_PU13f_101	76ODTUBE 200
7	4	LG16_PU_13_PU13f_052	CAPSULE DOCKPLATE B
6	1	LG16_PU_13_PU13f_042	MOSQUITO ENTRY TUBE A
5	3	LG16_PU_13_PU13f_041	EXTERIOR PANEL B
4	6	LG16_PU_13_PU13f_040	EXTERIOR PANEL A
3	2	LG16_PU_13_PU13f_038	CONNECTOR PLATE C
2	2	LG16_PU_13_PU13f_031	CONNECTOR PLATE B 76
1	6	LG16_PU_13_PU13f_030	CONNECTOR PLATE A 76

SIZE	A3	SCALE	1:6	MATERIAL	3MM ACRYLIC	
LINEAR TOL UOS	±0.2	DRAWING TO	BS8888	FINISH	CLEAN AND SCRATCH FREE	
ANGULAR TOL UOS	±0.5°	ALL DIMENSIONS	MM	DRAWN BY	F. SARATHCHANDRA	
				MODULE	PU-13f	
				TITLE	76 DIA ACOUSTIC TUNNEL	
				PART NR	LG16_PU_13_PU13f_803	
				DATE	REVISION	SHEET
				16/02/2021	A	1 OF 1

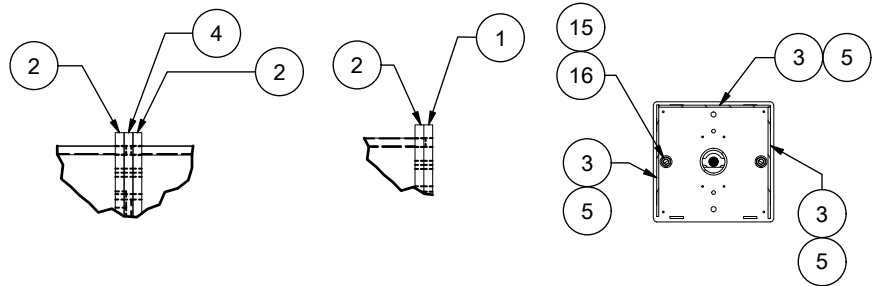
NOTE: DRAWING ILLUSTRATED WITH NOMINAL 3.3MM SHEET ACRYLIC!

D-D ( 1:8 )



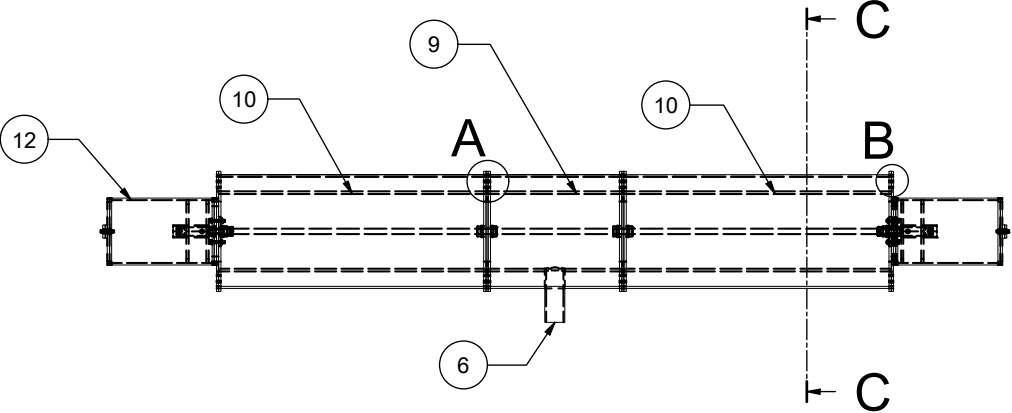
16	16	-	M8 FLANGED NUT
15	16	-	M8 WASHER
14	16	-	M3 WASHER
13	8	-	M3 X 20 SOCKET HEAD SCREW
12	8	-	M3 NUT
11	2	LG16_PU_13_PU13f_810	CAPSULE ASSY
10	2	LG16_PU_13_PU13f_401	M8 THREADED BAR 1040
9	2	LG16_PU_13_PU13f_106	40ODTUBE 400
8	1	LG16_PU_13_PU13f_105	40ODTUBE 200
7	4	LG16_PU_13_PU13f_052	CAPSULE DOCKPLATE B
6	1	LG16_PU_13_PU13f_042	MOSQUITO ENTRY TUBE A
5	3	LG16_PU_13_PU13f_041	EXTERIOR PANEL B
4	2	LG16_PU_13_PU13f_037	CONNECTOR PLATE B 40
3	6	LG16_PU_13_PU13f_040	EXTERIOR PANEL A
2	6	LG16_PU_13_PU13f_036	CONNECTOR PLATE A 40
1	2	LG16_PU_13_PU13f_038	CONNECTOR PLATE C
ITEM	QTY	PART NUMBER	DESCRIPTION

A ( 1:2 )    B ( 1:2 )    C-C ( 1:8 )

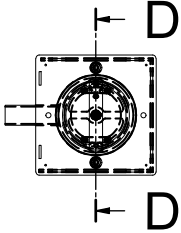
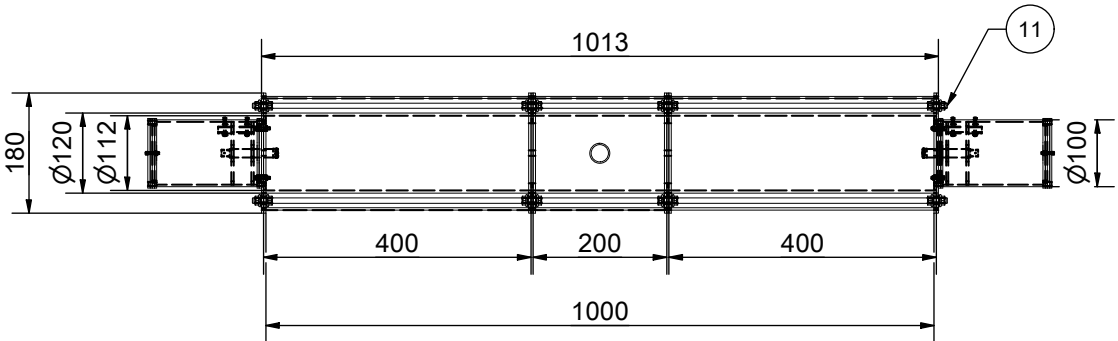
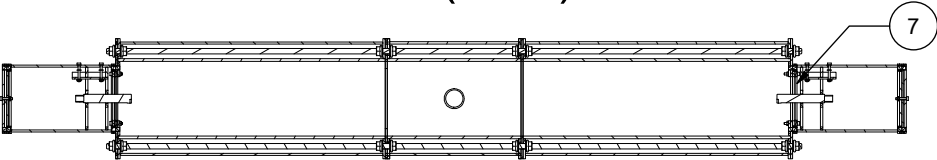


SIZE	A3	SCALE	1:6	MATERIAL	3MM ACRYLIC
LINEAR TOL UOS	±0.2	DRAWING TO	BS8888	FINISH	CLEAN AND SCRATCH FREE
ANGULAR TOL UOS	±0.5°	ALL DIMENSIONS	MM	DRAWN BY	F. SARATHCHANDRA
LONDON SCHOOL of HYGIENE & TROPICAL MEDICINE development LG16 		MODULE	PU-13f		
		TITLE	40 DIA ACOUSTIC TUNNEL		
		PART NR	LG16_PU_13_PU13f_805		
		DATE	REVISION		
		16/02/2021	A		
			SHEET	1 OF 1	

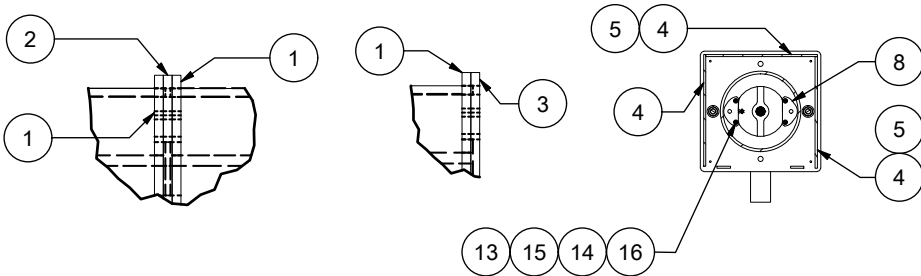
NOTE: DRAWING ILLUSTRATED WITH NOMINAL 3.3MM SHEET ACRYLIC!



D-D ( 1:8 )

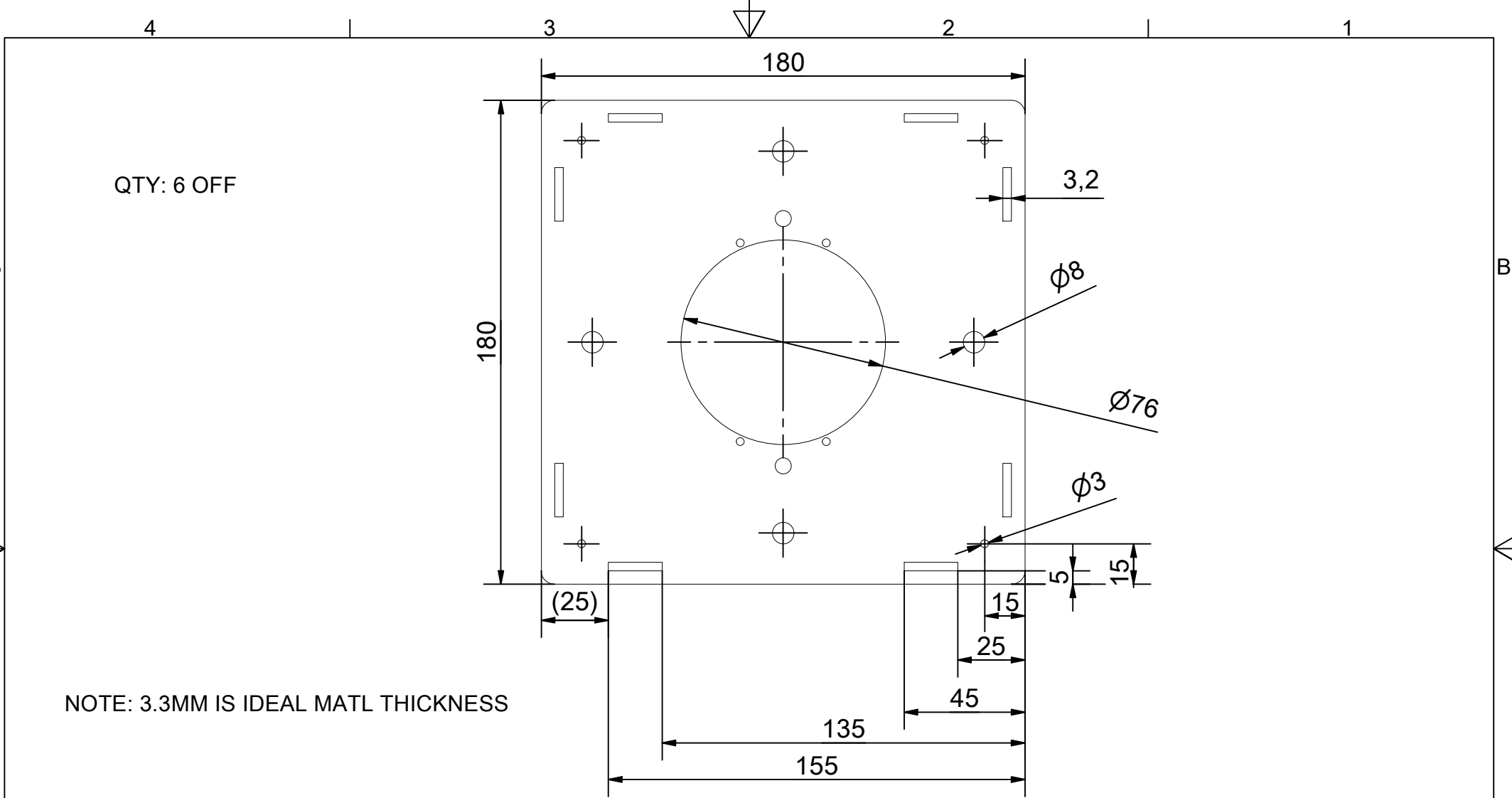


A ( 1:2 )    B ( 1:2 )    C-C ( 1:8 )



18	16	-	M8 WASHER
17	16	-	M8 FLANGED NUT
16	16	-	M3 WASHER
15	8	-	M3 NUT
14	4	-	M3 X 20 SOCKET SCREW
13	4	-	M3 X 16 SOCKET SCREW
12	2	LG16_PU_13_PU13f_810	CAPSULE ASSY
11	2	LG16_PU_13_PU13f_401	M8 THREADED BAR 1040
10	2	LG16_PU_13_PU13f_104	120ODTUBE 400
9	1	LG16_PU_13_PU13f_103	120ODTUBE 200
8	4	LG16_PU_13_PU13f_057	CAPSULE DOCK LATCH 120
7	4	LG16_PU_13_PU13f_052	CAPSULE DOCKPLATE B
6	1	LG16_PU_13_PU13f_042	MOSQUITO ENTRY TUBE A
5	3	LG16_PU_13_PU13f_041	EXTERIOR PANEL B
4	6	LG16_PU_13_PU13f_040	EXTERIOR PANEL A
3	2	LG16_PU_13_PU13f_038	CONNECTOR PLATE C
2	2	LG16_PU_13_PU13f_035	CONNECTOR PLATE B 120
1	6	LG16_PU_13_PU13f_034	CONNECTOR PLATE A 120
ITEM	QTY	PART NUMBER	DESCRIPTION

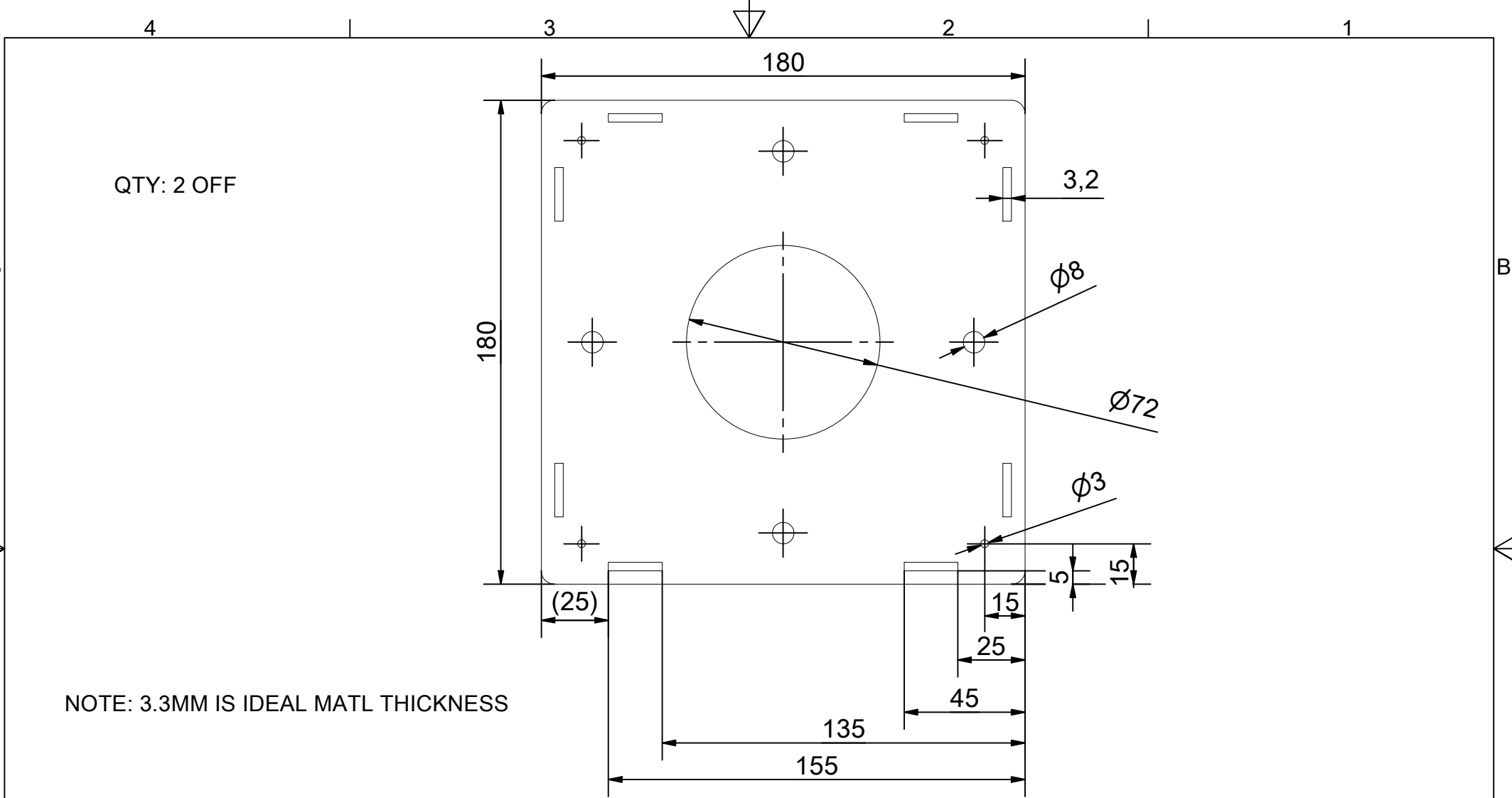
SIZE	A3	SCALE	1:6	MATERIAL	3MM ACRYLIC
LINEAR TOL UOS	±0.2	DRAWING TO BS8888		FINISH	CLEAN AND SCRATCH FREE
ANGULAR TOL UOS	±0.5°	ALL DIMENSIONS MM		DRAWN BY	F. SARATHCHANDRA
 LONDON SCHOOL of HYGIENE & TROPICAL MEDICINE		 development LG16		MODULE	PU-13f
				TITLE	120 DIA ACOUSTIC TUNNEL
				PART NR	LG16_PU_13_PU13f_806
				DATE	REVISION
				16/02/2021	A
				SHEET	1 OF 1



QTY: 6 OFF

NOTE: 3.3MM IS IDEAL MATL THICKNESS

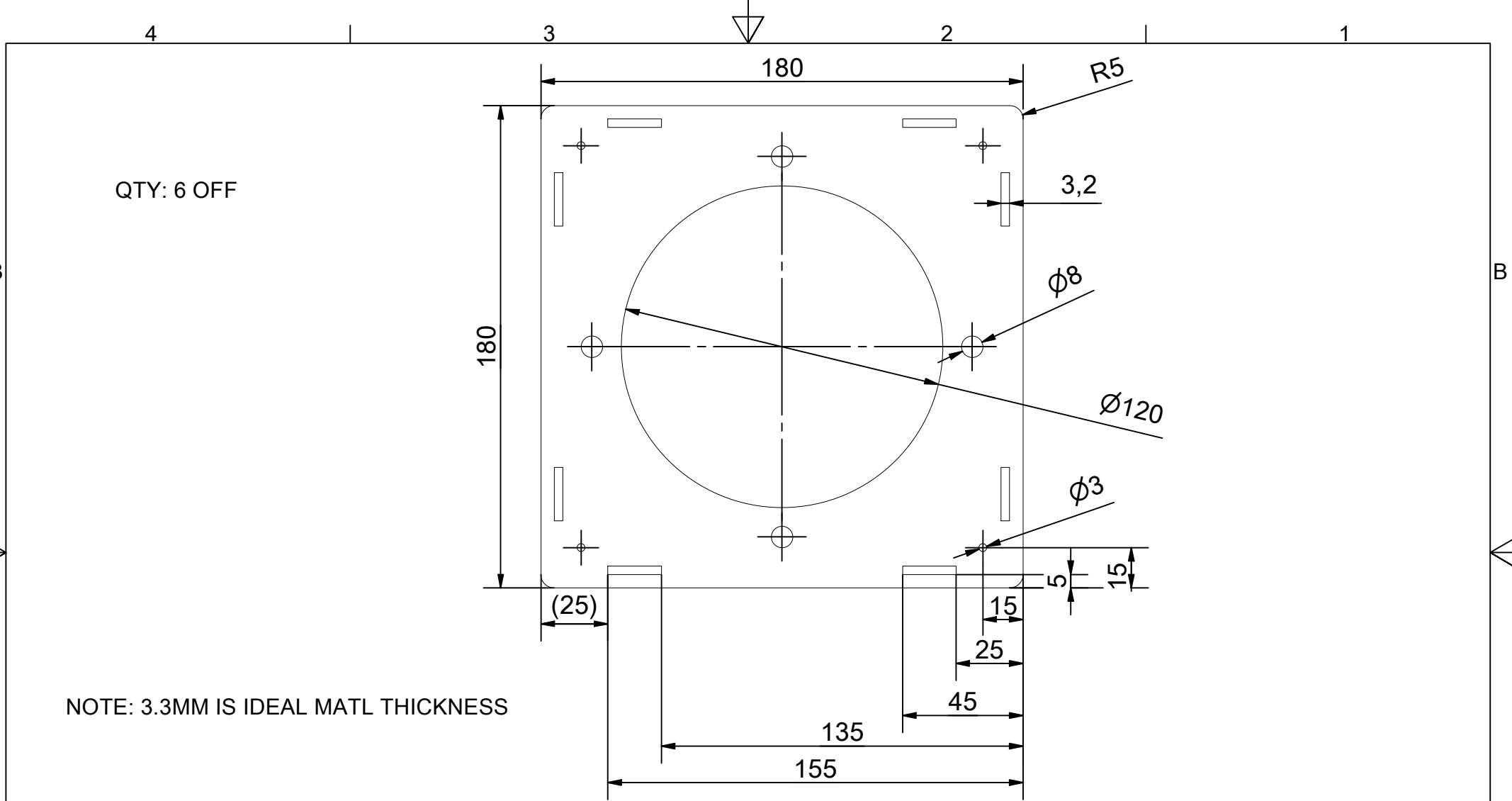
SIZE	A4	SCALE	1:2	MATERIAL	3MM ACRYLIC	
LINEAR TOL UOS	±0.2	DRAWING TO BS8888		FINISH	CLEAN AND SCRATCH FREE	
ANGULAR TOL UOS	±0.5°	ALL DIMENSIONS MM		DRAWN BY	F. SARATHCHANDRA	
				MODULE	PU-13f	
				TITLE	CONNECTOR PLATE A 76	
				PART NR	LG16_PU_13_PU13f_030	
				DATE	REVISION	SHEET
				16/02/2021	A	1 OF 1



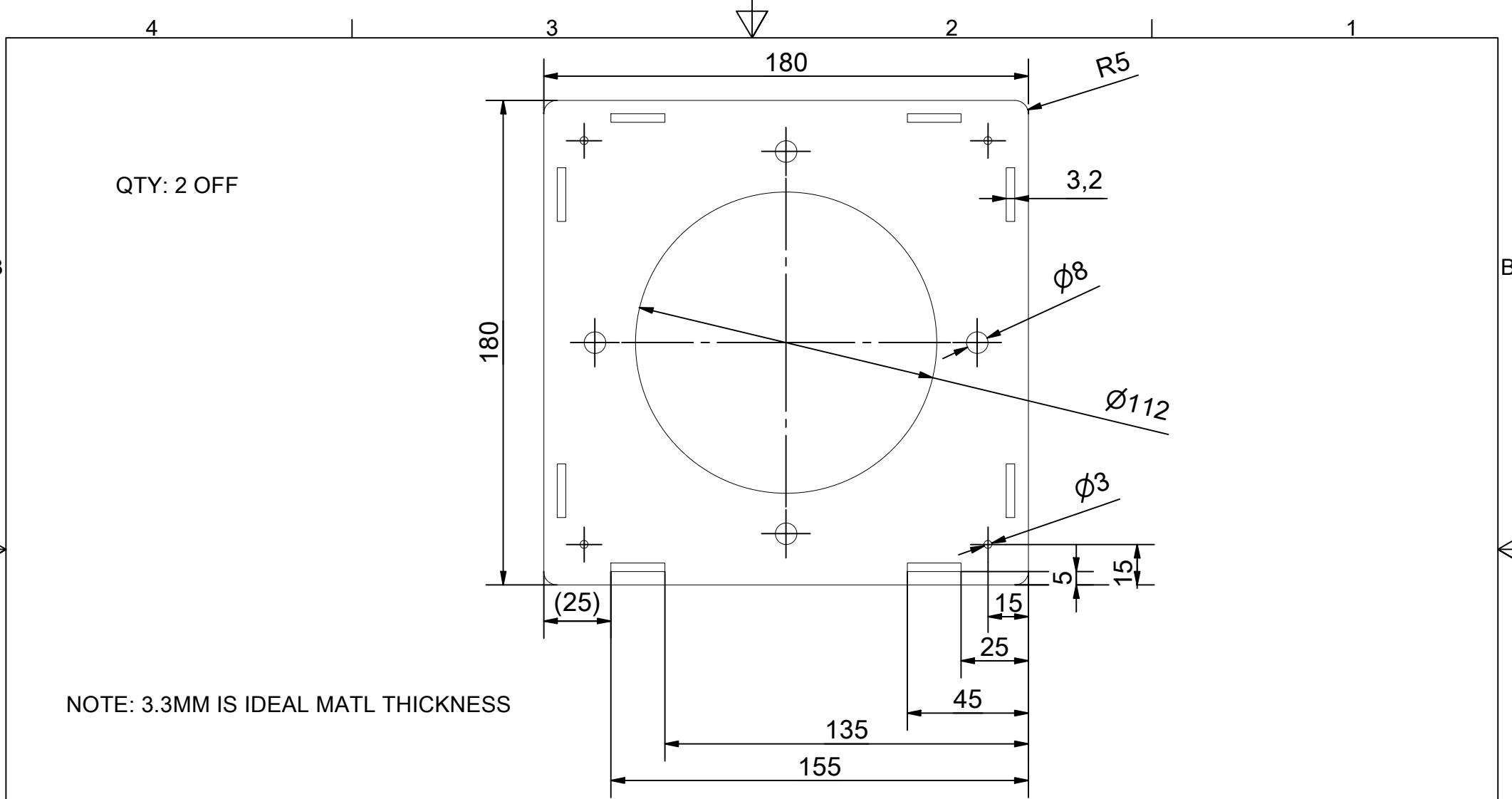
QTY: 2 OFF

NOTE: 3.3MM IS IDEAL MATL THICKNESS

SIZE	A4	SCALE	1:2	MATERIAL	3MM ACRYLIC	
LINEAR TOL UOS	±0.2	DRAWING TO BS8888		FINISH	CLEAN AND SCRATCH FREE	
ANGULAR TOL UOS	±0.5°	ALL DIMENSIONS MM		DRAWN BY	F. SARATHCHANDRA	
				MODULE	PU-13f	
				TITLE	CONNECTOR PLATE B 76	
				PART NR	LG16_PU_13_PU13f_031	
				DATE	REVISION	SHEET
				16/02/2021	A	1 OF 1

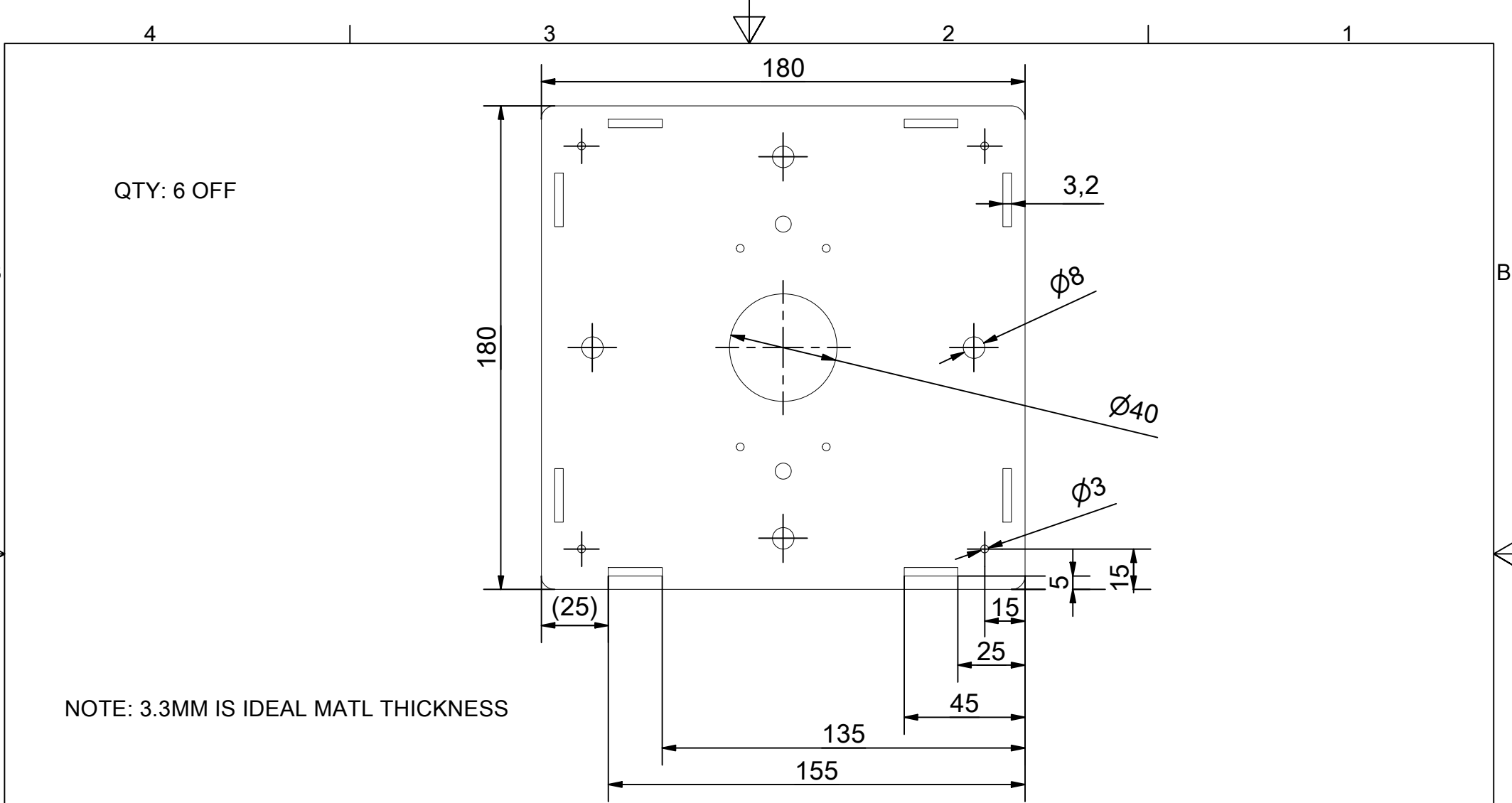


SIZE	A4	SCALE	1:2	MATERIAL	3MM ACRYLIC	
LINEAR TOL UOS	±0.2	DRAWING TO BS8888		FINISH	CLEAN AND SCRATCH FREE	
ANGULAR TOL UOS	±0.5°	ALL DIMENSIONS MM		DRAWN BY	F. SARATHCHANDRA	
				MODULE	PU-13f	
				TITLE	CONNECTOR PLATE A 120	
				PART NR	LG16_PU_13_PU13f_034	
				DATE	REVISION	SHEET
				16/02/2021	A	1 OF 1



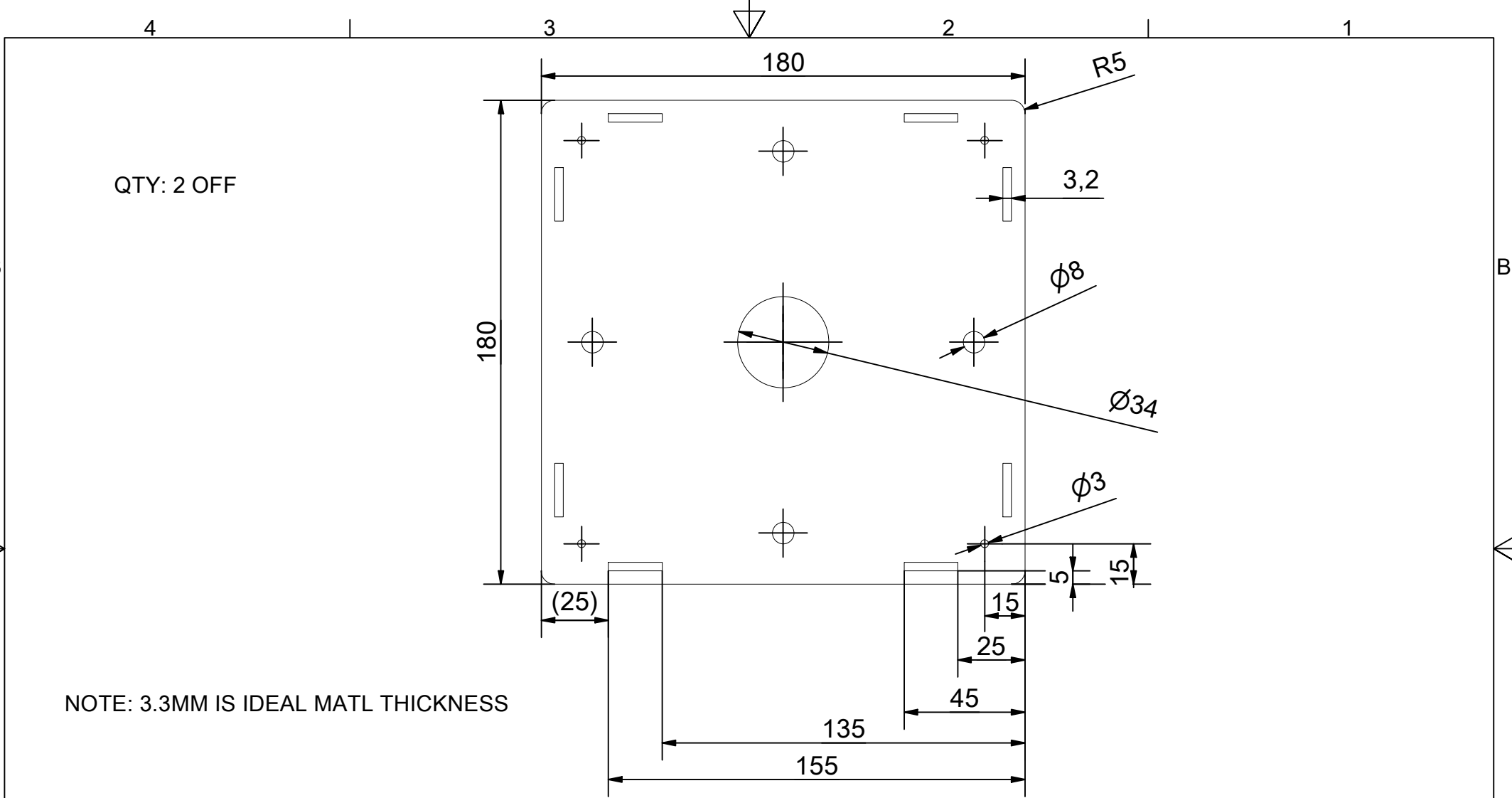
NOTE: 3.3MM IS IDEAL MATL THICKNESS

SIZE	A4	SCALE	1:2	MATERIAL	3MM ACRYLIC	
LINEAR TOL UOS	±0.2	DRAWING TO BS8888		FINISH	CLEAN AND SCRATCH FREE	
ANGULAR TOL UOS	±0.5°	ALL DIMENSIONS MM		DRAWN BY	F. SARATHCHANDRA	
				MODULE	PU-13f	
				TITLE	CONNECTOR PLATE B 120	
				PART NR	LG16_PU_13_PU13f_035	
				DATE	REVISION	SHEET
				16/02/2021	A	1 OF 1



NOTE: 3.3MM IS IDEAL MATL THICKNESS

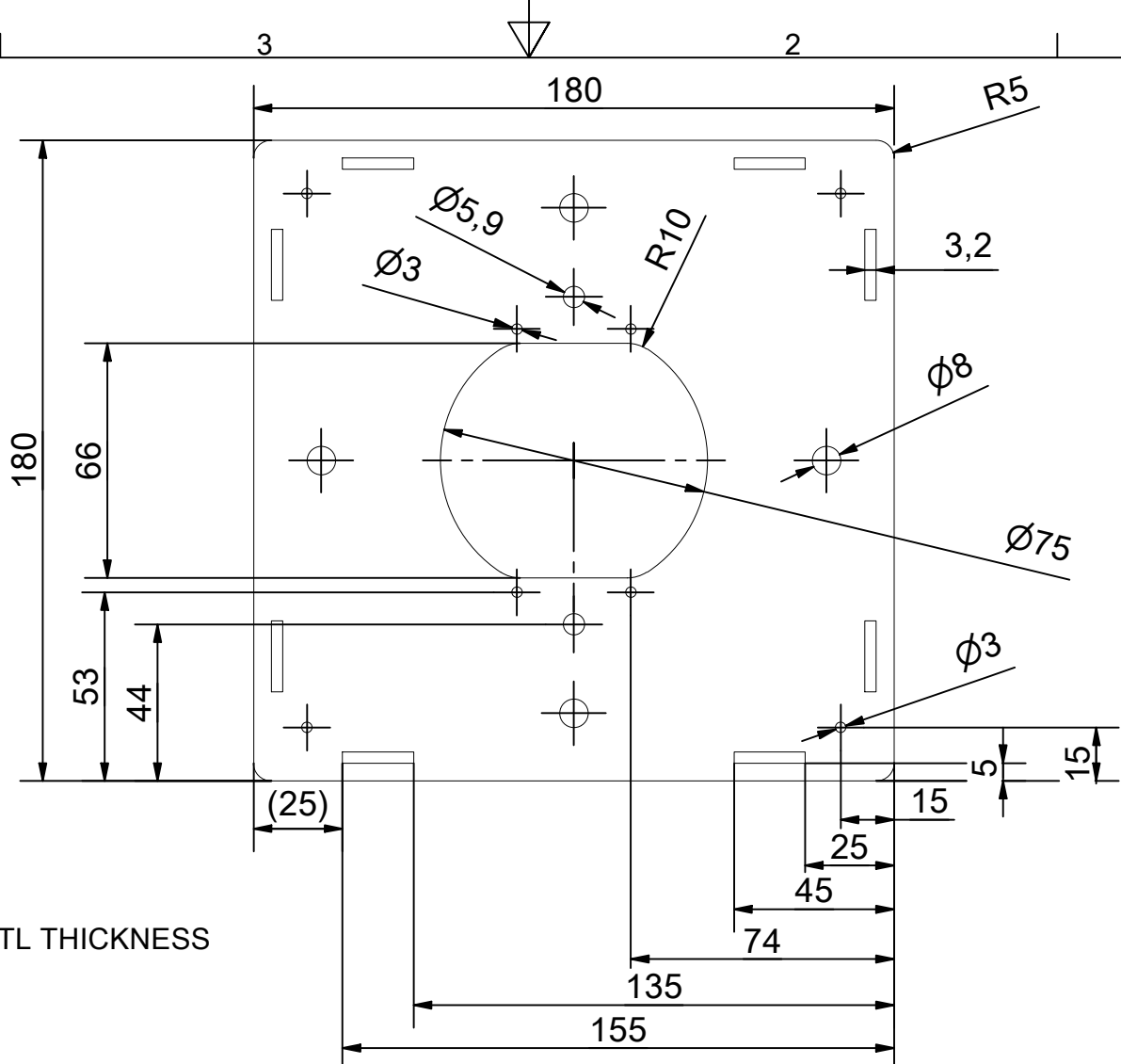
SIZE	A4	SCALE	1:2	MATERIAL	3MM ACRYLIC	
LINEAR TOL UOS	±0.2	DRAWING TO BS8888		FINISH	CLEAN AND SCRATCH FREE	
ANGULAR TOL UOS	±0.5°	ALL DIMENSIONS MM		DRAWN BY	F. SARATHCHANDRA	
				MODULE	PU-13f	
				TITLE	CONNECTOR PLATE A 40	
				PART NR	LG16_PU_13_PU13f_036	
				DATE	REVISION	SHEET
				16/02/2021	A	1 OF 1



NOTE: 3.3MM IS IDEAL MATL THICKNESS

SIZE	A4	SCALE	1:2	MATERIAL	3MM ACRYLIC	
LINEAR TOL UOS	±0.2	DRAWING TO BS8888		FINISH	CLEAN AND SCRATCH FREE	
ANGULAR TOL UOS	±0.5°	ALL DIMENSIONS MM		DRAWN BY	F. SARATHCHANDRA	
				MODULE	PU-13f	
				TITLE	CONNECTOR PLATE B 40	
				PART NR	LG16_PU_13_PU13f_037	
				DATE	REVISION	SHEET
				16/02/2021	A	1 OF 1

QTY: 6 OFF



NOTE: 3.3MM IS IDEAL MATL THICKNESS

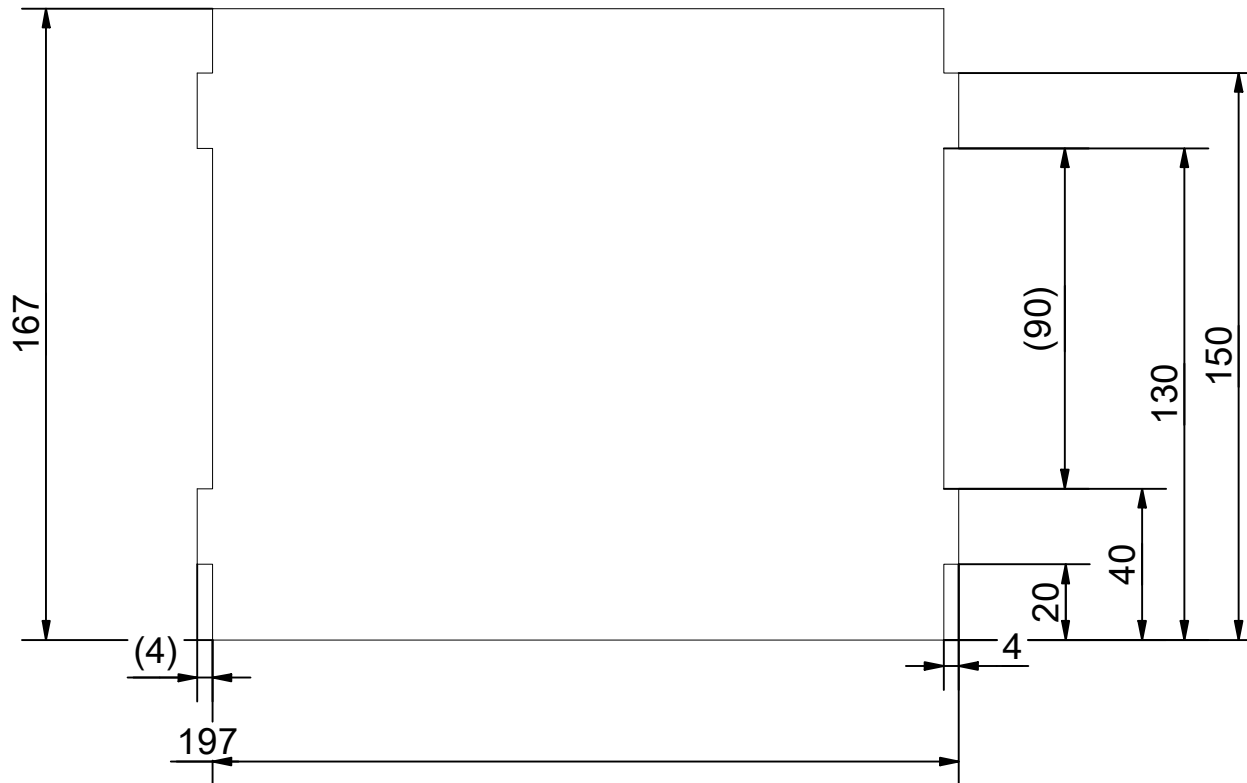
SIZE	A4	SCALE	1:2	MATERIAL	3MM ACRYLIC	
LINEAR TOL UOS	±0.2	DRAWING TO BS8888		FINISH	CLEAN AND SCRATCH FREE	
ANGULAR TOL UOS	±0.5°	ALL DIMENSIONS MM		DRAWN BY	F. SARATHCHANDRA	
				MODULE	PU-13f	
				TITLE	CONNECTOR PLATE C	
				PART NR	LG16_PU_13_PU13f_038	
				DATE	REVISION	SHEET
				16/02/2021	A	1 OF 1

QTY: MAX 24 OFF, MIN 6 OFF



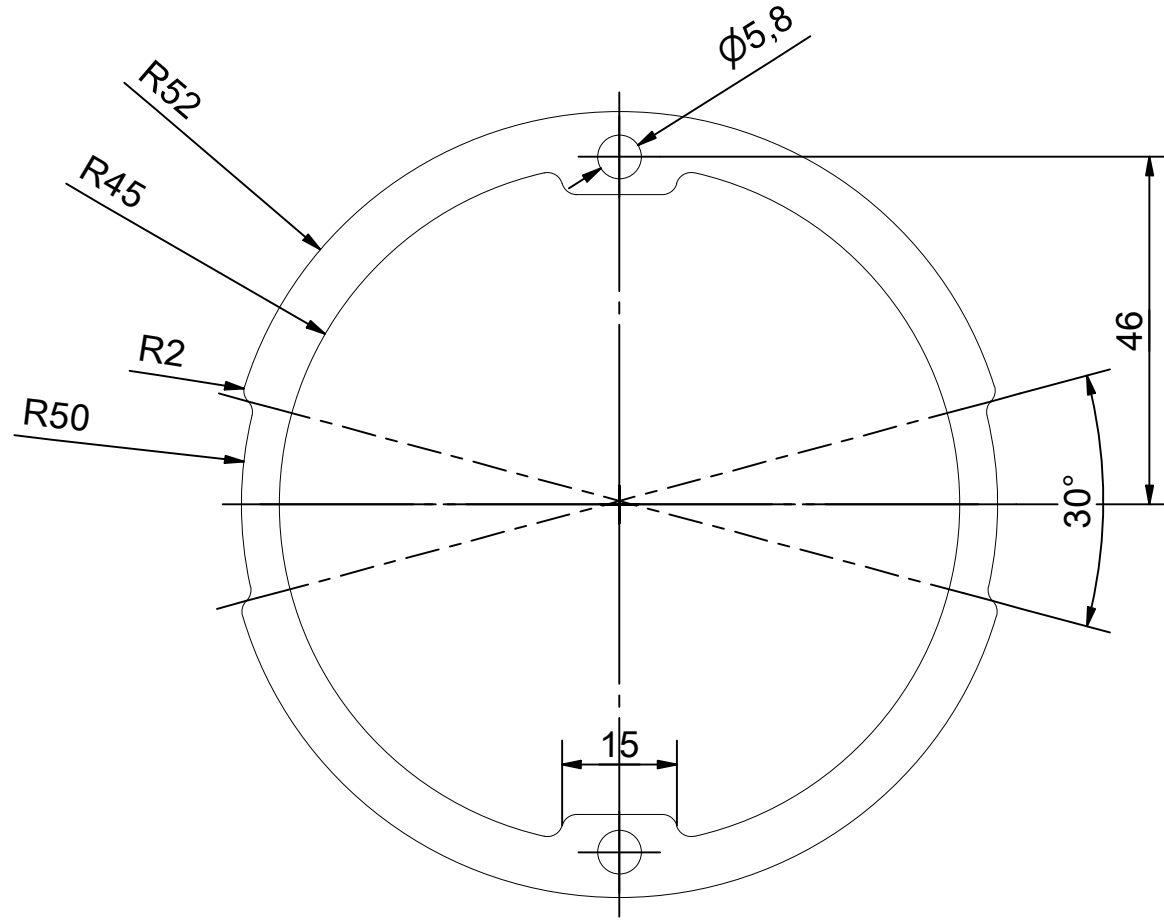
SIZE	A4	SCALE	1:2	MATERIAL	3MM ACRYLIC
LINEAR TOL UOS	±0.2	DRAWING TO BS8888		FINISH	CLEAN AND SCRATCH FREE
ANGULAR TOL UOS	±0.5°	ALL DIMENSIONS MM		DRAWN BY	F. SARATHCHANDRA
				MODULE	PU-13f
				TITLE	EXTERIOR PANEL A
				PART NR	LG16_PU_13_PU13f_040
				DATE	16/02/2021
				REVISION	A
				SHEET	1 OF 1

QTY: MAX 12 OFF, MIN 3 OFF



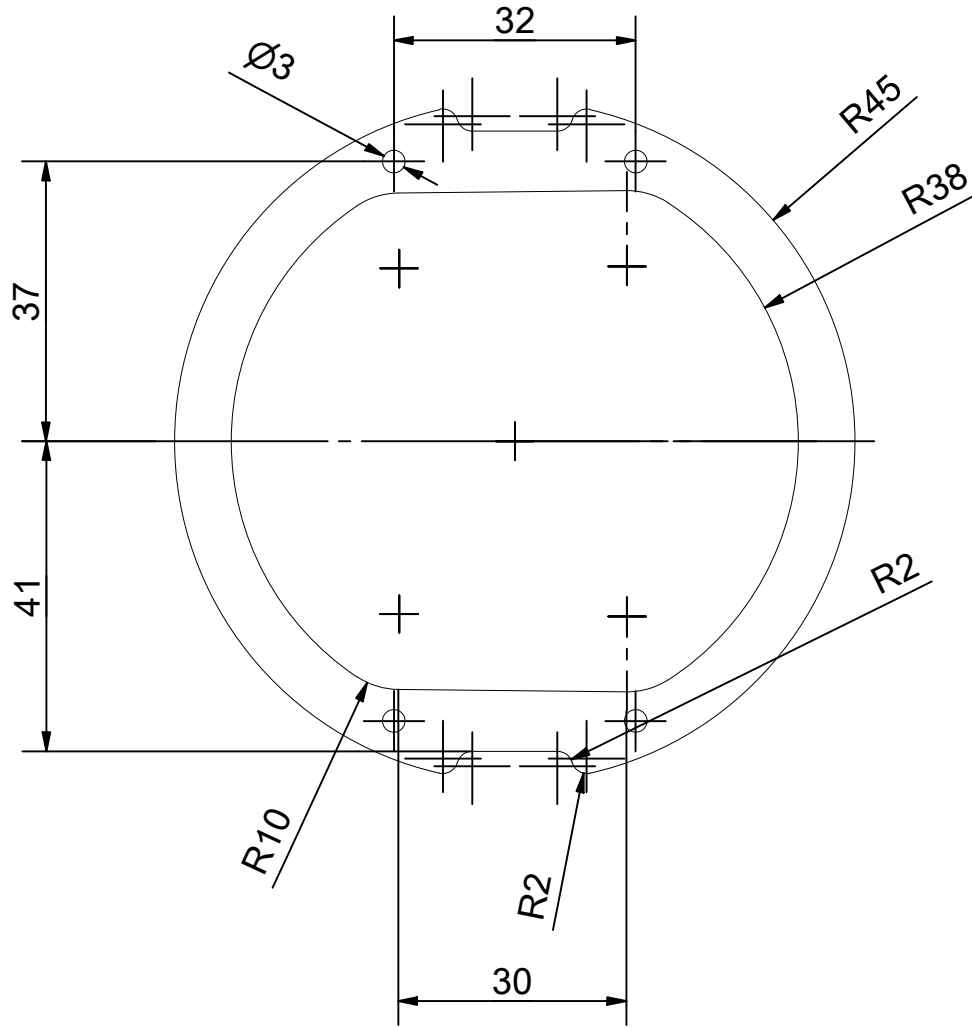
SIZE	A4	SCALE	1:2	MATERIAL	3MM ACRYLIC	
LINEAR TOL UOS	±0.2	DRAWING TO BS8888		FINISH	CLEAN AND SCRATCH FREE	
ANGULAR TOL UOS	±0.5°	ALL DIMENSIONS MM		DRAWN BY	F. SARATHCHANDRA	
				MODULE	PU-13f	
				TITLE	EXTERIOR PANEL B	
				PART NR	LG16_PU_13_PU13f_041	
				DATE	REVISION	SHEET
				16/02/2021	A	1 OF 1

QTY: 28 OFF



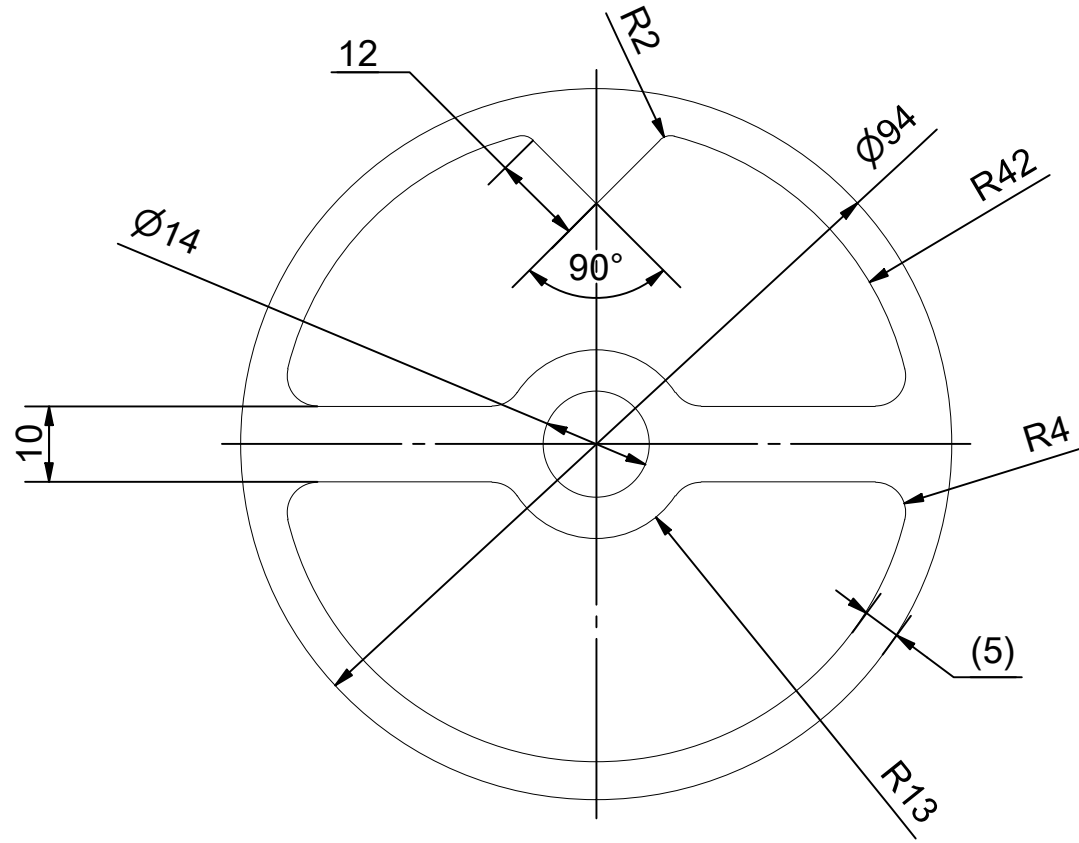
SIZE	A4	SCALE	1:1	MATERIAL	3MM ACRYLIC
LINEAR TOL UOS	±0.2	DRAWING TO BS8888		FINISH	CLEAN AND SCRATCH FREE
ANGULAR TOL UOS	±0.5°	ALL DIMENSIONS MM		DRAWN BY	F. SARATHCHANDRA
				MODULE	PU-13f
				TITLE	CAPSULE DOCK PLATE A
				PART NR	LG16_PU_13_PU13f_051
				DATE	16/02/2021
				REVISION	A
				SHEET	1 OF 1

QTY: 12 OFF



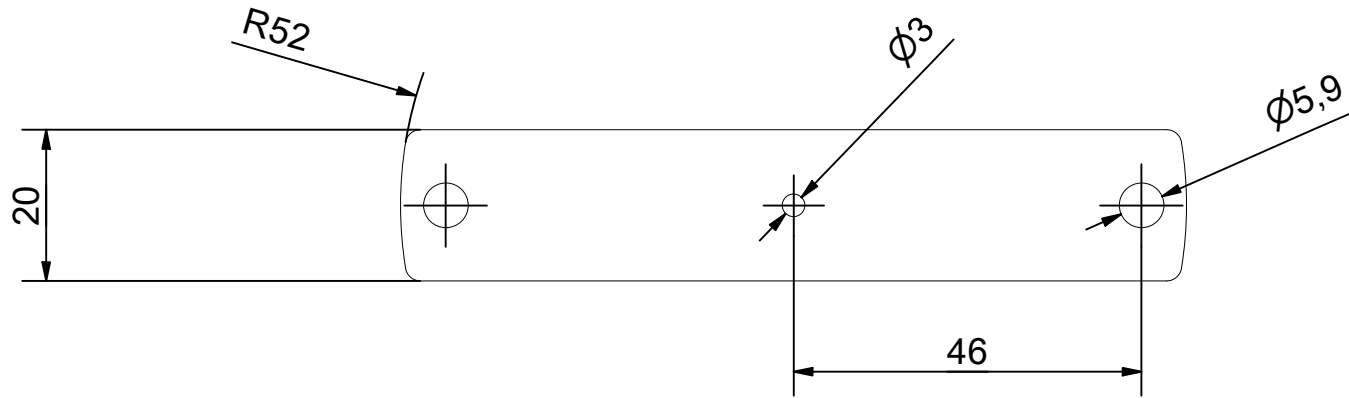
SIZE	A4	SCALE	1:1	MATERIAL	3MM ACRYLIC
LINEAR TOL UOS	±0.2	DRAWING TO BS8888		FINISH	CLEAN AND SCRATCH FREE
ANGULAR TOL UOS	±0.5°	ALL DIMENSIONS MM		DRAWN BY	F. SARATHCHANDRA
				MODULE	PU-13f
				TITLE	CAPSULE DOCKPLATE B
				PART NR	LG16_PU_13_PU13f_052
				DATE	16/02/2021
				REVISION	A
				SHEET	1 OF 1

QTY: 14 OFF



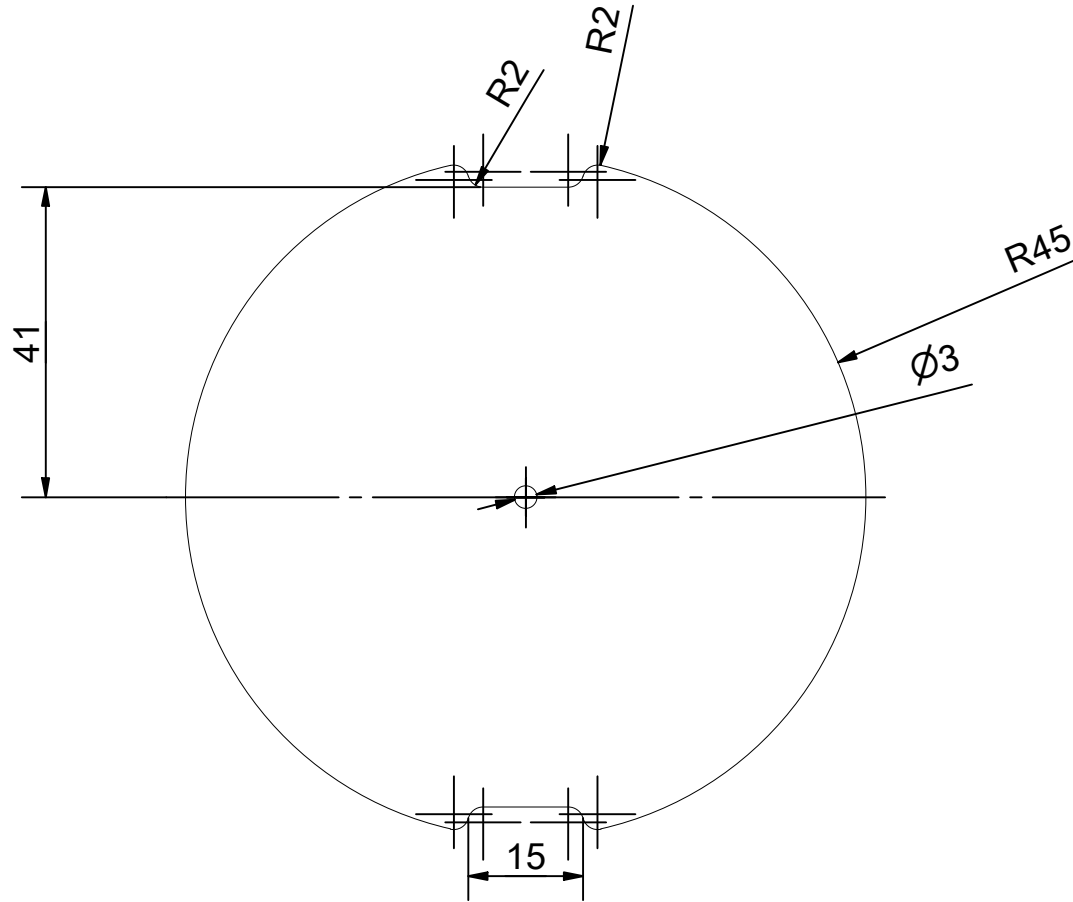
SIZE	A4	SCALE	1:1	MATERIAL	3MM ACRYLIC	
LINEAR TOL UOS	$\pm 0.2$	DRAWING TO BS8888		FINISH	CLEAN AND SCRATCH FREE	
ANGULAR TOL UOS	$\pm 0.5^\circ$	ALL DIMENSIONS MM		DRAWN BY	F. SARATHCHANDRA	
				MODULE	PU-13f	
				TITLE	CAPSULE DOCK PLATE C	
				PART NR	LG16_PU_13_PU13f_054	
				DATE	REVISION	SHEET
				16/02/2021	A	1 OF 1

QTY: 15 OFF



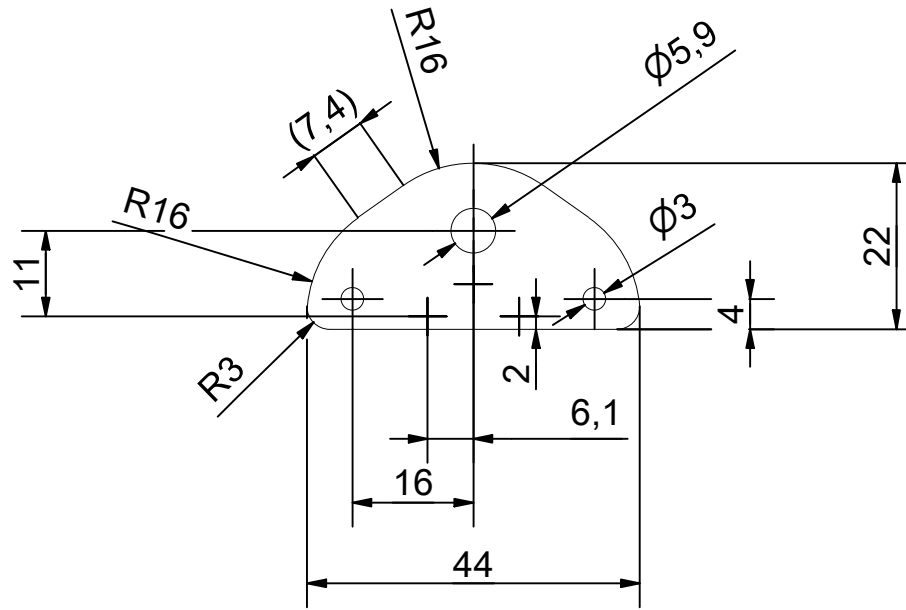
SIZE	A4	SCALE	1:1	MATERIAL	3MM ACRYLIC	
LINEAR TOL UOS	±0.2	DRAWING TO BS8888		FINISH	CLEAN AND SCRATCH FREE	
ANGULAR TOL UOS	±0.5°	ALL DIMENSIONS MM		DRAWN BY	F. SARATHCHANDRA	
				MODULE	PU-13f	
				TITLE	CAPSULE LOCK	
				PART NR	LG16_PU_13_PU13f_055	
				DATE	REVISION	SHEET
				16/02/2021	A	1 OF 1

QTY: 6 OFF



SIZE	A4	SCALE	1:1	MATERIAL	3MM ACRYLIC	
LINEAR TOL UOS	±0.2	DRAWING TO BS8888		FINISH	CLEAN AND SCRATCH FREE	
ANGULAR TOL UOS	±0.5°	ALL DIMENSIONS MM		DRAWN BY	F. SARATHCHANDRA	
				MODULE	PU-13f	
				TITLE	CAPSULE LID	
				PART NR	LG16_PU_13_PU13f_056	
				DATE	REVISION	SHEET
				16/02/2021	A	1 OF 1

QTY: 6 OFF



SIZE	A4	SCALE	1:1	MATERIAL	3MM ACRYLIC	
LINEAR TOL UOS	±0.2	DRAWING TO BS8888		FINISH	CLEAN AND SCRATCH FREE	
ANGULAR TOL UOS	±0.5°	ALL DIMENSIONS MM		DRAWN BY	F. SARATHCHANDRA	
				MODULE	PU-13f	
				TITLE	CAPSULE DOCK LATCH 120	
				PART NR	LG16_PU_13_PU13f_057	
				DATE	REVISION	SHEET
				16/02/2021	A	1 OF 1